MAX PLANCK INSTITUTE FOR HUMAN COGNITIVE AND BRAIN SCIENCES LEIPZIG

Christoph Herrmann: Bedeutung von 40-Hz-Oszillationen für kognitive Prozesse. Leipzig: Max Planck Institute of Cognitive Neuroscience, 2002 (MPI Series in Cognitive Neuroscience; 22)

Bedeutung von 40–Hz–Oszillationen für kognitive Prozesse

Der Fakultät für Biowissenschaften, Pharmazie und Psychologie
der Universität Leipzig
eingereichte

H A B I L I T A T I O N

zur Erlangung des akademischen Grades

DOCTOR HABILITATUS
(Dr. habil.)

von Dr. Christoph Herrmann

geboren am 20. August 1966 in Celle

Tag der Verleihung: 06.05.2002

Gutachter:
Prof. Dr. Thomas Elbert, Universität Konstanz
Prof. Dr. Angela Friederici, MPI für neuropsychologische Forschung, Leipzig
Prof. Dr. Erich Schröger, Universität Leipzig

Bibliographische Beschreibung

Name: Dr. Christoph S. Herrmann
Titel: Bedeutung von 40–Hz–Oszillationen für kognitive Prozesse
Universität Leipzig, Habilitation, 86 Seiten, 165 Referenzen, 35 Abbildungen

Referat:

Oszillatorische 40–Hz–Aktivität im Elektroenzephalogramm (EEG) hat in den letzten Jahren große Bedeutung gewonnen, nachdem im Tierexperiment gezeigt werden konnte, daß synchrone neuronale Aktivität in diesem Frequenzbereich für das Zusammenbinden von im Cortex getrennt repräsentierten Objektmerkmalen verantwortlich ist. Diese Befunde konnten anschließend im menschlichen EEG repliziert werden und 40–Hz–Oszillationen wurden seit dem hauptsächlich mit Merkmalsbindung in Zusammenhang gebracht. Spätere Arbeiten konnten darüber hinaus zeigen, daß aufmerksam verarbeitete Reize mehr 40–Hz–Oszillationen im EEG evozieren oder induzieren, als unaufmerksam verarbeitete. Neuere Arbeiten zeigen sogar, daß mehr 40–Hz–Aktivität im menschlichen EEG zu finden ist, wenn Versuchspersonen Reize memorieren müssen, als wenn sie diese nur wahrnehmen, aber nicht später erinnern müssen.

In der vorliegenden Arbeit wurden die Parameter 'Merkmalsbindung', 'Aufmerksamkeit' und 'Arbeitsgedächtnis' auf ihren Einfluß auf die 40–Hz–Aktivität im menschlichen EEG untersucht, indem diese Parameter in mehreren Experimenten systematisch variiert wurden. Dabei zeigte sich, daß Aufmerksamkeit für frühe, evozierte 40–Hz–Oszillationen von Bedeutung ist, während Merkmalsbindung für diese Art der 40–Hz–Aktivität keine Rolle spielt. Außerdem stellte sich heraus, daß insbesondere der Vergleich wahrgenommener Merkmale mit im Arbeitsgedächtnis gespeicherten Merkmalen derjenige Parameter zu sein schein, der für die Aufmerksamkeitsmodulation der 40–Hz–Oszillationen relevant ist. Weiterhin wird gezeigt, wie oszillatorische Reizdarbietung zu beschleunigtem Reaktionsverhalten führt und schließlich wird auf die Bedeutung anderer Oszillationsfrequenzen und auf die möglichen neurophysiologischen Grundlagen der 40–Hz–Aktivität eingegangen.

Vorwort

Die vorliegende Arbeit habe ich während meiner Zeit als wissenschaftlicher Mitarbeiter am Max Planck Institut für neuropsychologische Forschung in Leipzig erstellt. Während dieser angenehmen Zeit haben mir die vielen lieben Kollegen beigebracht, experimentalpsychologisch zu arbeiten. Ich kam als Ingenieur ans MPI und fühle mich inzwischen als Psychologe. Allen Kollegen, die mich in dieser Zeit so nett und zahlreich unterstützt haben, möchte ich hiermit herzlich danken. Mein besonderer Dank gilt Angela Friederici, die mich einerseits wissenschaftlich angeleitet hat und mir andererseits genügend Freihet für eigene Ideen ließ. Meinen Coautoren der in dieser Arbeit verwendeten Artikel, Andrew Chen, Mark Elliott, Axel Mecklinger, Herman Müller und Erdmut Pfeifer, sei ebenfalls mein Dank ausgesprochen. Auch möchte ich Andrea Gast–Sandmann und Stephan Liebig danken, die mir bei der Erstellung von Graphiken stets hilfreich zur Seite standen. Ulrike Barth, Heike Böthel, Ina Koch, Cornelia Schmidt, Kristiane Werrmann und Yvonne Wolff sei für die Unterstützung beim Aufnehmen der Daten gedankt.

Neben allen Kollegen gilt mein Dank aber auch den vielen mich unterstützenden Geistern außerhalb des Instituts: In erster Linie natürlich meiner Freundin Kerstin Kräling, die es humorvoll ertrug, wenn ich meine/unsere Freizeit am Institut oder auf Kongressen verbrachte. Ganz besonders muß ich aber auch denjenigen Kollegen danken, die mich durch ihre Unterstützung stets haben wissen lassen, daß wir alle gemeinsam am selben Thema forschen und einem stets jemand mit Rat und Tat zur Seite steht: Andreas Engel, Corinna Henschel, Jochen Kaiser und Daniel Strüber.

Leipzig, Juni 2002

Inhaltsverzeichnis

Teil I

Einleitung

Kapitel 1

Einleitung

1.1 Das Elektroenzephalogramm

Das Gehirn wird als dasjenige Organ des menschlichen Körpers angesehen, das für unsere kognitiven Leistungen verantwortlich ist. Dort ablaufende kognitive Prozesse können jedoch nicht direkt beobachtet werden, sondern es bedarf indirekter Messungen, wie der spätestens seit Wundt (1902) untersuchten Reaktionszeit. Reaktionszeitmessungen stellen jedoch nur ein Maß für die Gesamtdauer eines komplexen Prozesses dar, der in der Regel mehrere Subprozesse umfaßt. Eine andere Möglichkeit, die kognitiven Prozesse im Gehirn zu beobachten, stellt das Elektroenzephalogramm (EEG) dar, das in sehr kurzen zeitlichen Abständen (wenige Millisekunden) Gehirnpotentiale abbildet. Im Sinne des Informationsverarbeitungsansatzes (Lindsay und Norman, 1977) können kognitive Subprozesse bestimmten Ereignissen im EEG zugeordnet werden, wodurch eine genauere zeitliche Unterscheidung der an einem komplexen Prozess beteiligten Subprozesse erreicht wird.

Die an der Schädeldecke als elektrische Spannungen ableitbaren Gehirnpotentiale haben ihren Ursprung in der elektrischen Aktivität der Neurone im Gehirn. Durch die Weiterleitung im Gewebe ist auch an der Schädeldecke noch ein sogenanntes Summenpotential dieser neuronalen Aktivität meßbar. Abgeleitet werden die Gehirnströme mit Oberflächenelektroden, die zur Gewährleistung reproduzierbarer und vergleichbarer Befunde nach dem internationalen 10–20–System an definierten Lokalisationen der Schädeldecke plaziert werden (Klem et al., 1999). Der Name des Systems rührt von der Tatsache her, daß die Elektroden in Abständen von 10% und 20% bestimmter Verbindungslinien auf der Schädeldecke plaziert werden. Es werden 21 Elektroden verwendet, die nach den Hirnarealen benannt sind, die unter den Elektroden liegen, wie in Abbildung 1.1 dargestellt.

Bei der Auswertung kognitionspsychologischer EEG–Experimente wird in

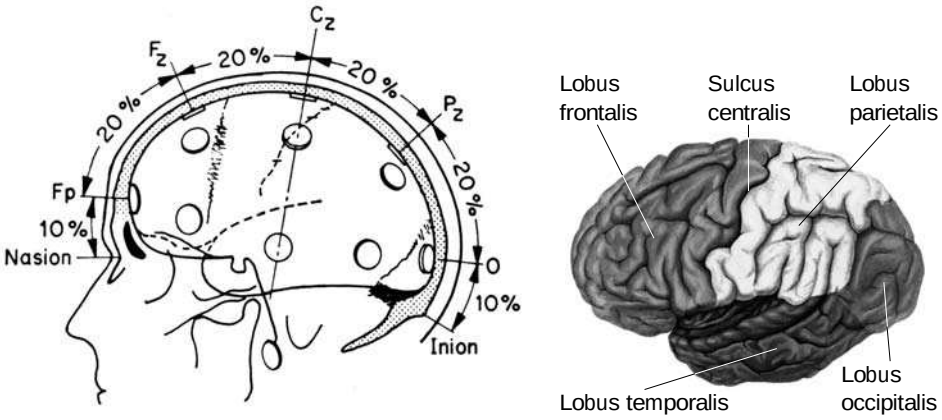

Elektrodenmontage des EEG Unterteilung des Gehirns

Abbildung 1.1: Die Montage von EEG–Elektoden nach dem internationalen 10–20–System (links, nach Platzer, 1994) erlaubt die Zuordnung gemessener Potentiale zu definierten Hirnregionen (rechts).

der Regel das ereigniskorrelierte Potential (EKP) auf Unterschiede zwischen experimentellen Bedingungen analysiert (Elbert et al., 2001). Das EKP wird berechnet, indem man für viele Wiederholungen einer experimentellen Bedingung jeweils eine Epoche des EEG betrachtet (z.B. eine Sekunde pro Wiederholung) und alle Epochen mittelt. Dieser Mittelwert aller EEG–Epochen stellt dann das EKP dar, in dem nur noch diejenige Aktivität vorkommt, die mit dem experimentellen Ereignis korreliert. Dabei werden positive und negative Potentiale, sogenannte EKP–Komponenten auf Unterschiede in ihrer Amplitude und Latenz untersucht. Die Polarität einer solchen Komponente und ihre Latenz in Millisekunden (ms) werden zu einem Akronym komponiert, das die Komponente bezeichnet. Ein 300 ms nach Beginn einer Stimulation auftretendes positives Potential im EKP würde daher als P300 bezeichnet.

1.2 Oszillationen

Neben diesen EKP–Unterschieden finden sich auch Unterschiede in der oszillatorischen EEG–Aktivität zwischen experimentellen Bedingungen (Başar und Schürmann, 2001). In den vergangenen Jahren wurde wiederholt gezeigt, daß oszillatorische Neuronenentladungen im Elektroenzephalogramm (EEG) mit Frequenzen um 40 Hz Korrelate kognitiver Prozesse darstellen (Tallon-Baudry und Bertrand, 1999; Başar et al., 2001). In der vorliegenden Arbeit soll gezeigt wer-

den, welche Bedeutung solche Oszillationen für Merkmalsbindung, Aufmerksamkeit und Arbeitsgedächtnis besitzen. Außerdem soll versucht werden, einen Zusammenhang zwischen den verschiedenen im Gehirn auftretenden Oszillationen herzustellen.

Oszillatorische Aktivität war der erste Hinweis darauf, daß man überhaupt elektrische Potentiale der Hirnaktivität zuordnen kann (Berger, 1929). Oszillationen im EEG werden anhand ihrer Frequenz in verschiedene Frequenzbänder eingeteilt:

- α Dieses Band beschreibt mit Frequenzen von ca. 8 bis 12 Hz die erstmals von Berger beschriebene vorherrschende Aktivität, die er Grundrhythmus nannte und mit dem griechischen Buchstaben α bezeichnete (Berger, 1929). In diesem Frequenzbereich sind bei 86% aller Menschen Amplituden von ca. $50\mu V$ und mehr zu erwarten (Kubicki und Höller, 1980).

- β Den chronologisch als nächsten beschriebenen Frequenzbereich physiologischer elektrischer Hirnaktivität bezeichnete Berger konsequenterweise mit dem Buchstaben β. Heute werden Frequenzen von ca. 12 bis 30 Hz als β–Aktivität gewertet (Zschocke, 1995, S. 106).

- γ Der sequentiell auf β folgende griechische Buchstabe γ wurde von Jasper und Andrews (1938) für Aktivität jenseits von 30 Hz eingeführt. Heute werden Freqeunzen zwischen ca. 30 und 80 Hz als γ–Frequenzen bezeichnet.[1]

- δ Der Bereich langsamer Wellen unterhalb des α-Bereichs wurde 1936 von Walter als der Delta-Bereich eingeführt (Walter, 1936).

- ϑ Walter selbst teilte anschließend die Frequenzen zwischen vier und acht Hertz als eigenen Bereich ab und gab ihnen die Bezeichnung ϑ, da er deren Ursprung im Thalamus vermutete.

In der vorliegenden Arbeit soll vor allem die Bedeutung der Gamma–Aktivität näher untersucht werden. In einem Überblicksartikel stellten Başar-Eroglu et al. (1996b) eine Taxonomie vor, die die Forschung auf dem Gebiet der Gamma–Aktivität in verschiedene Epochen unterteilt. Die erste Epoche begann laut dieser Taxonomie mit der Arbeit von Adrian (1942), der 40–Hz–Oszillationen beim Igel fand, als er sie mit Gerüchen stimulierte. Die zweite Phase wurde von Freeman (1975) initiiert, als er herausfand, daß 40–Hz–Oszillationen eine Schlüsselrolle bei der Wahrnehmung von Gerüchen im Bulbus Olfaktorius des Hasen spielen.

[1] Da die meisten der in der vorliegenden Arbeit beschriebenen Phänomene mit einer Frequenz von etwa 40 Hz auftreten, werden die Begriffe Gamma–Aktivität und 40–Hz–Oszillationen synonym verwendet.

In dieser Phase wurden 40–Hz–Oszillationen auch beim Menschen und im EKP gefunden (Başar und Ungan, 1973; Başar et al., 1976). Galambos et al. (1981) etablierte Gamma–Aktivität in menschlichen Studien, was die dritte Phase darstellt. Die vierte, und vorläufig prominenteste Phase der Untersuchung von 40–Hz–Oszillationen wurde von Gray et al. (1989) eingeleitet, als sie zeigten, daß synchrone Neuronenentladungen mit Merkmalsbindung in Zusammenhang stehen (siehe nächster Abschnitt). Karakaş und Başar (1998) zufolge befinden wir uns zur Zeit in der fünften Phase, in der eine Vielzahl von Forschern an der Lösung des von ihnen so bezeichneten 'Gammapuzzles' arbeiten.

1.3 Das Bindungsproblem

Das bisher bekannteste kognitive Korrelat der 40–Hz–Aktivität ist das Zusammenbinden verteilt repräsentierter Merkmale zu einem kohärenten Objekt. Einzelne Merkmale, wie etwa Form oder Farbe wahrgenommener physischer Objekte, werdem im menschlichen Cortex in getrennten Arealen repräsentiert (Thorpe, 1995). Das heißt, Farbe und Form werden in getrennten Arealen im visuellen Cortex repräsentiert. Einige Neurone im Areal für Farbcodierung feuern, wenn ein Objekt rot ist und andere wenn es blau ist. In einem anderen corticalen Areal feuern einige Neurone bei der Präsentation von vertikalen Balken und andere bei schrägen Balken. Nimmt man vier hypothetische Neurone, die die Merkmale `rot`, `blau`, `Dreieck` und `Viereck` repräsentieren, würde ein rotes Dreieck durch Aktivität der beiden Neurone `rot` und `Dreieck` codiert (vgl. Abb. 1.2).

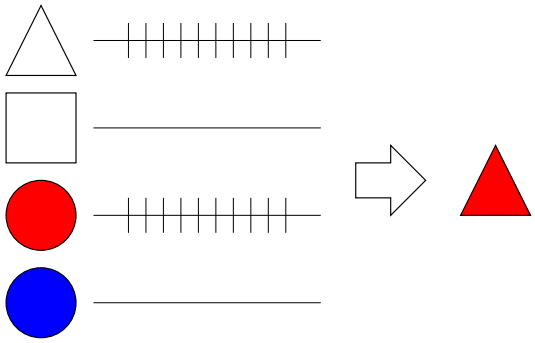

Abbildung 1.2: Das Feuern der beiden hypothetischen Neurone des frühen visuellen Cortex, die die Form Dreieck und die Farbe rot repräsentieren, signalisiert höheren visuellen Arealen, daß ein rotes Dreick wahrgenommen wurde.

Der Codierungsmechanismus basiert auf der Annahme, daß Merkmale durch die Entladungsrate von Neuronen codiert sind. Diese Annahme ist zwar zum Teil

richtig, reicht aber nicht aus, um Ambiguitäten bei der Wahrnehmung mehrerer gleichzeitig präsentierter Objekte aufzulösen. Wenn beispielsweise gleichzeitig ein rotes Dreieck und ein blaues Quadrat wahrgenommen würden, müßten alle vier Neurone feuern. Dann wäre allerdings nicht mehr klar, ob es sich um ein rotes Dreick und ein blaues Quadrat, oder um ein blaues Dreieck und ein rotes Quadrat handelt (vgl. Abb. 1.3). Dieses Dilemma bezeichnet man als das Bindungsproblem (Roskies, 1999).

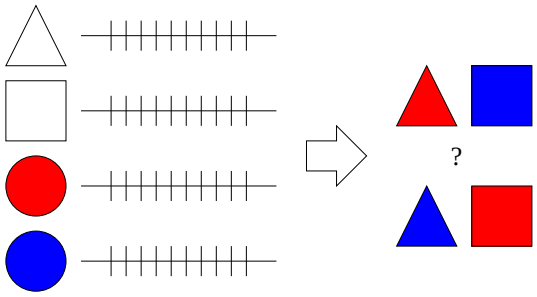

Abbildung 1.3: Würden die Merkmale mehrerer Objekte ausschließlich durch Feuerraten der sie repräsentierenden Neurone codiert, ergäbe sich das sogenannte Bindungsproblem: wenn die vier hier dargestellten Neurone im frühen visuellen Cortex gleichzeitig die Farben rot und blau, sowie die Formen Dreieck und Viereck codieren, können höhere Areale nicht unterscheiden, ob ein rotes Dreieck und blaues Viereck, oder ein rotes Viereck und blaues Dreieck wahrgenommen wurden.

1.4 Synchronizitätslösung des Bindungsproblems

Theoretische Lösung

Eine potentielle Lösung des Bindungsprobelms schlugen von der Malsburg und Schneider (1986) vor: Wenn diejenigen Neurone, die Merkmale desselben Objekts repräsentieren, gleichzeitig feuern und diejenigen, die Merkmale eines anderen Objekts repräsentieren, auch gleichzeitig, aber zu anderen Zeitpunkten, als Neurone, die ein anderes Objekt repräsentieren, würde die Ambiguität aufgelöst. Die Lösung ist in Abbildung 1.4 schmatisch dargestellt. Feuern die Neurone `rot` und `Dreieck` gleichzeitig, sowie die Neurone `blau` und `Viereck` gleichzeitig, aber die beiden Paare zu jeweils anderen Zeiten, können eindeutig ein rotes Dreieck und ein blaues Viereck codiert werden.

Neben dieser theoretischen Überlegung haben Simulationen in propositiona-

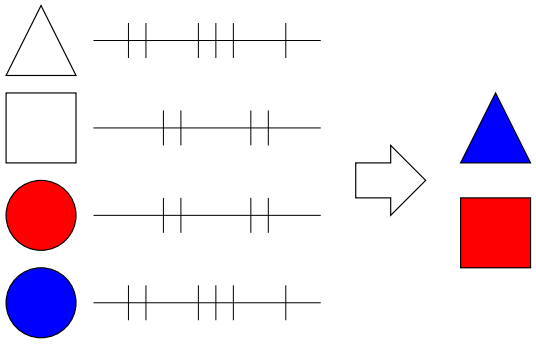

Abbildung 1.4: Gleichzeitiges Feuern von Neuronen, die Merkmale desselben Objekts repräsentieren, löst das Bindungsproblem.

len Netzwerken gezeigt, daß diese Lösung zumindest in künstlichen Anwendungen gut geeignet ist, dieselbe Proposition zum Codieren mehrerer Objekte zu verwenden (Ajjanagadde und Shastri, 1991; Shastri und Ajjanagadde, 1993).

40–Hz–Synchronizität bei der Katze

Gray et al. (1989) konnten später zeigen, daß dieses theoretische Konzept bei Neuronen im visuellen Cortex der Katze tatsächlich Verwendung findet. Sie leiteten die Entladungen von Neuronen ab, deren rezeptive Felder sie zuvor ermittelt hatten. Bewegten sie einen durchgehenden Balken über die beiden rezeptiven Felder, feuerten die entprechenden Neurone synchrone Aktionspotentiale mit einer Frequenz von etwa 40 Hz. Wurden zwei getrennte Balken mit gleicher Geschwindigkeit über die rezeptiven Felder bewegt, so daß der visuelle Eindruck entsteht, ein durchgehender aber in der Mitte nicht sichtbarer Balken würde bewegt, so feuerten die Neurone ebenfalls synchron (siehe Abb. 1.5). Sobald sie aber zwei getrennte Balken in verschiedene Richtungen bewegten, die auch perzeptuell als zwei Objekte wahrgenommen werden, feuerten die Neurone zwar noch, da sie ja vertikale Kanten detektierten, aber nicht mehr synchron.

Diese und ähnliche Befunde zeigen, daß die Synchronizität von Neuronenentladungen im Bereich von 40 Hz tatsächlich mit Merkmalsbindung korreliert (siehe beispielsweise auch: Eckhorn et al., 1988; Engel et al., 1992; Singer, 1999).

40–Hz–Synchronizität beim Menschen

Um zu testen, ob die Befunde aus dem visuellen Cortex von Tieren auch auf den Menschen übertragbar sind, haben Müller et al. (1996) das Paradigma von Gray

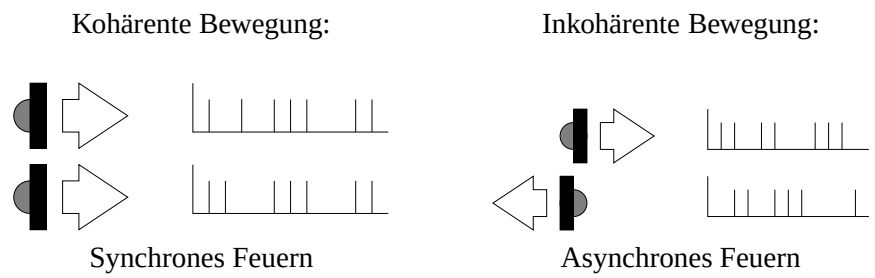

Abbildung 1.5: Kohärente Bewegung in den rezeptiven Feldern zweier Neurone führt zu synchronen Neuronenentladungen, während inkohärente Bewegung zu asynchronen Entladungen führt.

et al. (1989) am menschlichen EEG überprüft. Sie konnten zeigen, daß bei Makaken und Menschen ein durchgehender bewegter Balken mehr 40 Hz Oszillationen erzeugt, als zwei Balken, die in entgegengesetzte Richtungen bewegt werden.[2] Auch Lutzenberger et al. (1995) konnten zeigen, daß viele sich kohärent über den Bildschirm bewegende Balken mehr 40 Hz Aktivität im EEG hervorrufen, als gleich viele getrennte Balken, die sich in entgegengesetzte Richtungen bewegen.

Kritiker der Befunde zu diesen 40–Hz–Oszillationen beim Menschen haben argumentiert, daß es sich um harmonische Oberschwingungen der 10–Hz–Oszillationen handeln könnte (Jürgens et al., 1995). Solche 10–Hz–Oszillationen treten bei ca. 85% der gesunden Menschen im EEG auf (Zschocke, 1995, S. 127) und werden von präsentierten Stimuli synchronisiert (Brandt, 1997).

Müller et al. (1997) wiederholten ihre Messungen am Menschen und konnten einerseits ihre vorherigen Ergebnisse replizieren und weiterhin zeigen, daß die ebenfalls auftretenden 10–Hz–Oszillationen ein von den 40–Hz–Oszillationen verschiedenes zeitliches Muster und eine verschiedene topographische Verteilung über dem Cortex aufwiesen. Daher schlossen sie, daß es sich bei den Alpha– und Gamma–Antworten des menschlichen EEGs um verschiedene Phänomene handelt.

1.5 Visuelle Bindung beim Menschen

Neben diesen eher elementaren 40–Hz–Korrelaten der Merkmalsbindung, konnten auch beim Binden einzelner figürlicher Merkmale zu einem kohärenten Objekt 40–Hz–Oszillationen beim Menschen gefunden werden: Tallon et al. (1995) und Tallon-Baudry et al. (1996) fanden beim Zusammenbinden dreier Kreisscheiben

[2] Die 40–Hz–Oszillationen wurden hierbei und in den folgenden Experimenten zum Teil nicht von den Stimuli evoziert, sondern induziert, was eine schwächere zeitliche Kopplung zur Stumulation bedeutet und später genauer behandelt wird.

zu einem Kanizsa–Dreieck (Abb. 1.6a) mehr 40 Hz, als bei der Wahrnehmung dreier getrennter Kreisscheiben (Abb. 1.6b).

(a) (b)

Abbildung 1.6: Bei der Wahrnehumng eines Kanizsa–Dreiecks (a) müssen die drei Kreissegmente zusammengebunden werden. Bei der Wahrnehmung dreier getrennter Kreisscheiben (b) ist dies nicht der Fall.

Tallon-Baudry et al. (1997) konnten auch beim Zusammenbinden komplexerer Objekte 40–Hz–Oszillationen im menschlichen EEG beobachten: Wird in einem Suchbild ein schwer zu erkennender Dalmatiner inmitten von Flecken erkannt, die seinem Fell ähneln (siehe Abbildung 1.7), treten in diesem Moment vermehrt 40–Hz–Oszillationen auf. Aufgrund dieser Befunde, haben Tallon-Baudry und Bertrand (1999) das Auftreten von 40–Hz–Oszillationen mit der Repräsentation von Objekten assoziiert.

Abbildung 1.7: Dalmatiner–Suchbild von R.C. James.

Keil et al. (1999) konnten zeigen, daß ein rotierendes, skizziertes Gesicht bei solchen Rotationswinkeln Gamma–Aktivität induziert, bei denen es als Gesicht zu erkennen ist. Beim Betrachten autostereoskopischer Bilder stellte sich heraus, daß in dem Moment, in dem das im Rauschen versteckte dreidimensionale Bild plötzlich wahrgenommen wird, erhöhte 40–Hz–Aktivität im EEG zu sehen

ist (Revonsuo et al., 1997). Diese Erhöhung der 40–Hz–Aktivität bleibt aber nicht während der gesamten Zeit bestehen, während der man die Figur wahrnimmt, sondern besteht nur zum Zeitpunkt des Zusammenbindens der Figur. Auch bei der Wahrnehmung multistabiler Muster treten Gamma–Oszillationen auf, bevor das wahrgenommene Perzept bei gleichbleibender Stimulation wechselt (Başar-Eroglu et al., 1996a).

1.6 Aufmerksamkeit

Auch räumliche Aufmerksamkeit in einem Posner–Paradigma (Posner, 1980), in dem die Aufmerksamkeit vor der Stimulation nach links oder rechts gerichtet wird, beeinflußt die 40–Hz–Oszillationen im menschlichen EEG. Tiitinen et al. (1993) konnten zeigen, daß auditorische Stimuli, die dem beachteten Ohr präsentiert wurden mehr 40–Hz–Aktivität im menschlichen EEG hervorriefen als dem unbeachteten Ohr präsentierte. Richten Versuchspersonen ihre Aufmerksamkeit auf eine Hälfte des visuellen Felds, induzieren dort gezeigte Bewegungen mehr 40 Hz Oszillationen, als würde ihre Aufmerksamkeit zuvor auf die andere Hälfte gelenkt (Gruber et al., 1999).

Bei Katzen konnte gezeigt werden, daß Zielreize neben einer P300 im EKP außerdem erhöhte 40–Hz–Oszillationen erzeugen (Başar-Eroglu und Başar, 1991). Auch im menschlichen EEG evozieren Zielreize mehr 40 Hz Aktivität als Standardreize, wenn Versuchspersonen deviante Töne zählen (Fell et al., 1997).

1.7 Arbeitsgedächtnis

Auch die Funktionen des Arbeitsgedächtnisses wurden in Experimenten mit 40–Hz–Oszillationen im EEG korreliert. Dabei wurden sogenannte verzögerte Gedächtnis Paradigmen (engl. delayed matching to sample) verwendet, bei denen zunächst ein Reiz zum Zeitpunkt S1 memoriert werden muß und nach einem Behaltensintervall, zu einem späteren Zeitpunkt S2, ein weiterer Reiz mit dem ersten verglichen werden muß. Dabei wurden im Behaltensintervall 40–Hz–Oszillationen induziert, die in einer Kontrollbedingung, in der nichts memoriert werden mußte, nicht auftraten (Tallon-Baudry et al., 1998, 1999). De Pascalis und Ray (1998) konnten weiterhin zeigen, daß die 40–Hz–Aktivität beim Vergleichen des zweiten Stimulus mit dem ersten zum Zeitpunkt S2 mehr 40–Hz–Aktivität evozierte, je höher die Menge zu behaltender Information (engl. memory load) war. Auch Pulvermüller et al. (1999) argumentieren, daß diejenigen Stimuli, die bereits eine Gedächtnisrepräsentation besitzen, bei einer Präsentation zu mehr Gamma–Aktivität führen, als solche, für die noch keine existiert. Sie konnten zeigen, daß

Wörter mehr Gamma–Oszillationen induzieren als Pseudo–Wörter (Lutzenberger et al., 1994; Pulvermüller et al., 1996; Eulitz et al., 1996, 2000).

1.8 Arbeitshypothese

Aus den bisher geschilderten Ergebnissen läßt sich eine Arbeitshypothese ableiten, die für die Untersuchung von Aufmerksamkeit und Arbeitsgedächtnis lohnend erscheint.

Wird die Aufmerksamkeit beim Enkodieren auf verschiedene Stimuli verteilt, so werden die Stimuli später schlechter wiedererkannt, als wenn beim Enkodieren ungeteilte Aufmerksamkeit auf die Stimuli gelenkt wird (Iidaka et al., 2000; Ganor-Stern et al., 1998; Craik et al., 1996). Das zeigt, wie stark Aufmerksamkeit das Arbeitsgedächtnis beeinflussen kann. Alan Baddeley formuliert sogar die Hypothese, daß die Hauptaufgabe des Arbeitsgedächtnisses nicht in der Speicherung, sondern in den Exekutivfunktionen Aufmerksamkeit und Kontrolle liegt (Baddeley und Weiskrantz, 1995, S. 168). Auch in dem Arbeitsgedächtnismodell von Cowan (1997) liegt ein Hauptaspekt auf dem sogenannten Fokus der Aufmerksamkeit (Spotlight Metapher), der von der zentralen Exekutive gesteuert wird.

Aufmerksamkeit wiederum kann durch Stimuluseigenschaften beeinflußt werden. Experimente zur visuellen Suche haben gezeigt, daß Kanizsa–Figuren, die sich von den sie umgebenden Distraktoren nur durch zusammenbindbare kollineare Kanten unterscheiden, fast unabhängig von der Anzahl der Distraktoren gleich schnell erkannt werden (Davis und Driver, 1994). Das heißt, daß die Aufmerksamkeit automatisch auf solche Teile einer visuellen Szene gelenkt wird, an denen die einzelnen Elemente zu einer kohärenten Figur zusammengebunden werden können. Binding kann also Aufmerksamkeit und damit eventuell auch das Arbeitsgedächtnis beeinflussen. Luck und Vogel (1998) haben gezeigt, daß die Anzahl der Objekte, die im Arbeitsgedächtnis gehalten werden können, unabhängig von der Anzahl der Objekteigenschaften ist. Sie schlossen daraus, daß das Arbeitsgedächtnis auf dem abgeschlossenen Ergebnis eines Bindungsprozesses des perzeptuellen Systems operiert.

Binding, Aufmerksamkeit und Arbeitsgedächtnis sind also funktionell miteinander gekoppelt und rufen 40–Hz–Oszillationen im menschlichen EEG hervor. Daher ist im Sinne einer leitenden Arbeitshypothese festzuhalten, daß Merkmalsbindung, Aufmerksamkeit und Arbeitsgedächtnis Prozesse darstellen, die (zumindest partiell) aufeinander aufbauen:[3]

Merkmalsbindung $\rightarrow$ **Aufmerksamkeit** $\rightarrow$ **Arbeitsgedächtnis**

[3] Eine teilweise parallele Arbeitsweise ist dabei nicht auszuschließen.

Diese Reihenfolge von Merkmalsbindung und Aufmerksamkeit steht zwar im Widerspruch zu den Modellen von Treisman (1999) und Reynolds und Desimone (1999), die besagen, daß Aufmerksamkeit nötig ist, um korrekt zu binden. Diese Modelle betrachten aber Merkmalsbindung auf einem höheren kognitiven Niveau. Für den Prozeß der Bindung einzelner kollinearer Linien zu einer illusionären Figur, der im primären visuellen Cortex stattfindet (Peterhans und von der Heydt, 1989; Grosof et al., 1993), scheint aber die Merkmalsbindung der räumlichen Aufmerksamkeit vorauszugehen. Der von Davis und Driver (1994) gezeigte Effekt, daß Kanizsa–Quadrate unter einer beliebigen Anzahl von Distraktoren parallel erkannt werden, konnte mit den in dieser Arbeit verwendeten Kanizsa–Figuren repliziert werden (Herrmann, 2000).

In den in der vorliegenden Arbeit vorgestellten Experimenten soll untersucht werden, welcher der drei kognitiven Prozesse am ehesten für die Entstehung von 40–Hz–Oszillationen im EEG verantwortlich ist. Durch die Variation der in den Stimuli vorkommenden Merkmalsbindungen, der den Stimuli zugewandten Aufmerksamkeit und der an das Arbeitsgedächtnis gestellten Anforderungen soll die Beteiligung der drei Prozesse differenziert werden. Außerdem sollen die Interaktionen verschiedener Frequenzen und potentielle Generatoren der 40–Hz–Oszillationen untersucht werden.

Teil II

Methodische Grundlagen

Kapitel 2

Verschiedene Arten von Oszillationen

2.1 Zeitverschiebung und Phasenverschiebung

Bei der Betrachtung von Oszillationen aus den vielen einzelnen Epochen eines EEG Experiments ist es wichtig, zunächst die Begriffe der *Zeitverschiebung* und *Phasenverschiebung* zu erklären. In jeder einzelnen Epoche können Oszillationen zu einem bestimmten Zeitpunkt mit einer bestimmten Phase auftreten.

Die Bedeutung der Zeit– und Phasenverschiebung für Oszillationen mehrerer Epochen ist in Abb. 2.1 dargestellt. Würden die Signale aus (a) und (b) oder (c) und (d) aufsummiert, so würden sie sich im Mittelwert zu einer erkennbaren Oszillation aufaddieren, weil ihr Auftreten in den jeweiligen Epochen eine konstante Phase aufweist. Sind die Oszillationen aus den einzelnen Epochen zwar nicht zeitverschoben, aber phasenverschoben, wie in den Beispielen (a) und (c), würden sie sich im Mittelwert auslöschen. Dasselbe wäre der Fall, wenn die Oszillationen sowohl zeit– als auch phasenverschoben sind. Die Phasenverschiebung ist daher der kritische Parameter, der entscheidet, ob die Oszillationen der einzelnen Epochen im Mittelwert noch zu erkennen sind.[1]

Galambos (1992) hat im Wissen um diese mathematischen Gesetzmäßigkeiten eine Klassifikation verschiederner Arten von Oszillationen aufgestellt, die sie bezüglich ihrer Phasenverschiebung zu einem Stimulus unterscheidet. Er unterscheidet *spontane, induzierte,* und *evozierte* Oszillationen.[2]

[1] Es ist allerdings auch denkbar, daß oszillatorische Prozesse im Gehirn nicht mit verschiedenen Phasen beginnen können. In diesem Fall wäre ausschließlich die Zeitverschiebung relevant.

[2] Galambos hat weiterhin *emittierte* Oszillationen definiert, die in unserem Zusammenhang nicht bedeutend sind.

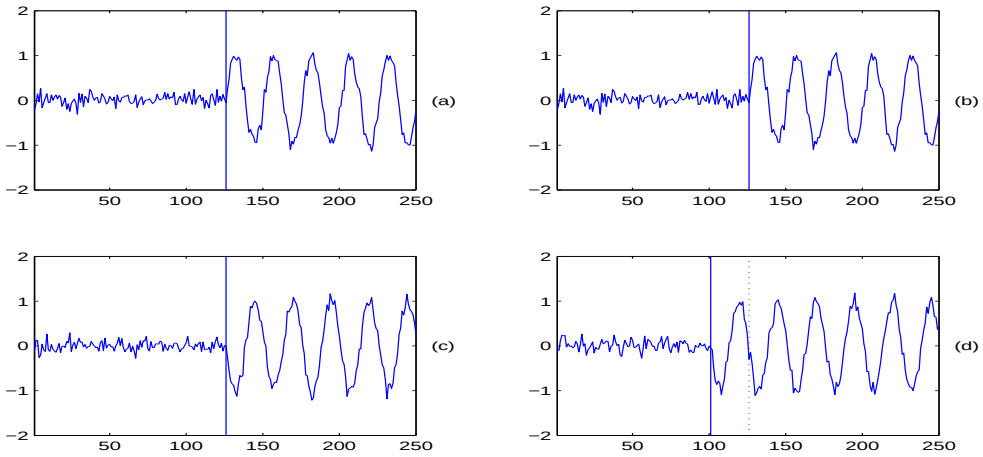

Signal:	Relation:	Mittelwert:
a + b	Weder zeit– noch phasenverschoben	Aufsummierung
a + c	Nicht zeit–, aber phasenverschoben	Auslöschung
c + d	Zeit–, aber nicht phasenverschoben	Aufsummierung
b + d	Zeit– und phasenverschoben	Auslöschung

Abbildung 2.1: Signale aus mehreren Epochen müssen phasenkonstant sein, damit sie sich im Mittelwert aufsummieren. Die Zeitverschiebung spielt dabei eine untergeordnete Rolle, solange sich die Oszillationen der verschiedenen Epochen noch überlappen.

Spontane Aktivität ist mit dem Auftreten von experimentellen Bedingungen (Stimuli) völlig unkorreliert.

Induzierte Aktivität wird zwar von einer experimentellen Bedingung ausgelöst, aber bei jedem Auftreten der Bedingung mit einer verschiedenen Phasenverschiebung und ist daher im Mittelwert nicht zu sehen.

Evozierte Aktivität wird von einer experimentellen Bedingung ausgelöst, weist keine Phasenverschiebung von Epoche zu Epoche auf und ist dadurch im Mittelwert gut zu erkennen.

Auch die hier untersuchten 40–Hz–Oszillationen treten mit und ohne Kopplung an experimentelle Bedingungen und mit und ohne Phasenverschiebung auf.

Spontane Gamma-Aktivität

Im menschlichen EEG tritt spontane Gamma-Aktivität auf, die nicht mit experimentellen Bedingungen in Zusammenhang steht und bei Mittelungen ausgelöscht wird. Wahrscheinlich ist sie mit kognitiven Prozessen korreliert, die im jeweiligen Experiment nicht kontrolliert werden. Spontane Gamma-Aktivität tritt im Wachsein und während des REM-Schlafs auf (Llinas und Ribary, 1993; Gross und Gotman, 1999), der wegen der auftretenden schnellen Augenbewegungen (rapid eye movements) so genannt wird und mit dem Auftreten von Träumen korreliert (Hobson, 1990). Da die Gamma–Aktivität während der nicht-REM Schlafphasen reduziert ist, vermutet man, daß sie mit bewußten Wahrnehmungsprozessen korreliert sein könnte. Strüber et al. (2000) und Strüber et al. (2001) haben gezeigt, daß die spontane Gamma-Aktivität bei solchen Probanden erhöht ist, bei denen die Wahrnehmung multistabiler Muster (z.B. des Necker–Würfels, vgl. Abb. 2.2) schneller wechselt als bei Vergleichspersonen. Eventuell korreliert die spontane Gamma-Aktivität daher mit dem allgemeinen Erregungsniveau des jeweiligen Individuums.

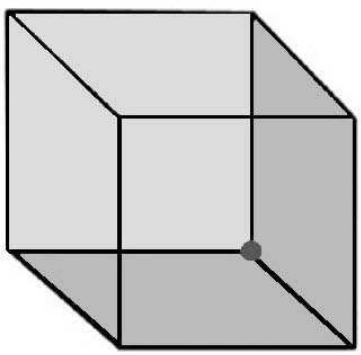

Abbildung 2.2: Der Necker–Würfel kann entweder so wahrgenommen werden, daß sich die markierte Ecke an seiner Vorder– oder Rückseite befindet. Diese beiden Wahrnehmungen wechseln sich rhythmisch mit einer bestimmten Geschwindigkeit ab.

Induzierte Gamma-Aktivität

Abb. 2.3 zeigt evozierte (links) und induzierte (rechts) Oszillationen in einer Simulation. Spezielle mathematische Verfahren müssen angewendet werden, um die

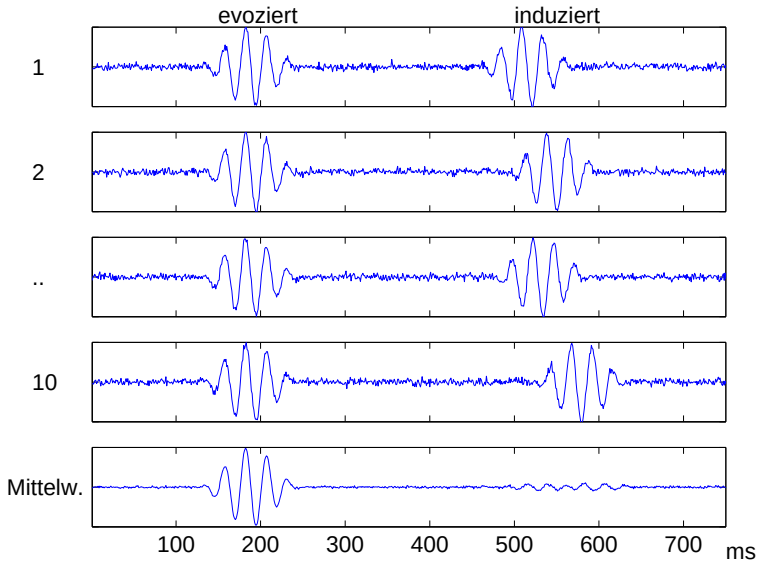

Abbildung 2.3: Simulation eines Mittelwerts aus 10 Einzelepochen. Treten Oszillationen in den Epochen ohne Phasenverschiebung auf (links), so sind sie im Mittelwert zu erkennen und werden als evozierte Aktivität betrachtet. Falls ihr Auftreten allerding mit einer Phasenverschiebung von Epoche zu Epoche behaftet ist, löschen sich diese Oszillationen meist aus und sind im Mittelwert nicht zu erkennen. Man bezeichnet sie dann als induzierte Aktivität.

induzierte Aktivität, die im Mittelwert nicht mehr zu erkennen ist, zu erfassen. Herrmann (2001a) gibt eine ausführliche Beschreibung der anwendbaren Verfahren inklusive einer Simulation, und später in diesem Kapitel ist die Vorgehensweise kurz skizziert. Induzierte Gamma-Aktivität tritt meist erst einige hundert Millisekunden nach Stimulusbeginn auf und wurde mit vielfältigen mentalen Prozessen in Zusammenhang gebracht: Merkmalsbindung (Tallon et al., 1995; Tallon-Baudry et al., 1996, 1997), Aufmerksamkeit (Müller et al., 2000; Gruber et al., 1999), Gestaltwahrnehmung (Keil et al., 1999) und Gedächtnisrepräsentationen (Tallon-Baudry et al., 1998, 1999).

Evozierte Gamma-Aktivität

Diejenigen 40–Hz–Oszillationen, die zwischen verschiedenen Epochen keine Phasenverschiebung aufweisen und als evozierte Aktivität beschrieben wurden, treten in der Regel bereits innerhalb der ersten 100 ms nach Stimulusbeginn auf (Fell et al., 1997; Pantev, 1995). Diese evozierte Aktivität wurde zunächst als

Korrelat exogener Prozesse, insbesondere der sensorischen Codierung, erachtet (Karakaş und Başar, 1998). Später konnte aber gezeigt werden, daß auch diese frühen evozierten Gamma Oszillationen kognitive Prozesse reflektieren (Karakaş et al., 2001). De Pascalis und Ray (1998) konnten beispielsweise zeigen, daß sich die Belastung des Arbeitsgedächtnisses in evozierter Gamma Aktivität widerspiegelt (siehe oben). In der vorliegenden Arbeit werden weitere Untersuchungen zu kognitiven Korrelaten evozierter Gamma Oszillationen vorgestellt.

2.2 Aufzeichnung von Gamma-Aktivität

Um Gamma-Aktivität im menschlichen EEG überhaupt registrieren zu können, müssen bestimmte Parameter der EEG–Verstärker richtig eingestellt sein.

Der Tiefpaß–Filter begrenzt die registrierten Frequenzen im EEG nach oben. Er läßt tiefe Frequenzen passieren. Deshalb muß die Grenzfrequenz des Tiefpaß–Filters, der in der Regel im analogen Verstärker integriert ist, auf mindestens die Frequenz eingestellt sein, die man analysieren möchte. Ein solcher Filter besitzt eine begrenzte Flankensteilheit, was bedeutet, daß er auch Frequenzen unterhalb der angegebenen Grenzfrequenz noch dämpft. Daher sollte der Wert idealer Weise deutlich über der zu analysierenden Frequenz liegen. Sollen 40 Hz betrachtet werden, empfiehlt sich beispielsweise ein Tiefpaß–Filter von 100 Hz.

Die Abtastrate muß auf einen Wert eingestellt werden, der mindestens das Doppelte der höchsten gemessenen Frequenz, also der Grenzfrequenz des Tiefpaß–Filters, beträgt. Bei einem Tiefpaß–Filter mit einer Grenzfrequenz von 100 Hz, müßte die Abtastrate mindesten 200 Hz betragen. Manche Hersteller verlangen eine Abtastrate, die das Vierfache der Grenzfrequenz des Tiefpaßfilters beträgt. Um sicher zu stellen, daß genügend hohe Frequenzen erfaßt werden, sollte bei Experimenten zur Gamma-Aktivität die Abtastrate mindestens 250 Hz (besser 500 Hz) betragen.

2.3 Potentielle Artefakte

Neben all den Artefakten, die in jedem EEG–Experiment auftreten können und vermieden oder von der Analyse ausgeschlossen werden müssen, können bei der Auswertung von Gamma–Aktivität weitere Artefakte zu falschen Interpretationen führen.

Harmonische von Alpha–Aktivität

Ein potentielles Problem stellt die im EEG wacher Vesuchspersonen häufig auftretede Alpha–Aktivität dar, die mit einer Frequenz von etwa 10 Hz und Amplituden von ca. 50 μV selbst in der Spontanaktivität zu sehen ist. Vielfältige kognitive Korrelate der Alpha–Aktivität zeigen, daß diese durchaus in vielen Experimenten auch ereigniskorreliert auftritt: Prozesse der Aufmerksamkeit (Başar et al., 1997), des Gedächtnisses (Klimesch et al., 1993, 2000) und der Motorik (Pfurtscheller und Berghold, 1989; Pfurtscheller und Neuper, 1992) korrelieren mit dem Auftreten von 10–Hz–Aktivität.

Das Auftreten solcher Alpha–Aktivität in kognitiven Experimenten stellt alleine noch kein Problem für die Auswertung von Gamma–Aktivität dar. Aber die folgende mathematische Besonderheit erfordert einige Vorsicht bei der Interpretation: Während eine reine 10–Hz–Oszillation im Frequenzspektrum tatsächlich auch nur genau einen Frequenzgipfel erzeugt (siehe Abb. 2.4 links), bewirkt eine leichte Formveränderung der 10–Hz–Aktivität, daß auch harmonische Frequenzgipfel bei 20 und 40 Hz im Spektrum auftreten (siehe Abb. 2.4 rechts). Deswegen muß stets überprüft werden, ob die kognitiven Korrelate der 40–Hz–Aktivität nicht auch Korrelate einer womöglich gleichzeitig vorhandenen 10–Hz–Aktivität sind (Jürgens et al., 1995). Ist allerdings entweder das zeitliche Auftreten, oder die topographische Verteilung der Gamma–Aktivität von derjenigen der Alpha–Aktivität verschieden, kann von separaten Generatoren ausgegangen werden (Müller et al., 1997).

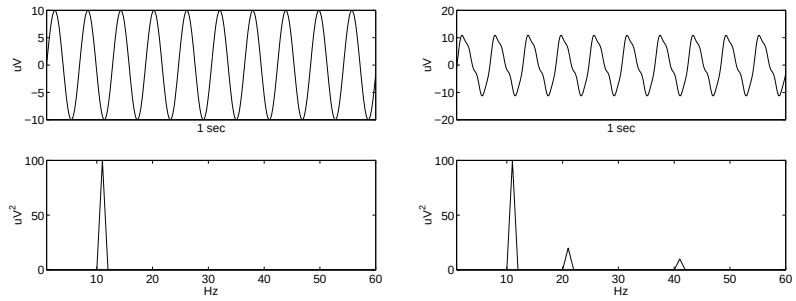

10–Hz–Sinuswelle Verformte 10–Hz–Welle

Abbildung 2.4: Eine sinusförmige 10–Hz–Schwingung (links) resultiert im Frequenzspektrum in genau einem Frequenzgipfel bei 10 Hz. Eine leichte Formveränderung führt bereits zu zusätzlichen harmonischen Frequenzgipfeln (rechts).

Elektromyographie

Eine weitere potentielle Fehlerquelle, die sich in dieser Form nicht so stark auf gewöhnliche EKPs auswirkt, ist die elektromyographische Aktivität der Muskeln (EMG), die auch im EEG erfaßt wird. Sitzt eine Versuchsperson verspannt, oder beißt sie während des Experiments die Zähne zusammen, so tritt EMG–Aktivität auf, die sich auch im Frequenzbereich von 40 Hz zeigt. Zunächst sollte deshalb noch größere Sorgfalt bei der Vorbereitung des Experiments aufgewendet werden, damit die Probanden entspannt sitzen und sich beim Experiment wohl fühlen. Weiterhin müssen alle Epochen eines Experiments visuell auf das Auftreten solcher Muskelaktivität überprüft und gegenenfalls von der Analyse ausgeschlossen werden. Fronto-temporale Elektroden (z.B. F7, F8, T7, T8) registrieren vornehmlich Kaubewegungen und occipitale Elektroden (O1, OZ, O2) spiegeln Verkrampfungen der Nackenmuskulatur wider.

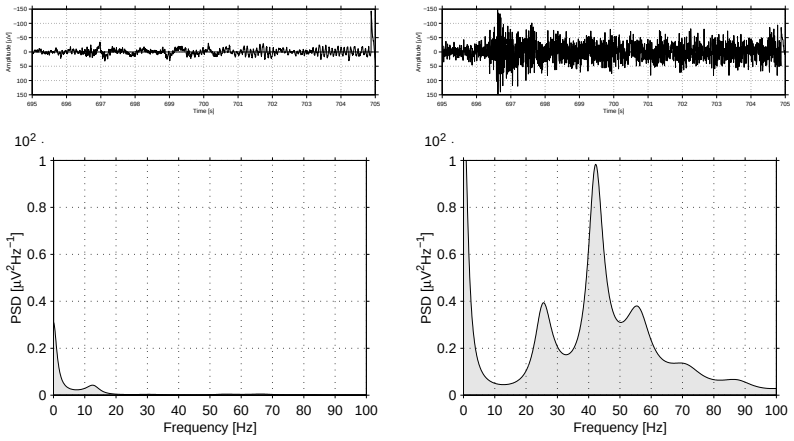

Abbildung 2.5: EMG–freie EEG–Aktivität und das entsprechende Frequenzspektrum (links) und das Auftreten von Muskelaktivität mit einem resultierenden Frequenzgipfel bei 40 Hz (rechts).

Abb. 2.5 zeigt 10 Sekunden eines EMG–freien EEGs (links) mit dem zugehörigen Frequenzspektrum. Das Auftreten von Muskelaktivität (rechts) kann zu Frequenzen um 40 Hz führen, ist aber in den Rohdaten durch die typische hochfrequente Zackenform gut detektierbar.

2.4 Analyse der Gamma-Aktivität

Verschiedene Ansätze der Frequenzanalyse

Es existieren verschieden Ansätze, die in einem EEG enthaltene oszillatorische Aktivität nach ihrer Frequenz zu analysieren. Am bekanntesten ist die Fourier Transformation, die ein beliebiges Signal in eine Reihe von Sinusschwingungen zerlegt (Dumermuth und Molinari, 1987; Jandó et al., 1993). Meist wird für diese Methode der Spektralschätzung das Akronym FFT für Fast Fourier Transform verwendet (Cooley und Tukey, 1965). Abb. 2.6 zeigt zwei EKPs nach einer Bandpaß–Filterung in einem Band von 35–45 Hz (links) und die FFT–Spektren der beiden EKPs (rechts). Die Spektren wurden für die ganze Sekunde des EKPs berechnet, weswegen die Unterschiede der 40–Hz–Aktivität zwischen den beiden Bedingungen, die beim gefilterten EKP zu erkennen sind, nicht mehr so deutlich sind. Im gefilterten EKP evoziert die gestrichelte Bedingung mehr 40–Hz–Aktivität nach ca. 100 ms, und nach etwa 200 ms verhält es sich umgekehrt. Da das Spektrum die 40–Hz–Aktivität der ganzen Sekunde darstellt, gleichen sich die beiden entgegengesetzten Unterschiede fast aus.

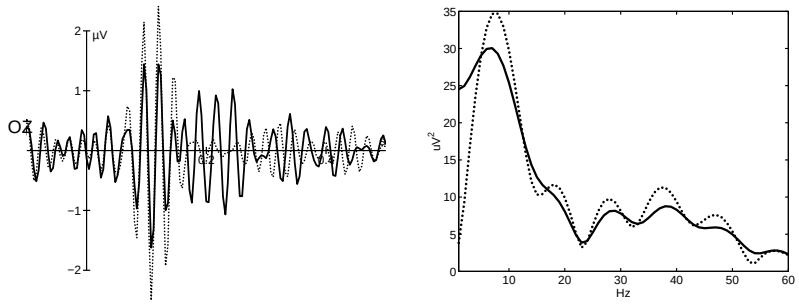

Filter (35–45 Hz) Fourier Spektrum

Abbildung 2.6: Zwei EKPs, die mit einem 35–45 Hz Bandpaß gefilter wurden (links) und die beiden entsprechenden Fourier Spektren (rechts). Die erhöhten 40–Hz–Oszillation für die gestrichelte Bedingung sind im Spektrum weniger deutlich zu sehen, als im gefilterten EEG.

Abb. 2.7 zeigt im Gegensatz dazu dieselben gefilterten EKPs wie in Abb. 2.6, aber anstelle der FFT–Spektren das Ergebnis einer Wavelet–Transformation mit einem 40–Hz–Wavelet. Diese Transformation bietet den Vorteil, daß der Zeitverlauf der 40–Hz–Aktivität erfaßt wird. Dadurch wird erkennbar, daß etwa 100 ms nach Beginn der Stimulation ein Unterschied zwischen den beiden Bedingungen besteht, der sich in einem späteren Zeitfenster umkehrt (ca. 200–300 ms).

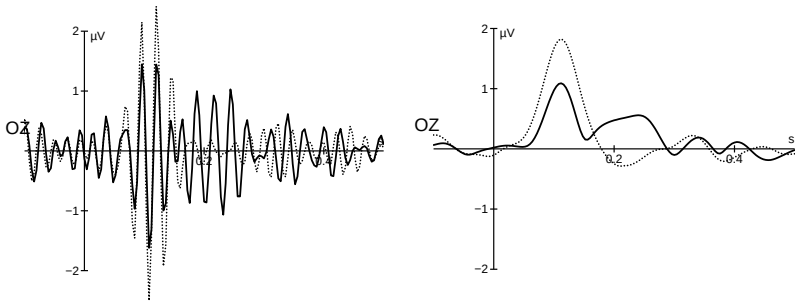

Filter (35–45 Hz) Wavelet–Transformation

Abbildung 2.7: Zwei EKPs, die mit einem 35–45 Hz Bandpaß gefilter wurden (links) und die beiden entsprechenden Wavelet–Transormationen (rechts). Der abwechselnde Verlauf der Unterschiede zwischen den beiden Bedingungen wird zeitlich erfaßt.

Im Gegensatz zu den gefilterten EKPs, die die Oszillationen deutlich erkennen lassen, zeigt die Wavelet–Transformation nur die Amplitude der Oszillation, die sogenannte Hüllkurve, an.

Die Wavelet–Transformation

Im folgenden soll die Methode der Wavelet–Transformtion (WT), die für die Frequenzanalyse der vorliegenden Arbeit benutzt wurde, kurz erläutert werden. Um eine WT zu berechnen, muß ein Signal wie das EEG mit einem sogenannten Wavelet (kleine Welle) gefaltet werden. Faltet man ein EEG mit einem solchen Wavelet mathematisch, ergibt sich daraus die Wavelet–Transformierte, die Amplitude und Verlauf derjenigen Frequenz im EEG anzeigt, die der Frequenz des Wavelets entspricht. Wie man in Abb. 2.7 sehen kann, ist das Ergebnis der Wavelet–Transformation dem eines Filters sehr ähnlich. Bei der WT erhält man allerdings eine komplexe Zahl zu jedem Zeitpunkt, deren Betrag oder Amplitude man darstellen kann. Der in Abb. 2.7 dargestellte Betrag ist quasi die Hüllkurve um die 40–Hz–Aktivität eines EEG, wenn man ein 40–Hz–Wavelet verwendet. [3]

Durch diese Betragsbildung kann man vermeiden, daß sich eine 40–Hz–Aktivität, die von Epoche zu Epoche leicht phasenverschobenen ist, auslöscht. Der Mittelwert des Betrags wird für phasenverschobene Signale nur etwas verschmiert. Abb. 2.8 zeigt schematisch, wie man sowohl evozierte, als auch induzierte 40–Hz–Aktivität mittels einer Wavelet–Transformation berechnen kann.

[3] Herrmann et al. (1999) und Herrmann und Mecklinger (2000) erklären die mathematischen Details der Wavelet–Transformation.

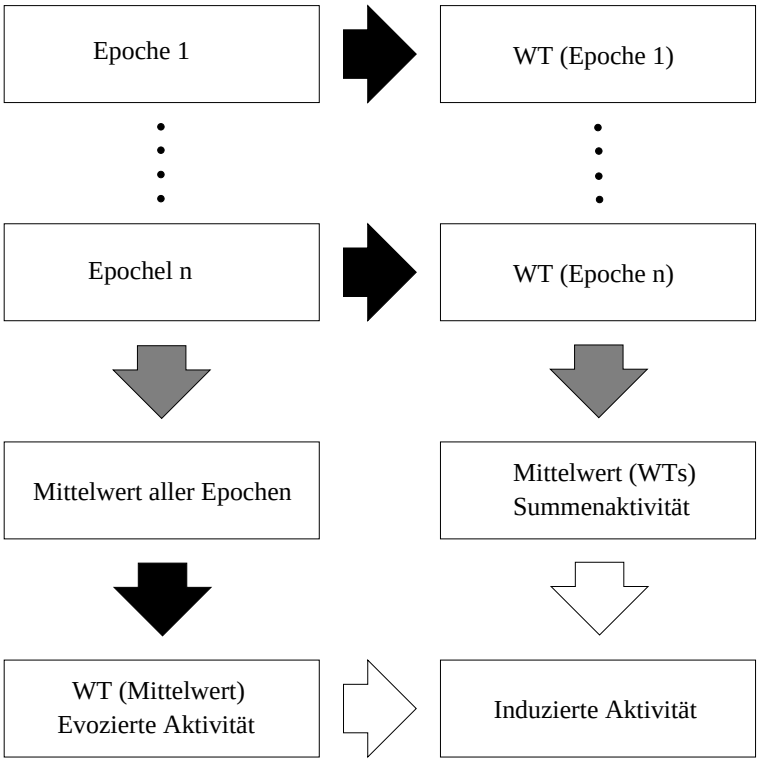

Abbildung 2.8: Berechnung der evozierten (links) und induzierten (rechts) Gamma Aktivität mit Hilfe der Wavelet–Transformation. Die WT des Mittelwertes der Epochen (links) enthält die evozierte 40–Hz–Aktivität und der Mittelwert der WTs der einzelnen Epochen (rechts) ergibt die Summe aus evozierter und induzierter Aktivität. Durch Subtraktion der evozierten Aktivität von der Summenaktivität kann die induzierte Aktivität berechnet werden. Die Berechnung einer WT ist durch schwarze Pfeile dargestellt, die Mittelwertbildung durch graue und die Subtraktion durch weiße.

2.5 Simulation

Um zu zeigen, wie das oben beschriebene Verfahren der Trennung evozierter und induzierter Oszillationen prinzipiell funktioniert, werden hier die in Abb. 2.3 dargestellten Daten einer Wavelet–Transformation unterzogen. Die Daten zeigen in 10 Epochen jeweils eine evozierte Oszillation bei etwa 200 ms ohne Phasenverschiebung und eine induzierte Oszillation mit variabler Phase zwischen 500 und 600 ms. Der Mittelwert der 10 Epochen enthält nur noch den evozierten Anteil. Daher enthält auch die WT des Mittelwertes (Abb. 2.9 oben) nur den evozierten

Anteil der 40–Hz–Aktivität bei 200 ms. Berechnet man jedoch zunächst von jeder einzelnen Epoche die WT und mittelt dann deren Beträge, sind sowohl evozierte, als auch induzierte Aktivität im Ergebnis enthalten (Abb. 2.9 Mitte). Die Differenz ergibt dann den induzierten Anteil (Abb. 2.9 unten).

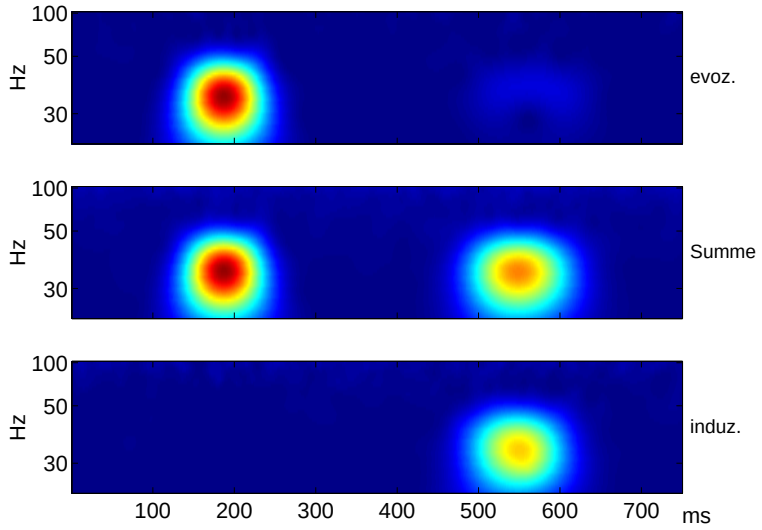

Abbildung 2.9: Ergebnis der Wavelet–Transformation der Simulation.

Bei den in Abb. 2.9 dargestellten Diagrammen handelt es sich um sogenannte Frequenz–Zeit–Darstellungen, da der zeitliche Verlauf einer Frequenzkomponente gezeigt wird. In der Vertikalen ist die Frequenz, in der Horizontalen die Zeit und durch die Färbung die Amplitude einer Komponente aufgetragen.

Teil III

Aufmerksamkeit und Arbeitsgedächtnis

Kapitel 3

Von der Merkmalsbindung zur Aufmerksamkeit

Die in diesem Kapitel beschriebenen Ergebnisse aus Experiment 1 wurden 1999 in *Clinical Neurophysiology* veröffentlicht (Herrmann et al., 1999). Der Vergleich der Experimente 1 und 2 wurde 2001 in *Visual Cognition* publiziert (Herrmann und Mecklinger, 2001).

3.1 Merkmalsbindung im EEG

Tallon et al. (1995) und Tallon-Baudry et al. (1996) haben gezeigt, daß beim Betrachten von Kanizsa–Dreiecken (Abb. 3.1b) in einem Zielreiz–Erkennungs–Paradigma Gamma–Oszillationen im EEG auftreten, die beim Betrachten physikalisch ähnlicher Stimuli ohne illusionäre Konturen (Abb. 3.1d) nicht auftreten und daher dem 'Zusammenbinden' der Kreissegmente zum Dreieck zugeordnet wurden. Der zu erkennende Zielreiz in diesen Experimenten war jedoch ebenfalls ein Kanizsa–Dreieck mit kleineren Öffnungswinkeln der induzierenden Kreissegmente (pacmen). Dadurch erweckte der Zielreiz den Eindruck eines Kanizsa–Dreiecks mit konkaven Kanten. Da Zielreize neben einer P300 auch zu erhöhten 40–Hz–Oszillationen führen (Başar-Eroglu und Başar, 1991; Fell et al., 1997), besteht die Gefahr, daß in den beschriebenen Experimenten eine Konfundierung durch die Ähnlichkeit der untersuchten Stimuli mit dem Zielreiz bestand.

Hypothese 1 *Die Amplitude der 40–Hz–Aktivität könnte von der Aufmerksamkeit, die auf Zielreize gelenkt wird, stärker moduliert werden, als von der Merkmalsbindung, die beim 'Zusammenbinden' von Kanizsa–Figuren auftritt.*

Experiment 1 (EEG)

Um die Funktion der Gamma-Aktivität nach Bindung und (durch die Erkennung des Zielreizes hervorgerufene) Aufmerksamkeit zu differenzieren, wurde ein Experiment mit Kanizsa–Dreiecken und zusätzlichen Vierecken durchgeführt. Die hierbei verwendeten Stimuli sind in Abb. 3.1 gezeigt. Während das Kanizsa–Quadrat als Zielreiz diente, können innerhalb der verbleibenden drei Standardreize das Kanizsa–Dreieck und das Nicht–Kanizsa–Dreieck miteinander verglichen werden, ohne daß eine Konfundierung mit der auf den Zielreiz gelenkten Aufmerksamkeit besteht. Zur Differenzierung der beiden Variablen wird der Einfluß der unabhängigen Faktoren Form (Quadrat vs. Dreieck) und Figur (Kanizsa vs. Nicht–Kanizsa) auf die abhängige Variable EKP-Amplitude in einer ANOVA mit Meßwertwiederholung untersucht.

Damit die elektrophysiologischen Messungen frei von 40–Hz–Aktivität bleiben, die bei motorischen Reaktionen auftreten (Pfurtscheller et al., 1992, 1994), sollte das Auftreten der Kanizsa–Quadrate gezählt werden.

(a) (b) (c) (d)

Abbildung 3.1: Um Aufmerksamkeitsprozesse und Bindungsprozesse zu differenzieren, wurden folgende vier Stimuli verwendet: (a) Kanizsa–Quadrat (Zielreiz), (b) Kanizsa–Dreieck, (c) Nicht–Kanizsa–Dreieck und (d) Nicht–Kanizsa–Quadrat.

Die EKPs des Experiments zeigten klare P1, N1 und P3 Komponenten, wie in Abbildung 3.2 (links) zu sehen ist. Zielreize evozierten signifikant höhere P3 Amplituden als Standardreize. Kanizsa–Figuren evozierten signifikant größere N1 Amplituden als Nicht–Kanizsa Figuren. [1] Außerdem evozierten Quadrate größere N1 Amplituden als Dreiecke.

[1] In einem nachträglichen Kontrollexperiment konnten wir zeigen, daß Kanizsa–Quadrate auch größere N1 Amplituden evozieren als Stimuli, die die gleiche Anzahl kollinearer Kanten besitzen, aber keine illusionäre Figur konstituieren (Herrmann und Bosch, 2001). Das zeigt, daß die N1 neben exogenen Prozessen und Aufmerksamkeit auch endogene Prozesse der Gestaltwahrnehmung reflektiert.

3.2 Aufmerksamkeit im EEG

Zwischen 50 und 150 ms nach Stimulusbeginn evozierte der Zielreiz signifikant mehr 40–Hz–Oszillationen als die Standardreize (siehe Abb. 3.3). Dieser Effekt deutet darauf hin, daß die den Zielreizen zugewandte Aufmerksamkeit erhöhte 40–Hz–Oszillationen evozieren.

Schlußfolgerung 1 *Die auf Zielreize gerichtete Aufmerksamkeit erhöht die frühen evozierten 40–Hz–Oszillationen im Vergleich zu Standardreizen.*

Allerdings handelt es sich bei dem verwendeten Zielreiz um eine Kanizsa–Figur, die gleichzeitig die höchste N1 Amplitude evozierte und aus Suchbildern sogar unter ähnlichen Distraktoren als 'pop-out' hervorspringt (Davis und Driver, 1994). Daher sollte in einem weiteren Experiment festgestellt werden, wie eine Variation der Aufgabenstellung bei Verwendung derselben Stimuli diese Ergebnisse verändert.

In der ebenfalls ausgewerteten, induzierten Gamma Aktivität konnten keine signifikanten Unterschiede zwischen den experimentellen Bedingungen gefunden werden.

Experiment 2 (EEG)

In einem zweiten Experiment wurde das Nicht–Kanizsa–Quadrat zum Zielreiz definiert, und sein Auftreten sollte wiederum gezählt werden. In Anlehnung an die Annahme, daß die den Zielreizen zugewandte Aufmerksamkeit die frühe Gamma Aktivität evoziert, oder deren Generierung moduliert, sollte jetzt das Nicht–Kanizsa–Quadrat die höchsten 40–Hz–Oszillationen hervorrufen und gleichzeitig die größte P3 evozieren.

Hypothese 2 *Bei Verwendung 'bindbarer' und 'nicht bindbarer' Stimuli evoziert jeweils der Zielreiz am meisten 40–Hz–Oszillationen, unabhängig von Merkmalsbindung.*

Abb. 3.2 zeigt die EKPs an Elektrode OZ aus Experiment 2 (rechts) im Vergleich zu denen aus Experiment 1 (links). EKPs von anderen Elektroden sind in der Originalarbeit abgedruckt (Herrmann und Mecklinger, 2001). Der Zielreiz (Nicht–Kanizsa–Quadrat, grün) evoziert signifikant größere P3 Amplituden als die drei Standardreize. Die frühen EKP–Komponenten P1 und N1 zeigen die gleichen Amplitudenreihenfolgen wie in Experiment 1. Sie reflektieren daher eher bottom-up Prozesse, da sie sich von der Aufgabenvariation nicht haben beeinflussen lassen.

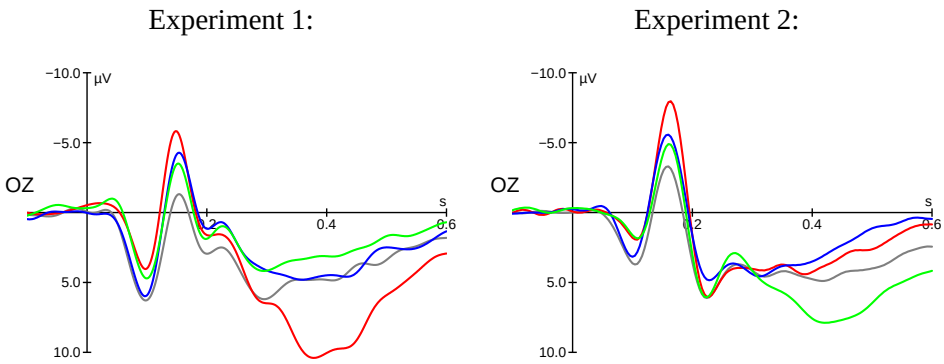

Abbildung 3.2: EKPs an der Elektrode OZ aus den Experimenten 1 und 2. P1 und N1 bleiben von der veränderten Aufgabenstellung unberührt. Die P3 verändert sich zwischen den beiden Experimenten und ist jeweils für den Zielreiz am größten. Kanizsa–Quadrat (Zielreiz in Experiment 1, rot), Kanizsa–Dreieck (blau), Nicht–Kanizsa–Quadrat (Zielreiz in Experiment 2, grün) und Nicht–Kanizsa–Dreieck (schwarz).

Abb. 3.3 zeigt die frühe evozierte Gamma-Aktivität (50 – 150 ms) für die vier verwendeten Stimuli aus den Experimenten 1 und 2.[2] Das Muster ist zwischen den Epxerimenten klar unterschiedlich, was bereits belegt, daß diese Aktivität ein Korrelat eines top-down Prozesses ist, der die Aufgabenstellung und nicht die physikalischen Stimuluseigenschaften widerspiegelt. Das Kanizsa–Quadrat (rot), das von den Versuchspersonen in Exp. 1 gezählt wurde, zeigt deutlich erhöhte Aktivität (links). In Experiment 2 dagegen evoziert das Nicht–Kanizsa–Quadrat (grün), das von den Versuchspersonen in Exp. 2 gezählt wurde, die höchste 40–Hz–Aktivität, obwohl es sich um eine 'nicht bindbare' Figur handelt. Das deutet darauf hin, daß diese Aktivität tatsächlich einen Aufmerksamkeitsprozeß widerspiegelt und nicht das Zusammenbinden der figuralen Merkmale.

Schlußfolgerung 2 *Frühe evozierte 40–Hz–Oszillationen reflektieren einen Aufmerksamkeitsprozeß.*

Interessanter Weise evoziert aber nicht nur der Zielreiz 40–Hz–Aktivität im Zeitraum von 50 – 150 ms nach Stimulusbeginn. Auch die anderen Figuren evozieren Gamma–Aktivität, wenngleich weniger als der Zielreiz.

[2]Die Elektroden wurden aufgrund unterschiedlicher Topograhien aus den jeweils am stärksten aktivierten Regionen ausgewählt. Die gesamte Topographie ist in der Originalarbeit abgedruckt (Herrmann und Mecklinger, 2001).

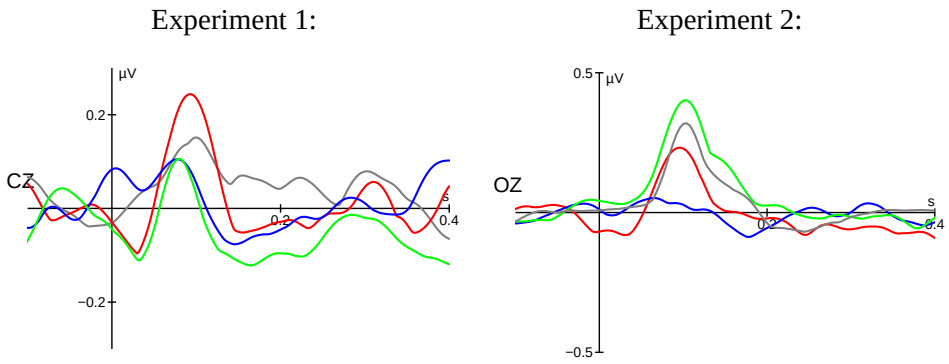

Abbildung 3.3: Die frühe evozierte 40–Hz–Aktivität aus den Experimenten 1 und 2 zeigt etwa 100 ms nach Stmimulationsbeginn einen deutlichen Zielreiz Effekt. Kanizsa–Quadrat (Zielreiz in Experiment 1, rot), Kanizsa–Dreieck (blau), Nicht–Kanizsa–Quadrat (Zielreiz in Experiment 2, grün) und Nicht–Kanizsa–Dreieck (schwarz).

3.3 Modell des Zielreiz–Erkennungs–Paradigmas

Um die Ergebnisse aus den Experimenten 1 und 2 zu erklären, soll hier zunächst ein Modell des Zielreiz-Erkennungs-Paradigmas aufgestellt werden, das dann anhand von behavioralen Daten präzisiert wird. In Anlehnung an frühere Modelle zur Informationsverarbeitung im Gehirn (Broadbent, 1958) und zur Steuerung der Aufmerksamkeit (Cowan, 1997) sollen diejenigen Prozesse, die an der Erkennung von Zielreizen beteiligt sind, schematisch dargestellt werden. Es soll insbesondere gezeigt werden, daß Zielreiz-Erkennung nicht ohne Zugriff auf das Kurzzeitgedächtnis möglich ist.

Abb. 3.4 zeigt schematisch, welche mentalen Prozesse in einem Zielreiz-Erkennungs-Paradigma zur Anwendung kommen:

1. Der präsentierte Reiz muß zunächst im visuellen Cortex encodiert werden.

2. Anschließend müssen die Merkmale des codierten Reizes mit denen des Zielreizes verglichen werden. Dazu wurde während der Instruktionsphase ein Muster des Zielreizes im Kurzzeitgedächtnis abgelegt.

3. Schließlich kann in Abhängigkeit des Vergleichsergebnisses die korrekte motorische Antwort generiert werden.

Der Vergleichsprozess, der den wahrgenommenen Reiz mit dem Muster im Kurzzeitgedächtnis vergleicht, ist im Sinne von Baddeley (1992a) ein Exekutiv-

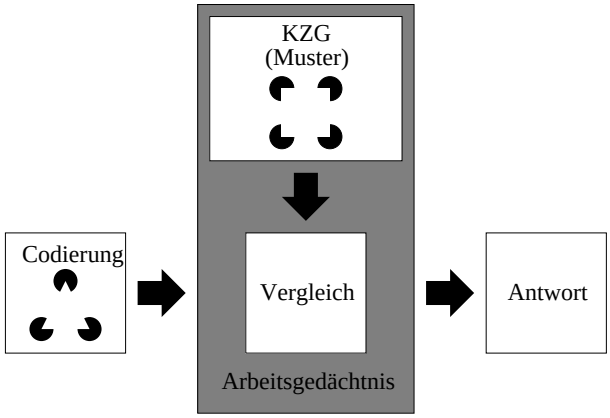

Abbildung 3.4: Schematischer Ablauf der Prozesse in einem Zielreiz-Erkennungs-Paradigma.

prozess, wodurch die Elemente 'Kurzzeitgedächtnis' und 'Vergleich' des Modells die Beteiligung des Arbeitsgedächtnisses an der Zielreizerkennung darstellen.

Experiment 3 (behavioral)

Um auf behavioraler Ebene mehr über die Verarbeitung von Kanizsa–Figuren in einem Zielreiz-Erkennungs-Paradigma zu erfahren, wurde Experiment 3 durchgeführt.

Experiment 3 wiederholte Experiment 2 mit Messung von Reaktionszeiten und Fehlern ohne EEG–Ableitung. Wieder wurden dieselben vier Stimuli verwendet, und in Experiment 3 diente das Nicht–Kanizsa–Quadrat als Zielreiz, auf den mit Drücken der rechten Hand auf eine Taste zu reagieren war. Die drei Standardreize erforderten einen Tastendruck mit der linken Hand auf eine andere Taste. Abb. 3.5 zeigt die Reaktionszeiten.

Es ist deutlich zu erkennen, daß der Zielreiz erwartungsgemäß die längste Reaktionszeit hervorruft (Teichner und Krebs, 1974). Das Kanizsa–Dreieck, das keine der beiden Figurmerkmale (Form, Kollinearität) mit dem Zielreiz gemeinsam hat, wurde am schnellsten diskriminiert. Die Figuren, die jeweils ein Merkmal mit dem Zielreiz gemeinsam haben, rufen mittlere Reaktionszeiten hervor. Diese Verteilungen der Reaktionszeiten zeigen, daß die beiden Merkmale Form und Kollinearität von separaten Prozessen mit dem Muster-Zielreiz im Arbeitsgedächtnis verglichen werden. Würde jede Figur als Gesamtheit mit dem Zielreiz verglichen, gäbe es keinen Grund für die unterschiedlichen Reaktionszeiten zwischen den drei

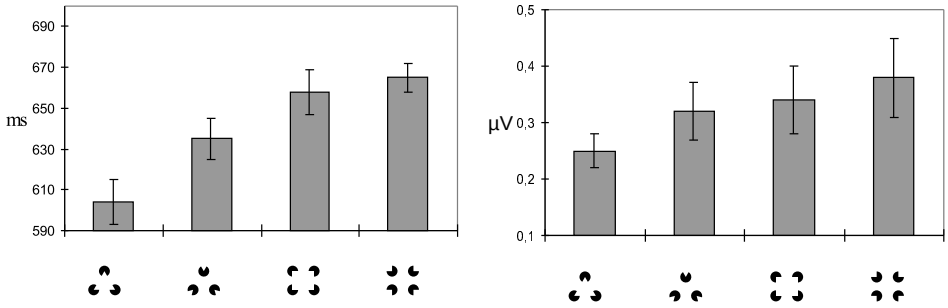

Reaktionszeiten aus Exp. 3 Frühe evozierte 40 Hz aus Exp. 2

Abbildung 3.5: Reaktionszeiten (Mittelwerte und Standardfehler) aus Experiment 3 (links) im Vergleich zur frühen evozierten Gamma–Aktivität aus Experiment 2 (rechts). Der Zielreiz (Nicht–Kanizsa–Quadrat) ruft die längste Reaktionszeit und die meiste Gamma–Aktivität hervor. Die dem Zielreiz unähnlichste Figur (Kanizsa–Dreieck) kann am schnellsten diskriminiert werden und evoziert am wenigsten Gamma–Aktivität.

Standardreizen, die mit der gleichen Hand erzeugt werden. Daher scheint der Vergleichsprozeß aus Abb. 3.4 ein zweistufiger Prozeß zu sein, der beide Merkmale der Figuren getrennt mit denen des Musters im Arbeitsgedächtnis vergleicht.

Die Reaktionszeiten aus Experiment 3 verhalten sich ähnlich der frühen evozierten Gamma–Aktivität aus dem EEG–Experiment 2: Der Zielreiz evoziert jeweils die meiste Aktivität, der dem Zielreiz unähnlichste Reiz die wenigste. Die beiden Figuren, die jeweils ein Merkmal mit dem Zielreiz gemeinsam haben, rufen eine mittlere Gamma–Amplitude hervor. Diese Ähnlichkeit mit den Reaktionszeiten legt nahe, daß der Vergleichsprozeß aus obigem Modell für die Generierung der Oszillationen verantwortlich ist. Je mehr Merkmale des wahrgenommenen Reizes mit denen des Musters im KZG übereinstimmen, desto mehr 40–Hz–Oszillationen werden evoziert.

Kapitel 4

Von der Aufmerksamkeit zum Arbeitsgedächtnis

Die in diesem Kapitel geschilderten Experimente 4 und 5 wurden 2000 im International Journal of Psychophysiology publiziert (Herrmann und Mecklinger, 2000).

4.1 Das Arbeitsgedächtnis

Das Modell des Zielreiz-Erkennungs-Paradigma sieht einen Vergleich des codierten wahrgenommenen Stimulus mit einem Muster im Arbeitsgedächtnis vor. Die 40–Hz–Oszillationen scheinen vom Vergleich der Merkmale eines Stimulus mit denen des Musters generiert zu werden. In zwei weiteren Experimenten soll gezeigt werden, wie die frühe evozierte Gamma–Aktivität darauf reagiert, ob die Merkmale eines Stimulus mit einem Muster im Arbeitsgedächtnis verglichen werden müssen, oder nicht.

Hypothese 3 *Der Vergleich wahrgenommener Merkmale eines Stimulus mit denen eines im KZG gespeicherten Stimulus evoziert frühe evozierte 40–Hz–Oszillationen.*

Bereits Baddeley und Weiskrantz (1995) wiesen darauf hin, daß Aufmerksamkeit und Arbeitsgedächtnis eng miteinander verwandt sind. In seinem Modell zum modularen Arbeitsgedächtnis stellt Baddeley die reinen Speichermodule für auditorische und visuelle Informationen neben die auf ihnen operierenden Prozesse, die sogenannten Exekutivprozesse (Baddeley, 1992a). Die Verarbeitung visueller Information wurde weiterhin in die Verarbeitung von Objekten und räumlichen Orten untergliedert, wobei jeweils verschiedene cortikale Regionen aktiviert werden (Ungerleider, 1995). Objektverarbeitung findet demnach in einem dorsalen

(a) (b) (c) (d) (e)

Abbildung 4.1: Die Stimuli (a) bis (d) wurden im Experiment 4 verwendet, wobei das Kanizsa–Quadrat (a) den Zielreiz darstellte. In Experiment 5 wurden alle 5 gezeigten Stimuli verwendet, und das rote Fixationskreuz (e) diente als Zielreiz.

Pfad statt, der vom occipitalen über den temporalen Cortex verläuft und im ventralen präfrontalen Cortex endet, während räumliche Information in einem dorsalen Pfad verarbeitet wird, der vom occipitalen zum parietalen und dann zum dorsolateralen präfrontalen Cortex läuft.

Experiment 4 (behavioral & MEG)

In Experiment 4 wird zunächst Experiment 1 im Magnetenzephalographen (MEG) wiederholt. Dabei müssen, wie zuvor, die beiden Merkmale Form und Kollinearität mit dem Muster im Arbeitsgedächtnis verglichen werden, um den Zielreiz – das Kanizsa–Quadrat – zu erkennen.

Experiment 5 (behavioral & MEG)

Im Gegensatz dazu, wird in Experiment 5 ein zusätzlicher Zielreiz eingeführt, der sich in einer anderen Dimension von den vier bisherigen Figuren unterscheidet: ein rotes Fixationskreuz. Daher müssen bei der Wahrnehmung einer der Figuren (a) bis (d) aus Abb. 4.1 die beiden Merkmale Form und Kollinearität der Figuren nicht mit dem Muster im Arbeitsgedächtnis verglichen werden.

Die behavioralen Ergebnisse zeigen, daß es sehr viel einfacher für das Gehirn ist, solche Zielreize zu erkennen, die aufgrund eines Merkmals detektiert werden können, das nur im Zielreiz enthalten ist: Die roten Fixationskreuze konnten nach etwa 450 ms und die Kanizsa–Quadrate erst nach etwa 750 ms erkannt werden. Die schwerer diskriminierbaren Zielreize aus Experiment 4 evozierten deutlich mehr frühe Gamma–Aktivität als die einfacher zu diskriminierenden aus Experiment 5 (siehe Abb. 4.2). Allerdings könnte dieser Unterschied auch an den unterschiedlichen verwendeten Zielreizen liegen. Deswegen ist der Vergleich der in beiden Experimenten verwendeten Standardreize (Kanizsa–Dreieck, Nicht–Kanizsa–Quadrat und Nicht–Kanizsa–Dreieck) entscheidend.

Zielreize:

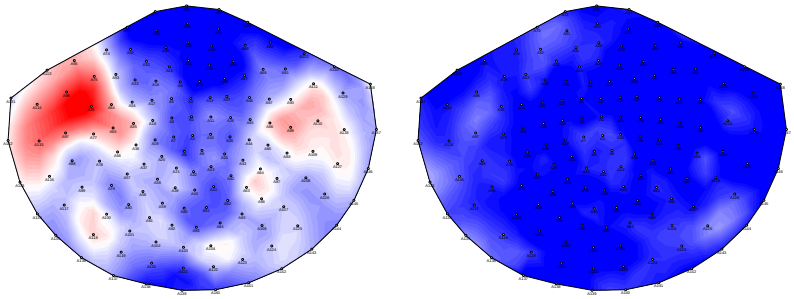

Experiment 4 Experiment 5

Abbildung 4.2: Topographische Verteilung der frühen evozierten Gamma–Aktivität für die Zielreize aus den Experimenten 4 und 5. Die Kanizsa–Zielreize, deren Merkmale von denen der anderen Figuren unterschieden werden müssen, evozieren viel Gamma–Aktivität (links). Die leicht zu diskriminierenden roten Fixationskreuze evozieren deutlich weniger Gamma–Aktivität.

Standardreize:

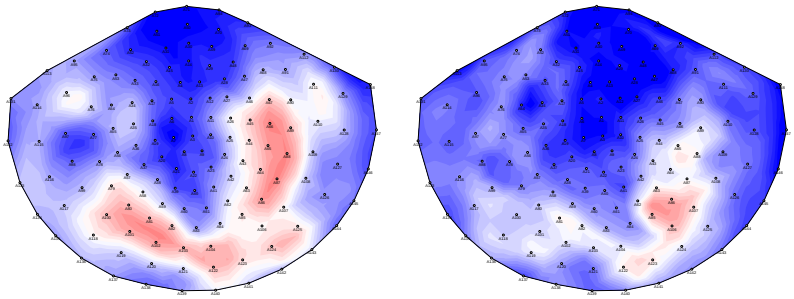

Experiment 4 Experiment 5

Abbildung 4.3: Topographische Verteilung der frühen evozierten Gamma–Aktivität für die Standardreize aus den Experimenten 4 und 5. Auch die Standardreize evozieren mehr Gamma–Aktivität, wenn ihre Merkmale mit einem Mustereiz verglichen werden müssen (links), als wenn die Zielreizerkennung aufgrund anderer, nicht in den Standardreizen enthaltener Merkmale (Farbe) durchgeführt werden kann (rechts).

Eine ANOVA, die die frühe evozierte Gamma–Aktivität zwischen den beiden Experimenten für diese drei Standardreize verglich, zeigte, daß diese in Experiment 4 signifikant höhere 40–Hz–Oszillationen als in Experiment 5 evozierten

(siehe Abb. 4.3). Da es sich um dieselben Stimuli handelte, unterschieden sie sich nur in dem in Experiment 4 notwendigen Vergleich ihrer Merkmale mit denen des Musterreizes im Arbeitsgedächtnis.

Schlußfolgerung 3 *Dieselben Stimuli evozieren höheramplitudige frühe 40–Hz–Oszillationen, wenn ihre Merkmale mit denen eines Musters im KZG verglichen werden.*

4.2 Generator der frühen evozierten 40 Hz

Da die Elektroenzephalographie zwar eine sehr gute zeitliche, aber nur begrenzte räumliche Auflösung besitzt, wurde zur Ermittlung der potentiellen Generatoren der 40–Hz–Aktivität die funktionelle Magnetresonanztomographie (fMRT) eingesetzt. Bei diesem Verfahren werden Sauerstoffkonzentrationsänderungen (BOLD, von engl. blood oxygenation level dependent) im Gehirn in Folge experimenteller Stimulation gemessen. Dabei ergibt sich jeweils für eine Schicht des Gehirns eine farbcodierte Karte der BOLD–Antworten, die einem anatomischen Hirnschnitt überlagert wird, um die genaue Lokalisation der Antwort zu gewährleisten.

Temporo–occipitale Generatoren

In den Experimenten 1, 2 und 4 trat die frühe frontale Gamma–Aktivität unter anderem in occipitalen und temporalen Elektroden/Sensoren auf (vgl. Abb. 4.3). Temporo–occipitale Hirnareale werden auch als die Generatoren der von allen Stimuli evozierten N1 Komponente angesehen (Gomez-Gonzales et al., 1994; Yamazaki et al., 2000). Abb. 4.4 zeigt die Aktivierung der vier Figuren aus Abb. 3.1 in einer Wiederholung von Experiment 1 im funktionellen Magnetresonanztomographen im Vergleich zu einer Kontrollbedingung, in der keine Stimuli präsentiert wurden (Kruggel et al., 2001). Die Stimuli aktivieren den ventralen Pfad vom occipitalen zum temporalen Cortex, der für die Verarbeitung von Objekten verantwortlich ist (Ungerleider, 1995; Ungerleider et al., 1998). Logothetis et al. (2001) haben kürzlich gezeigt, daß die BOLD–Antwort des Gehirns stark mit den lokalen Feldpotentialen (LFP) korreliert und weniger mit neuronaler Einzelzellaktivität. Sie weisen ausdrücklich darauf hin, daß diese LFPs meist oszillatorischer Natur sind. Daher erscheint es plausibel, anzunehmen, daß die in unserem fMRT–Experiment aktivierten Areale auch für die Entstehung eines Teils der frühen evozierten 40–Hz–Ozillationen verantwortlich sind.

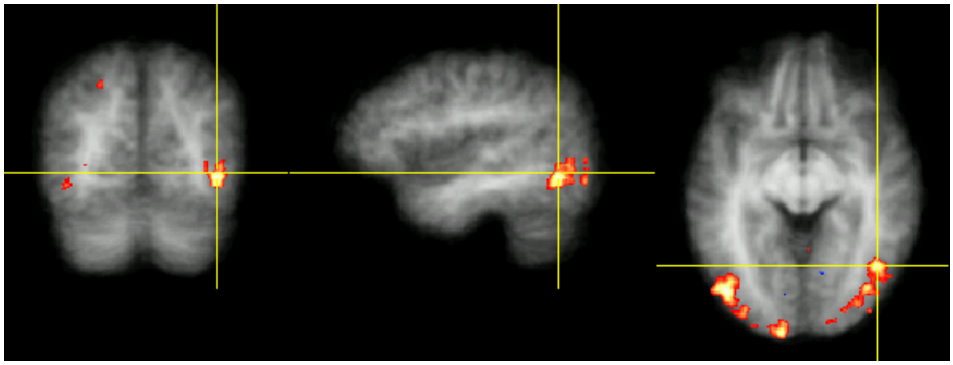

Abbildung 4.4: FMRT–Aktivierungen der vier Figuren im temporo–occipitalen Cortex in einem coronaren (links), saggitalen (Mitte) und tranversalen Schnitt (rechts).

Präfrontale Generatoren

Neben den occipitalen und temporalen Anteilen der frühen evozierten Gamma–Aktivität trat diese in den Experimenten 1, 2 und 4 für Zielreize auch über frontalen Arealen auf (vgl. Abb. 4.2). Mehrere fMRT–Experimente haben gezeigt, daß der präfrontale Cortex bei der Verarbeitung von Zielreizen aktiviert wird (McCarthy et al., 1997; Kirino et al., 2000). Gemäß dem obigen Modell zur Detektion von Zielreizen, generiert die zentrale Exekutive des Baddeleyschens Arbeitsgedächtnismodells diese Gamma–Aktivität. Experimente mit dem verzögerten Gedächtnisparadigma haben gezeigt, daß der laterale präfrontale Cortex für solche Exekutivfunktionen verantwortlich ist (Smith und Jonides, 1999; Desimone, 1999; Levy und Goldman-Rakic, 2000; Fuster, 2000). Abb. 4.5 zeigt den ventralen (rot) und dorsolateralen (grün) Teil des präfrontalen Cortex.

In einer Wiederholung des Experiments 1 als funktionelle Kernspinstudie konnte auch für das Erkennen von Zielreizen (Kanizsa–Quadraten) eine erhöhte Aktivierung des Gyrus frontalis medius gefunden werden (Herrmann et al., 2001). Abb. 4.6 zeigt diese Aktivierung des lateralen präfrontalen Cortex bei der Erkennung von Zielreizen.

Diese Übereinstimmung der frontalen Topographie der frühen evozierten Gamma–Aktivität für Zielreize mit der vermuteten cortikalen Lokalisation exekutiver Prozesse, die ebenfalls erhöhte Aktivierung für Zielreize zeigen, ist ein weiteres Indiz dafür, daß tatsächlich der Merkmalsvergleich im Arbeitsgedächtnis diese Gamma–Aktivität erzeugen könnte.

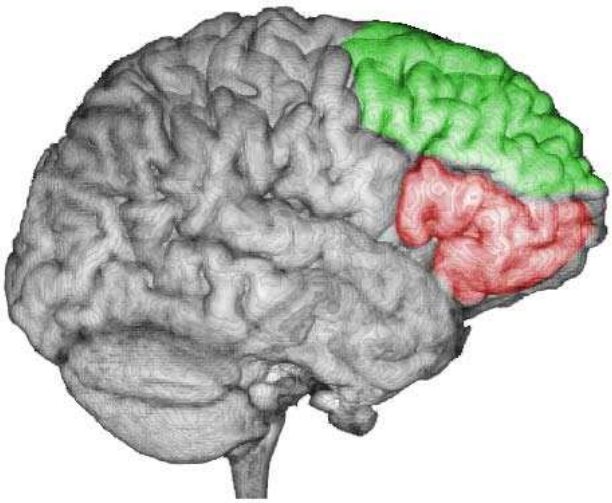

Abbildung 4.5: Folgende Hirnregionen werden von Gedächtnismodellen für Prozesse des Arbeitsgedächtnisses verantwortlich gemacht: der ventrale präfrontale Cortex (Brodman Areae 9 und 46, rot) und der dorsolaterale präfrontale Cortex (Brodman Areae 45 und 47, grün).

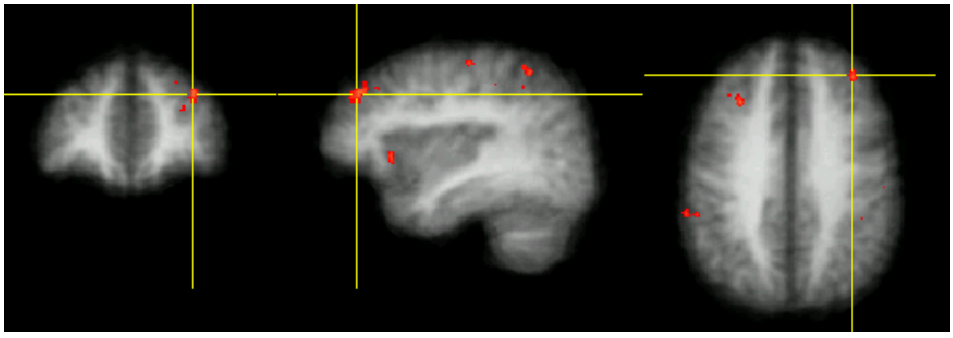

Abbildung 4.6: FMRT–Aktivierungen der Zielreize (Kanizsa–Quadrate) im Gyrus frontalis medius (Brodman Area 46) in einem coronaren (links), saggitalen (Mitte) und tranversalen Schnitt (rechts).

Teil IV

Exogene Beeinflussung endogener Prozesse

Kapitel 5

Das Elliott–Paradigma

Die Ergebnisse des in diesem Kapitel vorgestellten Experiments zur exogenen Beeinflussung endogener Prozesse wurden 2000 im *International Journal of Psychophysiology* veröffentlicht (Elliott et al., 2000).

5.1 Stimulus Präsentation mit 40 Hz

In der Einleitung wurde bereits gezeigt, daß das Zusammenbinden mehrerer Merkmale zu einer kohärenten Gestalt mit dem Auftreten von synchroner 40–Hz–Aktivität im visuellen Cortex der Katze (Gray et al., 1989; Engel et al., 1992) und des Menschen (Müller et al., 1996, 1997) assoziiert wurde. Weiterhin scheinen diese Oszillationen auch für exekutive Prozesse wie Aufmerksamkeit relevant zu sein (Tiitinen et al., 1993; Müller et al., 2000). Selbst die Speicherung im Arbeitsgedächtnis und der Zugriff auf das Arbeitsgedächtnis wurden mit dieser Gamma–Aktivität in Zusammenhang gebracht (De Pascalis und Ray, 1998; Tallon-Baudry et al., 1999; Herrmann und Mecklinger, 2001).

Nach all diesen Befunden liegt es nahe zu vermuten, daß man durch eine geeignete externe Stimulation mit Reizen, die mit einer Frequenz von 40 Hz dargeboten werden, solche endogenen Prozesse in ihrer Arbeitsweise günstig beeinflussen kann. Das wurde zunächst von mehreren Gruppen ohne Erfolg versucht (Fahle und Koch, 1995; Kiper et al., 1996). Schließlich gelang es Elliott und Müller (1998), mit Hilfe der in Abb. 5.1 gezeigten Anordnung, tatsächlich einen Reaktionszeiteffekt durch Verwendung unterschiedlicher Darbietungsfrequenzen zu erzielen.

Im Elliott–Paradigma wird zunächst für 600 ms eine sogenannte Prämaske dargeboten, die mit einer bestimmten Frequenz (z.B. 40 Hz) flickert, wobei neun Kreuze auf einem Oszilloskop–Bildschirm wahrgenommen werden. Anschließend bleiben von jedem Kreuz nur noch zwei Schenkel stehen, so daß in

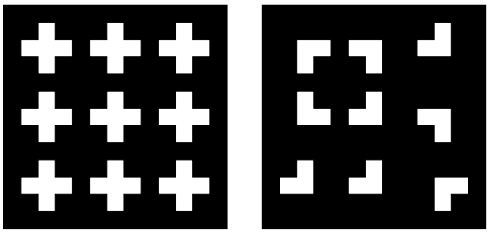

Prämaske (600ms) Zielreiz

Abbildung 5.1: Prämaske und Zielreiz im Elliott–Paradigma.

der Hälfte der Fälle ein Kanizsa–Quadrat induziert wird, das als Zielreiz erkannt werden soll. Auf diesen Zielreiz wird mit Drücken der rechten Hand reagiert, die Abwesenheit einer solchen Kanizsa–Figur wird mit der linken Hand angezeigt.

Die Prämaske besteht aber nicht wirklich aus neun konstant flickernden Kreuzen, sondern aus einer Abfolge von Einzelbildern, die nur einen Teil der neun Kreuze enthalten. Erst vier aufeinanderfolgende Teilbilder ergeben die komplette Matrix. Dabei wird bei einer Präsentationsfrequenz von 40 Hz jedes Teilbild für 25 ms dargeboten. In dieser so generierten Prämaske kann entweder ein Hinweisreiz versteckt sein (Abb. 5.2), der aber nicht bewußt wahrgenommen wird, oder nicht (Abb. 5.3).

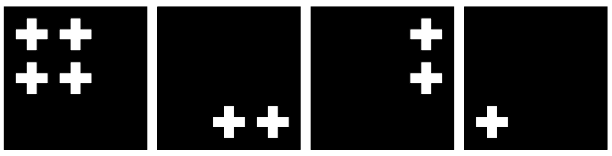

Abbildung 5.2: Prämaske mit verstecktem Hinweisreiz.

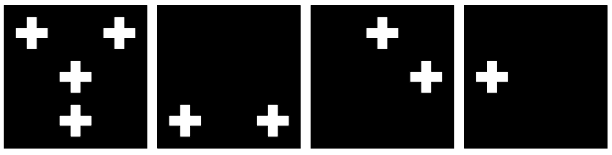

Abbildung 5.3: Prämaske ohne versteckten Hinweisreiz.

Wird in diesem Paradigma die Prämaske mit einer Frequenz von 40 Hz dargeboten und ist der Hinweisreiz in der Prämaske enthalten, so können die Ver-

suchspersonen signifikant schneller reagieren als ohne den versteckten Hinweisreiz oder bei anderen Frequenzen. Die Autoren gehen davon aus, daß es sich um einen Priming Effekt handelt, der die Figur–Grund–Segmentierung erleichtert (Elliott und Müller, 1998). Bei einer Variation des Intervalls zwischen Ende der Prämaske und Beginn des Zielreizes, stellte sich heraus, daß der Reaktionszeitvorteil nicht einfach kontinuierlich über der Zeit abnimmt, sondern mit ca. 40 Hz oszilliert (Elliott und Müller, 2000). Dies interpretieren die Autoren dahingehend, daß die Repräsentation des subliminal präsentierten Hinweisreizes im visuellen Kurzzeitgedächtnis auf einem oszillatorischen Prozeß basiert. Ähnliche Befunde, die eine oszillatorische Repräsentation von Stimuli im visuellen Kurzzeitgedächtnis vermuten, passen gut zu dieser Annahme (Lisman und Idiart, 1995; Jensen und Lisman, 1998; Burle und Bonnet, 2000). Daher sollte die Flickerstimulation mit verstecktem Hinweisreiz, die den Reaktionsvorteil auslöst, sich auch in Unterschiden elektrophysiologischer Parameter niederschlagen und die Latenz oder Amplitude von EKPs und/oder Oszillationen beeinflussen.

Hypothese 4 *Flickert ein versteckter Hinweisreiz im Elliott–Paradigma mit 40 Hz, so werden neben den Reaktionszeiten auch EEG Parameter davon beeinflußt.*

Experiment 6 (behavioral & EEG)

Eine periodische Stimulation, wie im Elliott–Paradigma, führt in der Regel zu einer periodischen Anregung des visuellen Cortex, die in Form sogenannter Steady–State–Potentiale ableitbar ist (Regan, 1989; Silberstein, 1995). Daher liegt es nahe zu vermuten, daß sich das Priming, das durch die flickernden Stimuli auftritt, im EEG in Form einer 40–Hz–Aktivität widerspiegelt. Eine Wiederholung des Elliott–Paradigmas mit gleichzeitiger Ableitung von EEG und Aufzeichnung von Reaktionszeiten sollte darüber Aufschluß geben.

Die Prämaske wurde für 600 ms dargeboten und der Zielreiz direkt im Anschluß an die Prämaske, ohne ein dazwischen liegendes Intervall, in dem der Priming Effekt abklingen könnte. Es wurde ausschließlich die Präsentationsfrequenz 40 Hz verwendet. Die folgenden vier Bedingungen wurden für die Reizdarbietung definiert:

1)	Hinweisreiz anwesend	Zielreiz anwesend	(RT–Vorteil erwartet)
2)	Hinweisreiz anwesend	Zielreiz abwesend	
3)	Hinweisreiz abwesend	Zielreiz anwesend	
4)	Hinweisreiz abwesend	Zielreiz abwesend	

Die Reaktionszeiten zeigten eine signifikante Abnahme der Reaktionszeiten bei anwesendem Zielreiz. Auch die Anwesenheit des Hinweisreizes erbrachte eine

signifikante Beschleunigung der Reaktion. Eine Interaktion Hinweisreiz × Zielreiz zeigte, daß die Beschleunigung durch den Hinweisreiz nur bei Anwesenheit des Zielreizes gelang. Dieses Muster von Reaktionszeiten repliziert die bisherigen Befunde, die mit dem Paradigma erzielt wurden.

Abb. 5.4 zeigt die EKPs der Zielreize an Elektrode O1, die über dem linken Occipitallappen (Sehzentrum) liegt. Das Erscheinen der flickernden Prämaske evozierte nach etwa 150 ms eine N1–Komponente sowohl für anwesende (rot), als auch für abwesende Hinweisreize (blau) — allerdings ohne signifikante Unterschiede. Der nach 600 ms präsentierte Zielreiz evozierte bei etwa 800 ms eine weitere N1–Komponente, die keine signifikanten Effekte zeigte. Etwa 1000 ms nach Beginn der Prämaske evozierte der Zielreiz eine P300, die signifikant früher für Zielreize als für Standarreize auftrat. Innerhalb der Zielreize wurde die P300 signifikant früher evoziert, wenn dem Zielreiz innerhalb der Prämaske ein Hinweisreiz vorausging (rot). Das zeigt, daß die nicht wahrgenommenen Hinweisreize neben der Reaktionszeit auch elektrophysiologische Indikatoren kognitiver Prozesse (P3) beeinflussen können, die die Dauer der Stimulusevaluierung widerspiegeln (Donchin und Coles, 1988).

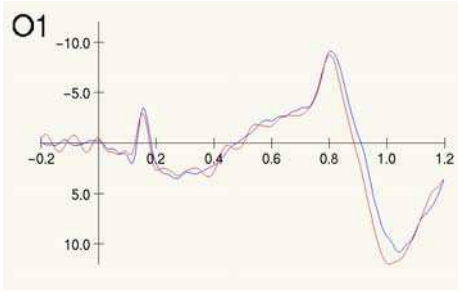

Abbildung 5.4: EKPs der Zielreize beim Elliott–Paradigma ab Beginn der Prämaske mit (rot) und ohne (blau) verstecktem Hinweisreiz.

Entgegen den Erwartungen evozierte die flickernde Prämaske kein Steady–State–Potential, das 600 ms andauert und den Priming Effekt widerspiegelt. Das lag vermutlich an der zu geringen Intensität der flickernden Stimuli auf dem kleinen Oszilloskop–Bildschrim.

5.2 40 Hz in der visuellen Wahrnehmung

Experiment 6 hat gezeigt, daß Versuchspersonen schneller auf Zielreize reagieren können, wenn zunächst eine Prämaske mit 40 Hz flickert, in der ein Hinweisreiz vorhanden ist, der aber nicht bewußt wahrgenommen wird. Dieser Reaktionszeit-

vorteil spiegelt sich auch in der Latenz der P3 wider.

Schlußfolgerung 4 *Flickert ein versteckter Hinweisreiz im Elliott–Paradigma mit 40 Hz, so wird eine signifikant frühere P3–Latenz evoziert, als wenn kein Hinweisreiz in der Prämaske enthalten ist.*

Bereits früher haben verschiedene Forschergruppen mit Hilfe kurz präsentierter Hinweisreize die Reaktion auf spätere Zielreize beeinflußt, ohne daß die Hinweisreize bewußt wahrgenommen wurden (Leuthold und Kopp, 1998; Vorberg, 2001). Dabei entstehende Reaktionszeitvorteile im Falle kongruenter Hinweisreize schreibt man subliminalem Priming zu, das eventuell auf verschiedenen Verarbeitungspfaden für die visuelle Wahrnehmung und visuo–motorische Reaktionen beruht (Goodale und Milner, 1992; Neumann et al., 1998).

Teil V

Interaktion von Frequenzen

Kapitel 6

Harmonische Oszillatoren

Die Ergebnisse des hier beschriebenen Experiments wurden 2001 in der Zeitschrift *Neuroscience Letters* veröffentlicht (Chen und Herrmann, 2001).

6.1 Multiple Frequenzen im menschlichen Gehirn

Während in der Regel der Begriff Gamma–Aktivität mit einer Frequenz von 40 Hz assoziiert wird, umfaßt dieser Frequenzbereich eigentlich 30–80 Hz. Die Besonderheiten, die diesen Gamma–Oszillationen anfänglich zugeschrieben werden, nämlich ihre Korrelation mit kognitiven Prozessen wie Aufmerksamkeit, Gestaltwahrnehmung, oder gar Bewußtsein (Engel et al., 1999; Engel und Singer, 2001; Singer, 2001), wurden später auch auch für höherfrequente Oszillationen gefunden. Curio et al. (1994) konnten im menschlichen EEG evozierte Oszillationen von bis zu 600 Hz finden. So wie die Gamma–Aktivität im Wachzustand und im REM–Schlaf stärker zu finden ist, als im Non–REM Schlaf (Llinas und Ribary, 1993; Gross und Gotman, 1999), können auch Oszillationen um 600 Hz diesen Bewußtseinszuständen zugeordnet werden (Halboni et al., 2000). Das legt nahe, daß nicht die Gamma–Aktivität alleine, sondern eventuell das Zusammenspiel mehrerer Oszillationen für bestimmte Wahrnehmungsphänomene zuständig ist.

6.2 80, 40, 20, 10 Hz

Hochfrequente Frequenzanteile im EKP setzen eine Mittelung über viele hundert Stimulationen voraus, die bei kognitiven Paradigmen sehr zeitaufwendig wäre und zur Habituierung der Antworten führt.

Hypothese 5 *Bei genügender Anzahl von Stimuluswiederholungen werden neben*

40 Hz auch höhere Frequenzen im EKP evoziert, die mit niedrigeren Frequenzen interagieren könnten.

Deswegen wurde ein somatosensorisches Experiment mit 600 Stimuluswiederholungen im 3 Hz Takt durchgeführt, um hohe Frequenzanteile im EKP zu evozieren.

Experiment 7 (EEG)

Zwölf gesunde, männliche Versuchspersonen wurden am linken Medianusnerven mit zwei Intensitäten elektrisch gereizt. Abb. 6.1 zeigt die EKPs an Elektrode C4' (über dem somatosensorischen Cortex) in Folge schmerzfreier (blau) und schmerzhafter Reizung (rot). Topographien wurden für die Zeitfenster früh (20–50 ms), mittel (50–100ms) und spät (100–250 ms) berechnet.

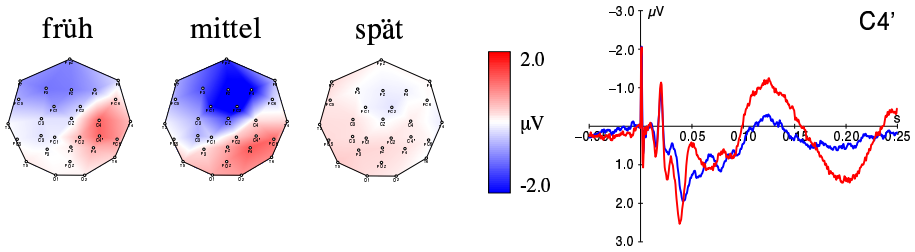

Abbildung 6.1: EKPs in Folge schmerzhafter (rot) und schmerzfreier (blau) elektrischer Reizung des linken Medianusnerven (rechts) und topographische Verteilung der schmerzhaften Potentiale in drei Zeitbereichen (links).

In diesem Paradigma traten vier Pakete evozierter Oszillationen auf, wie in Abb. 6.2 in der Freqeunz–Zeit–Darstellung zu sehen. In zeitlicher Abfolge evozierten schmerzhafte Stimuli Oszillationen von 80, 40, 20 und 10 Hz.

Um die zeitlichen und räumlichen Zusammenhänge dieser Oszillationen näher zu untersuchen, wurde für jede dieser vier Frequenzen ihre topographische Verteilung über dem Schädel und ihr zeitlicher Verlauf berechnet. Dies ist in Abb. 6.3 dargestellt.

Während die 80–Hz–Aktivität bereits 26 ms nach dem elektrischen Impuls fokal begrenzt über dem somatosensorischen Cortex contralateral zur stimulierten Hand ihr Maximum aufweist, erreicht die 40–Hz–Aktivität ihr Maximum erst nach etwa 40 ms und hat eine weiter ausgebreitete, auch frontale Areale umfassende Topographie. Die 40–Hz–Aktivität unterscheidet am deutlichsten zwischen schmerzhafter und schmerzfreier Stimulation. Zeitlich anschließend an die 40–Hz–Aktivität traten 20–Hz–Oszillationen mit einer ähnlichen Topographie auf.

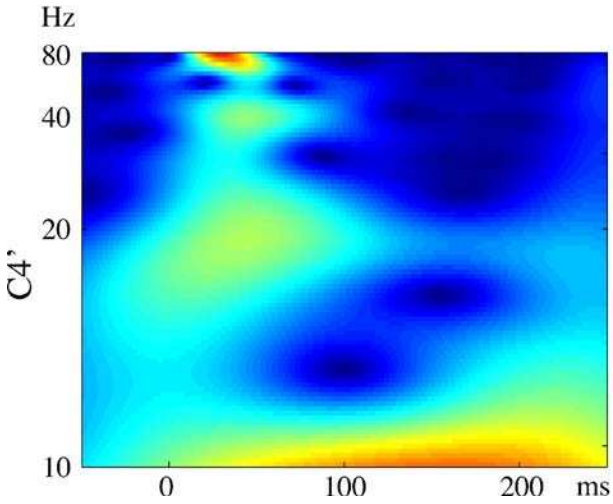

Abbildung 6.2: Frequenz–Zeit Diagramm der evozierten oszillatorischen Aktivität in Elektrode C4' in Folge schmerzhafter Medianusstimulation. Vier zeitlich aufeinanderfolgende Frequenzenanteile von 80, 40, 20 und 10 sind zu erkennen.

10–Hz–Oszillationen mit einer Ausbreitung über fast den gesamten Schädel konnten mit einem späten Maximum von etwa 120 ms gefunden werden. Langsamere Oszillationen konnten aufgrund der schnellen Stimulation von 3 Hz nicht berechnet werden, da sonst eine Konfundierung mit der Stimulationsfrequenz nicht auszuschließen gewesen wäre. Es ist aber zu vermuten, daß bei langsamerer Stimulation noch Frequenzen unterhalb von 10 Hz auftreten, die eine noch größere räumliche Ausbreitung besitzen.

Ähnliche Übergänge von schnellen zu langsameren Frequenzen wurden für Teile dieser Kette von Frequenzkomponenten bereits früher beschrieben: Traub et al. (1999) konnten für den Hippocampus von Ratten in–vitro zeigen, daß zunächst auftretende Beta–Oszillationen anschließend zu Gamma–Oszillationen wurden. Haenschel et al. (1999) konnten denselben Effekt im menschlichen EKP zeigen, wenn Versuchspersonen auditorisch stimuliert wurden, und vermuteten, daß ein solches Durchlaufen von Frequenzbändern physiologisch ist.

Schlußfolgerung 5 *Die hier gefundenen, sowohl zeitlich, als auch topographisch differenzierten Frequenzen deuten darauf hin, daß neuronale Oszillationen mit harmonischen Frequenzverhältnissen bei der bewußten Wahrnehmung von Reizen nacheinander auftreten.*

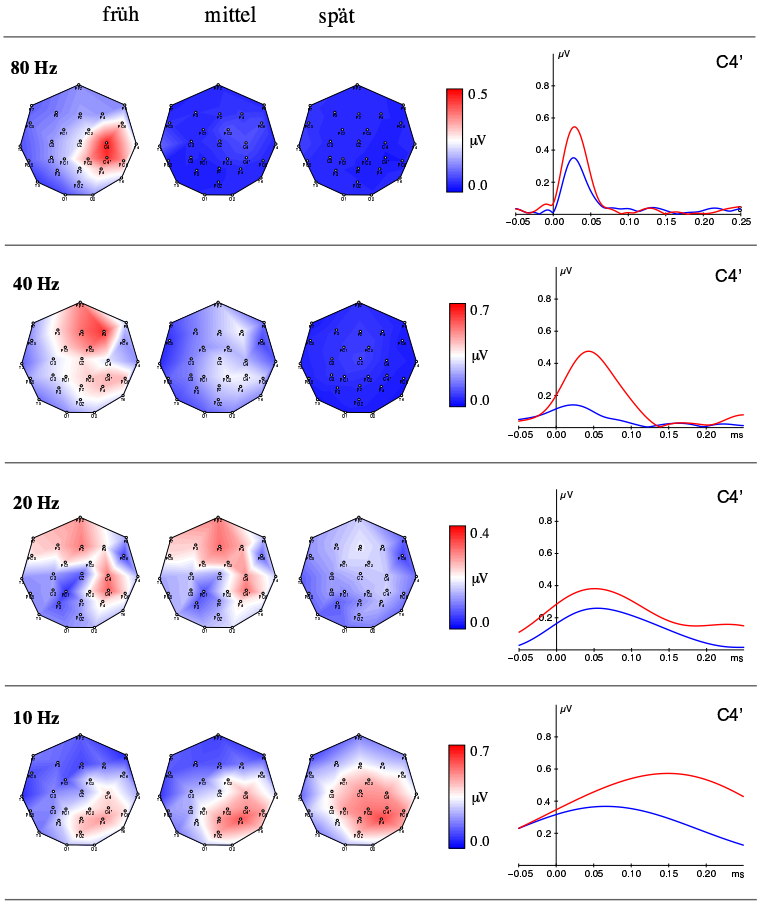

Abbildung 6.3: Zeitlicher Verlauf der evozierten Frequenzkomponenten (rechts) für schmerzhafte (rot) und schmerzfreie Reizung (blau) an Elektrode C4'. Die topographische Verteilung der Komponenten in drei Zeitfenstern (links) für die schmerzhafte Stimulation zeigt eine kontinuierliche Ausbreitung der aktivierten Cortexareale mit Zunahme der Zeit und Abnahme der Frequenz.

Kapitel 7

Resonanzfrequenzen im visuellen Cortex

Die Ergebnisse des hier beschriebenen Experiments wurden 2001 in der Zeitschrift *Experimental Brain Research* veröffentlicht (Herrmann, 2001b).

7.1 Flickerstimulation

In den vorigen Abschnitten wurde wiederholt gezeigt, daß bestimmte Frequenzen, vor allem 40, aber auch 80, 20 und 10 Hz, in verschiedenen kognitiven Paradigmen im menschlichen EEG auftreten. Dabei ist es irrelevant, welche Sinnesmodalität gereizt wird. Oszillatorische 40 Hz Aktivität tritt sowohl bei auditorischer (Pantev, 1995; Crone et al., 2001), visueller (Buchner et al., 1999; Bertrand und Tallon-Baudry, 2000) und somatosensorischer (Crone et al., 1998; Tomberg und Desmedt, 1998) Stimulation auf. Daher ist zu vermuten, daß es einen neuroarchitektonischen Grund für das Auftreten dieser Oszillationen gibt.

Es ist bekannt, daß einerseits einzelne Neurone zu oszillatorischem Verhalten neigen, was man als intrinsische Oszillationen bzeichnet (Gray und McCormick, 1996; Stanford et al., 1998). Weiterhin treten aber auch bei der Verschaltung mehrerer Neurone zu einem Netzwerk oszillatorische Frequenzphänomene auf (Jefferys et al., 1996; Eckhorn, 1999). Eine besondere Rolle in diesem Zusammenhang spielen sogenannte Resonanzfrequenzen. Ein neuronaler Oszillator, d.h. ein Ensemble von Neuronen, das so verschaltet ist, daß es oszilliert, besitzt dann eine Resonanzfrequenz, wenn er bei einer bestimmten Frequenz mit einer höheren Amplitude schwingt, als bei benachbarten Frequenzen. Dies ist ein von physikalischen Oszillatoren her wohl bekannter Effekt. Man kann kortikale Neurone dazu bringen, mit einer bestimmten Frequenz zu oszillieren, indem man sie mit einer Frequez kontinuierlich anregt. Flickert man etwa Licht mit einer bestimmten Fre-

quenz auf die Retina, so oszillieren Neurone im primären visuellen Cortex mit genau dieser Frequenz (Müller et al., 1997). Man nennt die im EEG dabei ableitbaren Oszillationen Steady–State–Potentiale (Regan, 1989; Silberstein, 1995).

Experiment 8 (EEG)

Um herauszufinden, wie der visuelle Cortex des Menschen auf bestimmte Flickerfrequenzen reagiert und insbesondere, ob er Resonanzfrequenzen aufweist, wurde ein Experiment mit Flickerstimulation durchgeführt. Versuchspersonen wurden dabei mit allen Frequenzen von 1 bis 100 Hz pseudo-randomisiert in Schritten von jeweils 1 Hz über eine Brille mit Leuchtdioden stimuliert. Bei jeder Frequenz wurden die Steady–State–Potentiale berechnet und ausgewertet.

Hypothese 6 *Das menschliche EEG weist infolge Flickerstimulation Resonanzfrequenzen bei denjenigen Frequenzen auf, bei denen auch in kognitiven Experimenten evozierte und induzierte Oszillationen auftreten.*

Abb. 7.1 zeigt die Steady–State–EKPs (oben, Elektrode O1) einer Versuchsperson bei 10 Hz (links) und 20 Hz (rechts) Stimulation. Es ist deutlich, daß die Stimulationsfrequenz jeweils die dominierende Frequenz der kortikalen Oszillation ist. Die FFT–Spektren (unten) zeigen, daß zusätzlich die erste Harmonische der Stimulationsfrequenz im EKP enthalten ist, d.h. 20 Hz bei 10 Hz Stimulation und 40 Hz bei 20 Hz Stimulation.

Extrahiert man jeweils aus dem zu einer Stimulationsfrequenz gehörenden Spektrum diejenige Frequenz, mit der stimuliert wurde, und trägt alle 100 so berechneten Amplituden in ein neues Diagramm, so ergibt sich Abb. 7.2. Ist die Amplitude bei einer bestimmten Stimulationsfrequenz stärker als bei den benachbarten Stimulationsfrequenzen, so handelt es sich um eine Resonanzfrequenz des zu Grunde liegenden neuronalen Oszillators. Deutliche Resonanzfrequenzen sind etwa bei 9, 18 und 43 Hz zu sehen.

7.2 Resonanzen und evozierte/induzierte Oszillationen

Die Tatsache, daß wir im visuellen Cortex des Menschen ohne kognitive Aufgabenstellung so deutliche Resonanzfrequenzen finden konnten, deutet darauf hin, daß die bei kognitiven Experimenten an diesen Frequenzen auftretenden Oszillationen auf denselben Resonanzmechanismen basieren. Es müssen nicht unbedingt dieselben neuronalen Generatoren sein, die Steady–State–EKPs und evozierte/induzierte Oszillationen generieren, aber es liegt nahe zu vermuten, daß eine bestimmte Art der Verschaltung kortikaler Neurone diese Resonanzfrequenzen hervorruft. Wenn der Cortex selbst ohne kognitive Anforderung bestimmte

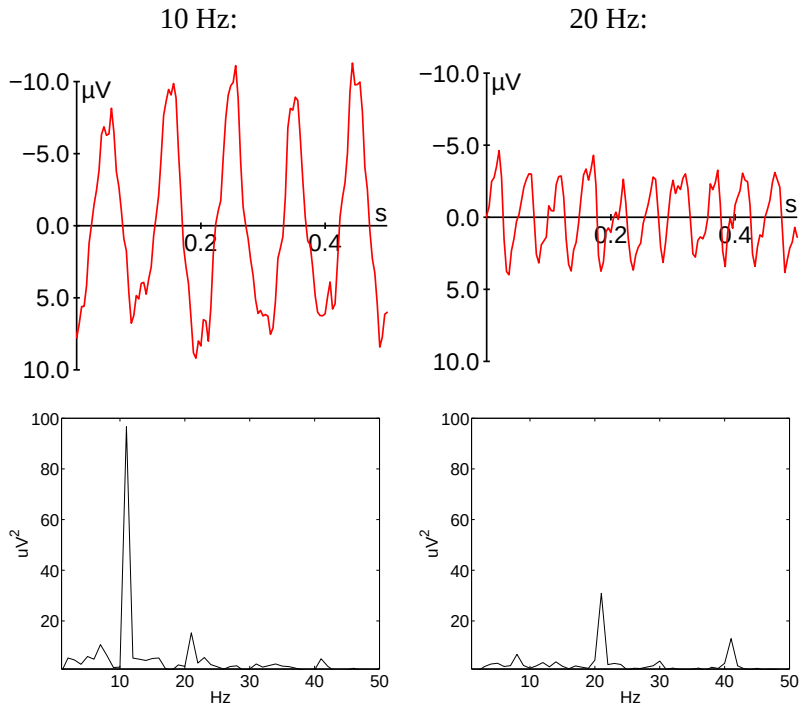

Abbildung 7.1: Steady–State–EKPs (oben) einer VP bei 10 Hz Stimulation (links) und 20 Hz Stimulation (rechts). Die entsprechenden FFT Spektren (unten) zeigen Frequenzanteile der Stimulationsfrequenz und der ersten Harmonischen.

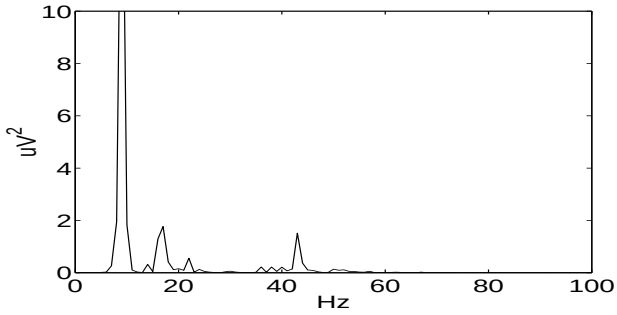

Abbildung 7.2: Steady–State–Amplituden der angeregten Frequenzen einer einzelnen Versuchsperson. Resonanzfrequenzen treten um 9, 18 und 43 Hz auf.

Frequenzen bevorzugt, scheinen diese Frequenzen auch bei kognitiven Prozessen aufzutreten.

Schlußfolgerung 6 *Neuronale Resonanzphänomene scheinen die Grundlage oszillatorischer EEG Aktivität in kognitiven Experimenten darzustellen.*

Teil VI

Diskussion und Schlußbemerkung

Kapitel 8

Diskussion

8.1 Kognitive Korrelate von 40–Hz–Oszillationen

Wie bereits dargestellt, spielen Oszillationen mit einer Frequenz von 40 Hz eine wichtige Rolle für kognitive Prozesse. Mindestens die folgenden vier Gruppen von Prozessen rufen 40–Hz–Oszillationen im menschlichen EEG hervor.

Merkmalsbindung

Das Zusammenbinden einzelner Merkmale zu einer kohärenten Figur ruft im menschlichen EEG induzierte 40–Hz–Oszillationen hervor (Müller et al., 1996, 1997; Tallon-Baudry et al., 1996, 1997; Revonsuo et al., 1997; Keil et al., 1999; Başar-Eroglu et al., 1996a). In den in dieser Arbeit vorgestellten Experimenten mit Kanizsa–Figuren traten allerdings ausschließlich evozierte 40–Hz–Oszillationen auf, die keine eindeutige Korrelation mit Merkmalsbindung zeigten.

Aufmerksamkeit

Tiitinen et al. (1993) konnte zeigen, daß räumliche Aufmerksamkeit auf auditorische Stimuli die von ihnen induzierte Gamma–Aktivität erhöht. Präsentiert man zwischen häufigen Standardtönen seltene, deviante Töne, die nicht beachtet werden müssen, so wird die Aufmerksamkeit automatisch (prä–attentiv) auf sie gerichtet und eine sogenannte Mismatch Negativierung evoziert (Schröger, 1996, 1997). Solche unbeachteten, devianten Töne riefen keine Erhöhung der evozierten oder induzierten 40–Hz–Aktivität hervor, während die Versuchspersonen ein Buch lasen (Tiitinen et al., 1994). Die beachtete Bewegung von Objekten in einem visuellen Halbfeld (Zielreiz) induziert jedoch mehr 40–Hz–Oszillationen als unbeachtete Bewegung (Gruber et al., 1999). Derartig beachtete Reize evozieren eine prominente P300 im EKP (Rösler, 1986; Mecklinger und Ullsperger, 1993),

die von 40–Hz–Oszillationen begleitet wird (Başar-Eroglu und Başar, 1991; Tomberg und Desmedt, 1998). Beachtete Zielreize evozierten in einem anderen Experiment mehr 40–Hz–Oszillationen als Standardreize (Fell et al., 1997).

In den hier vorgestellten Experimenten 1 und 2 evozierten Zielreize jeweils mehr frühe 40–Hz–Oszillationen als Standardreize. Dies war selbst dann der Fall, wenn in Experiment 2 ein nicht–figürlicher Stimulus als Zielreiz diente, dessen einzelne Merkmale nicht zu einer illusionären Figur zusammen gebunden werden mußten.

Anscheinend muß auf einen Stimulus bewußte Aufmerksamkeit gerichtet sein, damit er mehr 40 Hz evoziert als unbeachtete Stimuli.

Arbeitsgedächtnis

Tallon-Baudry et al. (1998) und Tallon-Baudry et al. (1999) konnten im Behaltensintervall eines verzögerten Gedächtnisparadigmas mehr induzierte 40–Hz–Aktivität finden, wenn Stimuli erinnert werden mussten, als wenn während des Intervalls nichts zu erinnern war. De Pascalis und Ray (1998) zeigten, daß in einem ähnlichen Paradigma zum Zeitpunkt S2 mehr 40–Hz–Oszillationen evoziert wurden, wenn die Belastung des Arbeitsgedächtnisses hoch war.

Im hier beschriebenen Experiment 4 war die evozierte 40 Hz Aktivität höher, wenn die Merkmale von Stimuli mit denen eines Musters im KZG verglichen werden mußten, als wenn sie nur wahrgenommen wurden, aber nicht aufgabenrelevant waren. Die frühe evozierte 40–Hz–Aktivität scheint daher den Prozess des Vergleichs wahrgenommener Stimuli mit solchen im KZG zu reflektieren. Insbesondere der positive Verlauf des Vergleich eines Merkmals führt zu frühen evozierten Gamma–Oszillationen. Dies könnte an einer Rückkopplung vom Gedächtnisprozess zum Wahrnehmungsprozess liegen, die die 40 Hz Oszillation verstärkt. Diese Interpretation erklärt die Gamma–Aktivität aus den Experimenten 1, 2, 4 und 5, sowie Experimente aus der Literatur: Im Experiment von Tiitinen et al. (1994) wurden beim Lesen eines Buches auditorische Stimuli nicht mit einem Zielreiz verglichen, wodurch deviante Töne keine erhöhten 40–Hz–Oszillationen evozierten. Bei De Pascalis und Ray (1998) und Fell et al. (1997) werden die Stimuli jedoch beachtet und mit Musterreizen im Arbeitsgedächtnis verglichen und evozieren daher erhöhte 40–Hz–Aktivität. In Bedingungen mit hoher Belastung des Arbeitsgedächtnisses bei De Pascalis und Ray (1998) werden mehr positive Vergleiche mit dem Musterreiz durchgeführt, als in der Bedingung mit niedriger Belastung. Die Zielreize von Fell et al. (1997) ergeben mehr Übereinstimmung mit dem Muster als die Standardreize. Wenn dieser Vergleichsprozess mit 40 Hz arbeitet, liegt es nahe zu vermuten, daß auch das Arbeitsgedächtnis selbst mit 40 Hz arbeitet, wie es von Lisman und Idiart (1995), Jensen und Lisman (1998) und Burle und Bonnet (2000) postuliert wurde. Allerdings weist wahrscheinlich

diese 40–Hz–Aktivität in Behaltensintervallen, die von den Stimuli, ab deren Beginn solche Aktivität aufgezeichnet wird, relativ weit entfernt sind (mehrere hundert ms bis einige Sekunden), leichte Phasenverschiebungen auf. Das könnte dazu führen, daß Tallon-Baudry et al. (1998, 1999) induzierte Gamma Oszillationen als Korrelat des Aktivhaltens von Stimuli im Arbeitsgedächtnis finden. Da allerdings der Vergleich stets kurz nach der Präsentation eines Reizes stattfindet, ist hier die Phasenverschiebung kleiner. Es könnte sein, daß es sich bei induzierter und evozierter Gamma–Aktivität um Oszillationen derselben neuronalen Generatoren handelt, deren Aktivität verschieden stark phasenverschoben ist. Yordanova et al. (1997) und Yordanova und Kolev (1997) haben gezeigt, daß Zielreize nicht wirklich die Amplitude von 40–Hz–Oszillationen verstärken, sondern die Phasenverschiebung von Epoche zu Epoche verringern, wodurch die evozierte 40–Hz–Aktivität anwächst, während die Summe aus evozierter und induzierter konstant bleibt. Man kann deswegen annehmen, daß ohnehin oszillierende 40–Hz–Generatoren durch Stimulation in ihrer Phase synchronisiert werden (siehe auch Tiitinen et al., 1994), wie es auch für 10 Hz Generatoren der Fall ist (Brandt, 1997).

Auch Csibra et al. (2000) konnten zeigen, daß Figuren bei Kleinkindern im Alter von acht Monaten, die bereits eine Gedächtnisrepräsentation der Figur besaßen, mehr Gamma–Aktivität hervorriefen, als bei sechs Monate alten Kleinkindern, die noch keine Repräsentation der Figuren besaßen. Eine alternative Erklärung der erhöhten Gamma–Aktivität im Csibra–Paradigma könnte allerdings auch die Aufmerksamkeit sein, die den Kanizsa–Figuren innerhalb von Sequenzen bunter Bilder zugewandt wurde (Herrmann und Friederici, 2001).

Eventuell basieren auch die Befunde über die Korrelation der 40 Hz Aktivität mit Schlaf– und Wachrhythmen (Llinas und Ribary, 1993; Gross und Gotman, 1999) mit diesem Zugriff auf das Gedächtnis. Sowohl im Wachzustand, als auch im REM Schlaf werden Wahrnehmungen mit Gedächtnisrepräsentationen verglichen, was vermutlich im nicht–REM Schlaf nicht der Fall ist.

Die frontale Topographie der hier beschriebenen Gamma–Aktivität ist ein weiteres Indiz dafür, daß sie sehr wohl einen sogenannten exekutiven Prozess reflektieren könnte, der auf dem Arbeitsgedächtnis operiert und dessen neuronale Quelle im frontalen Cortex vermutet wird (McCarthy et al., 1997). Auch die 40–Hz–Oszillationen in anderen Experimenten wiesen klar frontale Topographien auf, die ähnliche Prozesse vermuten lassen (Tiitinen et al., 1993; Başar-Eroglu et al., 1996a; De Pascalis und Ray, 1998; Tomberg, 1999).

Weitere kognitive Prozesse

Eine Reihe von Arbeiten berichtet außerdem, daß Wörter mehr 40 Hz Oszillationen induzieren als Pseudowörter (Lutzenberger et al., 1994; Pulvermüller et al.,

1996; Eulitz et al., 1996, 2000). Pulvermüller et al. (1999) vermuten, daß diese Aktivität daher rührt, daß Wörter, im Gegensatz zu Pseudowörtern, bereits im Gedächtnis repräsentiert sind. Diese Argumentation geht in dieselbe Richtung, wie die obige Erklärung des Vergleichs wahrgenommener Stimuli mit dem KZG.

Braeutigam et al. (2001) haben gezeigt, daß visuell präsentierte Sätze mehr Gamma–Aktivität im MEG evozieren, wenn sie semantische Fehler enthalten. Diese Aktivität trat in occipito–temporalen und links–frontalen Sensoren auf. Friederici et al. (2000) konnten zeigen, daß sowohl syntaktisch falsche Sätze, wie semantisch falsche Sätze, als auch Sätze aus Pseudowörtern mehr frontale Aktivität im fMRT hervorriefen, als korrekte Sätze. Der linke frontale Cortex wird sowohl für syntaktische (Friederici, 1995; Friederici et al., 1996), als auch für semantische Fehlerdetektion (Nyberg et al., 1998) verantwortlich gemacht. Daher könnte die von Braeutigam et al. (2001) gefundene Gamma–Aktivität die erhöhte Aufmerksamkeit in Folge der Detektion einer semantischen Verletzung reflektieren.

8.2 Schrittweise Frequenzmodulation

Die Abfolge der vier Frequenzkomponenten in Experiment 7 mit schrittweiser Halbierung der Frequenz und gleichzeitiger Ausbreitung der aktivierten Fläche läßt vermuten, daß eine solche Kette zur bewußten Wahrnehmung notwendig ist. Flickerndes Licht mit Frequenzen oberhalb von 40 Hz wird nicht mehr bewußt als intermittierend wahrgenommen, sondern als konstante Lichtquelle (Herrmann, 2001b). Die externe Frequenz des flickernden Lichts evozierte jedoch cortikale Aktivität derselben Frequenz innerhalb des primären visuellen Cortex. Crick und Koch (1995) haben als Erklärung für derartige Phänomene ein Modell aufgestellt, das darauf beruht, daß frühe visuelle Areale wie V1 keine direkten Verbindungen zu frontalen Hirnarealen besitzen und daher nur über den Weg höherer visueller Areale zu bewußter Wahrnehmung beitragen können. Ist diese Ausbreitung aber dadurch gestört, daß sich neuronale Aktivität nicht in ihrer Frequenz teilen und räumlich ausbreiten kann, kommt es nicht zu bewußter Wahrnehmung der in frühen visuellen Arealen vorkommenden Aktivität.

Ähnliche Befunde wurden von von Stein und Sarnthein (2000) berichtet: Sie fanden hochfrequente Kohärenzen (40 Hz) innerhalb primärer cortikaler Areale, die sensorische Integration reflektierten. Niederfrequente Kohärenzen (10 Hz) zwischen weiter auseinander liegenden Arealen (fronto–parietal) spiegelten kognitive Prozesse des Arbeitsgedächtnisses wider.

Die in Experiment 8 gefundenen Resonanzfrequenzen könnten die neurophysiologische Grundlage für das Vorkommen solcher Oszillationen sein: Da im menschlichen Cortex offensichtlich neuronale Oszillatoren existieren, die bereits ohne kognitive Aufgabenstellung bestimmte Frequenzen präferieren, scheinen die-

se Oszillatoren auch von kognitiven Prozessen aktiviert zu werden.

Kapitel 9

Schlußbemerkung

Insgesamt scheinen oszillatorische Prozesse eine überaus wichtige Rolle für kognitive Prozesse zu spielen. Neben kognitiven Prozessen basieren aber auch sensorische (Karakaş und Başar, 1998; Crone et al., 1998) und motorische Prozesse (Pfurtscheller et al., 1992, 1994) auf 40 Hz Oszillationen. Daher ist es in Zukunft wichtig, die Interaktion dieser drei Stufen menschlicher Wahrnehmungs–Reaktions–Abläufe zu erforschen.

9.1 40 Hz bei motorischen Prozessen

Es ist gut möglich, daß motorische Reaktionen nur zu bestimmten Zeitpunkten möglich sind, wie es oszillierende Reaktionszeiten vermuten lassen (Vorberg und Schwarz, 1987; Jokeit, 1990). Daher könnte man annehmen, daß frühere Stufen diese Quantisierung übernommen haben, um eine optimale Kopplung zwischen den Stufen zu erlauben. Dehaene (1993) konnte aber zeigen, daß Reaktionszeiten mit einer höheren Frequenz oszillieren, wenn auditorisch stimuliert wird, als wenn visuell stimuliert wird. Das läßt vermuten, daß eher die Wahrnehmungsmodalität die Oszillation bestimmt.

9.2 40 Hz bei sensorischen Prozessen

Es wäre gut möglich, daß sensorische Prozesse bereits eine Diskretisierung der Wahrnehmung durchführen, wie es sowohl die Ergebnisse aus der vorliegenden Arbeit vermuten lassen (Experiment 6), als auch die Ergebnisse von Elliott und Müller (1998). Eine solche Diskretisierung könnte auch die Zeitschwellen der Wahrnehmung erklären, die besagen, daß zwei auditorische Reize mindestens 2 ms getrennt sein müssen, um unterschieden werden zu können, während zwei

visuelle Reize 10–40 ms auseinander liegen müssen (Häcker und Stapf, 1998, S. 961).

9.3 40 Hz bei Wahrnehmungsprozessen

Dehaene (1993) konnte zeigen, daß die in Reaktionszeiten auftretenden Oszillationen unter anderem von der Schwierigkeit der Aufgabe abhingen. Eine Diskretisierung sensorischer oder motorischer Prozesse kann diesen Effekt nicht erklären. Daher legt dieser Befund nahe, daß die kognitive Verarbeitung in Zeitquanten unterteilt ist, wie von Geissler (1997) und Geissler et al. (1999) angenommen. Auch Elliott und Müller (2000) zeigten, daß eher das Arbeitsgedächtnis, als die Merkmalsbindung zu den beobachteten Oszillationen in Reaktionszeiten führten, als sie die Länge ihres Behaltensintervalls veränderten. Die in der vorliegenden Arbeit beschriebene Tatsache, daß auch nicht oszillierende Stimuli zu oszillatorischen Antworten im EEG führen (Experimente 1, 2, 4 und 5), die kognitive Prozesse widerspiegeln, könnte ein weiterer Hinweis darauf sein, daß Kognition in diskretisierten Schritten abläuft.

9.4 Ausblick

Die eventuelle Diskretisierung der menschlichen Wahrnehmung in Zeitquanten berührt interessante philosophische Fragen. Heidegger (1984) hat die Hypothese aufgestellt, daß das Sein über die Zeit definiert ist. Die oben beschriebenen Befunde bringen neurophysiologische Evidenz dafür, daß menschliches Bewußtsein entscheidend von Zeit und insbesondere von Zeitquanten abhängt. Läsionsstudien haben außerdem gezeigt, daß der präfrontale Cortex für die Zeitverarbeitung von entscheidender Bedeutung ist (Knight und Grabowecky, 2000). In der vorliegenden Arbeit wurde dargestellt, daß Gamma–Oszillationen, die vermutlich im präfrontalen Cortex generiert werden, exekutive Funktionen reflektieren, die wiederum der bewußten Wahrnemung zu Grunde liegen (Baddeley, 1992b; Baars, 1997). Daher ist es in Zukunft wünschenswert, den Ursprung oszillatorischer Hirnaktivität weiter zu untersuchen und auch die Wechselwirkung verschiedener Frequenzen dabei zu beachten.

Teil VII

Anhänge

Literaturverzeichnis

Adrian E.D., 1942. Olfactory reactions in the brain of the hedgehoc. Journal of Physiology (London), 100, 459–473.

Ajjanagadde V., Shastri L., 1991. Rules and variables in neural nets. Neural Computation, 3(1), 121–134.

Baars B.J., 1997. Some essential differences between consciousness and attention, perception, and working memory. Consciousness and Cognition, 6, 363–371.

Başar E., Schürmann M., 2001. Toward new theories of brain function and brain dynamics. International Journal of Psychophysiology, 39, 87–89.

Başar E., Ungan P., 1973. A component analysis and principles derived for the understanding of evoked potentials of the brain: Studies in the hippocampus. Kybernetik, 12, 45–54.

Başar E., Gönder A., Ungan P., 1976. Important relation between EEG and brain evoked potentials. II. A system analysis of electrical signals from the human brain. Biological Cybernetics, 25, 41–48.

Başar E., Schürmann M., Başar-Eroglu C., Karakaş S., 1997. Alpha oscillations in brain functioning: an integrative theory. International Journal of Psychophysiology, 26(1–3), 5–29.

Başar E., Başar-Eroglu C., Karakaş S., Schürmann M., 2001. Gamma, alpha, delta, and theta oscillations govern cognitive processes. International Journal of Psychophysiology, 39, 241–248.

Başar-Eroglu C., Başar E., 1991. A compound P300–40Hz response of the cat hippocampus. International Journal of Neuroscience, 13, 227–237.

Başar-Eroglu C., Strüber D., Kruse P., Başar E., Stadler M., 1996a. Frontal gamma-band enhancement during multistable visual perception. International Journal of Psychophysiology, 24, 113–125.

Başar-Eroglu C., Strüber D., Schürmann M., Stadler M., Başar E., 1996b. Gamma-band responses in the brain: a short review of psychophysiological correlates and functional significance. International Journal of Psychophysiology, 24, 101–112.

Baddeley A., 1992a. Working memory. Science, 255, 556–559.

Baddeley A., Weiskrantz L. (Hrsg.), 1995. Attention: selection, awareness and control. Oxford University Press, New York.

Baddeley A.D., 1992b. Consciousness and working memory. Consciousness and Cognition, 1, 3–6.

Berger H., 1929. Über das Elektrenkephalogramm des Menschen. Arch. Psychiat. Nerverkr., 87, 527–570.

Bertrand O., Tallon-Baudry C., 2000. Oscillatory gamma activity in humans: a possible role for object representation. International Journal of Psychophysiology, 38(3), 211–223.

Braeutigam S., Bailey A.J., Swithenby S.J., 2001. Phase-locked gamma band responses to semantic violation stimuli. Cognitive Brain Research, 10, 365–377.

Brandt M.E., 1997. Visual and auditory evoked phase resetting of the alpha EEG. International Journal of Psychophysiology, 26, 285–298.

Broadbent D.E., 1958. Perception & communication. Pergamon Press, New York.

Buchner H., Gobbele R., Waberski T.D., Wagner M., Fuchs M., 1999. Evidence for independent thalamic and cortical sources involved in the generation of the visual 40 Hz response in humans. Neuroscience Letters, 269(2), 59–62.

Burle B., Bonnet M., 2000. High-speed memory scanning: a behavioural argument for a serial oscillatory model. Cognitive Brain Research, 9, 327–337.

Chen A.C.N., Herrmann C.S., 2001. Perception of pain coincides with the spatial expansion of human EEG dynamics. Neuroscience Letters, 297(3), 183–186.

Cooley W., Tukey J., 1965. An algorithm for the machine calculation of complex Fourier series. Math. Comput., 19, 297–301.

Cowan N., 1997. Attention and memory: an integrated framework. Oxford University Press, New York.

Craik F.I.M., Govoni R., Naveh-Benjamin M., Anderson N.D., 1996. The effects of divided attention on encoding and retrieval processes in human memory. Journal of Experimental Psychology: General, 125(2), 159–180.

Crick F., Koch C., 1995. Are we aware of neural activity in primary visual cortex? Nature, 375, 121–123.

Crone N.E., Miglioretti D.L., Gordon B., Lesser R.P., 1998. Functional mapping of human sensorimotor cortex with electrocorticographic spectral analysis. ii. event-related synchronization in the gamma band. Brain, 121, 2301–2315.

Crone N.E., Boatman D., Gordon B., Hao L., 2001. Induced electrocorticographic gamma activity during auditory perception. Clinical Neurophysiology, 112, 565–582.

Csibra G., Davis G., Spratling M.W., Johnson M.H., 2000. Gamma oscillations and object processing in the infant brain. Science, 290, 1582–1585.

Curio G., Mackert B.M., Burghoff M., Koetitz R., Abraham-Fuchs K., Harer W., 1994. Localization of evoked neuromagnetic 600 Hz activity in the cerebral somatosensory system. Electroencephalography and Clinical Neurophysiology, 91(6), 483–487.

Davis G., Driver J., 1994. Parallel detection of Kanizsa subjective figures in the human visual system. Nature, 371, 791–793.

De Pascalis V., Ray W.J., 1998. Effects of memory load on event-related patterns of 40 Hz EEG during cognitive and motor tasks. International Journal of Psychophysiology, 28, 301–315.

Dehaene S., 1993. Temporal oscillations in human perception. Psychological Science, 4(4), 264–270.

Desimone R., 1999. Neural mechanisms for visual memory and their role in attention. Proceedings of the National Acadamy of Sciences USA, 93, 13494–13499.

Donchin E., Coles M.G.H., 1988. Is the P300 component a manifestation of context updating? Behavioural Brain Science, 11, 357–374.

Dumermuth G., Molinari L., 1987. Spectral analysis of EEG background activity. In: Gevins A.S., Rémond A. (Hrsg.), Methods of Analysis of Brain Electrical and Magnetic Signals (Handbook of Electroencephalography and Clinical Neurophysiology), Kapitel 4, S. 85–130. Elsevier.

Eckhorn R., 1999. Neural mechanisms of visual feature binding investigated with microelectrodes and models. Visual Cognition, 6(3/4), 231–265.

Eckhorn R., Bauer R., Jordan W., Brosch M., Kruse W., Munk M., Reitboeck H.J., 1988. Coherent oscillations: a mechanism of feature linking in the visual cortex? Biological Cybernetics, 60, 121–130.

Elbert T., Junghöfer M., Rockstroh B., Roth W.T., 2001. Physiologische Grundlagen und psychophysiologische Meßmethoden der Hirnaktivität. In: Rösler F. (Hrsg.), Enzyklopädie der Psychologie: Grundlagen und Methoden der Psychophysiologie, Band 4 von Biologische Psychologie, S. 179–236, Göttingen. Hogrefe Verlag.

Elliott M.A., Müller H.J., 1998. Synchronous information presented in 40–Hz flicker enhances visual feature binding. Psychological Science, 9(4), 277–283.

Elliott M.A., Müller H.J., 2000. Evidence for a 40 Hz oscillatory short-term visual memory revealed by human reaction-time measurements. Journal of Experimental Psychology: Learning, Memory, and Cognition, 26(3), 703–718.

Elliott M.A., Herrmann C.S., Mecklinger A., Müller H.J., 2000. The loci of oscillatory visual-object priming: a combined electroencephalographic and reaction-time study. International Journal of Psychophysiology, 38(3), 225–242.

Engel A.K., Singer W., 2001. Temporal binding and the neural correlates of sensory awareness. Trends in Cognitive Science, 5(1), 16–25.

Engel A.K., König P., Kreiter A., Schillen T.B., Singer W., 1992. Temporal coding in the visual cortex: new vistas on integration in the nervous system. Trends in Neuroscience, 15(6), 218–226.

Engel A.K., Fries P., König P., Brecht M., Singer W., 1999. Temporal binding, binocular rivalry, and consciousness. Consciousness and Cognition, 8, 128–151.

Eulitz C., Maess B., Pantev C., Friederici A.D., Feige B., Elbert T., 1996. Oscillatory neuromagnetic activity induced by language and non-language stimuli. Cognitive Brain Research, 4(2), 121–132.

Eulitz C., Eulitz H., Maess B., Cohen R., Pantev C., Elbert T., 2000. Magnetic brain activity evoked and induced by visually presented words and nonverbal stimuli. Psychophysiology, 37(4), 447–455.

Fahle M., Koch C., 1995. Spatial displacement, but not temporal asynchrony, destroys figural binding. Vision Research, 35(4), 491–494.

Fell J., Hinrichs H., Röschke J., 1997. Time course of human 40 Hz EEG activity accompanying P3 responses in an auditory oddball task. Neuroscience Letters, 235(3), 121–124.

Freeman W.J., 1975. Mass Action in the Nervous System. Academic Press, New York.

Friederici A.D., 1995. The time course of syntactic activation during language processing: a model based on neuropsychological and neurophysiological data. Brain and Language, 50, 259–281.

Friederici A.D., Mecklinger A., Hahne A., 1996. The temporal structure of syntactic parsing: Early and late event-related brain potentials elicited by syntactic anomalities. Journal of Experimental Psychology: Learning, Memory, and Cognition, 22, 1219–1248.

Friederici A.D., Meyer M., von Cramon D.Y., 2000. Auditory language comprehension: an event-related fMRI study on the processing of syntactic and lexical information. Brain and Language. in press.

Fuster J., 2000. Executive frontal functions. Experimental Brain Research, 133, 66–70.

Galambos R., 1992. A comparison of certain gamma band (40 Hz) brain rhythms in cat and man. In: Başar E., Bullock T.H. (Hrsg.), Induced rhythms in the brain, S. 201–216. Birkhäuser, Boston.

Galambos R., Makeig S., Talmachoff P., 1981. A 40 Hz auditory potential recorded from the human scalp. Proceedings of the National Acadamy of Sciences USA, 78, 2643–2647.

Ganor-Stern D., Seamon J.G., Carrasco M., 1998. The role of attention and study time in explicit and implicit memory for unfamiliar visual stimuli. Memory & Cognition, 26(6), 1187–1195.

Geissler H.G., 1997. Is there a way from behavior to non-linear brain dynamics? on quantal periods in cognition and the place of alpha in brain resonances. International Journal of Psychophysiology, 26(1–3), 381–393.

Geissler H.G., Schebera F.U., Kompass R., 1999. Ultra-precise quantal timing: evidence from simultaneity thresholds in long-range apparent movement. Perception and Psychophysics, 61(4), 707–726.

Gomez-Gonzales C.M., Clark V.P., Fan S., Luck S.J., Hillyard S.A., 1994. Sources of attention-sensitive visual event-related potentials. Brain Topography, 7(1), 41–51.

Goodale M.A., Milner A.D., 1992. Separate visual pathways for perception and action. Trends in Neuroscience, 15, 20–25.

Gray C.M., McCormick D.A., 1996. Chattering cells: Superficial pyramidal neurons contributing to the generation of synchronous oscillations in the visual cortex. Science, 274, 109–113.

Gray C.M., König P., Engel A.K., Singer W., 1989. Oscillatory response in the cat visual cortex exhibit intercolumnar synchronization which reflects global stimulus properties. Nature, 338, 334–337.

Grosof D.H., Shapley R.M., Hawken M.J., 1993. Macaque v1 neurons can signal 'illusory' contours. Nature, 365(6446), 550–552.

Gross D.W., Gotman J., 1999. Correlation of high-frequency oscillations with the sleep-wake cycle and cognitive activity in humans. Neuroscience, 94(4), 1005–1018.

Gruber T., Müller M.M., Keil A., Elbert T., 1999. Selective visual-spatial attention alters induced gamma band responses in the human EEG. Clinical Neurophysiology, 110, 2074–2085.

Häcker H., Stapf K.H. (Hrsg.), 1998. Dorsch Psychologisches Wörterbuch. Verlag Hans Huber, Bern.

Haenschel C., Baldweg T., Croft R.J., Whittington M.A., Gruzelier J., 1999. Gamma and beta frequency oscillations in response to novel auditory stimuli: A comparison of human electroencephalogram (EEG) data with in vitro models. Proceedings of the National Acadamy of Sciences USA, 97(13), 7645–7650.

Halboni P., Kaminski R., Gobbele R., Waberski T.D., Herrmann C.S., Töpper R., Buchner H., 2000. Sleep stage dependant changes of the high-frequency part of the somatosensory evoked potentials. Clinical Neurophysiology, 111(12), 2277–2284.

Heidegger M., 1984. Sein und Zeit. Max Niemeyer Verlag, Tübingen.

Herrmann C.S., 2000. Kanizsa figures pop out of visual search displays. Psychophysiology, 37(suppl. 1), S 47.

Herrmann C.S., 2001a. Gamma activity in the human EEG. In: Polich J. (Hrsg.), Detection of change: event-related potential and fMRI findings, Dordrecht. Kluwer Academic. in press.

Herrmann C.S., 2001b. Human EEG responses to 1–100 Hz flicker: Resonance phenomena in visual cortex and their potential correlation to cognitive phenomena. Experimental Brain Research, 137, 345–353.

Herrmann C.S., Bosch V., 2001. Gestalt perception modulates early visual processing. Neuroreport, 12(5), 901–904.

Herrmann C.S., Friederici A.D., 2001. Object processing in the infant brain. Science, 292(5515), 163.

Herrmann C.S., Mecklinger A., 2000. Magnetoencephalographic responses to illusory figures: Early evoked gamma is affected by processing of stimulus features. International Journal of Psychophysiology, 38(3), 265–281.

Herrmann C.S., Mecklinger A., 2001. Gamma activity in human EEG is related to high-speed memory comparisons during object selective attention. Visual Cognition, 8(3/4/5), 593–608.

Herrmann C.S., Mecklinger A., Pfeifer E., 1999. Gamma responses and ERPs in a visual classification task. Clinical Neurophysiology, 110(4), 636–642.

Herrmann C.S., Kruggel F., Wiggins C.J., von Cramon D.Y., 2001. Gestalt perception and target detection in EEG/MEG and fMRI. Journal of Psychophysiology. (in press).

Hobson J.A., 1990. Schlaf: Gehirnaktivität im Ruhezustand. Spektrum–Verlag, Heidelberg.

Iidaka T., Anderson N.D., Kapur S., Cabeza R., Craik F.I.M., 2000. The effect of divided attention on encoding and retrieval in episodic memory revealed by positron emission tomography. Journal of Cognitive Neuroscience, 12(2), 267–280.

Jandó G., Siegel R.M., Horváth Z., Buzsáki G., 1993. Pattern recognition of the electroencephalogram by artificial neural networks. Electroencephalography and Clinical Neurophysiology, 86, 100–109.

Jasper H.H., Andrews H.L., 1938. Electroencephalography. III. Normal differentiation of occipital and precentral regions in man. Arch. Neurolog. Psychiat., 39, 96–115.

Jefferys J.G.R., Traub R.D., Whittington M.A., 1996. Neuronal networks for induced 40 Hz rhythms. Trends in Neuroscience, 19(5), 202–208.

Jensen O., Lisman J.E., 1998. An oscillatory short-term memory buffer model can account for data on the Sternberg task. The Journal of Neuroscience, 18(24), 10688–10699.

Jokeit H., 1990. Analysis of periodicities in human reaction times. Naturwissenschaften, 77, 289–291.

Jürgens E., Rösler F., Henninghausen E., Heil M., 1995. Stimulus-induced gamma oscillations: harmonics of alpha activity. NeuroReport, 6, 813–816.

Karakaş S., Başar E., 1998. Early gamma response is sensory in origin: a conclusion based on cross-comparison of results from multiple experimental paradigms. International Journal of Psychophysiology, 31, 13–31.

Karakaş S., Başar-Eroglu C., Özesmi C., Kafadar H., Erzengin Ö.Ü., 2001. Gamma response of the brain: a multifunctional oscillation that represents bottom-up with top-down processing. International Journal of Psychophysiology, 39, 137–150.

Keil A., Müller M.M., Ray W.J., Gruber T., Elbert T., 1999. Human gamma band activity and perception of a gestalt. The Journal of Neuroscience, 19(16), 7152–7162.

Kiper D.C., Gegenfurtner K., Movshon A., 1996. Cortical oscillatory responses do not affect visual segmentation. Vision Research, 36(4), 539–544.

Kirino E., Belger A., Goldman-Rakic P.S., McCarthy G., 2000. Prefrontal activation evoked by infrequent target and novel stimuli in a visual target detection task: an event-related functional magnetic resonance imaging study. The Journal of Neuroscience, 20(17), 6612–6618.

Klem G.H., Lüders H.O., Jasper H.H., Elger C., 1999. The Ten-Twenty Electrode System of the International Federation. In: Deuschl G., Eisen A. (Hrsg.), Recommendations for the Practice of Clinical Neurophysiology – Guidelines of the International Federation of Clinical Neurophysiology (EEG Suppl. 52), Kapitel 1.1, S. 3–6. Elsevier, Amsterdam, second Ausgabe.

Klimesch W., Schimke H., Pfurtscheller G., 1993. Alpha frequency, cognitive load, and memory performance. Brain Topography, 5(3), 241–251.

Klimesch W., Doppelmayr M., Rohm D., Pollhuber D., Stadler W., 2000. Simultaneous desynchronization and synchronization of different alpha responses in the human electroencephalograph: a neglected paradox? Neuroscience Letters, 284(1-2), 97–100.

Knight R.T., Grabowecky M., 2000. Prefrontal cortex, time, and consciousness. In: Gazzaniga M.S. (Hrsg.), The new cognitive neurosciences, S. 1319–1339. MIT press, Cambridge.

Kruggel F., Herrmann C.S., Wiggins C.J., von Cramon D.Y., 2001. Hemodynamic and electroencephalographic responses to illusory figures: recording of the event-related potentials during functional MRI. Neuroimage. in revision.

Kubicki S., Höller L., 1980. Systematische Einteilung der EEG–Grundrhythmen und –Normvarianten. Das EEG–Labor. Zeitschrift für Neurophysiologische Funktionsdiagnostik, 2, 32–53.

Leuthold H., Kopp B., 1998. Mechanisms of priming by masked stimuli: Inferences from event-related brain potentials. Psychological Science, 9(4), 263–269.

Levy R., Goldman-Rakic P.S., 2000. Segregation of working memory functions within the dorsolateral prefrontal cortex. Experimental Brain Research, 133, 23–32.

Lindsay P.H., Norman D.A., 1977. Human Information Processing: An Introduction to Psychology. Academic Press, New York.

Lisman J.E., Idiart M.A.P., 1995. Storage of 7 ± 2 short-term memories in oscillatory subcycles. Science, 267, 1512–1515.

Llinas R., Ribary U., 1993. Coherent 40 Hz oscillation characterizes dream state in humans. Proceedings of the National Acadamy of Sciences USA, 90, 2078–2081.

Logothetis N.K., Pauls J., Augath M., Trinath T., Oeltermann A., 2001. Neurophysiological investigation of the basis of the fMRI signal. Nature, 412, 150–157.

Luck S.J., Vogel E.K., 1998. Response to nelson cowan: Visual and auditory working memory capacity. Trends in Cognitive Science, 2(3), 78–80.

Lutzenberger W., Pulvermüller F., Birbaumer N., 1994. Words and pseudowords elicit distinct patterns of 30 Hz activity in humans. Neuroscience Letters, 176, 115–118.

Lutzenberger W., Pulvermüller F., Elbert T., Birbaumer N., 1995. Visual stimulation alters local 40 Hz response in humans: an EEG study. Neuroscience Letters, 183, 39–42.

McCarthy G., Luby M., Gore J., Goldman-Rakic P.S., 1997. Infrequent events transiently activate human prefrontal and parietal cortex as measured by functional MRI. Journal of Neurophysiology, 77(3), 1630–1634.

Mecklinger A., Ullsperger P., 1993. P3 varies with stimulus categorization rather than probability. Electroencephalography and Clinical Neurophysiology, 86, 395–407.

Müller M.M., Bosch J., Elbert T., Kreiter A., Sosa M.V., Sosa P.V., Rockstroh B., 1996. Visually induced gamma-based responses in human electroencephalographic activity - a link to animal studies. Experimental Brain Research, 112(1), 96–102.

Müller M.M., Junghöfer M., Elbert T., Rockstroh B., 1997. Visually induced gamma-band responses to coherent and incoherent motion: a replication study. NeuroReport, 8, 2575–2579.

Müller M.M., Gruber T., Keil A., 2000. Modulation of induced gamma band activity in the human EEG by attention and visual processing. International Journal of Psychophysiology, 38(3), 283–300.

Neumann O., Ansorge U., Klotz W., 1998. Funktionsdifferenzierung im visuellen Kortex: Grundlage für motorische Aktivierung durch nicht bewußt wahrgenommene Reize? Psychologische Rundschau, 49(4), 185–196.

Nyberg L., Cabeza R., Tulving E., 1998. Asymmetric frontal activation during episodic memory: What kind of specificity? Trends in Cognitive Science, 2(11), 419–421.

Pantev C., 1995. Evoked and induced gamma-band activity of the human cortex. Brain Topography, 7(4), 321–330.

Peterhans E., von der Heydt R., 1989. Mechanisms of contour perception in monkey visual cortex. II. contours bridging gaps. The Journal of Neuroscience, 9(5), 1749–1763.

Pfurtscheller G., Berghold A., 1989. Patterns of cortical activation during planning of voluntary movements. Electroencephalography and Clinical Neurophysiology, 72, 250–257.

Pfurtscheller G., Neuper C., 1992. Simultaneous EEG 10 Hz desynchronization and 40 Hz synchronization during finger movements. NeuroReport, 3, 1057–1060.

Pfurtscheller G., Flotzinger D., Mohl W., Peltoranta M., 1992. Prediction of the side of hand movements from single-trial multi-channel EEG data using neural networks. Electroencephalography and Clinical Neurophysiology, 82, 313–315.

Pfurtscheller G., Flotzinger D., Neuper C., 1994. Differentiation between finger, toe and tongue movement in man based on 40 Hz EEG. Electroencephalography and Clinical Neurophysiology, 90, 456–460.

Platzer W. (Hrsg.), 1994. Pernkopf Anatomie – Atlas der topographischen und angewandten Anatomie des Menschen. Urban & Schwarzenberg, München, third Ausgabe.

Posner M.I., 1980. Orienting of attention. Quarterly Journal of Experimental Psychology, 32(1), 3–25.

Pulvermüller F., Eulitz C., Pantev C., Mohr B., Feige B., Lutzenberger W., Elbert T., Birbaumer N., 1996. High-frequency cortical responses reflect lexical processing: an MEG study. Electroencephalography and Clinical Neurophysiology, 98, 76–85.

Pulvermüller F., Keil A., Elbert T., 1999. High-frequency brain activity: perception or active memory. Trends in Cognitive Science, 3(7), 250–252.

Regan D., 1989. Human Brain Electrophysiology: Evoked Potentials and Evoked Magnetic Fields in Science and Medicine. Elsevier, New York.

Revonsuo A., Wilenius-Emet M., Kuusela J., Lehto M., 1997. The neural generation of a unified illusion in human vision. NeuroReport, 8, 3867–3870.

Reynolds J.H., Desimone R., 1999. The role of neural mechanisms of attention in solving the binding problem. Neuron, 24, 19–29.

Roskies A.L., 1999. The binding problem – Introduction. Neuron, 24(1), 7.

Rösler F., 1986. P300 complex: a manifestation of reactive or anticipatory processes of the brain? Electroencephalography and Clinical Neurophysiology, 38, 138–142.

Schröger E., 1996. A neural mechanism for involuntary attention shifts to changes in auditory stimulation. Journal of Cognitive Neuroscience, 8, 527–539.

Schröger E., 1997. On the detection of auditory deviations: a pre-attentive activation model. Psychophysiology, 34, 245–257.

Shastri L., Ajjanagadde V., 1993. From associations to systematic reasoning: A connectionist representation of rules, variables and dynamic bindings using temporal synchrony. Behavioural Brain Science, 16(3), 417–494.

Silberstein R.B., 1995. Steady-state visually evoked potentials, brain resonances, and cognitive processes. In: Nunez P.L. (Hrsg.), Neocortical dynamics and human EEG rhythms, S. 272–303. Oxford University Press, Oxford.

Singer W., 1999. Neuronal synchrony: a versatile code for the definition of relations. Neuron, 24, 49–65.

Singer W., 2001. Conciousness and the binding problem. Annals of the New York Academy of Sciences, 929, 123–146.

Smith E.E., Jonides J., 1999. Storage and executive processes in the frontal lobes. Science, 283, 1657–1661.

Stanford I.M., Traub R.D., Jefferys J.G.R., 1998. Limbic gamma rhythms II. synaptic and intrinsic mechanisms underlying spike doublets in oscillating subicular neurons. Journal of Neurophysiology, 80(1), 162–171.

Strüber D., Başar-Eroglu C., Hoff E., Stadler M., 2000. Reversal-rate dependant differences in the EEG gamma-band during multistable perception. International Journal of Psychophysiology, 38(3), 243–252.

Strüber D., Başar-Eroglu C., Miener M., Stadler M., 2001. EEG gamma-band response during the perception of Necker cube reversals. Visual Cognition, 8(3/4), 609–621.

Tallon C., Bertrand O., Bouchet P., Pernier J., 1995. Gamma–range activity evoked by coherent visual stimuli in humans. European Journal of Neuroscience, 7, 1285–1291.

Tallon-Baudry C., Bertrand O., 1999. Oscillatory gamma activity in humans and its role in object representation. Trends in Cognitive Science, 3(4), 151–162.

Tallon-Baudry C., Bertrand O., Delpuech C., Pernier J., 1996. Stimulus specificity of phase-locked and non-phase-locked 40 Hz visual responses in human. Journal of Neuroscience, 16(13), 4240–4249.

Tallon-Baudry C., Bertrand O., Delpuech C., Pernier J., 1997. Oscillatory γ-band (30–70 Hz) activity induced by a visual search task in humans. Journal of Neuroscience, 17(2), 722–734.

Tallon-Baudry C., Bertrand O., Peronnet F., Pernier J., 1998. Induced γ-band activity during the delay of a visual short–term memory task in humans. Journal of Neuroscience, 18(11), 4244–4254.

Tallon-Baudry C., Kreiter A., Bertrand O., 1999. Sustained and transient oscillatory responses in the gamma and beta bands in a visual short-term memory task. Visual Neuroscience, 16, 449–459.

Teichner W.H., Krebs M.J., 1974. Laws of visual choice reaction time. Psychological Reviews, 81(1), 75–98.

Thorpe S., 1995. Localized versus distributed representations. In: Arbib M.A. (Hrsg.), The handbook of brain theory and neural networks, S. 549–552. MIT Press, Cambridge.

Tiitinen H., Sinkkonen J., Reinikainen K., Alho K., Lavikainen J., Näätänen R., 1993. Selective attention enhances the auditory 40-Hz transient response in humans. Nature, 364, 59–60.

Tiitinen H., Sinkkonen J., May P., Näätänen R., 1994. The auditory 40-Hz response is insensitive to changes in stimulus features. Nature, 6(1), 190–192.

Tomberg C., 1999. Cognitive N140 electrogenesis and concomitant 40 Hz synchronization in mid-dorsolateral prefrontal cortex (area 46) identified in non-averaged human brain potentials. Neuroscience Letters, 266, 141–144.

Tomberg C., Desmedt J.E., 1998. Human perceptual processing: inhibition of transient prefrontal-parietal 40 Hz binding at P300 onset documented in non-averaged cognitive brain potentials. Neuroscience Letters, 255, 163–166.

Traub R.D., Whittington M.A., Buhl E.H., Jefferys J.G.R., Faulkner H.J., 1999. On the mechanism of the gamma $\rightarrow$ beta frequency shift in neuronal oscillations induced in rat hippocampal slices by tetanic stimulation. Journal of Neuroscience, 19(3), 1088–1105.

Treisman A., 1999. Feature binding, attention and object perception. In: Humphreys G.W., Duncan J., Treisman A. (Hrsg.), Attention, space and action: studies in cognitive neuroscience, S. 6–14, New York. Oxford University Press.

Ungerleider L.G., 1995. Functional brain imaging studies of cortical mechanisms for memory. Science, 270, 769–775.

Ungerleider L.G., Courtney S.M., Haxby J.V., 1998. A neural system for human visual working memory. Proceedings of the National Acadamy of Sciences USA, 95, 883–890.

von der Malsburg C., Schneider W., 1986. A neural cocktail-party processor. Biological Cybernetics, 54, 29–40.

von Stein A., Sarnthein J., 2000. Different frequencies for different scales of cortical integration: from local gamma to long range alpha/theta synchronization. International Journal of Psychophysiology, 38(3), 301–313.

Vorberg D., 2001. Ab wann wirken bewusste visuelle Reize anders als unbewusste? In: Zimmer A., Lange K., Bäuml K.H., Loose R., Scheuchenplug R., Tucha O., Schnell H., Findl R. (Hrsg.), Experimentelle Psychologie: Abstracts der 43. Tagung experimentell arbeitender Psychologen, S. 152, Lengerich. Pabst Science Publishers.

Vorberg D., Schwarz W., 1987. Oscillatory mechanisms in human reaction times? Naturwissenschaften, 74, 446–447.

Walter W.G., 1936. The location of cerebral tumors by electroencephalography. Lancet, 2, 305–308.

Wundt W., 1902. Physiologische Psychologie. Engelmann, Leipzig.

Yamazaki T., Kamijo K., Kenmochi A., Fukuzumi S., Kiyuna T., Kuroiwa Y., 2000. Multiple equivalent current dipole source localization of visual event-related potentials during oddball paradigm with motor response. Brain Topography, 12(3), 159–175.

Yordanova J., Kolev V., 1997. Effects of task variable on the amplitude and phase-locking of auditory gamma band responses in human. International Journal of Neuroscience, 92(3), 241–258.

Yordanova J., Kolev V., Demiralp T., 1997. The phase-locking of auditory gamma band responses in humans is sensitive to task processing. NeuroReport, 8, 3999–4004.

Zschocke S., 1995. Klinische Elektroenzephalographie. Springer, Berlin.

Autorenindex

Sachindex

Kumulierte Zeitschriftenartikel

Im Folgenden sind die kumulierten Zeitschriftenartikel abgedruckt.

1. C. S. Herrmann, A. Mecklinger & E. Pfeifer:
   Gamma responses and ERPs in a visual classification task. *Clinical Neurophysiology*, 110(4):636–642, 1999.
   Mit freundlicher Genehmigung von Elsevier Science

2. C. S. Herrmann & A. Mecklinger:
   Gamma activity in human EEG is related to high-speed memory comparisons during object selective attention. *Visual Cognition*, 8(3/4/5):593–608, 2001.
   Mit freundlicher Genehmigung von Psychology Press Limited, Hove (UK)

3. C. S. Herrmann & A. Mecklinger:
   Magnetoencephalographic responses to illusory figures: Early evoked gamma is affected by processing of stimulus features. *International Journal of Psychophysiology*, 38(3):265–281, 2000.
   Mit freundlicher Genehmigung von Elsevier Science

4. M. A. Elliott, C. S. Herrmann, A. Mecklinger & H. J. Müller:
   The loci of oscillatory visual-object priming: a combined electroencephalographic and reaction-time study. *International Journal of Psychophysiology*, 38(3):225–242, 2000.
   Mit freundlicher Genehmigung von Elsevier Science

5. A. C. N. Chen & C. S. Herrmann:
   Perception of pain coincides with the spatial expansion of human EEG dynamics. *Neuroscience Letters*, 297(3):183–186, 2001.
   Mit freundlicher Genehmigung von Elsevier Science

6. C. S. Herrmann:
   Human EEG responses to 1–100 Hz flicker: Resonance phenomena in visual cortex and their potential correlation to cognitive phenomena. *Experimental Brain Research*, 137:345–353, 2001.
   Mit freundlicher Genehmigung des Springer Verlags, Heidelberg

ELSEVIER

Clinical Neurophysiology 110 (1999) 636–642

Gamma responses and ERPs in a visual classification task

Christoph S. Herrmann*, Axel Mecklinger, Erdmut Pfeifer

Max-Planck-Institute of Cognitive Neuroscience, Postfach 500 355, 04303 Leipzig, Germany

Accepted 20 November 1998

Abstract

Objective: We examined event-related potentials (ERPs) and gamma range EEG activity in a visual classification task to assess which variables affect these responces.

Methods: Ten subjects silently counted the occurrence of rare Kanizsa squares (targets) among Kanizsa triangles and non-Kanizsa figures (standards). By applying a time-frequency analysis to the data and selectively calculating topographical maps of certain frequencies.

Results: We were able to find 3 different types of gamma responses to Kanizsa figures: an early phase-locked gamma response at 40 Hz in the N100 time range, late phase-locked gamma activity (200–300 ms) at 40 Hz and a continuous phase-locked gamma response at 80 Hz due to the monitor refresh frequency. The two 40 Hz responses were significantly higher for Kanizsa figures than for non-Kanizsa figures and within the Kanizsa figures were higher for the target figure than for the non-target.

Conclusion: The phase-locking of these two responses, previously found also as non-phase-locked activity, could be synchronized due to the monitor flicker frequency. Also, our findings suggest that the gamma responses are not solely associated with the binding of stimulus features, but reflect some processes related to target processing.

Keywords: Binding; Evoked potentials; Illusory contours; Kanizsa figures; Phase locking; Wavelet transform

1. Introduction

Currently, many investigations in cognitive neuroscience tackle the aspects of brain activity associated with binding multiple features together to form one coherent object. Synchronization of neuronal responses could in principle achieve this task (von der Malsburg and Schneider, 1986; Singer, 1993). Frequencies in the gamma range (γ) are believed to give a clue to which cortical areas are involved in the representation of the binding processes, since they have been found in single-cell studies with animals (Gray and Singer, 1989; Engel et al., 1992), as well as in scalp-recorded EEG of human subjects (Tallon-Baudry et al., 1997). While Jürgens et al. (1995) argued that γ responses are sometimes merely harmonics of changes in the α frequency band (8–12 Hz), Pulvermüller et al. (1995) found γ responses that discriminated between words and psuedo-words and found no evidence of correlation to power changes outside the γ range. A review and classification of γ band activity demonstrates the psychophysiological correlates and functional significance of these responses (Başar-Eroglu et al., 1996). Such γ frequencies can be found phase-locked (Tallon et al., 1995) and non-phase-locked to the onset of experimental stimuli (Eckhorn et al., 1990; Tallon-Baudry et al., 1996). Psychophysical experiments have recently shown that flickering stimuli in the gamma range can enhance visual binding (Elliott and Müller, 1998), providing further evidence for the relevance of γ activity for binding processes. In that study, Kanizsa-like figures had to be detected and reaction times significantly decreased when the targets were pre-attentively flickering at a frequency of 40 Hz prior to the detection period, as compared to other flickering frequencies.

In our experiment, 10 subjects silently counted the occurrence of rare Kanizsa squares (targets) among 3 types of standards – Kanizsa triangles, triangular non-Kanizsa figures and rectangular non-Kanizsa figures. In order to detect γ activity, a time-frequency analysis based on a wavelet transform was employed. The wavelet approach for the time-frequency analysis of electrophysiological signals has proven very efficient (Schiff et al., 1994; Halgamuge et al., 1996; Herrmann and Reine, 1996 ; Herrmann, 1997). Recently, some researchers have applied the technique of wavelet transforms for viewing time-frequency details of ERPs (Tallon-Baudry et al., 1997). In addition to computing the time-frequency planes, we extracted frequency bands from it for subsequent generation of topographical maps for certain frequencies.

* Corresponding author. Tel.: + 49-341-9940250; fax: + 49-341-9940113.

E-mail address: herrmann@cns.mpg.de (C.S. Herrmann)

1388-2457/99/$ - see front matter CLINPH 98727

PII: S1388-2457(99)00002-4

Fig. 1. The 4 stimulus types used in the experiment: (a) Kanizsa square (target), (b) Kanizsa triangle, (c) non-Kanizsa triangle, (d) non-Kanizsa square.

2. Methods

2.1. Subjects

Ten subjects with a mean age of 24.3 years (ranging from 20 to 35 years, 6 female) participated in the study. All subjects were right-handed and had normal or corrected-to-normal vision. They showed no signs of neurological or psychiatric disorders and all gave written informed consent.

2.2. Stimuli

As in the experiments of Tallon-Baudry et al. (1996), we used Kanizsa figures as stimulus material. According to Tallon-Baudry et al. (1996), it is advantageous to use a Kanizsa target which is different from the Kanizsa figure under investigation because this procedure allows us to evaluate the processing of Kanizsa figures while keeping the target shape different from the investigated one. We used the stimuli shown in Fig. 1. The stimuli consisted of either 3 or 4 pac-men and either constituted an illusory figure (Fig. 1a,b) or not (Fig. 1c,d).

The stimuli were presented for 700 ms with randomized inter-stimulus-intervals ranging from 1000 to 1500 ms. Figures were displayed together with a centered fixation cross on a computer monitor placed 1 m in front of the subjects. Subjects were instructed to count the appearances of the Kanizsa-squares. The experiment was run in four blocks with 100 stimuli per block. The 4 stimulus types were presented as equally probable in a pseudo-randomized order, resulting in a target probability of 0.25.

2.3. Data acquisition

The EEG was recorded with Neuro Scan amplifiers using 64 tin electrodes mounted in an elastic cap. Electrodes were placed according to the international 10–10 system. The ground electrode was C2 and all electrodes were referenced to the left mastoid (M1). Electrode impedance was kept below 5 kΩ. Horizontal and vertical EOG were registered with 4 additional electrodes. Data were sampled at 500 Hz and analog-filtered with a 0.05 Hz high-pass and a 100 Hz low-pass filter.

Averaging epochs lasted from 200 ms before to 900 ms after stimulus onset. All epochs were visually inspected for artifacts and rejected if eye-movement artifacts or electrode drifts were visible. Baselines were computed in the −200 ms to 0 ms interval in each single trial and subtracted prior to computing the ERP averages.

2.3.1. Data analysis

In order to compute a wavelet transform, the original signal is convolved with a so-called wavelet. In case of the Morlet wavelet used here, it is calculated according to

$$\Psi(t) = e^{j\omega_0 t} e^{-t^2/2} \tag{1}$$

which leads to sinusoidal waveforms. These wavelets can be compressed by a scaling factor a and shifted in time by a parameter b. Convolving the signal and the shifted and dilated wavelet leads to a new signal

$$s_a(b) = \frac{1}{\sqrt{a}} \int \bar{\Psi}\left(\frac{t-b}{a}\right) x(t)dt \tag{2}$$

where $\bar{\Psi}$ is the conjugate of the complex wavelet and $x(t)$ is the original signal. These new signals $s_a(b)$ are computed for different scaling factors a and are displayed as colored lines in a diagram where the color represents the amplitude of $s_a(b)$ (cf. Fig. 4).

To represent phase-locked activity, the wavelet transform of the average over the single trials (WTAv) is computed. Since the wavelet transform returns complex numbers, the absolute values are calculated.

$$\mathrm{WTAv} = \left|\frac{1}{\sqrt{a}} \int \bar{\Psi}\left(\frac{t-b}{a}\right) \frac{1}{n} \sum_{i=1}^{n} x_i(t)dt\right| \tag{3}$$

This time-frequency representation contains only that part of the activity which is phase-locked to stimulus onset. In order to also compute the activity which is not phase-locked to stimulus onset and therefore cancels out in the average, we calculate the sum of all activity. To calculate the sum of all activity, the absolute values of the wavelet transforms of the single trials are averaged (AvWT).

$$\mathrm{AvWT} = \frac{1}{n} \sum_{i=1}^{n} \left|\frac{1}{\sqrt{a}} \int \bar{\Psi}\left(\frac{t-b}{a}\right) x_i(t)dt\right| \tag{4}$$

This new time-frequency representation contains all activity that occurred after stimulus onset, no matter whether it was phase-locked to the stimulus or not. The difference of this sum of activity and the phase-locked activity (AvWT-WTAv) yields the non-phase-locked activity. A derivation of the publicly available wavelet toolbox UVI-Wave (the UVI-Wave package for use with MATLAB® can

be downloaded from http://www.tsc.uvigo.es/~wavelets/uvi_wave.html) running under MATLAB® was used in our approach.

In order to generate maps of γ activity, we extracted the 40 Hz and the 80 Hz frequencies out of the time-frequency maps. The topographical distribution of these signals can be displayed using a linear interpolation method, as for ERP averages. Color coding is blue for close-to-zero values and red for close-to-maximum values.

In order to avoid a loss of statistical power that is inherent when repeated measures ANOVAs are used to quantify multi-channel EEG data (Oken and Chiappa, 1986), selected electrode sites were pooled to 6 topographical regions of interest (ROIs) (Mecklinger and Pfeifer, 1996). According to Homan et al. (1987) who set out to establish a correspondence between electrode placements and the underlying cerebral region, the anterior region is approximately over Brodmann areas 45 and 46. The central region can approximately be located over Brodmann areas 1–4 and the posterior region overlies Brodmann areas 17–19, 37 and 39. The regions included the following electrodes which are shaded in gray in Fig. 2. Left anterior region (LAR): FP1, AF7, AF3, F7, F3 and F5. Left central region (LCR): FT7, FC3, T7, C5, C3 and CP5. Left posterior region (LPR): P7, P5, P3, PO7, PO3 and O1. Regions over the right hemisphere included the homologous electrodes. For statistical analyses ERP amplitudes were pooled across the electrodes in each of the ROIs. ERP components were defined as mean amplitudes in the following time intervals: 30–60 ms (N20), 70–110 ms (P50), 130–180 ms (N100) and 300–500 ms (P300).

3. Results

All of the subjects performed well on the detection of the Kanizsa squares. The mean error rate was 2.3% (SD 4.8%). One of the subjects showed strong technical artifacts in several electrodes and had to be excluded from further analysis.

3.1. ERPs

As apparent from Fig. 3, showing the grand average ERPs for all 4 conditions at selected electrodes, all stimuli evoked the typical visual N20, P50 and N100 ERP responses, as shown in Fig. 3. The target condition (Kanizsa square) also evoked a very prominent P300 with a parietal maximum. There is another N100 visible at approx. 800 ms due to pattern-offset (Fig. 3). The close-up of electrode P4 shows a very early differentiation between square and triangular form (N20), as well as a later differentiation between Kanizsa figures and non-Kanizsa figures (N100).

Repeated-measures ANOVAs with factors topography (anterior, central, posterior), hemisphere (left, right), form (3 pac-men vs. 4 pac-men) and figure (illusory, non) were conducted to assess the effects of the experimental variables on a variety of dependent variables.

In the N20 time interval, the ANOVA yielded a significant effect of form ($F(1,8) = 5.98$, $P < 0.05$). Square figures elicited a higher N20 than the triangular ones. No significant effect was found for the figure factor. In the time interval of the P50, no significant effects of figure or form were found. For the N100, the ANOVA yielded an interaction between topography and figure ($F(2,16) = 17.85$, $P < 0.001$). A post-hoc analysis showed significant effects of figure for the two posterior ROIs (LPR: $F(1,8) = 7.75$, $P < 0.05$, RPR: $F(1,8) = 16.33$, $P < 0.005$), but not for the remaining ROIs. The N100 was more negative for the two Kanizsa figures than for the two non-Kanizsa figures. For the P300, the ANOVA yielded effects of figure ($F(1,8) = 12.66$, $P < 0.01$), and form ($F(1,8) = 7.02$, $P < 0.05$) and an interaction figure × form ($F(1,8) = 17.20$, $P < 0.005$), indicating that P300 was largest for the Kanizsa square (target).

3.2. 40 Hz (γ_1)

Fig. 4 shows the average phase-locked time-frequency diagram for electrode FC4 over all subjects. For sake of simplicity, we will call the oscillations at 40 Hz γ_1 and those at 80 Hz γ_2 in the following. Three main γ responses can be identified. Between 50 and 150 ms a phase-locked 40 Hz component is visible (which we will call early γ_1 component), between 200 and 300 ms another phase-locked 40 Hz component (late γ_1) emerges and spurious 80 Hz activity is intermittently present over the whole interval (γ_2).

The grand average ($n = 9$) topography of the early phase-locked γ_1 response in the interval 50–150 ms is shown in Fig. 5. The early γ_1 response shows a significant main effect for figure ($F(1,8) = 5.65$, $P < 0.05$), indicating higher γ_1 oscillations for the Kanizsa figures than for non-Kanizsa figures. Moreover, there is an interaction figure × form ($F(1,8) = 14.55$, $P < 0.01$), indicating that γ_1 activity was higher for the Kanizsa square (target) than the other non-target conditions. The topographical distribution of this early γ_1 response is illustrated in Fig. 5.

Fig. 6 shows the topography of the late phase-locked γ_1 response. An ANOVA yielded a significant main effect of figure ($F(1,8) = 7.13$, $P < 0.05$), indicating that late γ_1 activity is higher for the two Kanizsa figures than for the two non-Kanizsa figures. As in the early time interval, there is an interaction figure × form ($F(1,8) = 8.46$, $P < 0.05$), reflecting the stronger activity for the target within the Kanizsa figures. In addition, the ANOVA yielded a significant effect for the factor topography ($F(1,8) = 4.05$, $P < 0.05$), indicating the decreasing amount of activity in posterior regions, irrespective of condition.

An ANOVA was also performed for the sum of γ_1 activity (AvWT), obtained from single trials, including phase-locked and non-phase-locked oscillations. This analysis did

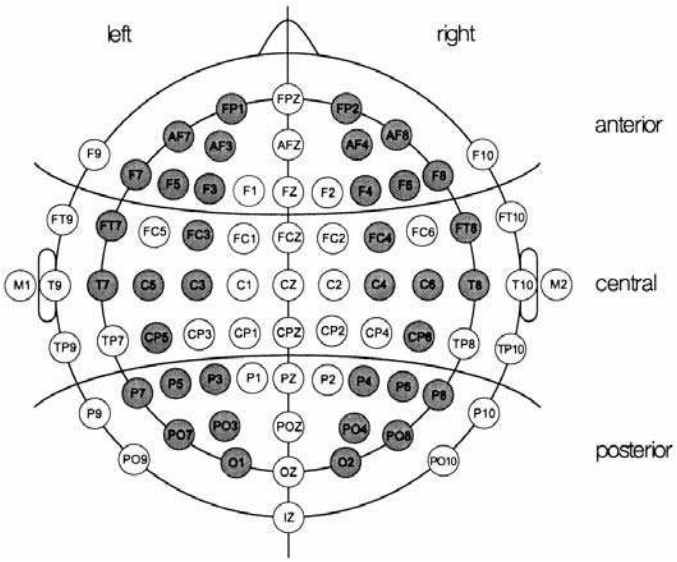

Fig. 2. Six regions of interest (left anterior, right anterior, left central, right central, left posterior and right posterior), as indicated by the shaded electrodes.

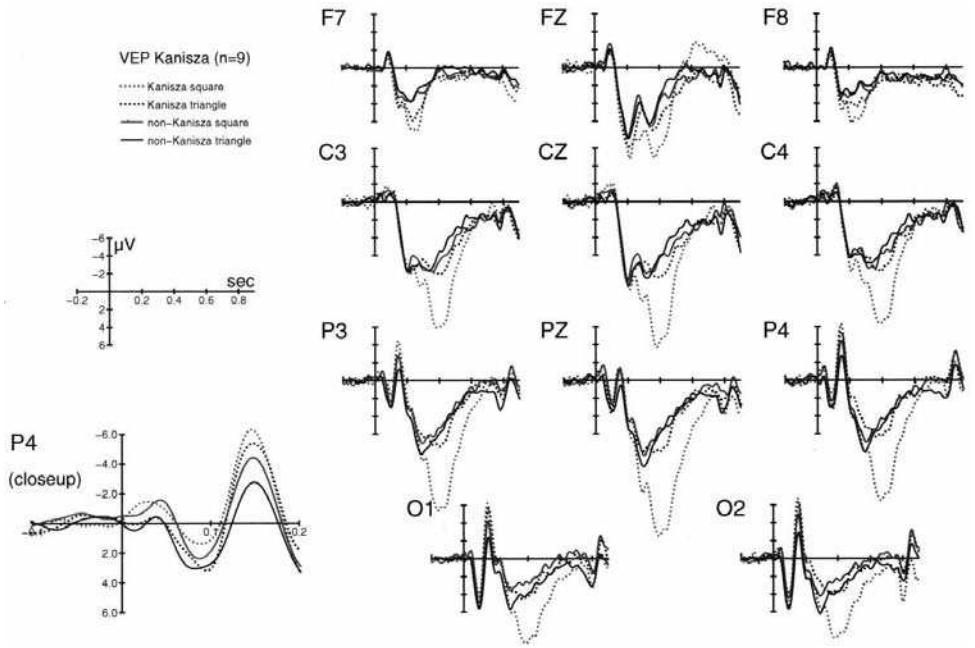

Fig. 3. Twenty-five Hz low-pass filtered evoked response potentials showing N20, P50 and N100 components for all conditions and a P300 for the target (Kanizsa square).

not reveal any significant results including the form or figure factors, neither in the early nor in the late time interval.

3.3. 80 Hz (γ_2)

As apparent from Fig. 4, there were evoked gamma responses in the cortex around 80 Hz. The activity appeared during the whole experiment, as well as during the stimulus presentation intervals, and during the inter stimulus intervals (cf. Fig. 4). An ANOVA yielded no significant differences between conditions. Fig. 7 shows the occipital topography for the whole stimulus presentation time. This

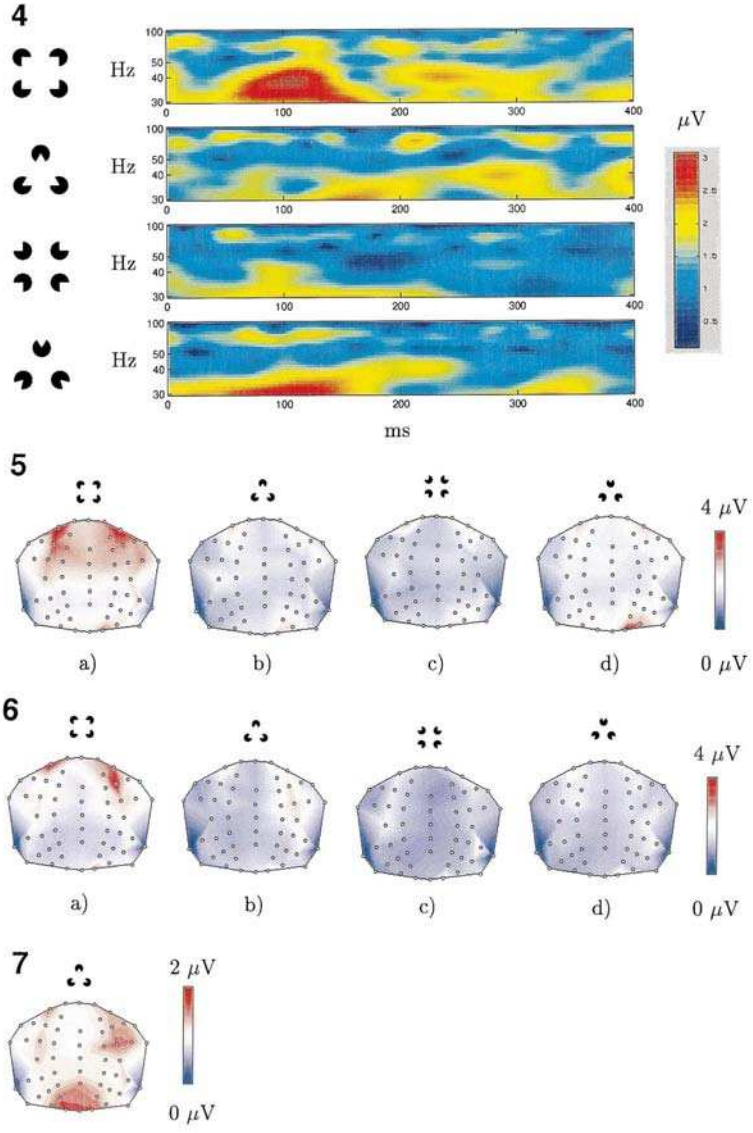

γ_2 activity corresponds to monitor-induced steady-state potentials which are known to be evoked by external flickering stimuli (Lyskov et al., 1998).

4. Discussion

Our ERP results are consistent with the view that visual stimulus properties are being processed in two stages. In a first stage, purely physical stimulus properties like changes in illumination play the dominant role. This is reflected in the amplitude of the N20 (30–60 ms) which is higher for the squares as compared to the triangles. We argue that this is due to the fact that four pac-men, when flashed onto the screen, lead to a greater change in overall brightness than only three of them. In a later stage, Gestalt-like properties that emerge from binding individual elements seem to become more relevant, as revealed by the N100 amplitude, which is higher for Kanizsa than for non-Kanizsa figures. This amplitude difference might be related to an increased perceived brightness as a result of the illusory contours, as reported by Lesher (1995). In addition, it is known that unexpected or novel stimuli also evoke higher N100 amplitudes (Altenmüller, 1993. This makes it plausible to expect the targets to evoke the highest N100 amplitude, which we in fact did find.

Consistent with a large variety of previous studies (Mecklinger and Ullsperger, 1993), the rare target stimuli elicited largest P300 amplitudes.

Concerning the γ responses, our results show similarities as well as differences to the results of Tallon-Baudry and colleagues (Tallon et al., 1995; Tallon-Baudry et al., 1996, 1997, 1998). Consistent with Tallon et al. (1995) we found early and late phase-locked γ_1 activity which was more pronounced for Kanizsa figures than for non-Kanizsa figures. Our results reveal that this activity is also larger for targets than for non-targets. The early differentiation of targets and non-targets around 100 ms is consistent with ERP findings revealing evidence for attentional modulation of automatic perceptual processes in this time interval (LaBerge, 1997) and a study showing pronounced increase of phase-locked γ activity in an auditory oddball task before 80 ms after stimulus onset (Fell et al., 1997). In contrast to Tallon-Baudry et al. (1996), no late non-phase-locked γ_1 activity to Kanizsa figures was obtained in the present study. Similarly, in a recent study using MEG recording, the late non-phase-locked γ_1 response to Kanizsa figures was also not obtained (Tallon-Baudry et al., 1997). According to these findings, it seems as if the phase-locked oscillations are more salient during the processing of Kanizsa figures than are the non-phase-locked. Which factors, however, do influence the phase-locking of this late γ_1 response?

From photic driving experiments it is known that external visual stimulation at a certain frequency can evoke steady-state-responses over human occipital cortex (Chiappa, 1997). In addition, it has been shown that the existence of synchronized activity can significantly influence ERP components and reaction times (Haig and Gordon, 1998). Psychophysical experiments have recently shown that stimuli flickering in the gamma range can even enhance visual binding. In an experiment by Elliott and Müller (1998), priming stimuli that flickered at 40 Hz led to a reduction of the subjects' reaction times in detecting Kanizsa-like illusory figures relative to priming stimuli flickering at frequencies higher or lower than 40 Hz. Taken together, these findings lead to the assumption that it may be possible to influence neural processes by external stimulus frequencies.

In our experiment, we used a monitor with a refresh rate of 75 Hz, which is approximately twice the hypothesized binding frequency. Consistent with studies that show that even slightly flickering stimuli, such as a computer monitor, evoke steady-state-potentials over human visual cortex (Lyskov et al., 1998), it can be assumed that the 75 Hz monitor flicker evoked a γ_2 steady-state potential focused occipitally over the visual cortex, independent of the experimental conditions. It is conceivable that the neural circuits that tend to oscillate at an innate frequency near the subharmonic of 37.5 Hz are being synchronized by the external stimulation, i.e. their phase-locking increases. Due to this state of resonance, the monitor flicker under these circumstances does enhance internal oscillations, once they are initiated by other processes assumed to be related to binding. In our experiment, the presentation of the stimuli was time-locked to the monitor screen refresh, so the stimulus onsets were always in phase with the induced γ_2 oscillation. This might have led to the observed phase-locking of the γ_1 activity, which was maintained for several hundred milliseconds due to the external synchronization. It may be possible that the condition specific γ_1 responses are synchronized by the unspecific γ_2 activity.

To make sure that the γ responses are not merely harmonics of activity in the alpha-band as argued by Jürgens et al. (1995), we analyzed the alpha-band but did not find any corresponding changes in amplitude. In the unfiltered ERP

Fig. 4. Average of the phase-locked time-frequency planes (WTAvs) for electrode FC4 over 9 subjects.
Fig. 5. Topography of the early phase-locked γ_1 activity for the conditions Kanizsa square (a), Kanizsa triangle (b), non-Kanizsa square (c) and non-Kanizsa triangle (d) in the time interval 50–150 ms averaged over 9 subjects.
Fig. 6. Topography of the late phase-locked γ_1 activity for the conditions Kanizsa square (a), Kanizsa triangle (b), non-Kanizsa square (c) and non-Kanizsa triangle (d) in the time interval 200–300 ms averaged over 9 subjects.
Fig. 7. Topography of the phase-locked γ_2 activity for the condition Kanizsa-triangle averaged over 9 subjects for the whole time interval of stimulus presentation (0–700 ms).

averages, clear bursts of γ activity appear on top of the N100 peak, comparable to the finding of Pantev (1995), and also at the onset of the P300.

In addition to the larger γ_1 responses for the two conditions in which Kanizsa figures were present, we also found more pronounced γ_1 responses to Kanizsa targets than Kanizsa non-targets in the early (50–150 ms) and in the late (200–300 ms) time interval. Since both γ_1 responses showed either a widespread or even mainly anterior scalp topography, it is reasonable to assume that they are not solely associated with the binding of stimulus features, a process which should be dominant in cortical areas engaged in perceptual processing. Since the γ_1 response extends to 300 ms, a time period in which stimulus classification and target detection occur, it is not unlikely that the late γ_1 response reflects some processes related to target processing such as detection of the task-relevant features or initiation of the counting response. Further experimentation will be required to get a more detailed picture of functional significance of early and late phase-locked γ_1 responses.

References

Altenmüller E. Psychophysiology and EEG. In: Niedermeyer E, Lopes da Silva F, editors. Electroencephalography, Basic Principles, Clinical Applications and Related Fields, Baltimore, MD: William and Wilkins, 1993. pp. 597.

Başar-Eroglu C, Strüber D, Schürmann M, Stadler M, Başar E. Gamma-band responses in the brain: a short review of psychophysiological correlates and functional significance. Int J Psychophysiol 1996;24:101–112.

Chiappa K. Evoked potentials in clinical medicine. Philadelphia: Lippincott-Raven, 1997.

Eckhorn R, Dicke P, Kruse W, Reitböck H. Stimulus-related facilitation and synchronization among visual cortical areas: experiments and models. In: Schuster H, Singer W, editors. Non-linear dynamics and neural networks, Weinheim: VCH, 1990. pp. 57.

Elliott M, Müller H. Synchronous information presented in 40 Hz flicker enhances visual feature binding. Psycholog Sci 1998;9(4):277–283.

Engel A, König P, Kreiter A, Schillen T, Singer W. Temporal coding in the visual cortex: new vistas on integration in the nervous system. Trends Neurosci 1992;15(6):218–226.

Fell J, Hinrichs H, Roschke J. Time course of human 40 Hz EEC activity accompanying P3 responses in an auditory oddball task. Neurosci Lett 1997;235(3):121–124.

Gray C, Singer W. Stimulus-specific neuronal oscillations in orientation columns of cat visual cortex. Proc Natl Acad Sci USA 1989;86:1698–1702.

Haig A, Gordon E. Prestimulus EEC alpha phase synchronicity influences N100 amplitude and reaction time. Psychophysiol 1998;35:591–595.

Halgamuge S, Herrmann C, Jain L. Analysis of EEC signals with wavelets and knowledge engineering techniques. In: Amari S, Xu L, Chan L-W, King I, Leung KS, editors. Progress in neural information processing, 2. Berlin: Springer, 1996. pp. 1381.

Herrmann C. Wavelet networks for EEC analysis. In: Zimmermann HJ, editor. European congress on fuzzy and intelligent technologies (EUFIT), Mainz: Wissenschaftsverlag, 1997. pp. 443.

Herrmann C, Reine F. Wavelet transform as feature extraction for medical diagnosis of EEGs. In: Jamshidi M, Fathi M, Pierrot F, editors. Soft computing with industrial applications, 5. Albuquerque: TSI Press, 1996. pp. 313.

Homan R, Herman J, Purdy P. Cerebral location of international 10-20 system electrode placement. Electroenceph clin Neurophysiol 1987;66:376–382.

Jürgens E, Rösler F, Henninghausen E, Heil M. Stimulus-induced gamma oscillations: harmonics of alpha activity. Neuroreport 1995;(6):813–816.

LaBerge D. Attention, awareness, and the triangular circuit, Consciousness Cognition 1997;6:149–181.

Lesher C. Illusory contour formation. In: Arbib M, editor. Handbook of brain theory and neural networks, Cambridge, MA: MIT Press, 1995. pp. 481.

Lyskov E, Ponomarev V, Sandström M, Mild K, Medvedev S. Steady-state visual evoked potentials to computer monitor flicker. Int J Psychophysiol 1998;28:285–290.

Mecklinger A, Pfeifer E. Event-related potentials reveal topographical and temporal distinct neuronal activation patterns for spatial and object working memory. Cog Brain Res 1996;4:211–224.

Mecklinger A, Ullsperger P. P3 varies with stimulus categorization rather than probability. Electroenceph clin Neurophysiol 1993;86:395–407.

Oken B, Chiappa K. Statistical issues concerning computerized analysis of brainwave topography. Ann Neurol 1986;19:493–494.

Pantev C. Evoked and induced gamma-band activity of the human cortex. Brain Topogr 1995;7(4):321–330.

Pulvermüller F, Lutzenberger W, Preissi H, Birbaumer N. Spectral responses in the gamma-band physiological signs of higher cognitive processes. Neuroreport 1995;6(15):2059–2064.

Schiff S, Aldroubi A, Unser M, Sato S. Fast wavelet transformation of EEG. Electroenceph clin Neurophysiol 1994;91:442–455.

Singer W. Synchronization of cortical activity and its putative role in information processing and learning. Ann Rev Physiol 1993;55:349–374.

Tallon C, Bertrand O, Bouchet P, Pernier J. γ-range activity evoked by coherent visual stimuli in humans. Eur J Neurosci 1995;7:1285–1291.

Tallon-Baudry C, Bertrand O, Delpuech C, Pernier J. Stimulus specificity of phase-locked and non-phase-locked 40 Hz visual responses in human. J Neurosci 1996;16(13):4240–4249.

Tallon-Baudry C, Bertrand O, Peronnet F, Pernier J. Induced (-band activity during the delay of a visual short-term memory task in humans, . J. Neurosci. 1998;18(11):4244–4254.

Tallon-Baudry C, Bertrand O, Wienbruch C, Ross B, Pantev C. Combined EEG and MEG recordings of visual 40 Hz responses to illusory triangles in human. Neuroreport 1997;8:1103–1107.

von der Malsburg C, Schneider W. A neural cocktail party processor. Biol Cybern 1986;54:29–40.

VISUAL COGNITION, 2001, *8* (3/4/5), 593–608

Gamma activity in human EEG is related to high-speed memory comparisons during object selective attention

Christoph S. Herrmann and Axel Mecklinger

Max-Planck Institute of Cognitive Neuroscience, Leipzig, Germany

Among the most important processes of the brain in order to correctly perceive the outside world and act within it are binding, attention, and memory. All three functional mechanisms have been associated with brain activity in the gamma frequency range. It needs to be clarified, however, which subprocesses within the gamma frequency range relate to which perceptual or cognitive functions. In a visual discrimination task, we used Kanizsa figures whose constituent inducer disks need to be bound together to perceive the illusory contours. By a variation of the task requirements we manipulated the allocation of object selective attention as compared to a previous study. One out of four objects had to be detected. This detection process requires the comparison of two object dimensions (form and collinearity) with a working memory template. In order to get behavioural and electrophysiological measures, EEG and reaction times were recorded from 16 and 10 subjects, respectively. We demonstrated that the early evoked gamma activity reflects the process of allocating attention to a selected object as early as 50–150 ms after stimulus onset. We propose that the underlying mechanism is a high-speed memory comparison. In addition, we show that this early gamma activity also determines the reaction times needed to respond to the different stimuli.

INTRODUCTION

Binding and attention are both necessary for the correct function of perceptual processes in the brain. Binding is necessary to link together the different features of single objects that are represented in a distributed fashion in the brain.

Please address all correspondence to C. Herrmann, Max-Planck Institute of Cognitive Neuroscience, PO Box 500 355, 04303 Leipzig, Germany. Email: herrmann@cns.mpg.de

We would like to thank Mark A. Elliott for his editorial work and three anonymous referees for valuable comments on an earlier version of this manuscript. We also express our thanks to Diana Böttger who helped to prepare the experimental set up, to Cornelia Schmidt for collecting the data, and to Andrea Sandmann who helped to design the figures. Diana Böttger was partly supported by DFG grant SCHR 375/8-1.

http://www.tandf.co.uk/journals/pp/13506285.html DOI:10.1080/13506280143000142

The mechanism of attention serves to focus onto a small subset of the vast amount of incoming information. It is still unclear how exactly these two mechanisms operate or interact. Binding is believed to operate at a very early stage in human information processing. According to the temporal correlation hypothesis, the simultaneous firing of neurons indicates that they code features of the same object (Singer & Gray, 1995; von der Malsburg & Schneider, 1986). Electrophysiological studies on humans and animals show strong evidence that brain activity in the gamma frequency range (approximately 30–80 Hz, mostly 40 Hz) could be the correlate of feature binding (Gray, König, Engel, & Singer, 1989; Tallon-Baudry & Bertrand, 1999). Nevertheless, it has been questioned whether gamma activity in the human electroencephalogram (EEG) really reveals processes of feature binding or rather relates to memory access (Pulvermüller, Keil, & Elbert, 1999).

If binding elicits gamma activity in the brain it seems plausible to assume that stimuli which oscillate at a frequency in the gamma range result in enhanced processing by the brain. This lead to an experiment of Elliott and Müller (1998) who demonstrated that stimuli flickering in the gamma range can enhance visual binding. In that study, Kanizsa-like figures had to be detected and reaction time (RT) significantly decreased when target-relevant cues were preattentively flickering at a frequency of 40 Hz prior to the detection period, as compared to other flickering frequencies. Further investigation by Elliott and Müller (2000) with the same paradigm has revealed that an object representation persisted with a 40 Hz oscillatory code for several hundred milliseconds. These findings are in line with previous results about high-speed memory processes in the same frequency range: Jensen and Lisman (1998) demonstrated in simulations that high-speed access to working memory may operate at frequencies in the gamma range, and Burle and Bonnet (2000) performed an auditory interference task suggesting an oscillatory process in working memory. The paradigm of Elliott and Müller also evokes gamma oscillations in the human EEG that determine the enhanced processing when target-relevant cues are presented (Elliott, Herrmann, Mecklinger, & Müller, 2000).

Gamma activity has not only been correlated with binding and memory, but there is also evidence that the same type of activity correlates with attention (Başar-Eroglu, Strüber, Schürmann, Stadler, & Başar, 1996; Müller, Gruber, & Keil, 2000; Tiitinen et al., 1993). In a recent EEG-experiment, Herrmann, Mecklinger, and Pfeiffer (1999) showed that an early gamma response in a visual discrimination task was larger for target stimuli than for non-target stimuli. In that experiment, Kanizsa squares and triangles (Kanizsa, 1976) as well as non-Kanizsa squares and triangles were visually presented to the subjects. The four different stimuli (Figure 1) were comprised of the two features form (3 vs. 4 inducer disks) and collinearity (presence/absence of an illusory Kanizsa figure due to collinear arrangement of the inducer disks). The authors formulated

(a) (b) (c) (d)

Figure 1. The four stimulus types used in the experiment: (a) Kanizsa square, (b) Kanizsa triangle, (c) non-Kanizsa square (target), and (d) non-Kanizsa triangle.

the hypothesis that the target effect of the early gamma activity was reflecting an attentional top-down process of stimulus selection.

The objective of the present experiments was to further investigate the possibility of early gamma activity reflecting a process of object-selective attention. Especially, we wanted to investigate how such a process operates and interacts with working memory. In our experiments, we used the identical four stimuli used in the study of Herrmann et al. (1999) but changed the task requirements for the subjects. Whereas Herrmann et al. (1999) used the Kanizsa square as the target, we here defined the non-Kanizsa square as the target that had to be counted. If the assumption is true, that the early gamma activity reflects an attentional process of object selection, it should be largest for the non-Kanizsa square in our new experiment. The amplitude of the visual N170 (negative deflection around 170 ms) was assumed to reflect physical and perceptual properties of the stimuli in the experiment of Herrmann et al. (1999). If this is true, the order of N170 amplitude for the four stimuli should not change in our new experiment. The event-related potential P300 (positive deflection around 300 ms) is known to reflect attentional mechanisms and to be maximal in response to infrequent targets (Donchin & Coles, 1988; Mecklinger & Ullsperger, 1993). Thus, the P300 should also be largest for the non-Kanizsa square. In order to gain additional insights in the attentional mechanism engaged in object selection, we also recorded RTs from another group of subjects performing the same task.

In a previous experiment with the four previously-mentioned stimuli, in which MEG and RTs were recorded simultaneously, Herrmann and Mecklinger (2000) demonstrated that targets (Kanizsa squares) were processed slowest even though they constituted a Kanizsa figure, whereas faster non-targets did not constitute Kanizsa figures. The RT pattern suggested a two-fold mechanism of comparing the two dimensions form and collinearity of an encoded stimulus with a pattern held in working memory. The stimulus which was most dissimilar to the target (non-Kanizsa triangle) was processed fastest in their experiment. In our new experiment, we defined the non-Kanizsa square as the target and expected it to be processed slowest, whereas we expected the most dissimilar stimulus (Kanizsa triangle) to be processed fastest.

METHODS

In our EEG experiment, subjects had to count the occurrence of target stimuli among non-target stimuli. This made the experiment comparable to the one of Herrmann et al. (1999) and keeps EEG responses free from motor artefacts. In order to also acquire behavioural measures of the task, we conducted an additional reaction-time experiment (RT experiment). In the RT experiment subjects had to respond with their right index finger to targets and with their left index finger to non-targets, yielding RTs and error measures under stimulation conditions identical with the EEG experiment.

Subjects

Sixteen subjects with a mean age of 22.6 years (ranging from 18 to 26 years, 7 female) participated in the EEG experiment and ten subjects with a mean age of 23.1 years (ranging from 19 to 31 years, 7 female) participated in the RT experiment. All subjects were right-handed and had normal or corrected-to-normal vision. They showed no signs of neurological or psychiatric disorders and all gave written informed consent to participate in the study.

Stimuli

The stimuli used in this paradigm were composed of three or four inducer disks, which either constitute a Kanizsa figure due to their collinear arrangement (Figure 1a and b) or don't constitute one (Figure 1c and d). The stimuli were identical to those of Herrmann et al. (1999) and varied across two dimensions, which we will refer to as form and collinearity dimension. The dimension "form" determines whether a stimulus is composed of three or four inducer disks, whereas the dimension "collinearity" determines whether a stimulus constitutes a Kanizsa figure due to the collinear arrangement of its inducer disks.

The stimuli were presented for 700 ms with randomized intertrial-intervals ranging from 1000 to 1500 ms. Figures were displayed in black together with a black central fixation cross on white background. Stimuli subtended a visual angle of 4°17' including inducer disks, while the induced illusory figures subtended 2°86' (Figure 2). Thus, the whole stimulus is projected into the field of central vision, i.e., the central 5 degrees of the macular region (Zeki, 1993). Fixation crosses were displayed foveally (0.02°). The ratio of the radius of the inducer disks and the side-length of the illusory figures was 1:4.

Figures were displayed on a computer monitor placed 1 m in front of the subjects. Subjects were instructed to silently count the appearance of the non-Kanizsa square (targets). The experiment was run in four blocks with 100 stimuli per block. The four stimulus types were presented equally probable in a pseudo-randomized order resulting in a target probability of .25.

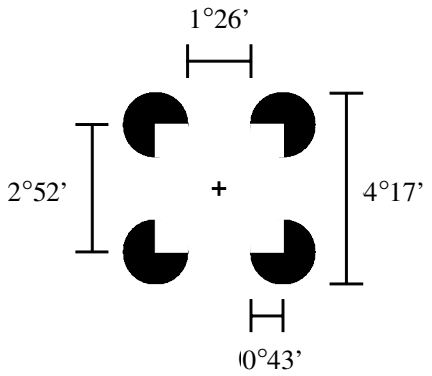

Figure 2. Size of the used stimuli in visual degrees.

Data acquisition

The EEG was recorded with NeuroScan amplifiers using 64 tin electrodes mounted in an elastic cap. Electrodes were placed according to the international 10-10 system. The ground electrode was placed near the left mastoid (M1) and all electrodes were referenced to the left mastoid. Electrode impedance was kept below 5kΩ. Horizontal and vertical electrooculogram (EOG) recordings were registered with four additional electrodes. Data were sampled at 500 Hz and analog-filtered with a 0.05 Hz high-pass and a 100 Hz low-pass filter. An additional, digital 20 Hz low-pass filter was applied before displaying the ERP data.

Averaging epochs lasted from 200 ms before to 900 ms after stimulus onset. All epochs were visually inspected for artefacts and rejected if eye-movement artefacts, muscle artefacts, or electrode drifts were visible. Three subjects had to be excluded from further analysis due to excessive eye-movements. Baselines were computed in the –200–0 ms interval in each single trial and subtracted prior to computing the event-related potential (ERP) averages.

Data analysis

For the interpretation of gamma activity it is assumed to be important that the oscillations occur either phase-locked to a stimulus (evoked activity) or with variable phase relative to a stimulus (induced activity). For the analysis of gamma activity, a wavelet transform based on Morlet wavelets was employed (Herrmann et al., 1999). To differentiate between evoked and induced activity, each subject's ERP is transformed yielding evoked gamma activity and averages of transforms of single epochs are computed yielding induced activity.

In order to avoid a loss of statistical power that is inherent when repeated measures ANOVAs are used to quantify multi-channel EEG data (Oken & Chiappa, 1986), selected electrode sites were pooled to four topographical regions of interest (ROIs). The left anterior region (LAR) was comprised of electrodes FP1, F7, F3, F5, AF7, and FC3; the left posterior region (LPR) included electrodes P7, P5, P3, PO7, PO3, and O1. Regions over the right hemisphere included the homologous electrodes. For statistical analyses, ERP amplitudes were pooled across the electrodes in each of the ROIs. ERP components were defined as mean amplitudes in the following time intervals: 130–180 ms (N170) and 300–500 ms (P300).

EEG data was analysed with two ANOVAs: In one of them, the two stimulus dimensions form and collinearity were used as factors with levels square vs. triangle and collinear vs. non-collinear, respectively. We will refer to this type of ANOVA as stimulus-ANOVA, since it differentiates between the features of a stimulus. In addition, we computed a second type of ANOVA contrasting the target with the mean of the three non-targets. We will refer to this as the response-ANOVA, since it reflects the response requirements. (See Table 1.) ANOVAs conducted for EEG data had an additional factor topography (anterior, posterior).

These repeated-measures ANOVAs were also computed for RTs and error rates of the RT experiment. RTs on trials in which a response error was made, were rejected from the data, as well as trials in which the RT exceeded 2.5 standard deviations of the mean.

Before analysing gamma responses, we evaluated the signal-to-noise ratio (SNR) of the time interval to be analyzed. In order to achieve this, we computed SNR-ANOVAs to determine whether the mean amplitude in specific time intervals (50–150 ms and 200–300 ms) differs significantly from the noise in the baseline (–100–0 ms). Only if this is the case, subsequent ANOVAs which test variations due to experimental conditions make sense.

TABLE 1
Overview of the statistical tests for the experimental variables

Statistical test	*Factors*	*Factor level*
Stimulus-ANOVA	form	(Kan4, Non4) vs. (Kan3, Non3)
	collinearity	(Kan4, Kan3) vs. (Non4, Non3)
Response-ANOVA	targetness	Non4 vs. (Kan4, Kan3, Non3)

The four figural stimuli are abbreviated as Kan (Kanizsa figures) and Non (non-Kanizsa figures) and numbers indicate the number of inducer disks.

RESULTS

Behavioural data

The response-ANOVA for the RTs of the RT experiment yielded a significant main effect, $F(1, 9) = 16.58$, $p < .005$, demonstrating that targets are processed slower (665 ms) than non-targets (632 ms). The stimulus-ANOVA yielded significant effects of collinearity, $F(1, 9) = 16.27$, $p < .005$, and form, $F(1, 9) = 42.26$, $p < .0001$, indicating longer RTs for squares than for triangles as well as longer RTs for non-Kanizsa figures than Kanizsa figures. In addition, the stimulus-ANOVA yielded a significant collinearity × form interaction, $F(1, 9) = 9.96$, $p = .01$. Post-hoc comparisons revealed that within the triangles there is a significant effect of collinearity, $F(1, 9) = 65.73$, $p < .0001$, but not within the squares (Figure 3, left).

The response-ANOVA for the error rates yielded a significant main effect of targetness, $F(1, 9) = 15.98$, $p < .005$, indicating more errors for targets (7.4%) than for non-targets (3.4%). The stimulus-ANOVA of the error rates yielded a significant form effect, $F(1, 9) = 14.70$, $p < .005$, revealing that error rates are higher for squares than for triangles. Basically, the pattern of the error rates resembles that of the RTs (Figure 3, right). The fact that the pattern of errors is not inverse to that of RTs indicates that we are not dealing with a speed-accuracy trade-off, but an effect of feature processing (Pachella, 1974).

ERP responses

Figure 4 shows the ERPs at selected electrodes over frontal, central, parietal, and occipital areas. In all conditions, there is a prominent N170 peak around 170 ms which is strongest in occipital electrodes. An additional P300 peaks around 400 ms and is strongest for the target condition.

The stimulus-ANOVA for the time interval of the N170 yielded significant effects of collinearity, $F(1, 12) = 39.12$, $p < .0001$, and form, $F(1, 12) = 13.40$, $p < .005$. Amplitudes were larger for squares than for triangles and larger for

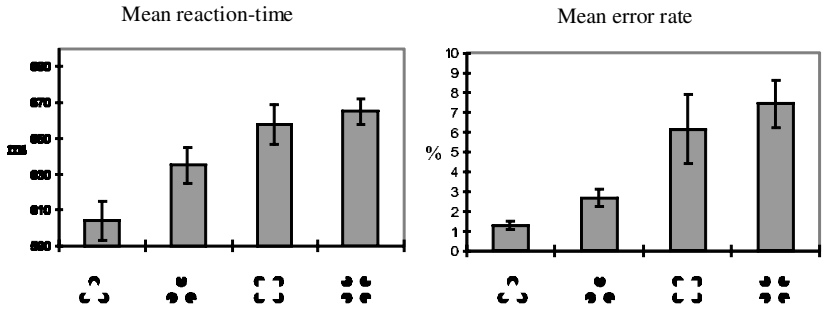

Figure 3. Mean RTs and error rates (means and standard errors of means) for the RT experiment.

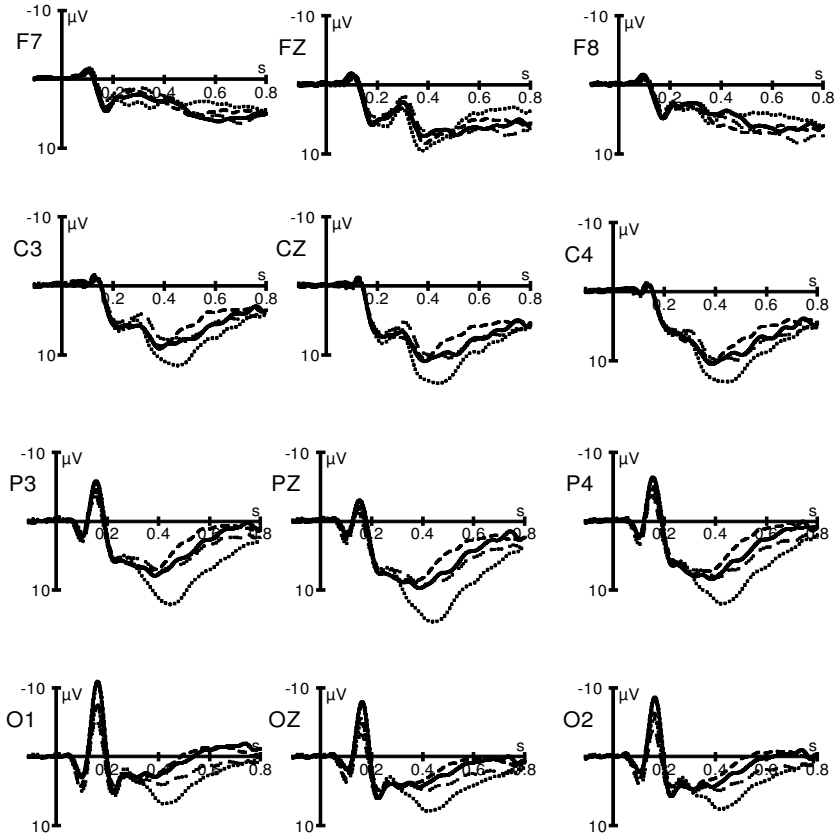

Figure 4. 20 Hz low-pass filtered ERPs averaged across 13 subjects in response to Kanizsa squares (solid), Kanizsa triangles (dashed), non-Kanizsa squares (target, dotted), and non-Kanizsa triangles (intermittently dotted).

Kanizsa figures than non-Kanizsa figures. A significant interaction of Topography × Collinearity, $F(1, 12) = 7.65$, $p < .05$, revealed that the collinearity effect was much stronger at posterior electrodes, $F(1, 12) = 28.02$, $p < .0005$, than in anterior ones, $F(1, 12) = 9.40$, $p < .01$. The post-hoc tests revealed that, even though the Topography × Form interaction was not significant in the ANOVA, a form main effect was significant at posterior electrodes, $F(1, 12) = 9.77$, $p < .01$. The order of response magnitude of the N170 was the same as in the previous experiment by Herrmann et al. (1999) as can be seen from the direct comparison in Figure 5. The order was: > Kanizsa square (7.9 µV) > Kanizsa triangle (6.4 µV) > non-Kanizsa square (5.9 µV) > non-Kanizsa triangle (4.5 µV); amplitudes were averaged across posterior electrodes. The response-ANOVA yielded no significant effect.

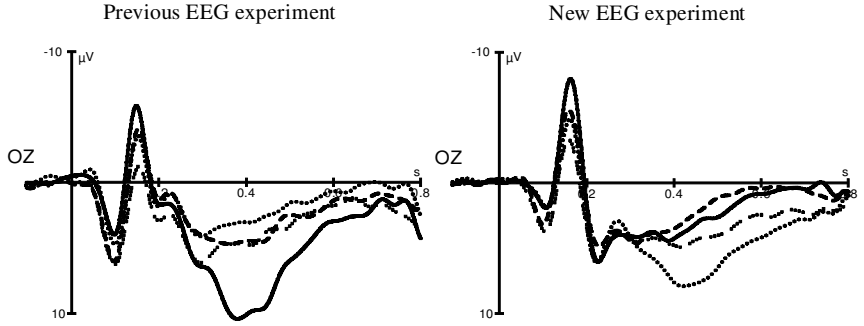

Figure 5. ERPs of electrode OZ for experiments 1 and 2. N170 components are independent of task requirements. The P300 component is affected by the task change between experiments and is delayed in latency and reduced in amplitude.

The response-ANOVA for the time interval of the P300 yielded a significant main effect for targetness, $F(1, 12) = 14.39$, $p < .005$, indicating larger potentials for targets (6.6 μV, amplitudes averaged across all electrodes) than non-targets (5.0 μV). A significant interaction of Topography × Targetness, $F(1, 12) = 7.80$, $p < .05$, justified post-hoc comparisons in the different regions. The target effect was only significant at posterior electrodes, $F(1, 12) = 27.30$, $p < .0005$, but not in anterior ones, $F(1, 12) = 0.12$. The stimulus-ANOVA yielded significant main effects of form, $F(1, 12) = 16.96$, $p < .005$, squares (6.3 μV) being greater than triangles (5.2 μV), and collinearity, $F(1, 12) = 4.75$, $p < .05$, collinear (5.4 μV) figures being greater than non-collinear ones (6.2 μV). Significant interactions were found for Topography × Form, $F(1, 12) = 6.91$, $p < .05$, Topography × Collinearity, $F(1, 12) = 5.36$, $p < .05$, and Form × Collinearity, $F(1, 12) = 5.61$, $p < .05$. Post-hoc comparisons in the individual regions revealed significant effects of form, $F(1, 12) = 20.42$, $p < .001$, squares (6.5 μV) being greater than triangles (4.7 μV) and collinearity, $F(1, 12) = 12.40$, $p < .005$, collinear (4.9 μV) figures being greater than non-collinear ones (6.3 μV) in posterior electrodes but no effects in anterior electrodes.

In the previous EEG experiment by Herrmann et al. (1999), the target-P300 had a latency of 382 ms and an amplitude of 18.1 μV at the PZ recording site. In the present EEG experiment, P300 latency was delayed (444 ms) and its amplitude reduced (14.5 μV).

Gamma responses

The SNR-ANOVA for the evoked gamma activity yielded a significant effect of SNR for the early time interval (50–150 ms), $F(1, 12) = 11.52$, $p < .01$, but not for the late time interval (200–300 ms). This is illustrated for three electrodes (O1, OZ, and O2) in Figure 6. A clear peak can be seen for three of the four

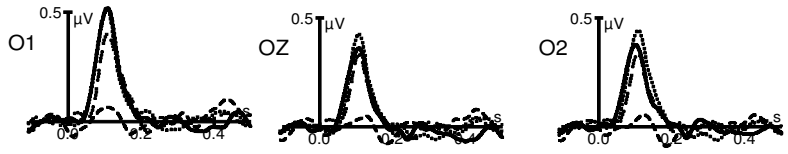

Figure 6. Grand average of the evoked gamma activity across 13 subjects in electrodes, O1, OZ, and O2. A clear peak is visible around 100 ms after stimulus onset.

conditions with a maximum around 100 ms. No difference from baseline is visible after this peak.

The SNR-ANOVA for the induced gamma activity yielded no significant effects. This implies that the SNR of induced gamma activity did not differ from the pre-stimulus baseline period. For this reason we refrained from further analysis of induced gamma activity. The induced gamma activity is illustrated for three electrodes (O1, OZ, and O2) in Figure 7 where no clear peaks can be seen that differ from the baseline activity.

The response-ANOVA for the time interval 50–150 ms of the evoked gamma activity yielded a significant main effect of targetness, $F(1, 12) = 4.93$, $p < .05$, indicating larger gamma activity for the target as compared to the non-targets. The stimulus-ANOVA yielded a significant main effect for form, $F(1, 12) = 5.04$, $p < .05$, indicating larger amplitudes for squares than for triangles. The topographical distribution of the early evoked gamma response is displayed in Figure 8.

Figure 9 shows the total amount of early evoked gamma activity summed across all analysed electrodes for the four conditions. It is obvious that the pattern resembles that of RTs and error rates, i.e., early evoked gamma activity is stronger the more similar a stimulus is to the target. A correlation analysis of the early evoked gamma activity (50–150 ms, averaged across all electrodes and 13 subjects) and the RTs (averaged across 10 subjects) of the four conditions ($n = 4$) revealed a correlation coefficient of 0.9749 ($p < .05$). Notably, the correlation of 0.18 between RT and N170 amplitude was not significant.

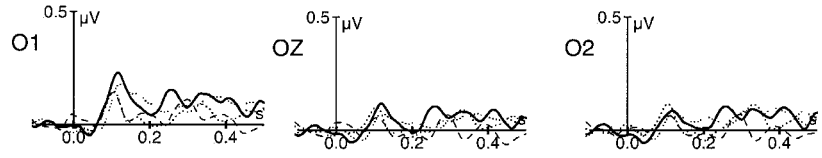

Figure 7. Grand average of the induced gamma activity across 13 subjects in electrodes, O1, OZ, and O2. No clear difference from baseline activity can be observed.

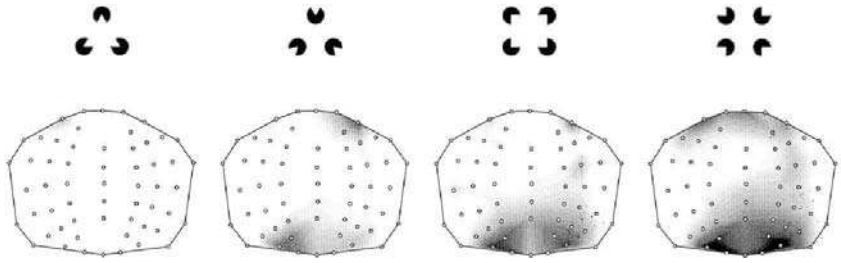

Figure 8. Topography of the early evoked gamma activity for the conditions Kanizsa triangle, non-Kanizsa triangle, Kanizsa square, and non-Kanizsa square (from left to right) in the time interval 50–150 ms averaged over 13 subjects. Gray-scale is from 0 μV (white) to 0.5 μV (black).

DISCUSSION

Behavioural data

From the behavioural data we can see that RTs and error rates show a typical pattern of target discrimination. As expected, the target, which occurs less frequently than the non-targets, is processed slowest (Teichner & Krebs, 1974). In a previous experiment by Herrmann and Mecklinger (2000) this was even the case when the Kanizsa square was the target which would otherwise be expected to be processed faster than a non-Kanizsa square due to its figural features (Pomerantz, 1983). As has been argued by Herrmann and Mecklinger (2000), the pattern of RTs is considered to represent a classification of the targets according to the two dimensions form and collinearity. In our new experiment, the Kanizsa-triangle is dissimilar in both dimensions which define the target: It is composed of three instead of four inducer disks (form) and in contrast to the target constitutes a Kanizsa figure (collinearity). Therefore, it is

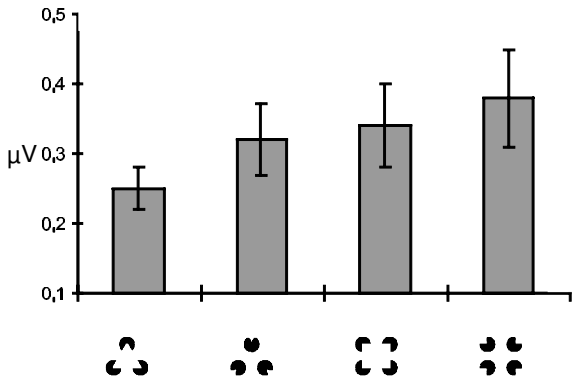

Figure 9. Total amount of early evoked gamma activity (50–150 ms) summed across all analysed electrodes as a function of experimental condition.

the easiest figure to differentiate from the target and by this is processed fastest. The fact that the non-Kanizsa triangle is processed faster than the Kanizsa square, even though they are both dissimilar from the target in one dimension, suggests that the selection process for target discrimination operates as a two-fold mechanism. This mechanism seems to include separate selection processes for comparisons of form and collinearity of the encoded stimulus with a template held in working memory. The fact that error rates did not differ significantly when stimuli varied only across the dimension collinearity while they did differ significantly when stimuli varied across the dimension form might be taken to indicate that the dimension form is more salient to the human visual system. This would also explain why the Kanizsa squares are processed slower than the non-Kanizsa triangles that both share one dimension with the target: The Kanizsa square varies across the less salient dimension collinearity, whereas the non-Kanizsa triangle varies across the more salient dimension form.

ERP responses

The order of N170 amplitude is the same as in the previous experiment by Herrmann et al. (1999) as can be seen from the direct comparison in Figure 5 (Kanizsa square > Kanizsa triangle > non-Kanizsa square > non-Kanizsa triangle). From the previous experiment it could have been concluded that the N170 reflects perceptual processes of illusory contour detection, since the N170 was larger for Kanizsa figures as compared to non-Kanizsa figures. But this effect might have been confounded by the Kanizsa square being the target, since attentional selection processes are known to sometimes influence early ERP components (Heinze et al., 1994). In our new experiment, the order of N170 amplitude did not change relative to the former experiment: The target now evoked the second smallest N170 amplitude showing that in our paradigm the N170 does not reflect attentional selection mechanisms. Thus, since the change in task requirements did not affect the order of N170 amplitude, the collinearity effect is really due to the collinearity of the stimuli and not a confound of the target. This nicely demonstrates that the N170 is driven by physical stimulus properties rather than task requirements. It is noteworthy that the N170 reflects not only physical stimulus properties (three vs. four inducer disks) but also perceptual features like the presence of illusory contours. This effect also suggests that illusory contours are in fact processed by the subjects.

The order of N170 amplitude which stays constant across experiments despite changes in task requirements also indicates that the stimuli possess a certain salience to our visual system. According to the order of N170 amplitude, stimuli that are composed of more inducer disks and stimuli which constitute illusory contours appear to be more salient.

The P300 showed a clear target effect in our EEG experiment. But it was delayed in latency and reduced in amplitude as compared to the previous EEG experiment (Herrmann et al., 1999). This suggests that the detection of the non-Kanizsa square is harder than the detection of the Kanizsa square which is more salient according to our above definition.

Gamma responses

It has been previously stated that the early evoked gamma activity is a purely stimulus-driven component, not being sensitive to perceptual/cognitive functions (Karakaş & Başar, 1998). In addition, comparable experiments with Kanizsa and non-Kanizsa figures failed to demonstrate differences between experimental conditions (real triangle, illusory triangle, non-triangle) in the early evoked gamma activity and the effects of targetness were not investigated (Tallon, Bertrand, Bouchet, & Pernier, 1995; Tallon-Baudry, Bertrand, Delpuech, & Pernier, 1996). We were able to show that changing the task across experiments while keeping the perceived stimuli identical changes the early evoked gamma response, whereas other early responses as the N170 were not affected by this attentional variable. Similar changes of early evoked gamma activity with task changes have been found in MEG recordings (Herrmann & Mecklinger, 2000). This indicates that early evoked gamma activity reflects a top-down mechanism involved in selecting the proper response to a stimulus that cannot be purely sensory in origin. In order to differentiate targets from non-targets, both features of a stimulus (form and collinearity) have to be compared to a template in working memory. It has been shown in simulations that high-speed access to working memory may operate at frequencies in the gamma range (Jensen & Lisman, 1998). Furthermore, Burle and Bonnet (2000) showed behavioural data from an auditory interference task, which also suggest an oscillatory process in working memory. Elliott and Müller (2000) showed that the representation of visual objects in working memory is accomplished by gamma oscillations. Therefore, the presence of a template in working memory may be critical for the generation of gamma activity in our task.

A model that accounts for our pattern of results can be sketched as follows: The plain access to working memory itself is probably not a candidate for generating the gamma response, since the amplitude of gamma activity varies for different stimuli and there is no apparent reason why the strength of memory access should vary across stimuli. But the process that compares the perceived stimuli with the template in working memory may well be the generator of the gamma activity. We demonstrated that within the three non-target stimuli the stimulus that is dissimilar to the target stimulus in two features (Kanizsa triangle) is processed faster than those that differ in only one feature. This indicates that the comparison process seems to operate as a two-fold process,

separately comparing the two features of which a target is composed. Whenever one of these two comparisons yields a positive result (Kanizsa square and non-Kanizsa triangle), this results in enhanced gamma activity as compared to both comparisons yielding negative results (Kanizsa triangle). When both comparisons yield positive results (non-Kanizsa square), we see the maximal amount of gamma activity. Thus, it seems plausible to assume that a positive comparison with working memory leads to a reinforced feedback of the frequency at which the process operates anyway, i.e., the 40 Hz are amplified more the better a perceived stimulus matches the template. This activity could then propagate to cortical areas that are relevant for correct task performance.

A further interesting result of our EEG and RT experiments was that the early evoked gamma activity correlates significantly with RTs, even though both measures were taken in different experiments. Thus, the gamma activity which peaks around 100 ms is an indicator for the much later motor reaction (approximately 600 ms). It has been reported previously that finger movements are accompanied by 40 Hz activity in the motor cortex (Pfurtscheller, Flotzinger, & Neuper, 1994). Therefore, it seems likely that early evoked gamma activity can be functionally related with motor gamma activity. Due to the additional fact that the evoked gamma activity is highly synchronized to the stimulus (evoked gamma), we think that the process underlying the correlation of early evoked gamma activity and the motor reaction is what Roelfsema, Engel, König, and Singer (1997) have described as visuomotor integration. Roelfsema et al. found highly synchronized gamma activity with zero time-lag between visual and motor areas in cats. If the selection process accessing working memory and the motor process both operate at 40 Hz, this constitutes an ideal mechanism for effective information transmission. Therefore, we render it important for future experiments to investigate the correlation of early evoked gamma activity and later motor gamma activity.

In the results of Herrmann et al. (1999) and Herrmann and Mecklinger (2000) the early evoked gamma activity was distributed more frontally than in this experiment. An unexpected result of this study was the rather occipital topography of the early evoked gamma activity. Further experiments will be needed to investigate the topography of the early evoked gamma activity in detail.

REFERENCES

Başar-Eroglu, C., Strüber, D., Schürmann, M., Stadler, M., & Başar, E. (1996). Gamma-band responses in the brain: A short review of psychophysiological correlates and functional significance. *International Journal of Psychophysiology, 24,* 101–112.

Burle, B., & Bonnet, M. (2000). High-speed memory scanning: A behavioural argument for a serial oscillatory model. *Cognitive Brain Research, 9,* 327–337.

Donchin, E., & Coles, M.G.H. (1988). Is the P300 component a manifestation of context updating? *Behavioural Brain Science, 11,* 357–374.

Elliott, M.A., Herrmann, C.S., Mecklinger, A., & Müller, H.J. (2000). The loci of oscillatory visual-object priming: A combined electroencephalographic and reaction-time study. *International Journal of Psychophysiology, 38*(3), 225–242.

Elliott, M.A., & Müller, H.J. (1998). Synchronous information presented in 40-Hz flicker enhances visual feature binding. *Psychological Science, 9*(4), 277–283.

Elliott, M.A., & Müller, H.J. (2000). Evidence for a 40 Hz oscillatory short-term visual memory revealed by human reaction-time measurements. *Journal of Experimental Psychology Learning, Memory and Cognition, 26*(3), 703–718.

Gray, C.M., König, P., Engel, A.K., & Singer, W. (1989). Oscillatory response in the cat visual cortex exhibit intercolumnar synchronization which reflects global stimulus properties. *Nature, 338*, 334–337.

Heinze, H.J., Mangun, G.R., Burchert, W., Hinrichs, H., Scholz, M., Münte, T.F., Gös, A., Scherg, M., Johannes, S., Hundeshagen, H., Gazzaniga, M.S., & Hillyard, S.A. (1994). Combined spatial and temporal imaging of brain activity during visual selective attention in humans. *Nature, 372,* 543–546.

Herrmann, C.S. & Mecklinger, A. (2000). Magnetoencephalographic responses to illusory figures: Early evoked gamma is affected by processing of stimulus features. *International Journal of Psychophysiology, 38*(3), 265–281.

Herrmann, C.S., Mecklinger, A., & Pfeiffer, E. (1999). Gamma responses and ERPs in a visual classification task. *Clinical Neurophysiology, 110*(4), 636–642.

Jensen, O., & Lisman, J. (1998). An oscillatory short-term memory buffer model can account for data on the Sternberg task. *Journal of Neuroscience, 18*(24), 10688–10699.

Kanizsa, G. (1976). Subjective contours. *Scientific American, 234*(4), 48–52.

Karakaş, S., & Başar, E. (1998). Early gamma response is sensory in origin: A conclusion based on cross-comparison of results from multiple experimental paradigms. *International Journal of Psychophysiology, 31,* 13–31.

Mecklinger, A., & Ullsperger, P. (1993). P3 varies with stimulus categorization rather than probability. *Electroencephalography and Clinical Neurophysiology, 86,* 395–407.

Müller, M.M., Gruber, T., & Keil, A. (2000). Modulation of induced gamma band activity in the human EEG by attention and visual processing. *International Journal of Psychophysiology, 38*(3), 283–300.

Oken, B.S., & Chiappa, K.H. (1986). Statistical issues concerning computerized analysis of brainwave topography. *Annals of Neurology, 19,* 493–494.

Pachella, R.G. (1974). The interpretation of reaction time in information processing research. In B. Kantowitz (Ed.), *Human information processing*. Hillsdale, NJ: Lawrence Erlbaum Associates Inc.

Pfurtscheller, G., Flotzinger, D., & Neuper, C. (1994). Differentiation between finger, toe and tongue movement in man based on 40 Hz EEG. *Electroencephalography and Clinical Neurophysiology, 90,* 456–460.

Pomerantz, J.R. (1983). Global and local precedence: Selective attention in form and motion perception. *Journal of Experimental Psychology: General, 112,* 516–540.

Pulvermüller, F., Keil, A., & Elbert, T. (1999). High-frequency brain activity: Perception or active memory. *Trends in Cognitive Science, 3*(7), 250–252.

Roelfsema, P.R., Engel, A.K., König, P., & Singer, W. (1997). Visuomotor integration is associated with zero time-lag synchronization among cortical areas. *Nature, 385,* 157–161.

Singer, W., & Gray, C.M. (1995). Visual feature integration and the temporal correlation hypothsis. *Annual Reviews in Neuroscience, 18,* 555–586.

Tallon, C., Bertrand, O., Bouchet, P., & Pernier, J. (1995). Gamma-range activity evoked by coherent visual stimuli in humans. *European Journal of Neuroscience, 7,* 1285–1291.

Tallon-Baudry, C., & Bertrand, O. (1999). Oscillatory gamma activity in humans and its role in object representation. *Trends in Cognitive Science, 3*(4), 151–162.

Tallon-Baudry, C., Bertrand, O., Delpuech, C., & Pernier, J. (1996). Stimulus specificity of phase-locked and non-phase-locked 40 Hz visual responses in human. *Journal of Neuroscience, 16*(13), 4240–4249.

Teichner, W.H., & Krebs, M.J. (1974). Laws of visual choice reaction time. *Psychological Reviews, 81*(1), 75–98.

Tiitinen, H., Sinkkonen, J., Reinikainen, K., Alho, K., Lavikainen, J., & Näätänen, R. (1993). Selective attention enhances the auditory 40-Hz transient response in humans. *Nature, 364,* 59–60.

von der Malsburg, C., & Schneider, W. (1986). A neural cocktail-party processor. *Biological Cybernetics, 54,* 29–40.

Zeki, S. (1993). *A vision of the brain*. Oxford, UK: Blackwell Scientific Publications.

ELSEVIER

International Journal of Psychophysiology 38 (2000) 265–281

INTERNATIONAL JOURNAL OF PSYCHOPHYSIOLOGY

www.elsevier.nl/locate/ijpsycho

Magnetoencephalographic responses to illusory figures: early evoked gamma is affected by processing of stimulus features

Christoph S. Herrmann*, Axel Mecklinger

Max-Planck-Institute of Cognitive Neuroscience, Postfach 500 355, 04303 Leipzig, Germany

Received 1 September 1999; accepted 20 April 2000

Abstract

We examined evoked and induced responses in event-related fields and gamma activity in the magnetoencephalogram (MEG) during a visual classification task. The objective was to investigate the effects of target classification and the different levels of discrimination between certain stimulus features. We performed two experiments, which differed only in the subjects' task while the stimuli were identical. In Experiment 1, subjects responded by a button-press to rare Kanizsa squares (targets) among Kanizsa triangles and non-Kanizsa figures (standards). This task requires the processing of both stimulus features (collinearity and number of inducer disks). In Experiment 2, the four stimuli of Experiment 1 were used as standards and the occurrence of an additional stimulus without any feature overlap with the Kanizsa stimuli (a rare and highly salient red fixation cross) had to be detected. Discrimination of collinearity and number of inducer disks was not necessarily required for task performance. We applied a wavelet-based time-frequency analysis to the data and calculated topographical maps of the 40 Hz activity. The early evoked gamma activity (100–200 ms) in Experiment 1 was higher for targets as compared to standards. In Experiment 2, no significant differences were found in the gamma responses to the Kanizsa figures and non-Kanizsa figures. This pattern of results suggests that early evoked gamma activity in response to visual stimuli is affected by the targetness of a stimulus and the need to discriminate between the features of a stimulus.

Keywords: Attention; Binding; Gamma activity; Illusory contours; Kanizsa figures; Magnetoencephalography; MEG; Wavelet transform

* Corresponding author. Tel.: +49-341-9940-250; fax: +49-341-9940-113.
E-mail address: herrmann@cns.mpg.de (C.S. Herrmann).

0167-8760/00/$ - see front matter
PII: S0167-8760(00)00170-7

1. Introduction

Oscillatory activity in the gamma-frequency range (30–80 Hz) of the human electroencephalogram (EEG) has been found to reveal some interesting correlates with cognitive processing. In particular, neurons in the animal brain, which oscillate at approximately 40 Hz, are believed to represent the binding of different features of one object to form a single coherent percept (Eckhorn et al., 1988; Engel et al., 1992; Gray et al., 1989). Since similar findings have been reported from the human EEG, it is assumed that gamma activity is associated with visual binding (e.g. Tallon et al., 1995; Tallon-Baudry et al., 1996; Müller et al., 1997).

It remains controversial whether binding requires attentional top-down mechanisms or arises from pre-attentive bottom-up processes in early vision (see, e.g. Reynolds and Desimone, 1999). Kanizsa figures (Kanizsa, 1976) have been used to study this question, since the perception of an illusory figure requires the binding of its inducer disks (Kojo et al., 1993). There has been psychophysical evidence (Davis and Driver, 1994) and results from positron emission tomography (Ffytche and Zeki, 1996) indicating pre-attentive stages to be responsible for feature binding. However, there has been speculation (Crick and Koch, 1990) and experimental evidence (Gurnsey et al., 1996) that searching for Kanizsa figures resembles a serial rather than a parallel process, i.e. it requires attention.

Reviews related to the functional relevance of gamma oscillations in humans and animals can be found in Başar-Eroglu et al. (1996). Reviews concerning the relation of gamma activity to human visual perception (Bertrand and Tallon-Baudry, 2000) and attentional mechanisms (Müller et al., 2000) can be found in this volume.

Psychophysical experiments have recently shown that stimuli flickering at 40 Hz can enhance visual binding (Elliott and Müller, 1998b), providing further evidence for the relevance of gamma activity for binding processes. RTs to target Kanizsa-type figures were expedited when the figures were preceeded by a flickering premask display, comprising collinear premask elements at the target location, only if the premask display flickered at approximately 40 Hz. The effects of 'priming' target detection at 40 Hz breakdown following stimulus-onset asynchronies of >240 ms between premask display offset and target display onset, although during this period, RTs show a modulatory pattern by ISI which indicates the operation of a 40-Hz process (Elliott and Müller, 1998a). Therefore, it seems plausible to assume that visual stimuli may be coded in short-term visual memory by an oscillatory process of approximately 40 Hz. In addition, Elliott et al. (2000) show that this visual representation is associated with gamma activity in the human EEG, indicating that binding operations of relevance to Kanizsa-type figure detection do adopt an oscillatory structure at 40 Hz.

Oscillatory activity in EEG can be phase-locked to the onset of an experimental stimulus, i.e. it starts at approximately the same latency after stimulus onset for every repetition of the stimulus. In this case the activity is called evoked. If, on the other hand, the oscillations occur after stimulation but with varying onset times (phase jitter), they are considered as being induced by the stimulus rather than evoked (Başar-Eroglu et al., 1996).

In a series of studies on the perception of illusory contours Tallon-Baudry and Bertrand have shown that illusory Kanizsa triangles (cf. Fig. 1b) elicited early and late gamma responses (Tallon et al., 1995; Tallon-Baudry et al., 1996, 1997). The early gamma response (approx. 100 ms) was phase-locked to stimulus onset (evoked activity) and showed no difference between conditions. The late response (200–300 ms) was not phase-locked to stimulus onset (induced activity) and was enhanced for Kanizsa figures as compared to non-Kanizsa figures. They concluded that the late induced gamma response is associated with the binding process needed to form the percept of a Kanizsa figure.

Herrmann et al. (1999) found a similar pattern of gamma responses but with different characteristics in a closely related target classification experiment using the stimuli shown in Fig. 1. In this experiment, the early gamma response was phase-locked, but, in contrast to the results of

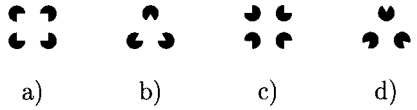

Fig. 1. The four stimulus types used in the experiment: (a) Kanizsa square (target); (b) Kanizsa triangle; (c) non-Kanizsa triangle; (d) non-Kanizsa square.

Tallon-Baudry and Bertrand, showed an enhancement for the target (the Kanizsa square) as compared to the non-targets. Due to its frontal topography, this effect was interpreted in terms of a top-down mechanism, which gates the bottom-up processing of visual stimuli. Consistent with this view, prefrontal cortex has been shown to be involved in the modulation of visual processing (Knight et al., 1999; Knight, 1997). As in the experiments of Tallon-Baudry and Bertrand, the late response was also larger for Kanizsa figures than for non-Kanizsa figures, but in contrast to Tallon-Baudry and Bertrand phase-locked to stimulus onset. In a further experiment, Herrmann and Mecklinger (1999) showed that varying the target stimulus while keeping all other parameters identical affects the early evoked gamma response. Therefore, it was argued that early gamma activity is affected by top-down processes that guide the visual coding process needed for discrimination of the target. One objective of the present paper is to further investigate how top-down processes modulate early gamma activity and to examine how these processes are reflected in MEG signals.

In the MEG experiments presented here, subjects viewed Kanizsa figures and non-Kanizsa figures comprised of either three or four inducer disks, spatially arranged as shown in Fig. 1. The subjects' tasks differed between experiments while stimuli were identical. According to the differentiation of a top-down and bottom-up process, the latter of which 'depends only on the visual stimulus but not on the task being performed' (Posner, 1989), such changes can only affect top-down processes. We wanted to investigate how changing top-down processing affects gamma responses. In Experiment 1, subjects had to respond with a button-press to rare Kanizsa squares (targets) among Kanizsa triangles and non-Kanizsa figures (standards). Here, the features of the presented figures had to be discriminated for successful task performance. In Experiment 2, the rare occurrence of a red fixation cross (target) in addition to the four stimuli of Experiment 1 (standards) had to be detected and reported with a button-press. Therefore, given the high salience of the target, discrimination of the features (number of inducer disks and presence of collinearity) of the standards was not necessarily required for task performance. In order to analyse gamma activity with a sufficiently high temporal resolution, a time-frequency analysis based on a wavelet transform was employed (Herrmann et al., 1999).

Our hypotheses were that we find larger evoked MEG gamma activity for the target as compared to the standards in an early time interval in Experiment 1, as it was the case in the EEG experiment of Herrmann et al. (1999). In addition, we expected to find higher gamma activity for the Kanizsa figures than for the non-Kanizsa figures in a later time interval. For Experiment 2, our hypothesis was not to find any differences in the early evoked gamma activity between the four standard stimuli. Nevertheless, we expected to find larger gamma activity in the late time interval for the Kanizsa figures, since this has been found to occur also for non-target Kanizsa figures (Herrmann and Mecklinger, 1999).

2. Methods

2.1. Stimuli

We used Kanizsa figures and non-Kanizsa figures as stimulus material as shown in Fig. 1. According to Tallon-Baudry et al. (1996), who used only triangular stimuli, it is advantageous to keep the target figure different from the Kanizsa figure under investigation. Therefore, we introduced the square arrangements of inducer disks which allows us to differentiate between the processing of Kanizsa figures and targets. The stimuli were identical to the ones used in a previous EEG experiment where a possible top-down modulation of gamma activity was discussed (Herr-

mann et al., 1999). The stimuli consisted of either three or four inducer disks which we will consider the shape feature and either constituted an illusory figure (Fig. 1a,b) or not (Fig. 1c,d) which we will consider the collinearity feature. The stimuli were presented for 700 ms with randomized inter-stimulus-intervals ranging from 1000 to 1500 ms to avoid contingent negative variations due to temporal predictability of the stimuli. Figures were displayed in black together with a black central fixation cross on white background. Stimuli subtended a visual angle of 4.28° including inducer disks, while the induced illusory figures (Fig. 1a,b) subtended 2.86°. Thus, the whole stimulus is projected into the field of central vision, i.e. the first 5° covered by the macula (Zeki, 1993). Fixation crosses were displayed foveally (0.02°). The ratio of the radius of the inducer disks and the side-length of the illusory figures was 1/4.

The fact that the late gamma activity in Herrmann et al. (1999) was phase-locked to the stimulus while it was not phase-locked in the results of Tallon-Baudry et al. (1996) could be attributed to a synchronization to the frequency of the monitor which oscillated at twice the frequency of the observed gamma activity. To exclude the possibility of such a synchronization, we used a liquid crystal display (LCD) monitor without a raster scan. In order to display the stimuli inside a shielded MEG cabin, where no electric devices may be operated which could interfere with MEG measurement, we used a VGA projector which projects the picture of an LCD screen into the cabin via mirrors. The projection plane was placed 1 m in front of the subjects. The stimuli on the projection screen inside the cabin were checked with a light-dependent resistor to show no flicker effects. Each experiment was run in four blocks with 100 figures each. Reaction times were registered with a special response button which interrupts a light beam in a fiber optic to avoid electric interference.

2.2. Experiment 1

As in Herrmann et al. (1999), in Experiment 1 the Kanizsa square served as the target figure. Subjects were instructed to press a button with their right index finger when a target appeared (with a probability of 0.25) and another button with their left index finger when one of the three standard stimuli appeared (with a probability of 0.75). In this experiment, the task requires the processing of both stimulus features, shape and collinearity.

Sixteen subjects participated in the study. Six of them had to be rejected due to excessive eye-movement artefacts, high-frequency artefacts (possibly resulting from EMG contamination) or behavioural measures (reaction time or error rate) not lying within 2.5 standard deviations from the mean. Ten subjects with a mean age of 21.7 years (ranging from 18 to 25 years, 6 female) were analyzed. All subjects had normal or corrected-to-normal vision. They showed no signs of neurological or psychiatric disorders and all gave written, informed consent.

2.3. Experiment 2

In Experiment 2 we employed a task in which the four stimuli from Experiment 1 were used as standard stimuli, to which we will refer as figural stimuli. An additional red fixation cross, appearing instead of a figural stimulus, was introduced as a target. The target stimulus is highly salient (red) such that the processing of shape and collinearity was not necessarily required for successful task performance. Target discrimination could be carried out by processing the color feature alone. The task was a go/no-go task and subjects had to respond with a button-press of their right index finger to the occurrence of rare red fixation crosses (with a probability of 0.2).

Twelve subjects participated in this study. Two of them had to be rejected due to the above-mentioned criteria. Ten subjects with a mean age of 22.4 years (ranging from 18 to 25 years, 6 female) were analyzed. All subjects had normal or corrected-to-normal vision. They showed no signs of neurological or psychiatric disorders and all gave written, informed consent.

2.4. Data acquisition

One issue of this study concerns the spatial resolution of MEG recording. In an earlier MEG experiment with a 32-channel device placed over the occipital cortex, no induced gamma activity could be found while evoked gamma activity was visible in MEG (Tallon-Baudry et al., 1997). In previous EEG experiments, gamma activity was found primarily over frontal areas (Herrmann et al., 1999 and Herrmann and Mecklinger, 1999). We used a whole-head MEG to be able to examine MEG gamma oscillations in various brain regions.

MEG was recorded with a BTI 148 channel whole-head system (MAGNES WHS 2500). Horizontal and vertical EOG were registered with four additional EEG electrodes. MEG data were sampled at 678.168 Hz (on-line 0.1 Hz analog high-pass and 200 Hz low-pass filtering). The subjects' head positions were recorded via four coils which were attached to anatomical landmarks and headshapes were digitized with a three-dimensional digitizer.

Averaging epochs lasted from 200 ms before to 900 ms after stimulus onset. All epochs were first automatically and then manually inspected for artefacts and rejected if eye movement artefacts or sensor drifts were detected. For automatic detection, we computed the standard deviation in a moving time window and epochs were rejected if a threshold was exceeded. EOG electrodes and MEG channels were checked with thresholds of 30 μV and 1100 fT, respectively. Window sizes were 200 ms for EOG and 3 s for MEG. Baselines were computed in the −200 to 0 ms interval in each single trial and subtracted prior to computing the averaged event-related fields (ERFs).

2.4.1. Data analysis

In order to compute a wavelet transform, the original signal is convolved with a so-called wavelet. In case of the Morlet wavelet used here it is calculated according to the formula

$$\Psi(t) = e^{j\omega_0 t} \cdot e^{-t^2/2}$$

where ω_0 is 2π times the frequency of the unshifted and uncompressed mother wavelet. Fig. 2 shows how these mathematical terms construct a wavelet.

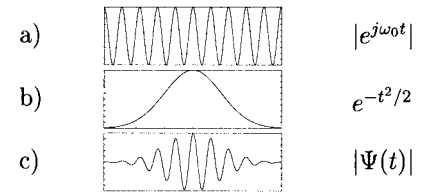

Fig. 2. Multiplying a sinusoidal function (a) and an envelope function (b) results in a wavelet.

Convolving wavelets with signals results in a new signal (the convolution) which can be interpreted as the similarity of the wavelet and the signal. Wavelets can be compressed by a factor a to get wavelets of different frequencies (substitute t by t/a). The mother wavelet ($a = 1$) has the same frequency as the sampling frequency (f_s) of the signal. Wavelets of lower frequencies are computed by increasing a (e.g. for $a = f_s$ the wavelet has a frequency of 1 Hz).

Convolving the signal and the shifted and compressed wavelet leads to a new signal

$$s_a(b) = A \int \overline{\Psi}\left(\frac{t-b}{a}\right) \cdot x(t)\mathrm{d}t$$

where $\overline{\Psi}$ is the conjugate of the complex wavelet and $x(t)$ is the original signal. These new signals $s_a(b)$ are computed for different scaling factors a. In our experiments we calculated the gamma activity by using a wavelet which was compressed to 40 Hz. The scaling factor $A = 1/\sqrt{a}$ is used to scale the wavelet prior to convolution.

To represent phase-locked (evoked) activity, the wavelet transform of the average over the single trials (WTAv) is computed. Since the wavelet transform returns complex numbers, the absolute values are calculated.

$$\mathrm{WTAv} = \left| A \int \overline{\Psi}\left(\frac{t-b}{a}\right) \cdot \frac{1}{n} \sum_{i=1}^{n} \mathrm{eeg}_i(t)\mathrm{d}t \right|$$

The baseline of the raw data in time interval

−200 to 0 ms is subtracted from each EEG epoch prior to averaging. Also, after calculating the gamma activity, the frequency-specific baseline activity at 40 Hz is subtracted to yield values which indicate gamma amplitude relative to baseline. When wavelet convolutions are computed, the convolution peaks at the same latency as the respective frequency component in the raw data. But, the width of the peak will be smeared. Therefore, the baseline was chosen from −400 to −100 ms to account for temporal smearing of post-stimulus activity into the interval directly preceding the stimulus. To avoid distortions by the rectangular window function which results from 'cutting out' a single epoch from continuous raw data, we computed the convolution starting and ending one wavelet length before the baseline and after the end of the investigated time interval, respectively.

The above time-frequency representation contains only that part of the activity which is phase-locked to stimulus onset. In order to also compute the activity which is not phase-locked to stimulus onset and therefore cancels out in the average, we calculate the sum of evoked and induced activity. To calculate the sum of all activity at one frequency, the absolute values of the wavelet transforms of the single trials are being averaged (AvWT).

$$\mathrm{AvWT} = \frac{1}{n}\sum_{i=1}^{n}\left|\frac{1}{\sqrt{a}}\int \overline{\Psi}\left(\frac{t-b}{a}\right)\cdot x_i(t)\mathrm{d}t\right|$$

This new time-frequency representation contains all activity of one frequency that occurred after stimulus onset, no matter whether it was phase-locked to the stimulus or not. As above, the 40 Hz activity in a pre-stimulus interval (−400 to −100 ms) is subtracted in order to get a relative measure.

Other authors refer to this sum of evoked and induced activity simply as induced activity (Tallon-Baudry and Bertrand, 1999). This may be a legitimate approximation, since the absolute amount of evoked activity is small compared to the much higher absolute values of the summed activity. Therefore, in the following, we will adapt to this terminology and refer to AvWT as induced activity.

A derivation of the publically available wavelet toolbox UVI-Wave[1] running under MATLAB® was used in our approach.

In order to generate maps of gamma activity, we computed the 40 Hz activity for each of the 148 sensors. The topographical distribution of these signals can be displayed using a linear interpolation method, as for ERP averages. Color coding is blue for values less than baseline amplitude (gamma decrease) and red for values which are higher (gamma increase).

2.5. Statistics

In order to avoid a loss of statistical power that is inherent when repeated measures ANOVAs are used to quantify multi-channel EEG data (Oken and Chiappa, 1986), selected electrode sites have to be pooled to topographical regions of interest (ROIs) (Mecklinger, 1998). This is even more important for MEG data where 148 channels are evaluated. We divided the MEG sensors into nine anatomical ROIs: anterior left (AL), anterior midline (AM), anterior right (AR), temporal/central left (TL), temporal/central midline (TM), temporal/central right (TR), posterior left (PL), posterior midline (PM), posterior right (PR). Fig. 3 shows the schematic locations of the nine ROIs and 148 sensors over the human scalp.

For statistical analyses, event-related field amplitudes were calculated for each experimental condition in each of the ROIs. ERF components were defined as mean amplitudes in the following time intervals: 100–140 ms (P1m), 140–200 ms (N1m), 200–300 ms (P2m) and 300–500 ms (P3m).

Before analyses were carried out on the gamma activity, we investigated whether the mean amplitude of the 40 Hz activity across all 148 sensors was significantly different from baseline activity. Four one-way ANOVAs with factor time interval were calculated to compare the early and late

[1]The UVI-wave package for use with MATLAB® can be downloaded from http://www.tsc.uvigo.es/~wavelets/uvi−wave.html.

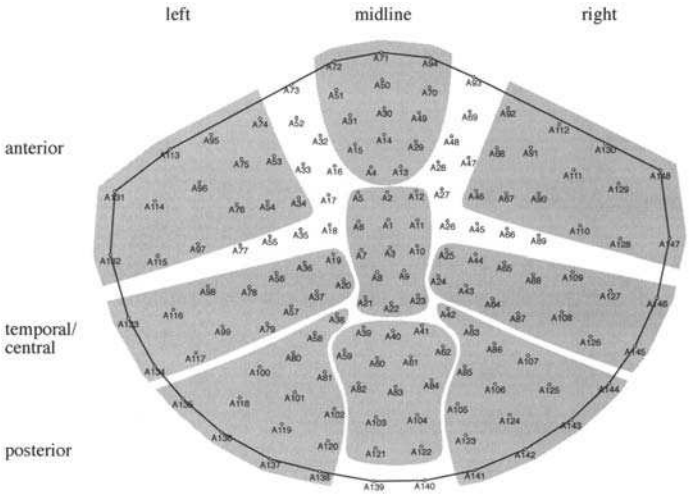

Fig. 3. The 148 sensors over a schematic head (nose at top).

time intervals of evoked and induced gamma activity with baseline gamma activity. We will refer to these ANOVAs as time-ANOVAs. Since the wavelet transform can widen peaks of gamma activity, the baseline interval was chosen from 200 to 100 ms before stimulus onset to avoid signal leakage into the baseline.

Repeated-measures ANOVAs with factors topography (anterior, temporal/central, posterior), hemisphere (left, midline, right) and condition were computed to assess the effects of the experimental variables on the ERF and gamma amplitudes. For Experiment 1, a target ANOVA, contrasting the target response with the response to standards (pooled across the three standards stimuli), was conducted (cf. Table 1). To investigate the effects within the standards, a further ANOVA was conducted which we will refer to as standard-ANOVA in the following. For Experiment 1, the standard-ANOVA was computed over the Kanizsa triangle, non-Kanizsa square and non-Kanizsa triangle. In case of Experiment 2, where a red cross was the target, also the Kanizsa square was included in the standard-ANOVA and no target-ANOVA was calculated. Repeated measures ANOVAs (target and standard version) were also computed for reaction times (RTs) and error rates of Experiment 1. In Experiment 2,

Table 1
Overview over the statistical tests conducted on the experimental conditions of the two experiments[a]

Exp.:	Statistical test:	Factor:	Factor levels:
1	Target-ANOVA	Target (2 levels)	Kan4 vs. (Kan3, Non4, Non3)
1	Standard-ANOVA	Condition (3 levels)	Kan3 vs. Non4 vs. Non3
2	Standard-ANOVA	Condition (4 levels)	Kan4 vs. Kan3 vs. Non4 vs. Non3
2	Post-hoc comp.	Shape (2 levels)	(Kan4, Non4) vs. (Kan3, Non3)
2	Post-hoc comp.	Collinearity (2 levels)	(Kan4, Kan3) vs. (Non4, Non3)

[a]The four figural stimuli are abbreviated as Kan (Kanizsa figures) and Non (non-Kanizsa figures) and numbers indicate the number of inducer disks.

means of RT and error rates were calculated, since the go/no-go paradigm required only responses to targets. RTs on trials in which a response error was made, were rejected from the data, as well as trials in which the RT exceeded 2.5 standard deviations of the mean. All effects with more than two degrees of freedom in the numerator were adjusted for violations of sphericity which are inherent in repeated-measures analyses according to the formula of Geisser and Greenhouse (1959) and Greenhouse-Geisser epsilons were used to compute the P values.[2]

3. Results

3.1. Experiment 1

3.1.1. Reaction times

The target-ANOVA revealed a significant main effect of target ($F_{1,9} = 21.28$, $P < 0.005$). Responses to the target stimulus were slower than to standard stimuli. The standard ANOVA yielded a main effect of condition ($F_{2,18} = 13.51$, $P < 0.0005$) indicating that standard RTs were also significantly different (cf. Fig. 4). Pairwise comparisons showed that all differences were significant: Kanizsa-triangle vs. non-Kanizsa triangle ($F_{1,9} = 10.46$, $P = 0.01$), Kanizsa triangle vs. non-Kanizsa square ($F_{1,9} = 5.75$, $P < 0.05$) and non-Kanizsa triangle vs. non-Kanizsa square ($F_{1,9} = 25.93$, $P < 0.001$).

For the error rates, neither the target- nor the standard-ANOVA yielded significant effects. However, Fig. 4 shows that the pattern of results for the error rates, even though not significant, resembles the one obtained for reaction times (Kanizsa square > non-Kanizsa square > Kanizsa triangle > non-Kanizsa triangle). The fact that the pattern of errors is not inverse to that of reaction times indicates that we are not dealing with a speed-accuracy trade-off, but an effect of feature processing (Pachella, 1974).

[2] The application of the Huynh-Feldt correction method yielded the identical pattern of results.

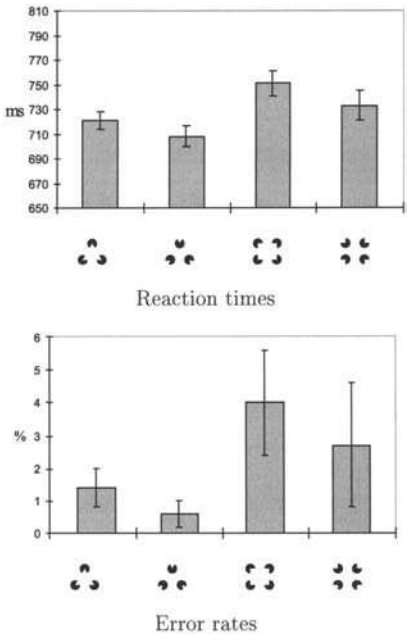

Fig. 4. Reaction times and errors (mean and standard error of mean) for Experiment 1. RTs were higher for squares than for triangles and within each shape higher for Kanizsa figures than for non-Kanizsa figures. A target main effect and all pairwise post-hoc comparisons were significant. Error rates did not differ significantly.

3.1.2. Event-related fields

Before reporting the results for event-related fields, we would like to draw the readers attention to the fact that magnetic field distributions differ from those of EEG. An electric current dipole generates a concentric magnetic field around it. Fig. 5 demonstrates how a simulated dipole in occipital cortex (a) generates EEG (b) and MEG (c). In Fig. 5c, red regions indicate that magnetic fields leave the scull and blue ones that they enter the scull. The source of magnetic activity is usually located underneath the steepest gradient of the magnetic fields.

In the P1m time interval (100–140 ms) the target-ANOVA yielded a significant interaction

of factors topography and hemisphere ($F_{4,36} = 5.47$, $P < 0.05$) indicating a polarity reversal from left (positive) to right hemisphere (negative) over temporal-central and posterior regions (cf. Fig. 6). The most probable source of this kind of magnetic brain activity can be assumed in occipital cortex and is probably resembled by two parallel dipoles in the left and right hemisphere which together generate fields similar to those of one dipole between the hemispheres (cf. Fig. 5). No significant differences between experimental conditions were obtained.

In the time interval of the N1m the target-ANOVA yielded a significant effect of hemisphere ($F_{2,18} = 28.25$, $P < 0.0001$) indicating a polarity reversal from positive (left) to negative amplitudes (right) which is shown in Fig. 6. This field pattern could again be generated by the occipital dipoles similar to those of the P1m but with a different orientation. The target-ANOVA also yielded a significant interaction of topography × hemisphere × target ($F_{4,36} = 6.98$, $P = 0.01$). Post-hoc analyses revealed a significant effect of the target factor over the left anterior ROI ($F_{1,9} = 5.30$, $P < 0.05$) revealing higher evoked fields for targets (146 fT) than for standard stimuli (121 fT).

Within the time window of the P2m (200–300 ms), no significant effects were found.

For the P3m time interval, the target-ANOVA yielded significant interactions of hemisphere × target ($F_{2,18} = 4.80$, $P < 0.05$) and topography × hemisphere × target ($F_{4,36} = 15.18$, $P < 0.0005$). Post-hoc analyses revealed larger absolute amplitudes for targets (−51 fT) than standards (14 fT) in the right anterior region ($F_{1,9} = 15.84$, $P < 0.005$). This can be seen in Fig. 7 by the deviation of the target response from the standard responses in channel A129. The patterns over each hemisphere for the P3m (cf. Fig. 6) suggests that it is generated by lateral sources.

No significant differences were revealed between experimental conditions by the standard-ANONA.

Fig. 7 shows the ERFs of Experiment 1 for nine sensors taken from the nine investigated ROIs. There are clear peaks of P1m (100–140 ms) and N1m (140–200 ms) over left- and right-hemispheric sensors. Midline sensors do not show strong activations which can also be seen in Fig. 6. The P2m (200–300 ms) shows an effect of factor target in sensors A114 and A116 which did not reach significance. Sensors A114 and A129 show a pronounced difference between targets and standards during the P3m (300–500 ms).

3.1.3. Gamma activity

Fig. 8 shows the evoked 40 Hz activity in Experiment 1 for the same nine sensors as the ERFs in Fig. 7. An early evoked response is visible between 100 and 200 ms. Therefore, this interval was chosen as the early gamma time interval and the late was chosen to be from 250 to 350 ms. The time-ANOVAs for evoked gamma activity yielded a significant main effect of time interval for the early time interval ($F_{1,9} = 37.91$, $P < 0.005$) indicating an increase with respect to baseline. No significant difference from baseline was found for the late time interval ($F_{1,9} = 0.43$). For the induced gamma activity the time-ANOVA yielded a significant main effect in the early time interval ($F_{1,9} = 10.44$, $P = 0.01$) again indicating an increase relative to baseline amplitudes. The differences of the induced gamma responses in the late time interval as compared to the baseline indicated a trend but did not reach significance ($F_{1,9} = 3.46$, $P = 0.10$). Target- and standard-ANOVAs on evoked and induced gamma activity were thus only calculated for the time interval 100–200 ms.

The target-ANOVA conducted on the early evoked gamma activity yielded a significant main effect of hemisphere ($F_{2,18} = 8.15$, $P = 0.005$) indicating larger evoked gamma activity over left and right as compared to midline regions. In addition, the target-ANOVA yielded a significant main effect of target ($F_{1,9} = 12.02$, $P = 0.01$) indicating larger evoked gamma activity for targets as compared to standards. Furthermore, a significant interaction topography × hemisphere ($F_{4,36} = 3.65$, $P < 0.05$) indicates that in frontal ROIs, the midline sensors showed lower amplitudes than sensors over the left and right hemisphere (cf. Fig. 9). This is due to the fact that the anterior peak is present only in left and right regions, while the posterior peak is also present in midline

Fig. 5

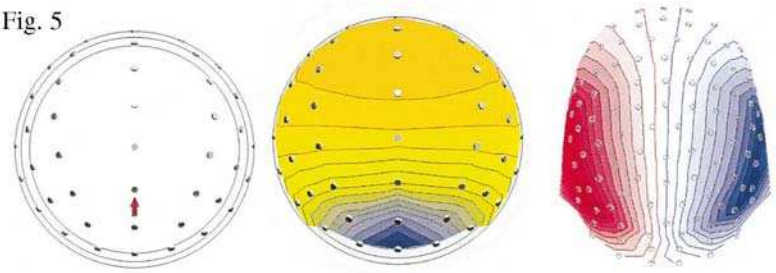

Fig. 6

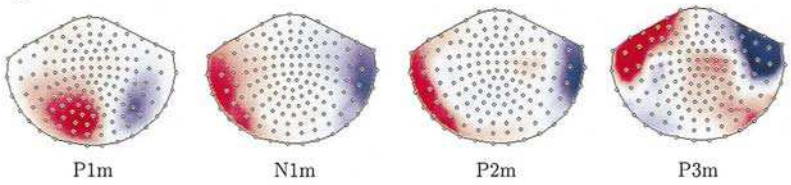

Fig. 9

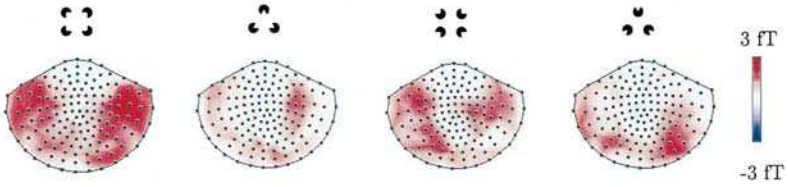

Fig. 10

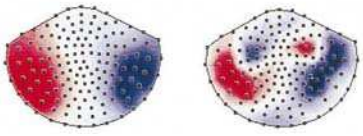

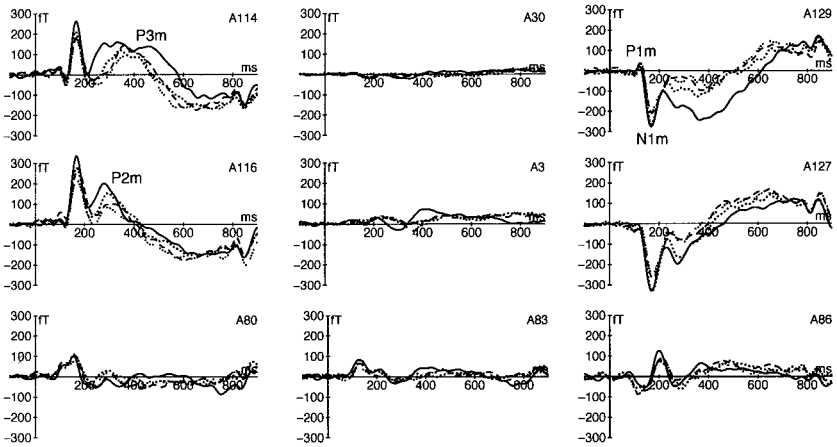

Fig. 7. ERFs of nine selected sensors in the nine ROIs averaged across 10 subjects for the four conditions of Experiment 1: Kanizsa square (solid), Kanizsa triangle (dashed), non-Kanizsa square (dotted) and non-Kanizsa triangle (intermittently dotted). Polarities of the ERFs need not correlate with the polarities of ERPs, e.g. P1 is positive in A129, while it is negative in A114.

regions. No significant differences between experimental conditions were revealed within the standards by the standard-ANOVA.

For the induced gamma activity, the ANOVAs yielded no significant effects.

3.1.4. Summary Experiment 1

To summarize the effects regarding experimental conditions, we found a target effect for the reaction times and for N1m amplitude in the left anterior as well as for P3m amplitude in the right anterior region. In addition, the early evoked gamma activity was larger for targets than standards, but no effects were found for late or induced gamma activity. Moreover, significant differences of the reaction times to the three standard stimuli indicate differential processing of these stimuli, but no electrophysiological correlate could be identified.

3.2. Experiment 2

To allow a comparison of ERF and gamma responses in Experiment 1 and 2, the following analyses will focus solely on the responses elicited by the four figural stimuli (standards). To allow a better comparison with the results of Experiment 1, the responses to the target (red fixation-cross) will not be further analyzed. However, as illustrated in Fig. 11, the ERFs showed a clear target response.

Fig. 5. A current dipole in the posterior part of a three-sphere volume conductor viewed from the top (a) generating electric potentials on the scalp (b) and magnetic fields in the sensors of the helmet over the scalp (c).

Fig. 6. Topographies of the event-related fields for the time intervals of the P1m, N1m, P2m and P3m in Experiment 1 for the stimulus Kanizsa square (target) averaged across 10 subjects. Color scales are adapted to maximum amplitudes. The polarity reversals revealed by the ANOVAs can be seen for P1m and N1m. For P2m and P3m there are bipolar patterns in each hemisphere, indicating at least one dipole per hemisphere.

Fig. 9. Topography of the early phase-locked gamma activity for the four conditions in the time interval 100–200 ms averaged over 10 subjects in Experiment 1. The activity is largest for the Kanizsa square (target, leftmost panel).

Fig. 10. Topographic maps of the event-related fields of Experiment 2 averaged across 10 subjects: the first peak of the target response (200–300 ms, left) and the second peak of the target response (300–500 ms, right).

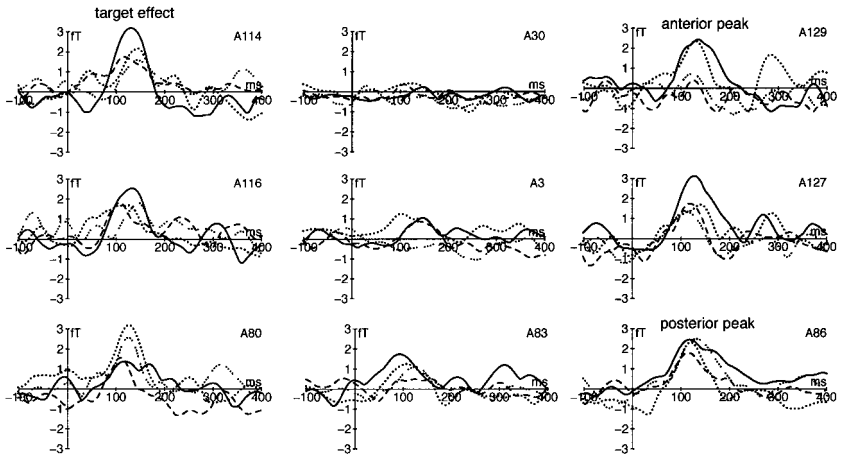

Fig. 8. Evoked 40 Hz activity for nine sensors in the nine ROIs averaged across 10 subjects for the four conditions of Experiment 1: Kanizsa square (solid), Kanizsa triangle (dashed), non-Kanizsa square (dotted) and non-Kanizsa triangle (intermittently dotted). A main effect of target was significant. Early evoked gamma significantly differed from baseline level. This was not only the case for posterior but even in anterior regions.

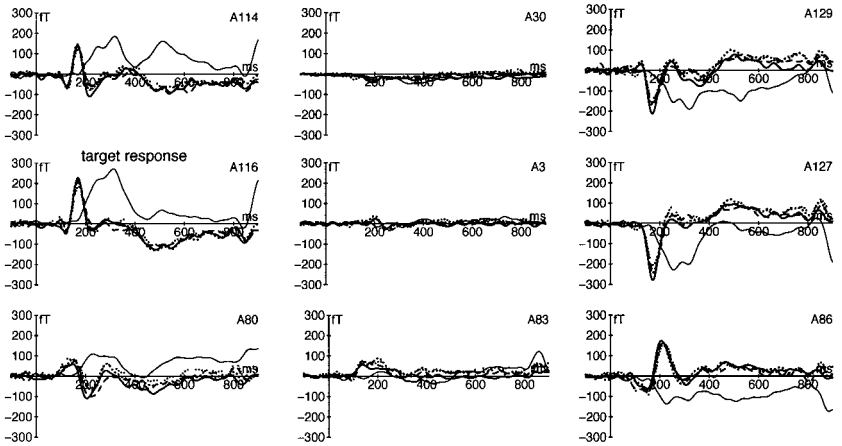

Fig. 11. ERFs of nine selected sensors in the nine ROIs averaged across 10 subjects for the five conditions of Experiment 2: Kanizsa square (thick solid), Kanizsa triangle (dashed), non-Kanizsa square (dotted), non-Kanizsa triangle (intermittently dotted) and the red fixation-cross which served as target stimulus (thin solid).

Fig. 10 shows the topographic distribution of the target response in Experiment 2. The topography of the first peak is related to that of the P1m and N1m of Experiment 1 and could be generated by an occipital source (cf. Fig. 5). The second peak of the target response (300–500 ms), which represents the P3m, clearly shows a bipolar pattern in each hemisphere indicating at least one dipole in each hemisphere. This topography is probably generated by two dipoles per hemisphere, like the target P3m of Experiment 1.

3.2.1. Reaction times

The average reaction time for responses to the red fixation cross (target) were 447 ms. The mean error rate was 6.6%. The only errors were timeouts where subjects did not press the button at all. There were no false-positive responses to standards.

3.2.2. Event-related fields

Within the time interval of the P1m, the standard-ANOVA yielded a significant main effect of hemisphere ($F_{2,18} = 4.78$, $P < 0.05$) indicating that amplitudes are positive over the left and negative over the right hemisphere. In addition, a significant interaction of topography × hemisphere ($F_{4,36} = 17.21$, $P < 0.005$) indicated that this polarity reversal is strongest over temporal-central and posterior regions. Furthermore, an interaction of hemisphere × condition ($F_{6,56} = 5.84$, $P < 0.005$) became significant. Post-hoc analyses found a significant main effect of condition over the right hemisphere ($F_{1,9} = 6.55$, $P < 0.01$). When post-hoc analyses were run with the two factors shape (triangular vs. square) and collinearity (absent vs. present) a significant main effect was found only for the factor shape ($F_{1,9} = 14.25$, $P < 0.005$).

In the N1m time interval, the standard-ANOVA yielded a significant main effect of hemisphere ($F_{2,18} = 16.28$, $P < 0.005$) indicating positive ERFs over the left and negative ERFs over the right hemisphere. In addition, the standard-ANOVA yielded a significant three-way interaction topography × hemisphere × condition ($F_{8,72} = 4.56$, $P < 0.05$). Post-hoc analyses revealed a significant main effect of condition ($F_{1,9} = 4.56$, $P < 0.05$) over the right temporal/central region only. When post-hoc analyses were run with the two factors shape (triangular vs. square) and collinearity (absent vs. present), a significant main effect of form was found ($F_{1,9} = 10.23$, $P = 0.01$).

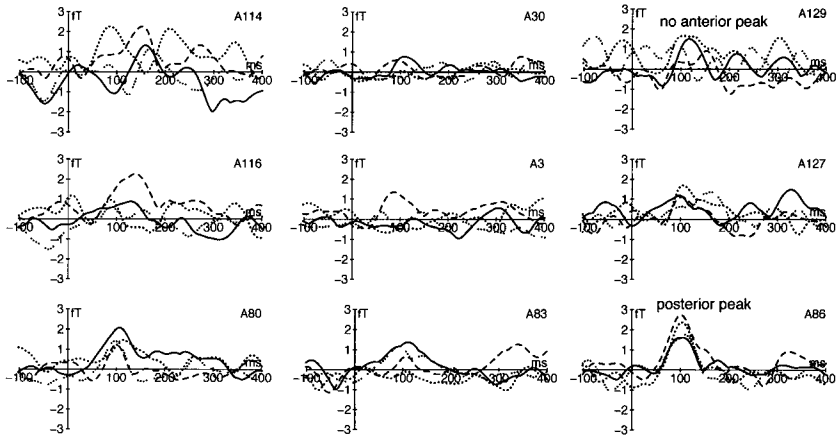

Fig. 12. Evoked 40 Hz activity of nine selected sensors in the nine ROIs averaged across 10 subjects for the four standard conditions of Experiment 2: Kanizsa square (solid), Kanizsa triangle (dashed), non-Kanizsa square (dotted) and non-Kanizsa triangle (intermittently dotted).

For the time interval of the P2m, the standard-ANOVA yielded a significant main effect for topography ($F_{2,18} = 5.25$, $P < 0.05$) indicating that ERFs are more positive in posterior regions.

Within the P3m time interval, the standard-ANOVA yielded no significant differences between the standards Fig. 11.

3.2.3. Gamma activity

In Experiment 2, the gamma responses were slightly earlier than in Experiment 1. Fig. 12 shows the evoked 40 Hz activity in Experiment 2 for nine sensors. An early response is visible between 50 and 150 ms. Consequently, this interval was chosen as the early gamma time interval and the late was chosen to be from 200 to 300 ms.[3] The time-ANOVA for evoked gamma activity yielded a significant main effect for the early time interval ($F_{1,9} = 36.49$, $P < 0.0005$) indicating an increase with respect to baseline. No significant difference from baseline for the late time interval was found ($F_{1,9} = 0.87$). For the induced gamma activity the time-ANOVA yielded a significant effect for the early time interval ($F_{1,9} = 4.82$, $P = 0.05$) indicating an increase relative to baseline. No significant difference from baseline was found for the late induced gamma activity ($F_{1,9} = 0.18$). Due to these results, target and standard-ANOVAs on gamma activity were only calculated in the time interval 50–150 ms.

The standard-ANOVA for the early evoked gamma activity yielded a significant main effect of hemisphere ($F_{2,18} = 4.89$, $P < 0.05$) indicating larger values over right than over left regions and slightly negative values over midline regions. No differences between experimental conditions were revealed.

3.2.4. Summary Experiment 2

To summarize the effects that concern the four figural stimuli, we found that square figures evoke slightly larger fields than triangular ones. This was the case over the right hemisphere for the P1m and over right temporal-central region for the N1m time interval. The other ERF components, as well as evoked and induced gamma activity, showed no significant differences between the four figural stimuli (standards).

[3] When the time intervals of Experiment 1 were adjusted to those of Experiment 2, or vice versa, no statistical differences were found.

4. Discussion

The main result of our experiments is that evoked gamma responses to figural stimuli are influenced by task requirements. In Experiment 1, where the features shape and collinearity of the four figural stimuli had to be discriminated because one of the four served as the target stimulus, we found that the gamma activity revealed differentiated processing of the four figural stimuli. In Experiment 2, the features of the four figural stimuli did not have to be discriminated, since the highly salient target (red fixation-cross) can be detected based on color discrimination. Here, no evidence for differentiated processing of the four figural stimuli was obtained in the gamma activity.

4.1. Reaction time

The effects of reaction times in Experiment 1 seem to indicate that the differentiation of the two features of the four figural stimuli (shape and collinearity) is actually processed in two steps by the brain. While it was to be expected that rare targets show longer reaction times than frequent standards (Teichner and Krebs, 1974), the significant differences between the three standards seem to represent a two-stage discrimination process. The non-Kanizsa triangle, which is dissimilar from the target (Kanizsa square) in both features, received the fastest no-response. The Kanizsa triangle, which can be differentiated from the target by its triangular shape, requires more processing time than the non-Kanizsa triangle. This could be due to the fact that it shares one of the target features while the non-Kanizsa triangle was dissimilar in both features. The non-Kanizsa square requires the most processing time of the standards — even though it also has only one feature in common with the target. However,

instead of having the feature collinearity in common with the target, the non-Kanizsa square shares the feature shape with the target. This indicates that the differentiation of the stimuli with the same shape is harder (RT differences 18 and 13 ms for Kan4/Non4 and Kan3/Non3 differentiation, respectively) than the differentiation of the stimuli with the same level of collinearity but different shape (RT differences 31 ms and 26 ms for Kan4/Kan3 and Non4/Non3 differentiation, respectively).

4.2. Event-related fields

The effects of pattern reversal for the P1m and N1m simply reflect the fact that an outgoing and an ingoing magnetic field are present over the hemispheres.

In Experiment 1, there were target effects on the N1m over the left anterior region and on the P3m over the right anterior region. A target effect on the P2m is also visible in Fig. 6 but did not reach significance. In Experiment 2, where all figural stimuli were non-targets, square figures showed differences as compared to the triangular ones over the right hemisphere within the P1m and over the right temporal-central ROI in the N1m time interval. This supports our interpretation that dissociating the shape is an individual process and different from the process which detects collinearity, which was inferred from reaction time results.

4.3. Gamma activity

In both experiments, evoked and induced gamma activity differed significantly from baseline level in the early time interval. Early gamma responses were argued to be sensory phenomena which do not differ with the degree of task complexity or attention (Karakaş and Başar, 1998). In Experiment 1, early evoked gamma activity was significantly larger for targets than standards. In Experiment 2, evoked gamma activity in the early time interval did not show any effects of experimental conditions. This demonstrates that the early evoked gamma response is modulated by task variables like discriminability of the target. Moreover, in Experiment 1, where the discrimination between the features of the figural stimuli was necessary for task performance, early evoked gamma activity was found not only at occipital but also at lateral frontal sensors. This is indicated by the topography × hemisphere interaction and further illustrated in Fig. 8. In contrast, in Experiment 2, where the target (red fixation-cross) could be discriminated without processing the shape and collinearity features of the figural stimuli, early evoked gamma activity was mainly found at occipital sensors. This can be seen in Fig. 12. From these findings, we conclude that frontal brain regions show early evoked gamma activity in response to certain stimuli only if processing of the features of these stimuli is crucial for task performance. Our results go well in line with fMRI findings that showed activity in dorsolateral prefrontal cortex in response to infrequent target stimuli which elicit P300 components (McCarthy et al., 1997). The discrimination of a target from the standards requires a comparison of the perceived stimulus to the one held in working memory. This matching process is assumed to take place in inferotemporal cortex and to depend upon top-down feedback from prefrontal cortex (Desimone et al., 1995). Our findings suggest that the early frontal gamma activity is associated with this top-down mechanism, that guides the matching process in working memory.

In Experiment 1, we found significant changes of evoked and induced gamma activity in the time interval from 100 to 200 ms. Only the evoked gamma activity showed significant differences between experimental conditions. The so-called induced activity really comprises phase-locked and non-phase-locked activity, since it simply adds up all activity in a certain frequency range-irrespective of the phase-locking. Thus, if the amount of induced activity remains unchanged while the amount of evoked activity varies, this can be due to the phase-locking of the activity. Thus, it seems plausible to assume that in Experiment 1, the target led to higher phase-locking of the gamma activity. Previous findings have indicated that evoked gamma activity increases after a stimulus while induced gamma activity decreases, which was interpreted as an increase in the phase-lock-

ing of the gamma activity after stimulation (Fell et al., 1997). Also Yordanova et al. (1997) found that targets lead to higher phase-locking in the gamma responses than did standards. In another article in this volume, Strüber et al. (2000) show that subjects who switch the perception of multistable patterns more frequently show higher phase-locking than subjects who switch less frequently. If one assumes that the sources of evoked and induced gamma activity are identical, it seems plausible to conclude that there is a stable early gamma response of approximately 100 ms after stimulus presentation for all perceived stimuli but with variable phase-locking. The more occipitally located part of this early gamma activity seems to represent the automatic bottom-up processing of the stimuli which occurs for all stimuli and was found in both experiments. This goes well in line with others findings of evoked and induced gamma activity during the perception of visual stimuli (e.g. compare reviews of Bertrand and Tallon-Baudry, 2000 and Müller et al., 2000 in this volume). On the other hand, the more frontally located part of the early evoked gamma activity seems to be only present when discrimination of the perceived features is relevant for task performance and seems to show a higher amount of phase-locking to targets than to standards. We hypothesize that the frontal gamma interacts with the occipital gamma, since its presence delays the occipital gamma in Experiment 1. This may result from a fronto-occipital feedback-loop.

We failed to find significant changes from baseline activity in the late time interval for evoked and induced activity. These findings are in line with those of Tallon-Baudry et al. (1997), who also found only early but no late gamma activity in MEG data. This is assumed to be due to a circular arrangement of neurons contributing to EEG but not to MEG gamma responses (Tallon-Baudry et al., 1999).

5. Conclusion

We were able to show that evoked and induced gamma activity in response to visually presented figural stimuli was enhanced compared to baseline in a time interval of approximately 100 ms. This was the case irrespective of whether the discrimination of the features of these stimuli was relevant for task performance. However, differences in the amplitude of the early evoked gamma activity could only be found when the features of the stimuli (shape and collinearity) had to be discriminated for adequate task performance. In that case, we found a clear enhancement for early evoked gamma responses to target stimuli.

Since this enhancement to target stimuli was only found in the evoked but not in the induced gamma activity, we argue that actually it was the phase-locking of the gamma activity which was enhanced in response to target stimuli.

Taken together, we showed that early evoked gamma activity is associated with a top-down process that might control the matching of a perceived stimulus to a template held in working memory rather than just reflecting sensory bottom-up processes.

Acknowledgements

We express our thanks to Yvonne Wolff who helped to acquire the data and to Stephan Rost who helped during data analysis.

References

Başar-Eroglu, C., Strüber, D., Schürmann, M., Stadler, M., Başar, E., 1996. Gamma-band responses in the brain: a short review of psychophysiological correlates and functional significance. Int. J. Psychophysiol. 24, 101–112.

Bertrand O., Tallon-Baudry C., 2000. Oscillatory gamma activity in humans: a possible role for object representation. Int. J. Psychophysiol. 38, 211–223.

Crick, R., Koch, C., 1990. Towards a neurobiological theory of consciousness. Semin. Neurosci. 2, 263–275.

Davis, G., Driver, J., 1994. Parallel detection of Kanizsa subjective figures in the human visual system. Nature 371, 791–793.

Desimone, R., Miller, E., Chelazzi, L., Lueschow, A., 1995. Multiple memory systems in the visual cortex. In: Gazzaniga, M. (Ed.), The Cognitive Neurosciences. MIT Press, Cambridge.

Eckhorn, R., Bauer, R., Jordan, W. et al., 1988. Coherent oscillations: a mechanism of feature linking in the visual cortex? Biol. Cybern. 60, 121–130.

Elliott M.A., Müller H., 1998a. Evidence for a 40 Hz oscillatory short-term visual memory revealed by human reaction-time measurements. J. Exp. Psychol. Learn. Mem. Cogn. 26(3), 703–718.

Elliott, M.A., Müller, H., 1998b. Synchronous information presented in 40-Hz flicker enhances visual feature binding. Psychol. Sci. 9 (4), 277–283.

Elliott M.A., Herrmann C.S., Mecklinger A., Müller H., 2000. The loci of oscillatory visual-object priming: a combined electroencephalographic and reaction-time study. Int. J. Psychophysiol. 38, 225–241.

Engel, A., König, R., Kreiter, A., Schillen, T., Singer, W., 1992. Temporal coding in the visual cortex: new vistas on integration in the nervous system. Trends Neurosci. 15 (6), 218–226.

Fell, J., Hinrichs, H., Roschke, J., 1997. Time course of human 40 Hz EEG activity accompanying P3 responses in an auditory oddball task. Neurosci. Lett. 235 (3), 121–124.

Ffytche, D., Zeki, S., 1996. Brain activity related to the perception of illusory contours. Neuroimage 3, 104–108.

Geisser, S., Greenhouse, S., 1959. On methods in the analysis of profile data. Psychometrika 24, 95–112.

Gray, C., König, R., Engel, A., Singer, W., 1989. Oscillatory response in the cat visual cortex exhibit intercolumnar synchronization which reflects global stimulus properties. Nature 338, 334–337.

Gurnsey, R., Poirier, J., Gascon, E., 1996. There is no evidence that Kanizsa-type subjective contours can be detected in parallel. Perception 25, 861–874.

Herrmann, C.S., Mecklinger, A., 1999. Target gamma response in visual ERPs. Psychophysiology 36, S59.

Herrmann, C.S., Mecklinger, A., Pfeiffer, E., 1999. Gamma responses and ERPs in a visual classification task. Clin. Neurophysiol. 110 (4), 636–642.

Kanizsa, G., 1976. Subjective contours. Sci. Am. 234 (4), 48–52.

Karakaş, S., Başar, E., 1998. Early gamma response is sensory in origin: a conclusion based on cross-comparison of results from multiple experimental paradigms. Int. J. Psychophysiol. 31, 13–31.

Knight, R.T., 1997. Distributed cortical network for visual attention. J. Cog. Neurosci. 9 (1), 75–91.

Knight, R.T., Staines, W., Swick, D., Chao, L., 1999. Prefrontal cortex regulates inhibition and excitation in distributed neural networks. Acta Psychol. 101, 159–178.

Kojo, I., Linasuo, M., Rovamo, J., 1993. Spatial and temporal properties of illusory figures. Vision Res. 33 (7), 897–901.

McCarthy, G., Luby, M., Gore, J., Goldman-Rakic, P., 1997. Infrequent events transiently activate human prefrontal and parietal cortex as measured by functional MRI. J. Neurophysiol. 77 (3), 1630–1634.

Mecklinger, A., 1998. On the modularity of recognition memory for object form and spatial location: a topographic ERP analysis. Neuropsychologia 36 (5), 441–460.

Müller, M.M., Junghöfer, M., Elbert, T., Rockstroh, B., 1997. Visually induced gamma-band responses to coherent and incoherent motion: a replication study. NeuroReport 8, 2575–2579.

Müller M.M., Gruber T., Keil A., Elbert T., 2000. Modulation of induced gamma band activity in the human EEG by attention and visual processing. Int. J. Psychophysiol. 38, 283–299.

Oken, B., Chiappa, K., 1986. Statistical issues concerning computerized analysis of brainwave topography. Ann. Neurol. 19, 493–494.

Pachella, R., 1974. The interpretation of reaction time in information processing research. In: Kantowitz, B. (Ed.), Human information processing. Erlbaum, Hillsdale, NJ.

Posner M., 1989. Foundations of Cognitive Sciences. MIT Press, Cambridge.

Reynolds, J., Desimone, R., 1999. The role of neural mechanisms of attention in solving the binding problem. Neuron 24, 19–29.

Strüber D., Başar-Eroglu C., Hoff E., Stadler M., 2000. Reversal-rate dependant differences in the EEG gamma-band during multistable perception. Int. J. Psychophysiol. 38, 243–252.

Tallon, C., Bertrand, O., Bouchet, P., Pernier, J., 1995. Gamma-range activity evoked by coherent visual stimuli in humans. Eur. J. Neurosci. 7, 1285–1291.

Tallon-Baudry, C., Bertrand, O., 1999. Oscillatory gamma activity in humans and its role in object representation. Trends Cog. Sci. 3 (4), 151–162.

Tallon-Baudry, C., Bertrand, O., Delpuech, C., Pernier, J., 1996. Stimulus specificity of phase-locked and non-phase-locked 40 Hz visual responses in human. J. Neurosci. 16 (13), 4240–4249.

Tallon-Baudry, C., Bertrand, O., Wienbruch, C., Ross, B., Pantev, C., 1997. Combined EEG and MEG recordings of visual 40 Hz responses to illusory triangles in human. Neuroreport 8, 1103–1107.

Tallon-Baudry, C., Bertrand, O., Pernier, J., 1999. A ring-shaped distribution of dipoles as a source model of induced gamma-band activity. Clin. Neurophysiol. 110, 660–665.

Teichner, W., Krebs, M., 1974. Laws of visual choice reaction time. Psychol. Rev. 81 (1), 75–98.

Yordanova, J., Kolev, V., Demiralp, T., 1997. The phase-locking of auditory gamma band responses in humans is sensitive to task processing. NeuroReport 8, 3999–4004.

Zeki, S., 1993. A Vision of the Brain. Blackwell Scientific Publications, Oxford.

ELSEVIER

International Journal of Psychophysiology 38 (2000) 225–241

INTERNATIONAL JOURNAL OF PSYCHOPHYSIOLOGY

www.elsevier.nl/locate/ijpsycho

The loci of oscillatory visual-object priming: a combined electroencephalographic and reaction-time study

Mark A. Elliott[a,*], Christoph S. Herrmann[b], Axel Mecklinger[b], Hermann J. Müller[a]

[a] *Institut Für Allgemeine Psychologie, Universität Leipzig, Leipzig, Germany*
[b] *Max-Planck Institute of Cognitive Neuroscience, Leipzig, Germany*

Received 28 September 1999; accepted 15 May 2000

Abstract

The detection of reaction-times (RTs) to a target Kanizsa-type square (an illusory square defined by the collinear arrangement of 90° corner junctions) within a matrix of distractor junctions are expedited when the target display is preceded by a 40-Hz flickering display of premask crosses presented prior to, and at the locations subsequently occupied by the junctions of the target display. Priming effects were obtained when four crosses (which together matched the Gestalt arrangement of the target) were presented at the display locations subsequently occupied by the junctions forming the target Kanizsa square (Elliott and Müller, 1998; Elliott and Müller, 2000). The present study was conducted with the aim of replicating the 40-Hz RT priming effects, while simultaneously recording the observers EEG in order to establish the presence and location of Gestalt priming in the brain. The statistical pattern obtained in the RT data corresponded well with previous studies and was matched by the pattern of target P300 latencies across bilateral central and posterior electrodes. Planned analyses focused upon the evoked 40-Hz activity that co-occurs with the P300, revealing a more specific pattern of 40-Hz priming over the visual cortex. A subsequent series of cross-correlational analyses examined the cortical distribution and timing of Gestalt-prime generation during and subsequent to premask-display presentation. Correlations were revealed between stimulus related 40-Hz activity over a range of cortical loci, including the right temporal lobe, which is considered important for figure coding. Taken together, these findings not only support the role of a distributed 40-Hz mechanism during Gestalt-figure priming, but also suggest that patterns of oscillatory brain activity may be directly influenced by, and interpretable in terms of equivalent temporal patterns of stimulus activity.

Keywords: Visual-Gestalt priming; Object coding; Kanizsa-type figure detection; Reaction time; EEG; Wavelet transform; Evoked gamma-band activity

* Corresponding author. Tel.: +49-341-973-5957; fax: +49-341-973-5969.
E-mail address: elliott@uni-leipzig.de (M.A. Elliott).

0167-8760/00/$ - see front matter
PII: S0167-8760(00)00167-7

1. Introduction

In order to successfully combine the separable feature-elements of a visual object into a single perceptual item, the feature-elements must be first differentiated and then recombined or 'bound' into a composite 'object' representation. Composite featural representations have been shown to be represented in the 'ventral' visual pathways (Ungerleider and Mishkin, 1982) which includes the temporal cortex and, particularly, the inferotemporal cortex (IT, see Desimone et al., 1984; Fujita et al., 1992; Moran and Desimone, 1985). In addition, motion-coding areas in the 'dorsal' visual pathways, such as the medial-temporal cortex (MT), are capable of responding to the motion of Gestalt configurations within their receptive fields (Logothesis and Schall, 1989). Neurophysiological studies have demonstrated that basic feature-elements are coded earlier than in either IT or MT, by anatomically and functionally specific visuo-cortical neurons tuned to particular physical attributes of the stimulus (e.g. Hubel and Wiesel, 1959; Livingstone and Hubel, 1988). It has also been demonstrated that feature-coding neurons in the visual cortex adjust their firing pattern and fire synchrony if separate stimulus features belong to the same object. These findings suggest that the 'binding' of feature-elements is achieved through temporal coordination of local activity in the visual cortex (e.g. Gray et al., 1989; Kreiter and Singer, 1992; Eckhorn et al., 1993; Frien et al., 1994), which supports the Gestalt grouping of stimulus elements according to criteria such as stimulus continuity, the proximity and common motion of stimuli (Engel et al., 1991; Gray et al., 1989).

Electroencephalographic (EEG) recordings have also shown that gamma-band activity specific to posterior electrodes varies with common stimulus motion (Lutzenberger et al., 1995; Müller et al., 1996, 1997) and is selectively enhanced when observers are asked to silently count targets that group according to continuity (Herrmann et al., 1999; Tallon et al., 1995). In addition, these and other EEG studies have also reported stimulus-specific gamma-band activity across a wider area of cortex: Başar-Eroglu et al. (1996a), Herrmann et al., (1999), Tallon-Baudry et al. (1996, 1997) have reported gamma-band activity across frontal, central and temporal electrodes as well as posterior electrodes during visuo-perceptual tasks, including the perception of multistable stimuli, visual classification and search for a target embedded amongst distractor items (respectively). The distribution of gamma-band activity across a range of brain areas corresponds well with the idea that performance on visuo-perceptual tasks such as visual grouping and object selection is mediated by mechanisms outside of the visual cortex, which has also encouraged speculation that the synchronization of neuronal firing at earlier stages of visual coding is influenced in a top-down fashion by activity at later stages (see Başar-Eroglu et al., 1996b; Singer, 1996).

In agreement with this idea, recent behavioral evidence has shown that an undetected, but figurally-relevant, priming stimulus may segment from a fully visible display of flickering premask crosses and thereby prime the reaction time (RT) response to a target-figure, subsequently presented at the same matrix location as the figural prime (i.e. the priming effect was spatially specific, see Elliott and Müller, 1998, Experiment 3). Priming was also both target- and frequency-specific and occurred only if the flicker frequency across the premask display was set at 40 Hz and not at the other mid-gamma-band frequencies tested (note that the premask display consisted of four temporally and spatially separate image frames that repeated at 10 Hz; image frames were presented sequentially, each frame for 25 ms with a 0-ms interval between frames). For a 40-Hz flicker, observers were unable to detect the spatio-temporal structure of the premask display, although the prime persisted as a form of short-term visual memory for 240–300 ms, a duration consistent with that of a 'visible' stimulus (Coltheart, 1980; Elliott and Müller, 2000). Furthermore, across the duration of prime persistence, the RTs to the target figure displayed a clear 40-Hz periodicity that was confined to trials upon which a figurally-relevant priming stimulus was presented. These findings confirmed that the internal response to prime display presentation was a process that matched the 40-Hz structure of the premask

display, which was specific to the figural coding mechanisms responsible for prime generation.

The figure-ground segmentation account for frequency-specific priming logically entails that the prime must be coded in the context of the premask display as a whole. The evidence outlined above supports this idea and also advances the idea that the prime becomes active across a number of contributive visual-coding mechanisms. Consider the finding that prime persistence is consistent with that of a visible stimulus, although the priming stimulus is not itself detected. In addition, the priming effects are spatially specific, suggesting that the prime becomes active at an early stage of visual coding where neurons respond to activity across relatively small regions of visual space (the products of which are not consciously available, see He et al., 1996), but inherits (persistence) properties consistent with the later coding of a visible stimulus; in this instance the premask display as a whole. One candidate location for the coding of the premask display has been suggested as IT (Elliott and Müller, 2000). Taken together, the accumulated evidence and speculations concerning the priming effect suggest that the prime develops an oscillatory structure across early visual-coding mechanisms through the backpropagation of an oscillatory code, which is generated across later mechanisms such as IT, and which would permit the prime to develop a periodic structure consistent with the 40-Hz periodicity of the premask-display as a whole.

In the current investigation, the RT paradigm described by Elliott and Müller (1998) was combined with EEG recording in order to examine a series of hypotheses related to the locus of the 40-Hz prime activity. Given that the previous evidence for 40-Hz oscillatory priming was based upon RT measures, as a first step, it was proposed to examine for prominent event-related potentials (ERPs) that showed evidence of prime activity matching the pattern of effects revealed within the accompanying RT data. The RTs were specifically expected to reveal target-specific priming (demonstrated by a significant interaction of target and prime) with no influence of priming on target-absent trials. Thus, for ERPs following target presentation, an equivalent pattern of effects would be considered characteristic of prime activity, although for ERPs revealed during premask display presentation (i.e. prior to presentation of the target display), this criterion was relaxed to include any significant evidence of prime activity, irrespective to the subsequent presentation of a target on those trials.

As mentioned above, the RT data of Elliott and Müller (2000) have also shown that the internal response to prime-display presentation was a figural-coding process with a 40-Hz structure. Accordingly, it was proposed to specifically examine the 40-Hz EEG response at those electrodes for which a target $\times$ prime interactions were examined in the ERP. There is evidence that the neural response to flickering stimulation matches the frequency of the stimulus (Gur and Snodderly, 1997), and a temporal correspondence between ERP components, such as the N1 or the P300, with stimulus-related 40-Hz activity has been suggested by previous studies (Başar et al., 1993; Herrmann et al., 1999). These findings influenced the choice of the wavelet analysis used in this study, which was primarily based upon the following considerations: Elliott and Müller (1998), Elliott and Müller (2000) have shown that the response to a 40-Hz flickering display which contains a figurally-relevant priming stimulus is the formation of a spatially-specific prime with a 40-Hz structure, which is phase-locked to the presentation sequence of the premask frames. This translation of the global 40-Hz rhythm to the local response to the priming stimulus might only be achieved if the 40-Hz neural response is backpropagated from visual coding areas such as IT, which code across the entire premask display, to mechanisms (in the visual cortex, for example), which code local subregions of the display. The idea that object representations are generated through recurrent activity in the brain is consistent with the findings of some recent EEG studies (see Tallon-Baudry and Bertrand, 1999), although the idea that the pattern of prime activity is 'evoked' by stimulus presentation is inconsistent with the findings of these researchers, who state that figure coding processes occur in the 'induced' (i.e. non-phase locked) gamma-band response to

stimulus presentation. However, other investigations of the gamma band response to figure presentation have shown the opposite pattern of effects (see, Herrmann et al., 1999). Herrmann et al. showed that a stimulus-specific response to illusory Kanizsa figures (also employed by Tallon et al., 1995) were precisely time locked to stimulus presentation. Given the consistency of the 'evoked' gamma-band account with the priming effects shown by Elliott and Müller (2000), it was proposed to focus upon the 40-Hz response, which was time locked to premask display presentation, for evidence of prime operation.

It was considered logical that those electrodes at which the 40-Hz EEG revealed differences between figurally relevant and non-relevant premasks, equivalent or similar to those found in the RTs, could be considered indicators of prime activity and, therefore, candidate loci for prime generation and persistence. Given that the priming effects may be principally determined by the 10-Hz EEG response to the repeat of the individual premask-frames, which should also be strongly represented in the evoked EEG response, additional (and identical) analyses examined the 10-Hz EEG response that co-occurred with the ERP. The separate analyses of 10- and 40-Hz EEG responses were considered legitimate on the basis of the proposal (see Başar-Eroglu and Başar, 1991) that the 10- and 40-Hz EEG should be considered in terms of qualitatively different types of stimulus-processing mechanisms. For the ERP, the 10- and 40-Hz EEG analyses, the likely loci of prime activity were expected to be indicated by the electrodes at which target-specific differences in prime amplitudes (i.e. target $\times$ prime interactions) were reliably obtained (i.e. given target $\times$ prime $\times$ electrode interactions).

Having identified the most likely loci for prime activity, a subsequent cross-correlational analysis was planned to examine the related hypothesis that the prime activity was not confined to single, independent mechanisms, but was generated across a series of visual coding areas. It was expected that the crosscorrelational analysis would reveal a relationship between loci at which (i) the synchronous prime might become 'locally' active at 40 Hz with (ii) loci at which the coding of global properties of the premask display might encourage the generation of the 40-Hz code adopted by the prime. Finally, the cross-correlational design was considered suitable across a series of time windows from the trial onset to target response in order to capture patterns of activity during time periods prior to the onset of the target stimulus (recall that the priming EEG effect can only occur in the time period during, or immediately after premask-display presentation).

2. Method

2.1. Observers

Eleven observers participated in the experiment (eight male; mean age 24.3 years; all with normal or corrected-to-normal vision).

2.2. Design and procedure

The experiment used a within-subject design, with stimulus parameters similar to those used previously (see Elliott and Müller, 1998). A trial always started with a brief (300-ms) 250-Hz computer-generated tone. Following a subsequent delay of 200 ms, observers were presented with the flickering 3×3 matrix of premask crosses, which after 600 ms, reduced to simple 90° corner junctions by the removal of redundant line segments (see Fig. 1a). Observers were informed that the flickering display did not require a response, but that they should fixate to the center of the display and avoid eye-movements during presentation. On removal of the redundant line segments, observers were asked to produce an RT response, as rapidly and accurately as possible, to the presence or absence of a target Kanizsa-type square within the matrix of 90° corner junctions (see Fig. 1a). In the event of an erroneous response, feedback was provided through a second (150-ms) 100-Hz computer-generated tone followed by a 500-ms delay.

The premask crosses comprised four separate frames, the members of which were presented simultaneously, but asynchronously relative to the

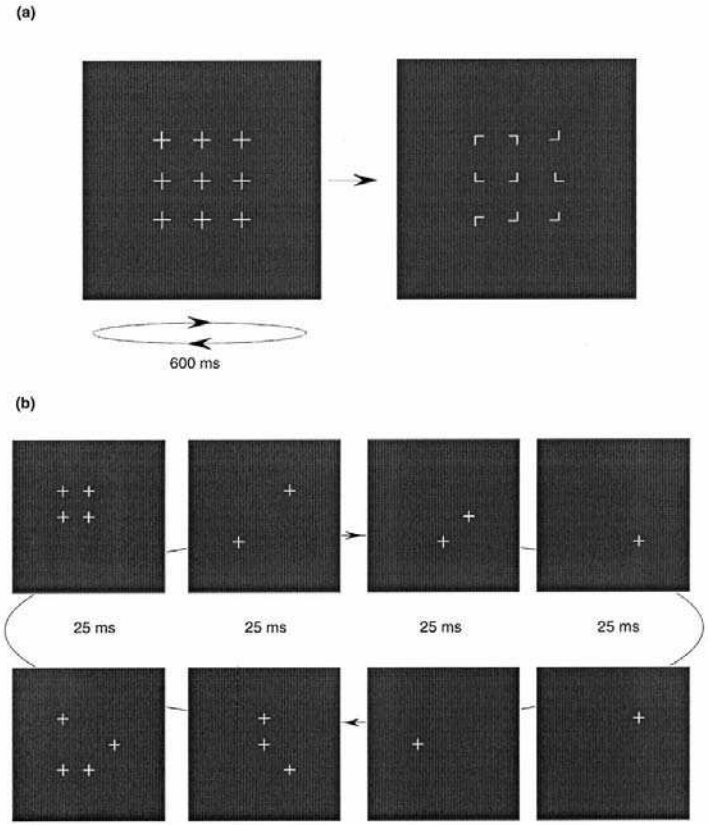

Fig. 1. The stimulus presentation paradigm. In (a), the premask-display presentation was followed by a target display to which the observers produced their target-present/absent RT responses. In (b) are shown example sequences of the four premask frames in both no-prime and prime condition, which includes a premask consisting of four elements presented in square arrangement (upper left panel).

members of other frames. As illustrated in Fig. 1b, this design permitted two premask conditions to be defined, the 'prime' and 'no-prime' conditions. In the prime condition, one subset of premask elements consisted of four crosses presented at the display locations subsequently occupied by corner junctions defining the target Kanizsa-type square. In the no-prime condition, there was also one subset comprising four elements, which were, however, presented in pseudo-random arrangement that did not correspond to a square. Pre-mask displays were presented for 600 ms and the presentation frequency across the entire premask display was maintained at 40 Hz. Thus, at 40 Hz, the entire premask matrix (i.e. the sequence of all four premask frames) was presented 10 times per 1000 ms (i.e. each premask frame repeated at 10 Hz), with a constant frame exposure duration of 25 ms and an inter-subset interval of less than 1 ms. In this

way, the premask sequence was continually 'recycled' during the lead time to target display onset. This produced the phenomenal experience of a flickering display of nine crosses, within which observers were unable to discern the structure of a given frame. Target and non-target displays did not oscillate, but were presented until a response keypress.

All conditions were presented in pseudo-random order within each of eight, 40-trial blocks and were preceded by one block of randomized practice trials immediately prior to the experiment proper. The observers were naive to the precise experimental conditions presented in each experiment and received payment at the rate of DM 15.00 per hour.

2.3. Apparatus and stimuli

Stimulus event timing and EEG trigger signals, data collection and image frame generation were controlled by a PC-compatible computer which also controlled oscilloscopic image presentation through an Interactive Electronics Systems point plotter buffer with a 8-Mb frame store memory (Finley, 1985). Image frames were presented on a 6″ Tektronix 608-oscilloscope monitor equipped with a very fast-decay P15 phosphor. The use of a P15 phosphor ensured that on-screen image persistence reduced to 10% of normal image intensity within 2.8 μs of image termination (Bell, 1970). The Interactive Electronic Systems point plotter buffer allowed pixels to be plotted at a rate of one pixel every microsecond. Although individual premask-image frames were repeatedly presented at 10 Hz, both oscillatory and static (target-display) frames were displayed at a background presentation frequency of 1 kHz.

In order to encourage EEG activity of sufficient amplitude to permit successful time-frequency analysis, both the size and brightness of the premask and target stimuli were increased in comparison with the stimulus dimensions previously employed. Stimulus luminance was increased to 1.2 cd/m^2 upon a background field of 0.075 cd/m^2 with a mean screen-surround luminance of 0.078 cd/m^2. Observers viewed the oscilloscope monitor at a distance of 38 cm (maintained via a chin rest), thereby increasing the retinal size of display elements by 150% relative to the size of similar 3×3 element displays to those used in previous experiments. Finally, both premask and target specified-to-total inducer length parameters were increased from 20% to 40%. The reliability of the 40% inducer length parameter for production of the RT priming effect was established by a pilot experiment.

Pre-mask crosses subtended 2°33′ of the visual angle, and exhibited horizontal and vertical separations of 2°42′. This produced premask displays in which the 3×3 matrix of premask elements subtended either $13°03' \times 13°03'$ of the visual angle (frame elements were arranged around the center of the monitor screen). Pre-mask crosses comprised 21 pixels and along each axis of the premask cross, pixels were separated by 16′03″ of visual angle. No gap was visible between each pixel and stimuli appeared as conjunctions of uninterrupted lines. Pre-mask frames could consist of one, two, three or four elements presented simultaneously; thus the amount of pixels presented in a given frame could be either 21, 42, 63 or 84. This could result in the brightness of premask stimuli varying across frames, with frames comprising fewer elements appearing brighter than those with more elements. In order to control for differential stimulus brightness, additional 979, 958, 937 and 916 pixels were plotted for one, two, three and four element frames (respectively). Each additional pixel was plotted to a corner of the display with {0, 0} x, y coordinates. This equalized the amount of pixels plotted in a single frame (although the extra pixels were invisible), thereby ensuring that: (i) stimulus frames were maintained at a constant 1 kHz presentation frequency; and (ii) each frame was equiluminant, despite changes in the amount of stimulus information presented.

Junction elements in the target display subtended at 1°17′ of the visual angle and were separated horizontally and vertically by between 2°42′ and 5°15′. Accordingly, target displays subtended $10°14'–13°03' \times 10°14'–13°03'$ of the visual angle. Kanizsa figures represented a 'good square' with a probability of approximately 0.45 (see Shipley and Kelman, 1992). Each target junc-

tion consisted of 11 pixels and along each axis of the junction, the pixels were separated by 16′03″ of visual angle. The target display overall consisted of 99 pixels. According to an identical procedure to that used for premask displays, an additional 901 pixels were plotted to the corner of the display. This measure ensured that premask and target displays were equiluminant.

The EEG was recorded with NeuroScan amplifiers using 19 electrodes mounted in an elastic cap. Electrodes were placed according to the international 10–20 system. The ground electrode was C2 and all electrodes were referenced to the left mastoid (M1). Electrode impedance was kept below 5 kOhm. Horizontal and vertical EOG were registered with four additional electrodes. Data were sampled at 500 Hz and analog-filtered with a 0.05-Hz high-pass and a 100-Hz low-pass filter. Averaging epochs lasted from 200 ms before premask presentation to response-button press. All epochs were visually inspected for artifacts and rejected if eye movement artifacts or electrode drifts were visible. Baselines were computed in the −200–0-ms interval for each trial and subtracted prior to subsequent ERP analyses.

2.4. Analyses

Trials on which response errors were made (3.13% of all trials), were removed from the data, before the removal of RTs above or below 2.5 S.D. from the means of all (correct) observations (1.8% of all trials). As mentioned above, RT trials were rejected on the basis of eye movement artifacts or electrode drifts revealed in the EEG (1.4% of all trials). These measures were taken to provide the basis for complementary analysis of the RT and EEG data. Accounting for these measures, all subsequent RT and EEG analyses were performed on the mean scores calculated from an average of 75 trials for each experimental condition, for each observer.

The corrected RT data (shown in Table 1) were examined by means of a repeated measures analysis of variance (ANOVA) with main terms of prime (prime, no prime) and target (present, absent). On the basis of previous research (Elliott and Müller, 1998; Elliott and Müller, 2000), the evidence for priming was expected to be indicated by a significant target × prime interaction, revealing enhancements for prime presentations on target but not target-absent trials.

Visual inspection of the mean EEG amplitudes revealed prominent premask and target N1s and a target P300. The peak amplitudes of the N1 and P300 components were obtained by picking the most negative (N1), or most positive (P300) amplitudes within appropriate time windows for each observer and for each experimental condition. By this method, the amplitudes of the premask N1 were taken as the lowest within the period 100–200 ms following premask stimulus onset, and, for the target N1, were taken as the lowest amplitudes within the period 700–900 ms from premask display onset. For the target P300, the highest amplitudes were taken from the period 800–1050 ms from premask display onset (recall that the premask display was presented for 600 ms and immediately replaced by the target display, see also Fig. 2). The latencies of each peak amplitude were also recorded for subsequent analyses. A series of (repeated measures) univariate F tests examined the possibility that the position of the reference electrode on the left mas-

Table 1
(a) Mean target-present and target-absent RTs in ms (and associated S.E. mean) and (b) mean% errors (and associated S.E. mean) as a function of prime[a]

	Target-present		$R-S$	Target-absent		$R-S$
	Prime	No prime		Prime	No prime	
(a)	451 (7)	481 (8)	30	504 (8)	506 (9)	2
(b)	2.2 (0.67)	4.01 (0.88)		3.24 (0.82)	3.06 (0.91)	

[a]*Note*: $R-S$ refers to the mean difference between prime and no-prime RTs.

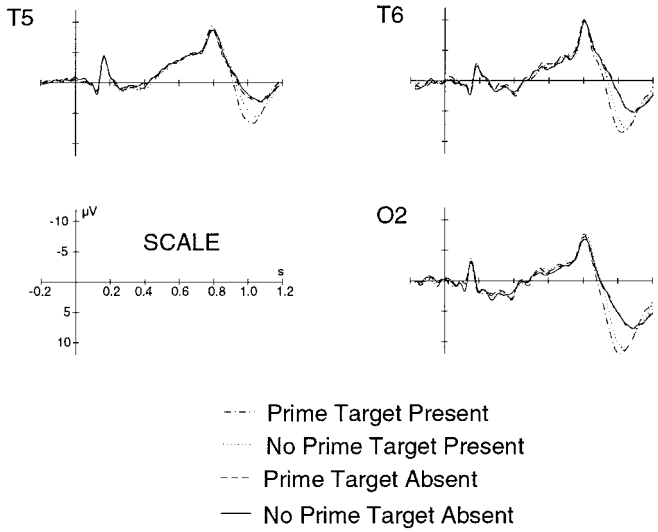

Fig. 2. Averaged ERPs for T5, T6 and O2 across an average trial duration of 1200 ms. ERPs are given for all combinations of target and prime conditions. The premask-display stimulus was presented across the first 600 ms of this period and was immediately followed by target-display presentation.

toid (M1) produced an asymmetry between the right and left hemisphere reference corrections of the EEG data. Tests were conducted for each ERP component (premask N1, target N1 and target P300) with a main term for hemisphere (right, left). For each test, hemisphere was revealed as non-significant ($F_{1,10} = 2.125$; $F_{1,10} = 0.776$; and $F_{1,10} = 2.816$, for the premask N1, target N1 and target P300, respectively), confirming that the referenced ERP amplitudes were not unilaterally biased by the position of the reference electrode.

The latency and amplitude of the N1 and P300 components at each electrode were collapsed across repeated measures and subject to principal components analyses (PCA), across observers and experimental conditions, to divide the ERP into a series of electrode subsets. The PCA is a standard, data-driven approach to analysis multiple time window and multiple electrode data with the purpose of identifying orthogonal, spatial sources of variance in the EEG (e.g. Donchin and Heffley, 1978; Donchin et al., 1997; Spencer et al., 1998; Spencer et al., in press). The PCA employed here used a correlational design with an equamax rotation, which aimed to classify the electrode amplitude/latencies into separate components (subsets) on the basis of maximum orthogonality between the mean amplitude/latencies and between the amplitude/latency subsets. The subsets of electrodes were defined for further analysis on the basis of eigenvalues > 1 and consisted of contributive amplitude/latencies (variables) with component weightings of ≥ 0.5. In practice, variable classification procedures terminated when weightings accounting for $> 50\%$ and $< 75\%$ of variance in each PCA had been extracted. Given that the target N1 potential was reliably obtained (for all observers) only at electrodes O1 and O2, no data reduction or classification procedures were applied to these data (note that the electrode subsets extracted from the PCAs conducted on the premask N1 and target P300 are given at the end of the following paragraph).

Examination of the EEG was conducted in three subsequent stages: firstly, a series of repeated-measures ANOVAs were conducted separately for all electrode subsets extracted from each PCA. These ANOVAs examined main terms for prime (prime, no prime), and electrode (variable, see below), with the additional factor target (present, absent) for the target N1 and target P300 responses. The principal object of the ERP analysis was to discover the loci of activity that displayed a similar pattern of effects to that revealed from analysis of the RT data. Specifically, and based upon the results of the RT data, the presence of target × prime and target × prime × electrode interactions in the target N1 and P300 components, with specific enhancements for primed relative to unprimed targets, were expected to indicate the likely loci at which activity across the prime and target interact. Analysis of the premask N1 was conducted with separate ANOVAs (excluding the factor target) for each of four subsets derived from the PCA. For the premask N1 the subsets consisted of: (i) amplitudes at frontal sites Fp1, Fp2, F4, F7 and F8; (ii) frontal and central amplitudes at Fz, F3, Cz, C3, C4 and T4; (iii) parietal amplitudes at Pz, P3 and P4; and (iv) occipito-parietal amplitudes at T5, T6, O1 and O2. Analysis of the target N1 was confined to occipital electrodes O1 and O2. For the target P300, amplitudes and latencies were also examined by means of separate ANOVAs for each of three subsets revealed by the PCA. These subsets could be characterized in terms of: (i) amplitudes distributed across frontal, central and temporal electrodes; (ii) centro-parietal amplitudes; and (iii) occipito-parieto-central latencies. Accordingly, the main terms for electrode in subsequent ANOVAs included: (i) amplitudes at T5, T3, T4, F3, F4, F7, F8 and FP1; (ii) amplitudes at P3, P4, CZ, C3, C4, FZ and FP2; and (iii) latencies at O1, O2, PZ, P3, P4, T5, T6 C3 and C4.

The second stage of analysis involved identical repeated measures ANOVAs to those performed on the ERP data. However, in this instance, the ANOVAs were performed on the 10-Hz and 40-Hz evoked EEG responses (time locked to premask display presentation) that co-occurred with the ERP and only for those electrode subsets within which target × prime interactions were revealed in the ERP data. For these time-frequency analyses, the ERP was convoluted with Morlet wavelets of the desired frequencies (10 and 40 Hz) to calculate specific frequency responses. The Morlet wavelet used here is calculated according to the following formula, which leads to sinusoidal waveforms.

$$\Psi(t) = e^{j\omega_0 t} e^{-t^2/2}$$

The wavelet was then compressed by a scaling factor α to obtain the desired frequency. By shifting the compressed wavelet with parameter b along the EEG signal, both the signal and the wavelet were convolved according to the following formula:

$$s_a(b) = \frac{1}{\sqrt{\alpha}} \int \overline{\Psi}\left(\frac{t-b}{\alpha}\right) x(t)\mathrm{d}t$$

where $\overline{\Psi}$ is the conjugate of the complex wavelet and $x(t)$ is the original EEG signal. To represent the phase-locked, time-frequency activity, wavelet transforms were computed across the average of single-trial data (WTAv, see below). Since the wavelet transform returns complex numbers, the absolute values were calculated. This time-frequency representation contains only that part of the activity that is phase locked to stimulus onset (i.e. the evoked gamma activity). For comparative purposes, note that in order to compute activity that is not phase locked to stimulus onset (and which cancels out in the grand average, i.e. the induced time-frequency activity), the sum of all activity should be calculated by averaging the absolute values of the wavelet transforms for the single-trial data (AvWT, see below). The application of this technique is detailed in full in Herrmann et al. (1999).

$$\mathrm{WTAv} = \left| \frac{1}{\sqrt{\alpha}} \int \overline{\Psi}\left(\frac{t-b}{\alpha}\right) \frac{1}{n} \sum_{i-1}^{n} x_i(t)\mathrm{d}t \right|$$

$$\mathrm{AvWT} = \frac{1}{n} \sum_{i=1}^{n} \left| \frac{1}{\sqrt{\alpha}} \int \overline{\Psi}\left(\frac{t-b}{\alpha}\right) x_i(t)\mathrm{d}t \right|$$

For the evoked time-frequency data, visual inspection of the amplitudes of the 10-Hz and 40-Hz responses to premask and target presentation found little variation across the range 8–12 Hz and 36–42 Hz (respectively).

The final stage of analysis involved the investigation of crosscorrelations between the (mean) subtraction of the prime from no-prime amplitudes, at 40-Hz, during the time period from premask-display onset to the target P300 response. These analyses were focused upon those electrodes at which a pattern of effects corresponding to the pattern of effects obtained in the RT data were obtained for the 40-Hz EEG response (i.e. those electrodes revealed as being of significance on the basis of a significant target × prime × electrode interaction).

3. Results

3.1. RT analysis

Analyses were conducted on the RT data prior and subsequent to correction for EEG artifacts and the pattern of effects was found to be identical. An ANOVA revealed no significant patterns within the error data. In addition, no speed-accuracy trade offs were revealed in the RT data.

Target-absent RTs were slower than target-present RTs [$F_{1,10} = 24.14$; $MS_e = 685.7$; $P = 0.001$; mean RT enhancement (and associated S.E. mean): 39 (8) ms]. Furthermore, the main effect of prime was significant ($F_{1,10} = 15.65$, $MS_e = 186.456$, $P < 0.005$). Consistent with previously reported findings (Elliott and Müller, 1998; Elliott and Müller, 2000), RT effects were confined to trials in which the flickering premask display was followed by a target Kanizsa figure [significant target × prime interaction: $F_{1,10} = 13.54$, $MS_e = 165.9$, $P < 0.005$; RT enhancements (and S.E. means) were 30 (8) ms and 2 (4) ms for target-present and target-absent conditions, respectively]. This result confirmed previously reported findings showing that figurally relevant information presented within premask-display flicker primes subsequent target detection.

3.2. EEG analyses

The ANOVAs conducted on the subsets of electrodes (revealed by the PCA analyses) for both premask and target N1's revealed no significant pattern of effects, although, as illustrated in Fig. 2, both the amplitude and latency of the target P300 was found to vary according to the presence or absence of a prime in the premask display. For the P300, the ANOVA performed on subset (i) (P300 amplitudes distributed across frontal, central and temporal electrodes) revealed no significant main effects or interactions in either the amplitudes of the ERP or 40-Hz responses. Even though the 10-Hz response varied across electrodes ($F_{7,70} = 5.563$, $MS_e = 0.0726$, $P < 0.001$) this was not significantly influenced by the presence of either target or prime. The ERP data from subset (ii) (P300 centro-parietal amplitudes) revealed a significant [2.5 microvolt (μV)] increase in (overall) amplitude for the target compared with the non-target response ($F_{1,10} = 11.5$, $MS_e = 45.532$, $P < 0.01$) and an increase in amplitude at central and posterior compared with frontal electrodes ($F_{6,60} = 7.67$, $MS_e = 41.12$, $P < 0.001$), although there was no main effect of prime nor any interactions with prime. As with subset (i), no pattern of effects were revealed from analyses of either the 10- or 40-Hz responses.

For subset (iii) (P300 occipito-parieto-central latencies) the ANOVA revealed a main effect for target ($F_{1,10} = 28.61$, $MS_e = 8688.6$, $P < 0.001$): target-present P300 latencies were faster than target absent latencies [mean latencies (and associated S.E. mean): 441 (12) and 491 (13) ms, respectively], while ERP latency on trials in which a prime was presented were, overall, faster than those in which no prime was presented (prime main effect: $F_{1,10} = 6.9$, $MS_e = 2607.83$, $P < 0.025$). Importantly, and consistent with the pattern of effects revealed in the RT data, the target × prime interaction was significant ($F_{1,10} = 10.21$, $MS_e = 3303.974$, $P = 0.001$) and was due to an earlier peak for prime compared with no-prime activity on target trials only [mean enhancements (and associated S.E. mean) 31 (12) ms and −5 (14) ms, for target-present and target-absent trials respectively; see Fig. 2]. No main effect was ob-

tained for electrode in subset (iii), nor were there any interactions with electrode, suggesting bilateral coherence in the P300 timing from central through posterior brain areas. Importantly, the target × prime interaction indicates an equivalent pattern of effects to those obtained from the RT data, which is supported by the similarity of the priming effects for the P300 and RT responses (i.e. 31 and 30 ms enhancements for target-present, compared with −5 and 2 ms for target-absent trials for the P300 and RT enhancements, respectively).

No specific loci were revealed from the ANOVA conducted on the amplitudes of the 10-Hz response (non-significant three-way interaction), although a significant target × prime interaction ($F_{1,10} = 6.05$, $MS_e = 0.0291$, $P < 0.05$) was based upon mean enhancements (no prime minus prime) of −0.56 μV for target-present and 0.28 μV for target-absent trials (respectively). A more specific indication of target priming was revealed in the corresponding evoked 40-Hz response, which accompanied the P300. For the 40-Hz response, neither target nor prime main effects were obtained, although the electrode main effect and a significant target × prime × electrode interaction were significant ($F_{8,80} = 4.55$, $MS_e = 0.0046$, $P < 0.001$; $F_{8,80} = 3.93$, $MS_e = 0.0011$, $P = 0.001$; note that the prime × electrode interaction was non-significant). The significant three-way interaction was explored by simple-main-effects analysis, which indicated the effects of prime presentation for target trials only at O2 [target present: $F_{1,10} = 81.92$, $P < 0.001$; target absent: $F_{1,10} = 0.027$, n.s, mean enhancements (and S.E. means) were 0.5 (0.02) and 0.07 (0.2) μV for target-present and -absent trials, respectively] and T6 [target present: $F_{1,10} = 8.94$, $P < 0.025$; target absent: $F_{1,10} = 0.038$, n.s, 0.4 (0.3) and 0.03 (0.5) μV for target-present and -absent trials, respectively; note that for the significant differences at O2 and T6, the no-prime response was significantly higher than the prime response]. Consistent with other findings (i.e. Hirsch et al., 1995), these results suggest that Kanizsa-type figures are coded in visuo-cortical mechanisms located principally in the right cortical hemisphere. The notion of a relationship between the figural priming effects obtained in the 40-Hz response amplitudes and the equivalent pattern of effects in the RT response gains additional support from the finding that the mean amplitude of the 40-Hz responses in O2 and T6 correlated well with the timing of RT response to the target Kanizsa-type squares. The partial correlations between the 40-Hz response amplitudes and the target-present RTs [which controlled for the 40-Hz activity at other electrodes in subset (iii)] were −0.651 and −0.029 ($P < 0.05$ and $P > 0.93$, for prime and no-prime conditions, respectively) at O2, and 0.902 and 0.911 ($P < 0.001$ and $P < 0.001$, for prime and no-prime conditions, respectively) at T6. Given the different patterns of partial correlation between the 40-Hz activity at O2 and T6 with the target-present RTs, activity at these electrodes was considered to relate differently to the process of RT response generation, with more evidence for figural priming in the differing correlations between RT and 40-Hz EEG for the prime and no-prime conditions at O2. Specifically and consistent with similar observations of 40-Hz activity during response execution reported elsewhere (e.g. Haig et al., 1999), the negative correlations obtained at O2 represent a reduction in 40-Hz amplitude accompanying target detection. One possible explanation for this finding is that the strength of 40-Hz target-coding activity over the right visual cortex is inversely proportional to the strength of 40-Hz activity induced during synchronous-premask presentation. In other words, a relatively strong pattern of existing and target-relevant 40-Hz activity appears to require a lower amplitude 40-Hz response during target detection, suggesting that some proportion of the 40-Hz response to target presentation has been prepared in advance by a synchronous-premask presentation. That the 40-Hz activity accompanying the P300 may be contrasted in terms of the priming of figure coding compared with the generation of a figurally-neutral spatio-temporal pattern of activity is supported by the absence of a correlation for no-prime conditions at O2. For the no-prime condition, an enhanced target response cannot logically result from the synchronization of neural assemblies specific to the spatial arrangement of feature elements across the target.

In summary, the pattern of results obtained from subset (iii) (P300 occipito-parieto-central latencies) are consistent with the idea that priming is a target-specific phenomenon, while in contrast to the ERP data, the corresponding evoked 40-Hz response offers more specific evidence for target priming and the associated RT effects at electrodes lying over primary visual and extrastriate visual cortex.

3.3. Cross-correlational analyses

Although the effects of target priming (i.e. the convergence of activity coding the target with that coding the prime) are evident in the 40-Hz EEG that accompanies the target P300 at O2 and T6, logically, the prime must have been generated at some point during premask-display presentation. As outlined in Section 1, it was suggested that a 40-Hz prime becomes active in the visual cortex, although prime generation is likely to require concurrent patterns of activity across more than one brain region, particularly in areas able to code across the spatial extent of the premask display. In addition, some distribution of prime activity across more than one cortical region would be necessary for coding and generating prime activity consistent with the 40-Hz frequency of premask-display frame presentation. This is logical, given that visuo-cortical neurons possess receptive fields of insufficient dimensions to code across the entire premask display, which rejects the possibility that the temporal structure of premask-display presentation is encoded exclusively by activity in early visual cortex (most likely to underlie electrodes positioned at O2 and T6). Instead, neurons within other visual processing regions (e.g. IT, MT of pre-frontal cortex) are able to respond to stimuli across a sufficiently wide region of visual space to account for the premask display as a whole and could, in principle, encode the temporal structure of premask display presentation.

In order to examine this hypothesis within the EEG, a cross-correlational analysis was employed following the standard formula described in most time series references (e.g. Box and Jenkins, 1976). Cross correlations were performed using the mean amplitude difference between the prime and no-prime conditions as this offered a more parsimonious account of the extent of priming at a given electrode and at a given point in time. The procedure used was as follows: for the 40-Hz response data for both prime and no-prime conditions, the mean amplitudes were calculated for each observer, at each electrode and across each of 11 consecutive 100-ms time windows (i.e. averaged across each successive presentation of the entire premask-display sequence from 0 to 600 ms, and in equivalent time steps, until the peak of the target P300 at between 1000 and 1100 ms). The mean amplitude differences were then calculated by subtracting the amplitude of the prime response from that of the no-prime response. In this way the extent of priming was correlated across different electrodes. Cross-correlational analyses were then performed between the 40-Hz prime responses at O2 and T6 with the 40-Hz subtractions at the remaining electrodes. Given that, overall, 36 cross correlations were calculated, a corresponding value of $\alpha = 0.0015$ was set for statistical significance. Significant cross-correlations are given in Table 2 and Fig. 3a; note that in each case the magnitude of the cross correlations exceeds the value of 0.7, described by Nunez et al. (1999) as the automatic correlation for volume conductance between electrodes separated by 4 cm or less. As illustrated in Fig. 3a, the pattern of cross correlations occurs exclusively about the lag of zero observations, which includes subtractions across temporal, parietal and central electrodes (T4, P3 and C3 for O2 and P4 for T6).

Inspection of both panels in Fig. 3b shows similar patterns of prime and no-prime 40-Hz

Table 2
Significant cross correlations (associated S.E. mean = 0.29) between priming effects at O2 and T6 with the 40-Hz subtractions at other electrodes[a]

O2	T6
T4 (0.802)	P4 (0.763)
P3 (0.802)	
C3 (0.781)	

[a] *Note*: All cross correlations are with lag 0 and differ significantly from chance performance with $\alpha \leq 0.0015$.

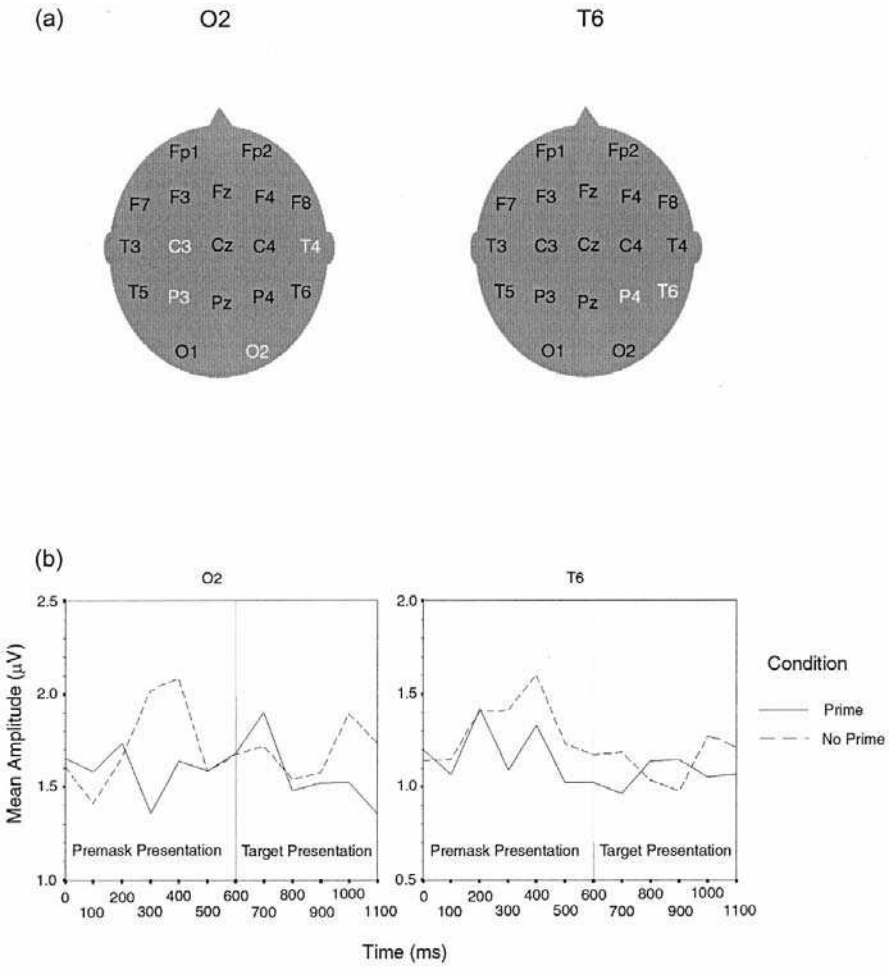

Fig. 3. (a) Significant cross correlations between the subtraction (the no-prime minus prime response) derived from the 40-Hz wavelet at O2 and T6 with the equivalent subtractions for the evoked 40-Hz response at other loci. Note that all cross correlations occurred with lag 0 and were computed for data collapsed across 11, 100 ms bins (i.e. across trial periods extending from trial onset at 0 ms to the P300 response at approx. 1100 ms). Given the number of comparisons (36), cross correlations were considered to differ significantly from chance (i.e. a correlation of 0.00) according to an α criterion of ≤ 0.0015. The cross correlations are also given in numeric form in Table 2. In (b), the mean amplitudes of the 40-Hz response for prime and no-prime conditions at O2 and T6 are plotted as a function of the time from premask display onset to the time period of the P300 (0–1100 ms). The reference line denotes the time of premask-display offset. Note the different slopes of the prime and no-prime conditions for O2 and T6 during the rise of the P300 (800–1100 ms).

activity. A major division between the 40-Hz prime and no-prime responses at both O2 and T6 occurs after 100 ms of premask-display presentation, which is characterized by an elevation of the no-prime response at between 200 and 300 ms, accompanied by a sharper decrease in the prime response at 200 ms. For both prime and no-prime responses, this pattern repeats at O2 during the rise of P300 activity to reach a maximum at 1100 ms. The positive cross correlations with activity at O2 (see Table 2) tend to indicate that the stimulus response at other electrodes exhibits a qualitatively similar character. This is supported by reference to Fig. 3b, which shows an elevated no-prime relative to a prime response at T6.

4. Discussion

Consistent with previously reported research, the RT data indicated that the presence of a figurally-relevant premask stimulus, embedded within a flickering premask display of distractor items, primes the subsequent presentation of a target according to the Gestalt configuration of the premask, even though the premask and subsequent prime are not detectable. Analysis of the parallel EEG data revealed that the statistical pattern obtained in the RT data was also found in the timing of the target P300 response at central, bilateral-parietal and occipital electrodes. The overall pattern of P300 timing across these loci did not, however, permit a more precise estimation of the locus for the RT priming effects, although a more precise correspondence between the RT and EEG priming effects was revealed within the evoked 40-Hz EEG over the right visual cortex (O2) and over extrastriate areas of the right ventral visual pathway (T6). Although this pattern of results is inconsistent with the idea that object representation may only occur as a property of induced gamma-band activity (i.e. Tallon-Baudry and Bertrand, 1999), this evidence supports other research revealing figurally-specific patterns of evoked gamma-band activity (Herrmann et al., 1999) and is entirely consistent with the idea that the prime becomes generated through the entrainment of figural coding mechanisms by a 40-Hz stimulus (see, Elliott and Müller, 1998; Elliott and Müller, 2000).

It was suggested in Section 1 that evidence of priming recorded temporal cortex (in this case at electrodes T3 and T4, which overlie the middle and superior temporal gyri; see Homan et al., 1987) might indicate the location at which the separate premask-display frames bring about a (combined) response at 40 Hz. Examination of Fig. 3a shows that the 40-Hz prime response at O2 does indeed correlate well with the 40-Hz subtraction at T4, which, like T6, lies over the right ventral visual pathway. As previously noted, given the non-detectability of the priming stimulus and spatial specificity of the priming effect (Elliott and Müller, 1998, Experiments 2 and 3), coupled with the finding that the prime exhibits a temporal structure and persistence consistent with the premask display as a whole, although the prime is most likely to be located in neural mechanisms underlying O2 and T6, the 40-Hz structure of the prime may be generated and subsequently back projected from neural mechanisms in IT, which underlies T4 in the right ventral visual pathway. This account is also consistent with the feedforward-feedback account of 40-Hz prime generation given by Elliott and Müller (2000).

The significant cross correlation of 40-Hz prime activity in both O2 and T6 with parietal electrodes (P3 and P4, respectively) cannot rule out the possibility that the spatial specificity of the priming effect is, to some extent, mediated by corresponding activity in the dorsal visual pathway, although the previous findings of Elliott and Müller (1998) argue against the priming effect as primarily dependent upon the deployment of spatial-attentional mechanisms (considered to be mediated by dorsal pathway mechanisms responding to transient signals in the visual field). Instead it seems possible that parietal mechanisms responding to the flicker across the premask display may also respond specifically to the Gestalt configuration within the flicker (as might be suggested by the findings of Logothesis and Schall, 1989). Allowing for facultative interactions between dorsal and ventral visual pathways, the contribution of parietal mechanisms may enhance, but are unlikely to be of singular signifi-

cance in generating figural priming in earlier stages. A similar conclusion may be assumed with regards to the cross correlation of activity in O2 with that in C3. C3 overlies the motor cortex and is likely to represent activity in the right hand (responsible for the target-present response). Accordingly, the possibility cannot be ruled out that generation of a 40-Hz code during visual coding also involves the generation of a response prime across mechanisms preparing the manual keypress. However, the RT data of Elliott and Müller (2000) examined the hypothesis that the 40-Hz prime was relatively non-specific to the Gestalt arrangement of synchronous-premask elements and found no evidence to support this notion, which tends to suggest the involvement of 40-Hz motor mechanisms support, rather than fully describe the 40-Hz priming effects.

One remaining puzzle concerns the differences between prime and no-prime activity at O2 and other related electrodes in which the no-prime activity achieves maximum amplitudes of a greater magnitude than those across the prime. This is shown in Fig. 3b, in which maximum 40-Hz amplitudes occur following 200–300 ms of premask-display presentation and later, with the rise of the target P300. One potential account for these phenomena includes the idea that, as the premask display is coded, the separate frames are represented in particular and different phases of the 40-Hz premask-display code. In no-prime conditions, the representation of elements across both the premask and subsequently the target displays would be coded within various phase angles determined by the location of those elements within the sequence of premask frames. During target coding, the convergence of target and premask activity early in visual processing might be expected to occur across neural assemblies coding local target elements. Accordingly, an additional latency (as was evident in the P300 response overall) combined with increased 40-Hz activity, might be expected if the neural mechanisms coding the target-display elements need to align the phase of their 40-Hz responses, which had been (randomly) shifted according to the asynchronous presentation of premask display elements at the locations subsequently occupied by the target Kanizsa-type square. The sharp increase in no-prime activity in O2 compared with the shallower slopes characterizing the no-prime responses in subsequent visual-coding areas such as T6 (see Fig. 3b) tends to support the idea that local visuo-cortical 40-Hz mechanisms are particularly susceptible to the effects of randomized premask-frame presentation. In contrast, for extrastriate neurons, receptive fields may be sufficiently large to code more than one (but not all) premask-display frames. Thus, some of the presentation asynchronies associated with premask-display frame presentation may become resolved by extrastriate neurons coding a sufficient degree of visual angle to account for the spatial separation between some of the premask frame elements. Consistent with the results shown in Fig. 3b, this should result in shallower 40-Hz target-coding activity due to the alignment of relatively fewer phase shifted neural assemblies during target coding. This account provides one hypothesis for examination in further RT and RT/EEG studies.

In conclusion, the influence of prime formation based upon the presentation of a flickering (40-Hz) visual-premask stimulus was revealed within the RTs to a subsequently presented target, with an equivalent pattern of effects obtained within the timing of the target P300 across central and posterior electrodes. A more specific pattern of effects was revealed from an analysis of the evoked 40-Hz response that accompanied the P300 at electrodes over visual cortex, specifically at O2 and T6. Subsequent cross-correlation analyses revealed that prime activity was distributed across occipital, parietal, temporal and central electrodes. On this basis, an account for Gestalt-prime generation was offered which emphasized the role of the right ventral visual pathway (responsible for visual Gestalt coding) for 40-Hz prime formation, which may be supported by both stimulus and task-specific activity recorded at parietal and central electrodes.

Importantly, the account of 40-Hz priming given here is based upon a parametric equivalence between the pattern of RT effects specific to visual-stimulus presentation within 40-Hz flicker, and a corresponding pattern of EEG effects re-

vealed within the evoked 40-Hz response to stimulus presentation. These findings not only support the role of a 40-Hz mechanism during figure-ground segmentation, but also suggest that patterns of oscillatory brain activity may be directly influenced by, and interpretable in terms of, equivalent patterns of stimulus activity.

Acknowledgements

This study is supported by Deutsche Forschungsgemeinschaft project grant No. SCHR 375/8-1. The authors' thanks are extended to D. Böttger and J. Wendt for assistance in subject recruitment and data analysis and to two anonymous reviewers for comments on an earlier draft of this manuscript. This work represents an equal contribution by the first two authors.

References

Başar, E., Başar-Eroglu, C., Demiralp, T., Schürmann, M., 1993. The compound P300-40 Hz response of the human brain. Elec. Clin. Neurophysiol. 87, 14.

Başar-Eroglu, C., Başar, E., 1991. A compound P300-40 Hz response of the cat hippocampus. Int. J. Neurosci. 13, 227–237.

Başar-Eroglu, C., Strüber, D., Kruse, P., Başar, E., Stadler, M., 1996a. Frontal gamma-band enhancement during multistable visual perception. Int. J. Psychophysiol. 24, 113–125.

Başar-Eroglu, C., Strüber, D., Schürmann, M., Stadler, M., Başar, E., 1996b. Gamma-band responses in the brain: a short review of psychophysiological correlates and functional significance. Int. J. Psychophysiol. 24, 101–112.

Bell, R.A., 1970. Application note 115. Principles of Cathode-Ray Tubes, Phosphors, and High-Speed Oscillography. Hewlett Packard Company/Colorado Springs Division, Garden of the Gods Road, Colorado Springs, Colorado, USA.

Box, G.E.P., Jenkins, G.M., 1976. Time Series Analysis: Forecasting and Control. Holden-Day, San Francisco.

Coltheart, M., 1980. Iconic memory and visible persistence. Percept. Psychophys. 27, 183–228.

Desimone, R., Albright, T.D., Gross, C.G., Bruce, C., 1984. Stimulus-selective properties of inferior temporal neurons in the macaque. J. Neurosci. 4, 2051–2062.

Donchin, E., Heffley, E., 1978. Multivariate analysis of event-related potentials: a tutorial review. In: Otto, D. (Ed.), Multidisciplinary Perspectives in Event-Related Potential Research (EPA-600/9-77-043). US Government Printing Office, Washington, DC, pp. 555–572.

Donchin, E., Spencer, K.M., Dien, J., 1997. The varieties of deviant expectancies: ERP manifestations of deviance processors. In: van Boxtel, G.J.M., Bocker, K.B.E. (Eds.), Brain and Behavior: Past, Present and Future. Tilburg UP, Tilburg, pp. 67–91.

Eckhorn, R., Frien, A., Bauer, R., Woelbern, T., Kehr, H., 1993. High frequency (60–90 Hz) oscillations in primary visual cortex of awake monkey. Neuroreport 4, 121–130.

Elliott, M.A., Müller, H.J., 1998. Synchronous information presented in 40-Hz flicker enhances visual feature binding. Psyc. Sci. 9, 277–283.

Elliott, M.A., Müller, H.J. (2000). Evidence for a 40-Hz oscillatory short-term visual memory revealed by human reaction time measurements. J. Exp. Psychol.: Learning Memory Cogn. 26(3), 703–718.

Engel, A.K., König, P., Kreiter, A.K., Singer, W., 1991. Interhemispheric synchronization of oscillatory neuronal responses in cat visual cortex. Science 252, 1177–1179.

Finley, G., 1985. A high-speed point plotter for vision research. Technical Note. Vis. Res. 25, 1993–1997.

Frien, A., Eckhorn, R., Bauer, R., Woelbern, T., Kehr, H., 1994. Stimulus-specific fast oscillations at zero phase between visual areas V1 and V2 of awake monkey. Neuroreport 5, 2273–2277.

Fujita, I., Tanaka, K., Ito, M., Cheng, K., 1992. Columns for visual features in monkey inferotemporal cortex. Nature 360, 343–346.

Gray, C.M., König, P., Engel, A.K., Singer, W., 1989. Oscillatory responses in cat visual cortex exhibit inter-columnar synchronization which reflects global stimulus properties. Nature 338, 334–337.

Gur, M., Snodderly, D.M., 1997. A dissociation between brain activity and perception: chromatically opponent cortical neurons signal chromatic flicker that is not perceived. Vis. Res. 37, 377–382.

Haig, A.R., De Pascalis, V., Gordon, E., 1999. Peak gamma latency correlated with reaction time in a conventional oddball paradigm. Clin. Neurophysiol. 110, 158–165.

He, S., Cavanagh, P., Intriligator, J., 1996. Attentional resolution and the locus of visual awareness. Nature 383, 334–337.

Herrmann, C.S., Mecklinger, A., Pfeifer, E., 1999. Gamma responses and ERPs in a visual classification task. Clin. Neurophysiol. 110, 636–642.

Hirsch, J., DeLaPaz, R.L., Relkin, N.R. et al., 1995. Illusory contours activate specific regions in human visual cortex: evidence from functional magnetic resonance imaging. Proc. Natl. Acad. Sci. USA. 92, 6469–6473.

Homan, R.W., Herman, J., Purdy, P., 1987. Cerebral location of international 10–20 system electrode placement. Elec. Clin. Neurophysiol. 66, 376–382.

Hubel, D.H., Wiesel, T.N., 1959. Receptive fields of single neurones in the cat's striate cortex. J. Physiol. London 148, 574–591.

Kreiter, A.K., Singer, W., 1992. Stimulus-dependent synchronization of neuronal responses in the visual cortex of the awake macaque monkey. J. Neurosci. 16, 2381–2396.

Livingstone, M.S., Hubel, D.H., 1988. Segregation of form, color, movement and depth: anatomy, physiology and perception. Science 240, 309–356.

Logothesis, N.K., Schall, J.D., 1989. Neuronal correlates of subjective visual perception. Science 245, 761–763.

Lutzenberger, W., Pulvermüller, F., Elbert, T., Birbaumer, N., 1995. Visual stimulation alters local 40-Hz responses in humans: an EEG study. Neurosci. Lett. 183, 1–4.

Moran, J., Desimone, R., 1985. Selective attention gates visual processing in the extrastriate cortex. Science 229, 782–784.

Müller, M.M., Bosch, J., Elbert, T. et al., 1996. Visually induced gamma-band responses in human electroencephalographic activity-a link to animal studies. Exp. Brain Res. 112, 96–102.

Müller, M.M., Junghöfer, M., Elbert, T., Rockstroh, B., 1997. Visually induced gamma-band responses to coherent and incoherent motion: a replication study. Neuroreport 8, 2575–2579.

Nunez, P.L., Srinivasan, R., Westdorp, A.F. et al., 1999. EEG coherency I: statistics, reference electrode, volume conductance, Laplacians, cortical imaging, and interpretation at multiple scales. Elec. Clin. Neurophysiol. 103, 499–515.

Shipley, T.F., Kelman, P.J., 1992. Strength of visual interpolation depends on the ratio of physically specified to total edge length. Percept. Psychophys. 52, 97–106.

Singer, W., 1996. Neuronal synchronization: a solution to the binding problem? In: Llinás, R., Churchland, P.S. (Eds.), The Mind–Brain Continuum: Sensory Processes. MIT Press, Cambridge, Mass, pp. 101–131.

Spencer, K.M., Mecklinger, A., Friederici, A.D., Donchin, E., 1998. Using a forest of electrodes to clear a garden path: Identifying the ERP components elicited by disambiguating words. Psychophysiology 35, S78.

Spencer, K.M, Dien, J., Donchin, E. (in press). A componential analysis of the ERP elicited by novel events using a dense electrode array. Psychophysiol.

Tallon, C., Bertrand, O., Bouchet, P., Pernier, J., 1995. Gamma-range activity evoked by coherent visual stimuli in humans. Eur. J. Neurosci. 7, 1285–1291.

Tallon-Baudry, C., Bertrand, O., 1999. Oscillatory gamma activity in humans and its role in object representation. Trends. Cogn. Sci. 3, 151–162.

Tallon-Baudry, C., Bertrand, O., Delpeuch, C., Pernier, J., 1996. Stimulus specificity of phase-locked and non-phase-locked 40 Hz visual responses in human. J. Neurosci. 16, 4240–4249.

Tallon-Baudry, C., Bertrand, O., Delpeuch, C., Pernier, J., 1997. Oscillatory γ-band (30–70 Hz) activity induced by a visual search task in humans. J. Neurosci. 17, 722–734.

Ungerleider, L.G., Mishkin, M., 1982. Two cortical visual systems. In: Ingle, D., Goodale, M., Mansfield, R. (Eds.), Analysis of Visual Behavior. MIT Press, Cambridge, MA, pp. 549–586.

ELSEVIER

Neuroscience Letters 297 (2001) 183–186

Neuroscience Letters

www.elsevier.com/locate/neulet

Perception of pain coincides with the spatial expansion of electroencephalographic dynamics in human subjects

Andrew C.N. Chen[a,*], Christoph S. Herrmann[b]

[a]*Human Brain Mapping and Cortical Imaging Laboratory, The International Doctoral School in Biomedical Sciences and Engineering, SMI, Aalborg University, Fred Bayers Vej 7D3, DK-9220, Aalborg, Denmark*
[b]*Max-Planck-Institute of Cognitive Neuroscience, Postfach 500 355, 04303 Leipzig, Germany*

Received 12 October 2000; received in revised form 17 October 2000; accepted 20 November 2000

Abstract

The dynamics of cortex driven by painful median nerve stimulation were investigated in event-related oscillation (ERO). We applied a wavelet time-frequency analysis to differentiate the brain dynamics between painful and non-painful somatosensory stimulation. The observed pattern to pain-induced effects exhibited a stepwise decrease of frequencies over time, starting around 26 ms over somatosensory cortex at 80 Hz, intermediate oscillations at 40 and 20 Hz around 40 ms, and reaching down to 10 Hz after 160 ms. This step-wise frequency decrease of ERO, coincident with spatial shift from the contralateral somatosensory area at 80 Hz to the centro-frontal brain at 40/20 Hz and final spatial expansion to the large region of centro-parietal areas at 10 Hz, may represent the cortical processes necessary to transfer sensory information from perceptual stages to subsequent cognitive stages in consciousness.

Keywords: Electroencephalogram; Event-related oscillation; Gamma activity; Pain; Perception; Somatosensory evoked potentials

Thalamocortical neurones are capable to produce spontaneously occurring fast oscillations, which closely resemble the induced gamma responses by external stimuli [19]. Further, both the spontaneous and induced fast polarization in the thalamic relay neurons are highly coherent with fast rhythms in cortical areas. These responses in the gamma frequency range (30–100 Hz) are considered a hallmark of brain activation pattern [19]. Induced gamma responses are part of event-related oscillations resonating between activity of single neurons and whole assemblies of neurons in a network of neocortex. Recently, it has been proposed [3] that selectively distributed electroencephalogram (EEG) oscillations in the delta, theta, alpha, beta, and gamma frequency range represent the activity of certain neural assemblies in a large web of neural networks. For example, the theta and gamma rhythms have been demonstrated to act as an integrated function in attention [14,17], short-term memory [18], perception [8,13], visual imagery [9,11], learning [10,15], and even pathological hallucination in schizophrenia [1]. Thus, event-related oscillation (ERO) in the brain and its scalp EEG dynamics can be considered as probable correlates of sensory and cognitive functions [3,4,16].

The hypothesis of gamma rhythm and ERO in the brain for feature extraction and binding common features of an object from both local and widely distributed neural systems to generate one integrated percept demands a cohesive process of spatio-temporal dynamics of EEG resonance [3]. Although significant works on gamma-binding have been rapidly accumulated in the recent years [2], the cardinal feature of the binding hypothesis which states that 'spatio-temporal dynamics of EEG rhythm at specific bandwidth acts as distributed information processing' has rarely been demonstrated or unequivocally proven. Here, we report the characteristics of the spatio-temporal dynamics of event-related oscillation upon median nerve stimulation in human pain revealing such phenomena. Our analysis of the ERO in the well-controlled experimental noxious stimulation of the median nerve adds to the understanding of cortical processing of pain, and perhaps the conscious mechanisms, in man.

Informed written consent was obtained from each subject in accordance with the Helsinki Declaration. Somatosensory evoked potentials (SEPs) were recorded from 12

* Corresponding author. Tel.: +45-9635-9826; fax: +45-9815-4008.
E-mail address: ac@smi.auc.dk (A.C.N. Chen).

0304-3940/01/$ - see front matter
PII: S0304-3940(00)01696-7

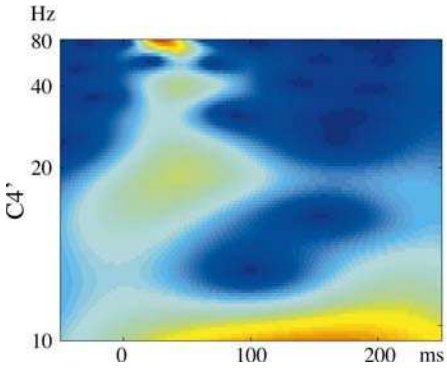

Fig. 1. Time-frequency plane of electrode C4′ (grand average across all subjects). Four individual frequency responses are evoked after stimulation: three early frequency components are at 80, 40 and 20 Hz and a late component at 10 Hz.

healthy, right-handed males (age: 26.8 ± 5.2) with 31 EEG and one electrooculogram electrodes (bandwidth 0.05–500 Hz, 2 kHz sampling, referenced to bilateral earlobes, impedance at <5 kΩ) in response to median nerve stimulation at the wrist of the left hand. Electrodes montage (cf. Fig. 2, upper left panel) followed the international 10–10 system and two extra electrodes (C3′ and C4′) were placed 2 cm posterior to C3 and C4, respectively. Baselines were computed (50 ms prior to stimulation) and subtracted before averaging. Epochs were scrutinized to be free from eye-movement and blink artefacts. Subjects were stimulated (600 trials, stimulation rate: 3 Hz) at two stimulation intensities (non-pain at 7.9 ± 3.6 mA and pain at 25.8 ± 7.6 mA) tailored individually with an average of five trials by method ascending limit. The averaged SEPs (artefact-rejected, baseline-corrected, linear detrended) of each individual subject were then subjected to a wavelet analysis in order to investigate oscillatory activity. After wavelet transformation, averages were computed across subjects, as described recently [8]. It has been shown that the perception of sensory events is accompanied by the occurrence of responses in the alpha and beta range [5]. But, in addition, gamma-band activity also has been reported during the perception of sensory perception [6]. This led us to investigate individual frequency bands of our EEG data. In a first step we computed the time-frequency representation of electrode C4′ for frequencies in the range from 10 to 80 Hz. This was conducted by calculating the convolution of the SEP signal and a wavelet of a specific frequency. The amplitudes of the convoluted signals are colour-coded and integrated into the time-frequency plane (cf. Fig. 1). The SEP was convoluted with Morlet wavelets. In order to generate topographical maps of oscillatory activity, we extracted frequency lines from the time-frequency planes that represent the absolute amount of oscillations for all electrodes in a certain period of time. We extracted only those frequencies at which activity actually occurred (80, 40, 20 and 10 Hz) that are shown in Fig. 2.

Selected electrode sites were pooled [12] to six topographical regions of interest (ROIs) in both hemispheres. The regions included the following electrodes, (e.g. ipsilateral left hemisphere): anterior region FP1, F7, F3, FC5; central region: C3, C3′, T3, PC5; posterior region: P3, T5, O1, PC1. Regions over the contralateral right hemisphere included the homologous electrodes. For statistical analyses amplitudes of oscillatory activity were pooled across the electrodes in each of the ROIs for each of the time intervals. Analysis of variances (ANOVAs) were computed for the following time intervals: 20–50 ms (early), 50–100 ms (middle) and 100–

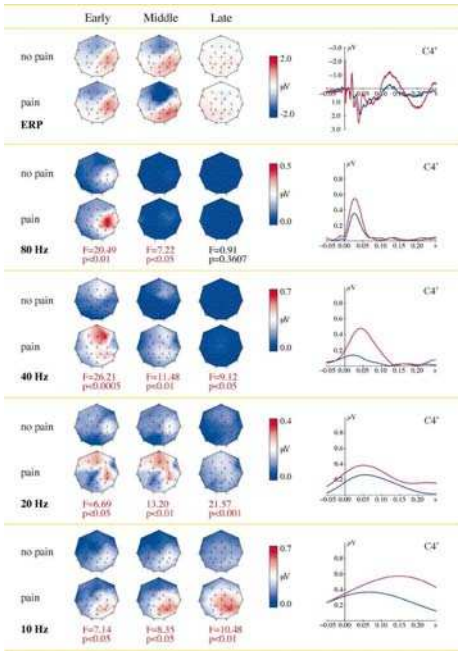

Fig. 2. Topographical distribution and time courses in response to painful and non-painful stimulation for the wide-band SEP response and the individual frequency bands. Maps are shown for the two conditions painful (lower row) and non-painful (upper row) stimulation. Each row of maps is split up into the three time intervals early (20–50 ms), middle (50–100 ms) and late (100–250 ms). Significant differences between conditions pain and no pain ($P < 0.05$) are indicated by red text. Time courses are also shown for painful (red) and non-painful (blue) stimulation. Top panel (SEPs): The maps for the wide-band (0.1–100 Hz) SEP response do not show clear differences between stimulation conditions while the time courses reveal especially a late differentiation. Oscillatory activity (lower panels) differentiate well between the two stimulation conditions.

250 ms (late). Repeated-measures ANOVAs with factors topography (anterior, central, posterior), hemisphere (left, right), frequency (80, 40, 20 and 10 Hz) and condition (pain, no-pain) were conducted to assess the effects of the experimental variables on a variety of dependent variables. All effects with more than two degrees of freedom in the numerator were adjusted for violations of sphericity which are inherent in repeated-measures analyses according to the formula of Geisser, and Greenhouse–Geisser epsilons were used to compute the *P*-values. Differences for the factor condition are shown in Fig. 2, while all other differences are reported in the text.

The time-frequency representation of the SEPs for electrode C4′ revealed four individual activities at different frequencies, i.e. at 80, 40, 20 and 10 Hz (cf. red and yellow activity in Fig. 1). Maps were calculated for each of these frequencies to determine the individual topographic distributions of each frequency and time interval. Fig. 2 shows the topographic maps for all frequencies and for the unfiltered event-related potential (SEPs, top-right panel) for the time intervals early (20–50 ms), middle (50–100 ms) and late (100–250 ms). An ANOVA resulted in significant main effects of factors hemisphere (early: $F_{1,11} = 97.44$; $P < 0.0001$; middle: $F_{1,11} = 101.19$; $P < 0.0001$; late: $F_{1,11} = 16.03$; $P < 0.005$; always the contralateral right > the ipsilateral left), frequency (early: $F_{1,11} = 3.07$; $P < 0.05$; 10 > 40 > 20 > 80 Hz; middle: $F_{1,11} = 19.43$; $P < 0.0001$: 10 > 20 > 40 > 80 Hz; late: $F_{1,11} = 44.41$; $P < 0.0001$; 10 > 20 > 40 > 80 Hz) and condition (early: $F_{1,11} = 21.24$; $P < 0.001$; middle: $F_{1,11} = 24.35$; $P < 0.0005$; late: $F_{1,11} = 14.23$; $P < 0.005$; always pain > no pain) for all time windows. In addition, significant interactions were found for topography*hemisphere (early: $F_{2,22} = 19.31$; $P < 0.0001$; middle: $F_{2,22} = 10.30$; $P < 0.001$), topography*frequency (early: $F_{6,66} = 4.48$; $P < 0.001$; middle: $F_{6,66} = 5.42$; $P < 0.001$; late: $F_{6,66} = 4.18$; $P < 0.05$), hemisphere*frequency (middle: $F_{3,33} = 10.34$; $P < 0.0001$; late: $F_{3,33} = 9.98$; $P < 0.0001$), topography*condition (middle: $F_{2,22} = 5.59$; $P < 0.05$; late: $F_{2,22} = 5.13$; $P < 0.05$), and freqency*condition (late: $F_{3,33} = 8.40$; $P < 0.05$). Post-hoc analyses for individual frequencies revealed significant main effects of hemisphere (contralateral > ipsilateral) for all frequencies and time intervals except the late 40 Hz and the middle and late 80 Hz where virtually no activity was present. Main effects for topography were only found significant in the middle time interval for 10 and 20 Hz. Main effects of condition are printed below the maps in Fig. 2. Significant interactions of topography*hemisphere were found for 10, 20 and 80 Hz in the early and for 10 Hz in the middle time interval. An interaction of hemisphere*condition was found to be significant only for the early time interval of the 80 Hz response. The latency of the amplitude maxima of all frequency components were located and summarized in a Fig. 3.

As early as 26 ms after stimulation, the difference between pain and non-pain was most pronounced in the 80 Hz activity in the hand area over C4′ contralateral to the stimulated hand with a very focal central-parietal topography. Following this early activation, a 40 Hz activity peaked at 44 ms and was significantly higher for the pain condition at the same site in C4′. This activity had two foci in frontal and central regions. Immediately after that, an ensuing 20 Hz activity peaked at 46 ms which was again higher for the pain condition than the no-pain condition, with a fronto-central topography around C4′. While the frontal activity was bilateral, the central activity was only present over the stimulated sensory area. Finally, the 10 Hz activity had its maximum in the late time window at 160 ms (C4′). The 10 Hz topography was centro-parietal, had its maximum over the contralateral right hemisphere and covered the largest region over the scalp.

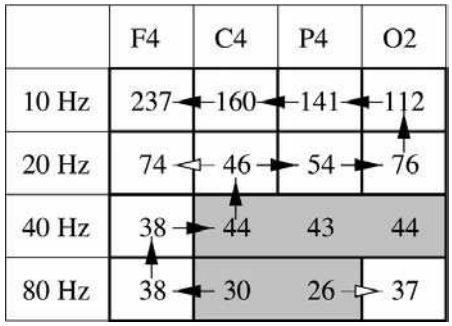

Fig. 3. Latency of maxima in four electrodes over the right hemisphere for all investigated frequency bands. Solid arrows indicate a possible path of propagation of brain electrical activity through space and frequency. Electrodes, which are activated almost simultaneously, are shaded grey. The electric response of the brain to somatosensory stimulation is first recorded under electrodes C4′/P4 at 26/30 ms in the 80 Hz frequency range and then spreads from there to more frontal and more posterior regions. The earliest maximum of the 40 Hz activity is at the same electrode as the latest maximum of the 80 Hz activity (F4), indicating a down-modulation of the frequency. The latest maximum of this 40 Hz activity at 44 ms is again the earliest maximum of the 20 Hz activity in the same electrode (C4′). When the 40 Hz activity reaches O2 it is finally down-modulated to 10 Hz activity. Propagation through the brain is indicated by horizontal arrows, and down-modulation of the frequency by vertical arrows. The temporal propagation clearly involves the step-wise transitions from 80 to 40 to 20 to 10 Hz.

The results of the peaks of the individual frequency components showed a clear increase in latency while the frequency decreased (cf. right column of Fig. 2). The 80 Hz activity peaks 26 ms after stimulation, 40 Hz after 43 ms, 20 Hz after 46 ms and 10 Hz after 112 ms. We summarized this stepwise decrease of frequency over time and topography in Fig. 3. Black arrows indicate a possible path through frequencies and brain. The activity starts over somatosensory brain early after stimulation and covers

only this primary somatosensory brain. Then the activity is propagated to frontal brain. There it was down-modulated to 40 Hz and spread towards more posterior regions again. When the 40 Hz activity reached somatosensory cortex, it was being down-modulated to 20 Hz and spread to more posterior regions. There it was down-modulated to 10 Hz, remaining in posterior regions.

Our findings showed shifts in frequencies in the electric activity of neural ensembles. It has been shown how initial gamma oscillations are being down-modulated to beta oscillations in in-vitro studies [20]. These findings indicate that during the time course of perception there is a spreading of electrical activity starting at higher frequencies and being down-modulated to sub-harmonic frequencies. Our results show that this is even true for a much broader range of frequencies, starting very locally at 80 Hz and ending rather wide-spread at 10 Hz. In addition, we also found a frontal/parietal 40 Hz response that has been hypothesized as conscious somatic perception [7]. After 26 ms, only somatosensory cortex contralateral to the stimulated hand (hemisphere*condition interaction) is activated at 80 Hz. Then the activity is down-modulated in frequency and spreads over brain. It is possible that the frequency of the EEG activity needs to be down-modulated to lower frequencies in order to activate large parts of the brain. Initial high frequencies may be capable of binding across small areas only, while lower frequencies can evoke synchronous activity in larger areas.

Time-frequency analysis of EEG proves to be highly sensitive in differentiating painful from non-painful somatosensory stimulation. This study established a spatio-temporal EEG frequency resonance model in sensory processing. Early processes are fast and focal while later processes spread out spatially and temporally. This could be due to different neural oscillators, which trigger each other and propagate their activity over the brain.

This study was supported by fundings from the Danish National Research Foundation.

[1] Baldeweg, T., Spence, S., Hirsch, S.R. and Gruzelier, J., Gamma-band electroencephalographic oscillations in a patient with somatic hallucinations, Lancet, 352 (1998) 620–621.
[2] Basar, E., Brain Functions and Oscillations. II. Integrative Brain Function. Neurophysiology and Cognitive Processes, Springer, Berlin, 1999.
[3] Basar, E., Basar-Eroglu, C., Karakas, S. and Schurmann, M., Are cognitive processes manifested in event-related gamma, alpha, theta and delta oscillations in the EEG? Neurosci. Lett., 259 (1999) 165–168.
[4] Basar, E., Demiralp, T., Schurmann, M., Basar-Eroglu, C. and Ademoglu, A., Oscillatory brain dynamics, wavelet analysis, and cognition, Brain Lang., 66 (1999) 146–183.
[5] Crone, N.E., Miglioretti, D.L., Gordon, B., Sieracki, J.M., Wilson, M.T., Uematsu, S. and Lesser, R.P., Functional mapping of human sensorimotor cortex with electrocorticographic spectral analysis: I. Alpha and beta event-related desynchronization, Brain, 121 (1998) 2271–2299.
[6] Crone, N.E., Miglioretti, D.L., Gordon, B. and Lesser, R.P., Functional mapping of human sensorimotor cortex with electrocorticographic spectral analysis: II. Event-related synchronization in the gamma band, Brain, 121 (1998) 2301–2315.
[7] Desmedt, J.E. and Tomberg, C., Transient phase-locking of 40 Hz electrical oscillations in prefrontal and parietal human brain reflects the process of conscious somatic perception, Neurosci. Lett., 168 (1994) 126–129.
[8] Herrmann, C.S., Mecklinger, A. and Pfeiffer, E., Gamma responses and ERPs in a visual classification task, Clin. Neurophysiol., 110 (1999) 636–642.
[9] Keil, A., Muller, M.M., Ray, W.J., Gruber, T. and Elbert, T., Human gamma band activity and perception of a gestalt, J. Neurosci., 19 (1999) 7152–7161.
[10] Miltner, W.H., Braun, C., Arnold, M., Witte, H. and Taub, E., Coherence of gamma-band EEG activity as a basis for associative learning, Nature, 397 (1999) 434–436.
[11] Nikolaev, A.R. and Anokhin, A.P., EEG frequency ranges during perception and mental rotation of two- and three-dimensional objects, Neurosci. Behav. Physiol., 28 (1998) 670–677.
[12] Oken, B.S. and Chiappa, K.H., Statistical issues concerning computerized analysis of brainwave topography, Ann. Neurol., 19 (1986) 493–494.
[13] Rodriguez, E., George, N., Lachaux, J.P., Martinerie, J., Renault, B. and Varela, F.J., Perception's shadow: long-distance synchronization of human brain activity, Nature, 397 (1999) 430–433.
[14] Shibata, T., Shimoyama, I., Ito, T., Abla, D., Iwasa, H., Koseki, K., Yamanouchi, N., Sato, T. and Nakajima, Y., Attention changes the peak latency of the visual gamma-band oscillation of the EEG, NeuroReport, 10 (1999) 1167–1170.
[15] Singer, W., Synchronization of cortical activity and its putative role in information processing and learning, Annu. Rev. Physiol., 55 (1993) 349–374.
[16] Singer, W., Consciousness and the structure of neuronal representations, Philos. Trans. R. Soc. Lond. B Biol. Sci., 353 (1998) 1829–1840.
[17] Sokolov, A., Lutzenberger, W., Pavlova, M., Preissl, H., Braun, C. and Birbaumer, N., Gamma-band MEG activity to coherent motion depends on task-driven attention, NeuroReport, 10 (1999) 1997–2000.
[18] Tallon-Baudry, C., Kreiter, A. and Bertrand, O., Sustained and transient oscillatory responses in the gamma and beta bands in a visual short-term memory task in humans, Vis. Neurosci., 16 (1999) 449–459.
[19] Timofeev, I. and Steriade, M., Fast (mainly 30-100 Hz) oscillations in the cat cerebellothalamic pathway and their synchronization with cortical potentials, J. Physiol. (Lond.), 504 (1997) 153–168.
[20] Traub, R.D., Whittington, M.A., Buhl, E.H., Jefferys, J.G.R. and Faulkner, H.J., On the mechanism of the gamma - beta frequency shift in neuronal oscillations induced in rat hippocampal slices by tetanic stimulation, J. Neurosci., 19 (1999) 1088–1105.

Exp Brain Res (2001) 137:346–353
DOI 10.1007/s002210100682

RESEARCH ARTICLE

Christoph S. Herrmann

Human EEG responses to 1–100 Hz flicker: resonance phenomena in visual cortex and their potential correlation to cognitive phenomena

Received: 19 June 2000 / Accepted: 9 January 2001 / Published online: 1 March 2001

Abstract The individual properties of visual objects, like form or color, are represented in different areas in our visual cortex. In order to perceive one coherent object, its features have to be bound together. This was found to be achieved in cat and monkey brains by temporal correlation of the firing rates of neurons which code the same object. This firing rate is predominantly observed in the gamma frequency range (approx. 30–80 Hz, mainly around 40 Hz). In addition, it has been shown in humans that stimuli which flicker at gamma frequencies are processed faster by our brains than when they flicker at different frequencies. These effects could be due to neural oscillators, which preferably oscillate at certain frequencies, so-called resonance frequencies. It is also known that neurons in visual cortex respond to flickering stimuli at the frequency of the flickering light. If neural oscillators exist with resonance frequencies, they should respond more strongly to stimulation with their resonance frequency. We performed an experiment, where ten human subjects were presented flickering light at frequencies from 1 to 100 Hz in 1-Hz steps. The event-related potentials exhibited steady-state oscillations at all frequencies up to at least 90 Hz. Interestingly, the steady-state potentials exhibited clear resonance phenomena around 10, 20, 40 and 80 Hz. This could be a potential neural basis for gamma oscillations in binding experiments. The pattern of results resembles that of multiunit activity and local field potentials in cat visual cortex.

Keywords Alpha · EEG · Gamma · Flicker · Resonance · SSVEP · Steady-state potentials

C.S. Herrmann (✉)
Max-Planck Institute of Cognitive Neuroscience,
Postfach 500 355, 04303 Leipzig, Germany
Tel.: +49-341-9940250, Fax: +49-341-9940113

Introduction

Oscillations in the electroencephalogram (EEG) are classified according to their relation to stimulation and can be spontaneous, evoked or induced (Başar-Eroglu et al. 1996). Spontaneous oscillations are not related to stimulation (also called background activity) while evoked oscillations appear after stimulation and are phase-locked to the stimulus. Induced oscillations also occur after stimulation but without phase-locking to the stimulus. Therefore, induced oscillations cannot be observed in averaged signals, since they cancel out due to their random phase relation to the stimulus.

The data presented here suggest a possible correlation between evoked/induced oscillations from cognitive experiments and oscillatory EEG activity which results from repetitive stimulation: so-called steady-state visual evoked potentials (SSVEPs).

Electrophysiological experiments have shown that neurons in human visual cortex synchronize their firing to the frequency of flickering light, leading to EEG responses which show the same frequency as the flickering stimulus – namely SSVEPs (Regan 1989; Silberstein 1995). This phenomenon is also called photic driving and is routinely used as an activation method in clinical EEG recordings (Takahashi 1993). SSVEPs can be evoked at weak stimulation intensities such as the monitor refresh flicker at frequencies up to at least 75 Hz when the flickering is no longer consciously perceived (Lyskov et al. 1998; Herrmann et al. 1999).[1]

Neurons in visual cortex are selectively responsive to certain features of stimuli, such as contours of specific orientation, color or motion. In order to perceive coherent objects which are composed of all these features, the brain needs to bind together the responses of the single neurons. This has been demonstrated to be done via syn-

[1] It has been argued that the reason for not perceiving stimulus changes which are still processed by cortical neurons is due to a lack of cortical connections from frontal brain areas, where memory and executive functions are supposed to reside, to area V1 (Crick and Koch 1995).

chronization of the neural spikes in cat visual cortex (Gray et al. 1989). Especially spike discharge rates in the gamma frequency range (30–80 Hz, mainly around 40 Hz) have been found to represent such binding functions in animal brains (Engel et al. 1992). Experiments with humans were able to reproduce these findings showing that so-called induced gamma oscillations are present in the human EEG when the two parts of a moving bar are perceived as one coherent object (Müller et al. 1997). If frequencies in the gamma frequency range are responsible for feature binding in visual cortex, stimuli presented at those frequencies should be bound better than stimuli presented at other frequencies. Indeed, psychophysical experiments have recently shown that stimuli which flicker at a frequency in this frequency range lead to faster processing by the brain than stimuli which flicker at other frequencies (Elliott and Müller 1998). In that study, Kanizsa-like arrangements of L-shaped angles had to be detected among randomly arranged angles. Reaction times significantly decreased when target-relevant primes were preattentively flickering at a frequency of 40 Hz prior to the detection period. These behavioral differences were also reflected by latency differences of the evoked 40-Hz response to the stimuli (Elliott et al. 2000). Evoked and induced oscillations in the gamma frequency range have been found by many researchers and have been proposed to be responsible for visual binding (Tallon et al. 1995; Herrmann et al. 1999), Gestalt perception (Keil et al. 1999), attention (Tiitinen et al. 1993; Herrmann and Mecklinger 1999) and memory representations (Tallon-Baudry et al. 1998; Pulvermüller et al. 1999).

Since 40-Hz oscillations seem to play a key role in human perception, it seems plausible to assume a neuroanatomical reason for the constant appearance of this brain response in multiple functional roles. One possible reason for such a preference to a frequency is a resonance phenomenon in the brain, i.e., the brain responds more strongly to that frequency than to others. Such a resonance phenomenon is known to exist for frequencies in the alpha frequency range (approximately 8–12 Hz), which also has been associated with a variety of perceptual and cognitive functions ranging from primary sensory coding (Schürmann et al. 1997) to memory representations (Klimesch 1997). An overview is given by Başar et al. (1997).

The objective of this experiment is to test whether a similar resonance phenomenon exists for frequencies around 40 Hz in human visual cortex by driving the visual cortex at all frequencies from 1 to 100 Hz in 1-Hz steps.

Previous experiments, which nicely demonstrated SSVEPs in animal (Başar et al. 1998) and human brains (Schürmann and Başar 1994), have computed so-called amplitude-frequency characteristics. Such diagrams indicate how the amplitude of the SSVEP changes in response to the stimulation frequency. A more detailed analysis of the frequency content of signals was used in a recent animal study where recordings from cat visual cortex were analyzed with respect to which frequencies in the recording are evoked by which stimulation frequency (Rager and Singer 1998). This method is able to differentiate between response frequencies which are identical, harmonic, subharmonic or unrelated to the stimulation frequency. Therefore, this analysis method was used here to investigate the resonance phenomena of SSVEPs in the human cortex.

Another objective was to test the correlation of human and animal data with respect to oscillatory brain responses, since a recent article has requested that such comparisons shall be made for better comparability of the two (Juergens et al. 1999). Thus, we plot our results in the same fashion as Rager and Singer (1998) plotted their animal data and compare the observed phenomena in the human brain to their findings.

Materials and methods

Subjects

Ten subjects with a mean age of 24.5 years (ranging from 19 to 34 years, six female) took part in the experiment. All subjects had normal or corrected-to-normal vision. They showed no signs of neurological or psychiatric disorders and all gave written, informed consent. All subjects were explicitly informed that flicker stimulation might lead to seizures in epileptics and reported that neither they nor any members of their families had ever suffered from epilepsy.

Stimuli

Special goggles were manufactured for this experiment with one light-emitting diode (LED) placed in front of each eyepiece. White LEDs with a light intensity of 3000 mcd (no. 153745, Conrad Electronic, 92240 Hirschau, Germany) were mounted in polished, concave metal reflectors. Thus, the full visual field was lit by the light of the two LEDs, i.e., we presented unstructured stimuli driving predominantly magnocellular (M) cells (Silberstein 1995). A frequency generator (Wavetek, 10 MHz Function generator, model *29*) was used to drive the LEDs at all frequencies from 1 to 100 Hz in 1-Hz steps. Frequencies were pseudo-randomized and the same sequence of frequencies was presented to all subjects. Each stimulation frequency was presented for 30 s with a 5-s pause in between. Whenever the LEDs received a pulse from the frequency generator, a trigger impulse was transmitted to the EEG amplifier to record all stimulation events.

Data acquisition

The EEG was recorded with TMS amplifiers (Twente Medical Systems, Enschede, The Netherlands) using 19 tin electrodes mounted in an elastic cap. Electrodes were placed according to the international 10-20 system. The ground electrode was placed over the left mastoid and all electrodes were referenced to an additional reference electrode, also placed over the left mastoid (M1). Electrode impedance was kept below 5 kΩ. Horizontal and vertical EOG were registered with four additional electrodes. EEG amplitudes were sampled at 256 kHz with an analog, first-order, anti-aliasing RC low-pass filter at 5 kHz. Data were stored at 500 samples/s after digital downsampling and digital low-pass filtering at 135 Hz with a decimating filter (inside the hardware). Data were then digitally high- and low-pass filtered offline with a finite impulse response filter (FIR) at 0.05 and 100 Hz, respectively. Due to the filter settings, frequencies below 1 Hz and above 95 Hz may have been attenuated.

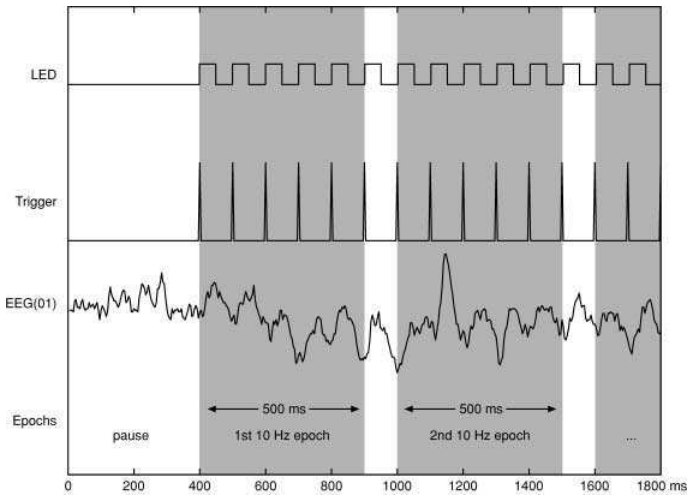

Fig. 1 Schematic of the procedure to extract 0.5-s stimulation epochs. Each 0.5-s epoch is extracted from the raw EEG data (e.g., electrode O1) where a light impulse (*LED*) starts. The beginning of every light impulse is indicated by a trigger

Data analysis

From the 30 s of each stimulation with one frequency, approximately 60 consecutive 0.5-s epochs were extracted from the EEG. Each epoch was extracted exactly at one of the trigger events where a single light stimulus started to ensure phase-locked averaging (cf. Fig. 1). All epochs were visually inspected for artifacts and were rejected if eye-movement artifacts or electrode drifts were visible. Baselines were computed in the 100-ms interval prior to the relevant event trigger for each single epoch and subtracted before computing the ERP averages.

Frequency spectra were computed for ERP averages of electrode O1 with the autoregressive method (AR, e.g., Lopes da Silva 1993). This method of estimating a frequency spectrum assumes that a spectrum can be generated by filtering white noise with zero mean and variance σ^2. Parameters a_i are estimated which set a virtual filter in such a manner that only the observed frequency components pass the filter.

The method is called autoregressive, since each digital EEG value can be predicted from the preceding values and the noise:

$$\mathrm{eeg}(k) + \sum_{i=1}^{M} a_i \,\mathrm{eeg}(k-i) = \mathrm{noise}(k) \qquad (1)$$

M is the maximum number of frequency components in the spectra and was set to 20. Once these parameters have been estimated by a special algorithm, spectral power values can be computed at each frequency f (here, j is the imaginary number and ω is 2π times the frequency):

$$S(f)\frac{\sigma^2}{\left|1+\sum_{i=1}^{M} a_i\, e^{-jwi}\right|^2} \qquad (2)$$

Spectral values were multiplied by their frequency to correct for the $1/f$ characteristic of the typical frequency spectrum. The 100 frequency spectra were arranged in a two-dimensional plane and power values were coded in gray scales, i.e., one horizontally arranged spectrum was represented in gray scale for each stimulation frequency on the vertical axis (cf. Fig. 5). These spectral planes were averaged across all ten subjects.

Since the AR does not provide information on the phase angle of a frequency component, FFT spectra were computed to estimate the phase shift of an SSVEP relative to the stimulation and were used for some of the figures (where mentioned) for easy comparison with other studies.

Results

Subjects reported perceiving flickering light below and constant dim light above a frequency of about 30 Hz (flicker fusion frequency). In addition, most subjects reported form (stars or stripes) and color (blue, red or purple) illusions at frequencies around 10–15 Hz.

Event-related potentials

Figure 2 shows the SSVEP (top row) of one subject in response to stimulation frequencies of 10 (left), 20 (middle) and 30 Hz (right). In the bottom row, the corresponding frequency spectra (computed with an FFT) are displayed. For 10 Hz stimulation the SSVEP shows a clear 10-Hz and a harmonic 20-Hz response. At 20 Hz stimulation, only a 20-Hz response is visible in the SSVEP and at 30 Hz stimulation a 15-Hz subharmonic appears in addition to the 30-Hz response.

Figure 3 demonstrates the frequency selectiveness of the visual system of one subject for three adjacent frequencies. While the responses to 35 and 37 Hz stimulation lead to corresponding frequency peaks of about 17 μV^2, a stimulation frequency of 36 Hz leads to 27 μV^2.

A similar frequency selectivity can be observed for the 10-Hz SSVEP which was often evoked by flicker frequencies higher than 10 Hz. Figure 4 shows the SSVEP of one subject to frequencies of 79, 80 and 81 Hz. At 80 Hz a clear 10-Hz response was evoked which was not present at adjacent frequencies.

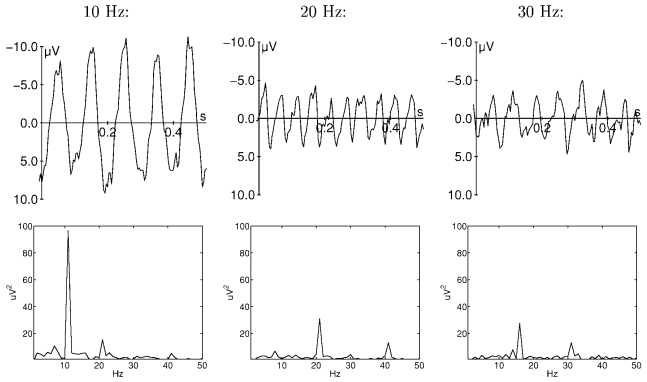

Fig. 2 SSVEPs of a single subject in response to 10 Hz (*left*), 20 Hz (*middle*) and 30 Hz (*right*) stimulation (*top row*) and the corresponding FFT frequency spectra (*bottom row*)

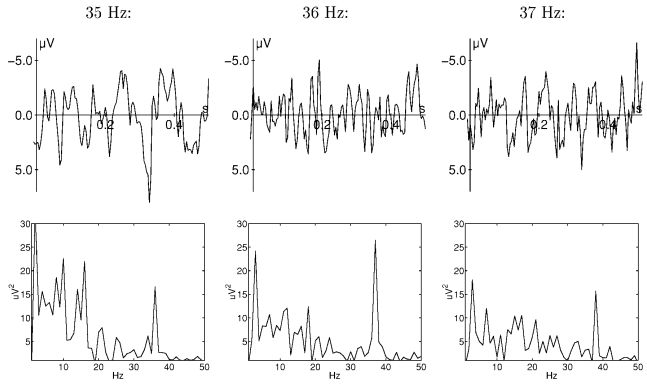

Fig. 3 SSVEPs of a single subject in response to 35 Hz (*left*), 36 Hz (*middle*) and 37 Hz (*right*) stimulation (*top row*). The corresponding FFT frequency spectra show an increase of power at 36 Hz for 36 Hz stimulation (*middle*) as compared to adjacent frequencies (*left and right*)

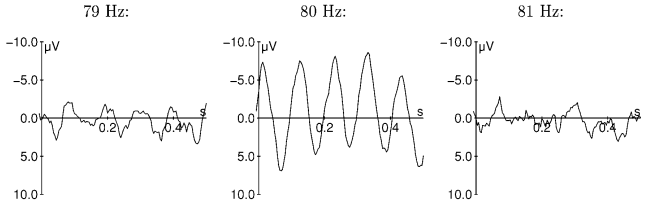

Fig. 4 SSVEPs in response to flicker frequencies 79 (*left*), 80 Hz (*middle*) and 81 Hz (*right*). The VEP shows clear 10-Hz oscillations at 80 Hz which are not as prominent for the adjacent frequencies

Frequency plane

Figure 5 shows the SSVEP response frequency as a function of the stimulation frequency. A clear fundamental can be seen as the diagonal which indicates that the visual cortex is driven by the flickering stimulus at precisely the stimulation frequency. In addition, a first and second harmonic are clearly visible and a third and even fourth harmonic can be marginally detected. This shows that response frequencies which are integer multiples of the stimulus frequency are also evoked by the flicker. Moreover, also subharmonic oscillations can be seen at the intersection with the 10-Hz alpha response. The alpha response is evoked not only by stimulation at and around 10 Hz, but also at higher frequencies which are possibly harmonics (compare with vertical 10-Hz line in Fig. 5). At 39 Hz stimulation frequency, a response in the SSVEP is seen at numerous frequencies which are all multiples of 13.5 Hz (cf. horizontal line at 39 Hz in Fig. 5). Here, the fundamental response frequency is shifted from 39 Hz to 40.5 Hz (3×13.5 Hz).

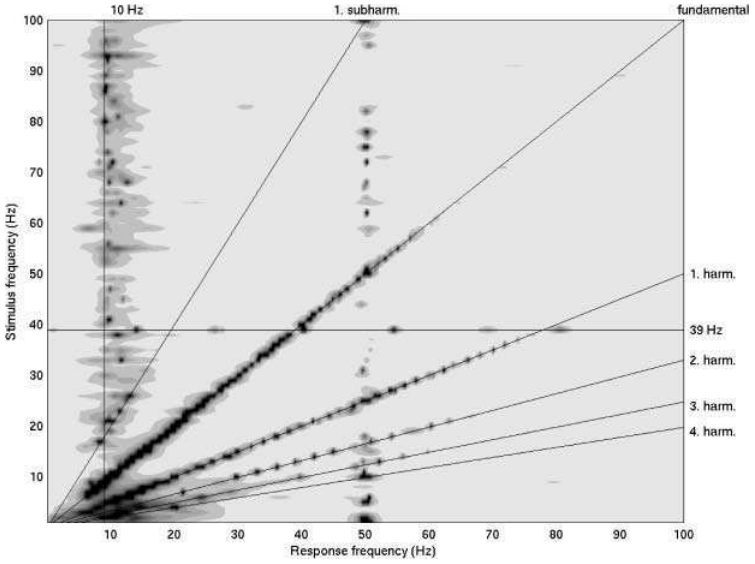

Fig. 5 Response frequency (*x-axis*) as a function of stimulation frequency (*y-axis*). The fundamental frequency (stimulus freq. = response freq.) can be seen as well as a first and second harmonic. Alpha (around 10 Hz) responds to many stimulation frequencies and preferably at intersections with the subharmonics. An enhanced response to 39 Hz stimulation can be observed

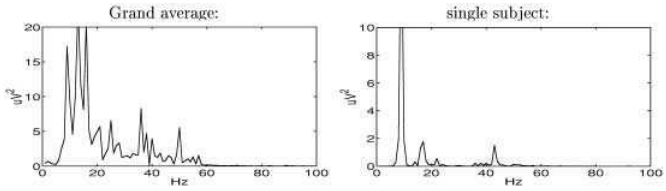

Fig. 6 Profile of the fundamental frequency for the average across all ten subjects (*left*) and for one single subject (*right*). Clear resonance peaks are visible around 10, 20 and 40 Hz

The profile along the fundamental frequency is shown in Fig. 6 for the average across all ten subjects (left) and for a single subject (right). The average exhibits strong resonance peaks around 10 Hz and weaker peaks in the 20- to 30- and 35- to 45-Hz range (the 50-Hz peak is due to the German line frequency). The single subject data show that each subject contributes only one of the spectral peaks per frequency range, i.e., one at 10, one at 16 and one at 42 Hz in the shown case.

Figure 7 shows SSVEP spectrum peaks at response frequencies 10, 20, 30, 40 and 50 Hz computed at the given frequency plus/minus 1 Hz from spectra of all stimulation frequencies (vertical profiles in Fig. 5). In each spectrum a peak is visible at the stimulation frequency. For higher frequencies, subharmonic peaks are also observed, e.g., a 10-Hz and a 15-Hz peak in response to the 30-Hz stimulation. The system mainly responds to the stimulation frequency and to frequencies which are subharmonic to the stimulation frequency.

Figure 8 shows the topographical distribution of the 10-Hz activity evoked by 10-Hz stimulation in a single subject. The map was computed for one positive peak in

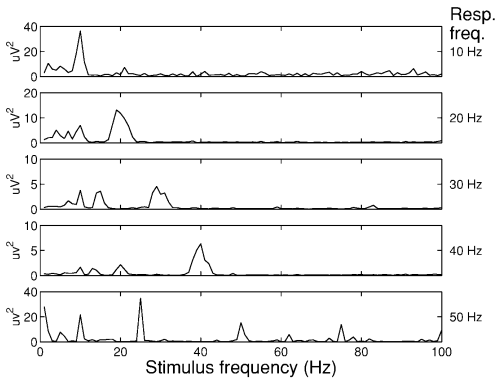

Fig. 7 Vertical profiles at certain response frequencies show that the system mainly responds to the stimulation frequency and subharmonic frequencies

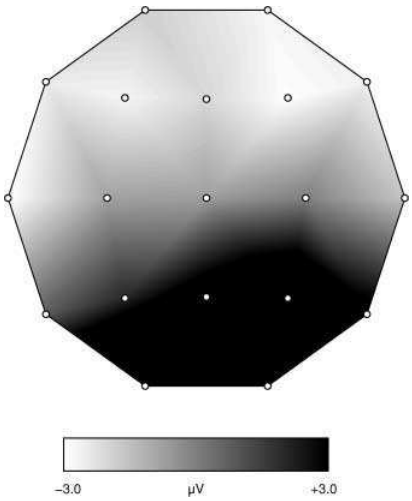

Fig. 8 Topographical distribution of the 10-Hz SSVEP of a typical subject. Occipital positivities and frontal negativities suggest an occipital source of the activity which projects to frontal regions

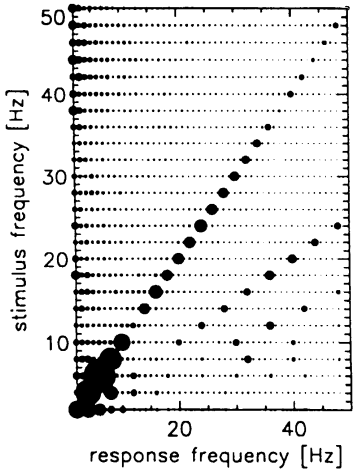

Fig. 9 Response frequency as a function of stimulation frequency for local field potentials of area 17 of cat visual cortex. Adapted from Rager and Singer (1998, Fig. 7) with permission of the corresponding author

the SSVEP and shows a positivity over occipital cortex with a simultaneous negativity over frontal cortex.

Discussion

The topographical distribution of the SSVEP shown in Fig. 8 is typical for occipital dipoles in visual cortex as they are assumed for primary visual ERP components, such as the P100 in response to checkerboard onset (Ossenblok and Spekreijse 1991). Therefore, it seems plausible to assume that the generators of the visual SSVEP also lie in visual cortex. This has also been found by functional magnetic resonance imaging (fMRI) experiments (Hillyard et al. 1997).

In a recent experiment, local field potentials (LFPs) and multiunit activity (MUA) were recorded from cat visual cortex during flicker stimulation from 2 to 50 Hz (Rager and Singer 1998). Our results are the first human SSVEPs which have been evaluated with the surface-plot method which was introduced for steady-state responses by Rager and Singer (1998). Our results demonstrate a high correlation of the cortical MUA and LFPs from cat visual cortex with human scalp EEG during flicker stimulation. The strong correlation is demonstrated by the marked similarity of Fig. 5 (our data) and Fig. 9 (cat data). Both recordings demonstrate that the visual cortex can be driven by external stimulation up to frequencies of at least 50 Hz. In addition, the brain oscillates at harmonic frequencies of the stimulation frequency. Juergens et al. (1999) have recently demanded that animal MUA and LFPs be correlated with human EEG recordings to gain further insights into the similarities and differences of the two measures. Our results give rise to the assumption that oscillatory multiunit activity and local field potentials evoked by flickering light in cat visual cortex are closely related to the SSVEP recorded from the human scalp. In addition to the similarity with the cat data, our results also reveal a difference: the strong responsiveness of the alpha frequency range, especially where the subharmonic of the stimulation frequency intersects with the alpha band, was not found in the cat data. This may be due to the fact that the generators responsible for alpha oscillations are constituted of larger networks of neurons which are not captured when MUA or LFPs are recorded.

The SSVEPs in response to some frequencies show resonance phenomena indicating a selective frequency preference of the neural oscillators. Resonance phenomena occurred in the 10-, 20-, 40- and 80-Hz frequency range, i.e., human visual cortex responds to flickering stimuli at these frequencies more strongly than to stimuli flickering at adjacent frequencies, even though the stimuli are otherwise identical. Therefore, this resonance property may be the underlying phenomenon resulting in enhanced response characteristics when stimuli flicker at around 40 Hz, as demonstrated by Elliott and Müller (1998). This is especially probable, since those stimuli also resulted in EEG oscillations in the gamma frequency range (Elliott et al. 2000). At the same time, the resonance phenomena observed here may explain the predominance of 40-Hz rhythms in binding experiments that occur in human EEG (Tallon Baudry and Bertrand 1999; Keil et al. 1999), MEG (Herrmann and Mecklinger

2000) and animal MUA (Engel et al. 1992; Eckhorn 1994).

The axonal connections between the neurons of an oscillating ensemble have certain temporal characteristics which will propagate spikes at much the same delay after every spike discharge. This can lead to a preferred oscillation frequency and may be the neuroanatomical reason for 40-Hz oscillations even if the generators of evoked/induced and steady-state oscillations are not identical but share common feedback properties.

Our results demonstrate that the neural oscillators which underlie the observed SSVEP oscillations constitute a non-linearly coupled system. Harmonic oscillators show exactly one resonance peak in the frequency spectrum which is the systems resonance frequency. Taking into account that our results show harmonic as well as subharmonic resonance peaks in the spectral plane leads to the conclusion that the involved oscillators constitute a non-linearly coupled system. This interpretation goes in line with previous findings suggesting that the human alpha rhythm behaves in a non-linear fashion (Stam et al. 1999).

The observed hallucinations could be due to the oscillating SSVEP propagating across retinotopic areas of visual cortex. One area then is successively excited and inhibited, thus leading to hallucinations. This phenomenon is known from certain kinds of epilepsies and has been simulated in mathematical models (Tass 1995, 1997). Some of our subjects were retrospectively shown the hallucinations calculated by Tass (1995) and reported them to be identical to the ones observed. An alternative explanation might be that of the so-called Fechner colors. Fechner demonstrated that black and white images lead to color illusions when alternated at certain frequencies (Fechner 1938).

Last but not least, we find it notable that the SSVEP spectrum had clear 50-Hz peaks not only for 50 Hz stimulation frequency, but also for 1, 5, 10, 25, 75 and 100 Hz. Had the 50-Hz spectral peak been present at all stimulation frequencies to a similar extent, it would have just been an artifact of the German line frequency. However, the selective responsiveness to certain stimulation frequencies which are in harmonic relation to 50 Hz suggests that there is a clear interaction of the line frequency and brain oscillations.

Acknowledgements We express our thanks to Diana Böttger and Stefan Röttger, who helped during data analysis, to Markus Bauer, who helped with writing the stimulation software, and to Thomas Arnold, who helped to adapt the AR method to the paradigm. Thomas Arnold was supported by BMBF grant 0311462 and Diana Böttger was partly supported by DFG grant SCHR 375/8-1.

References

Başar-Eroglu C, Strüber D, Schürmann M, Stadler M, Başar E (1996) Gamma-band responses in the brain: a short review of psychophysiological correlates and functional significance. Int J Psychophysiol 24:101–112

Başar E, Schürmann M, Başar-Eroglu C, Karakaş S (1997) Alpha oscillations in brain functioning: an integrative theory. Int J Psychophysiol 26:5–29

Başar E, Demiralp T, Schürmann M, Başar-Eroglu C (1998) Cross-modality experiments on the cat brain. In: Başar E (ed) Brain functions and oscillations, vol. 2. Springer-Verlag, Berlin, pp 37–59

Crick F, Koch C (1995) Are we aware of neural activity in primary visual cortex? Nature 375:121–123

Eckhorn R (1994) Oscillatory and non-oscillatory synchronization in the visual cortex of cat and monkey. In: Pantev C (ed) Oscillatory event-related brain dynamics. Plenum Press, New York, pp 115–134

Elliott MA, Müller HJ (1998) Synchronous information presented in 40-Hz flicker enhances visual feature binding. Psychol Sci 9:277–283

Elliott MA, Herrmann CS, Mecklinger A, Müller H (2000) The loci of oscillatory visual-object priming: a combined electroencephalographic and reaction-time study. Int J Psychophysiol 38:225–242

Engel A, König P, Kreiter AK, Schillen TB, Singer W (1992) Temporal coding in the visual cortex: new vistas on integration in the nervous system. Trends Neurosci 15:218–226

Fechner GT (1938) Ueber eine Scheibe zur Erzeugung subjectiver Farben. In: Poggendorf JC (ed) Annalen der Physik und Chemie. Verlag von Johann Ambrosius Barth, Leipzig, pp 227–232

Gray CM, König P, Engel AK, Singer W (1989) Oscillatory response in the cat visual cortex exhibits intercolumnar synchronization which reflects global stimulus properties. Nature 338:334–337

Herrmann CS, Mecklinger A (1999) Target gamma response in visual ERPs. Psychophysiology 36:S59

Herrmann CS, Mecklinger A (2000) Magnetoencephalographic responses to illusory figures: early evoked gamma is affected by processing of stimulus features. Int J Psychophysiol 38:265–281

Herrmann CS, Mecklinger A, Pfeiffer E (1999) Gamma responses and ERPs in a visual classification task. Clin Neurophysiol 110:636–642

Hillyard SA, Hinrichs H, Tempelmann C, Morgan ST, Hansen JC, Scheich H, Heinze HJ (1997) Combining steady-state visual evoked potentials and fMRI to localize brain activity during selective attention. Hum Brain Mapping 5:287–292

Juergens E, Guettler A, Eckhorn R (1999) Visual stimulation elicits locked and induced gamma oscillations in monkey intracortical and EEG potentials, but not in human EEG. Exp Brain Res 129:247–259

Keil A, Müller MM, Ray WJ, Gruber T, Elbert T (1999) Human gamma band activity and perception of a gestalt. J Neurosci 19:7152–7162

Klimesch W (1997) EEG-alpha rhythms and memory processes. Int J Psychophysiol 26:319

Lopes da Silva F (1993) Computer-assisted EEG diagnosis: pattern recognition and brain mapping. In: Niedermeyer E, Lopes da Silva F (eds) Electroencephalography, basic principles, clinical applications and related fields. William & Wilkins, Baltimore, pp 1063–1086

Lyskov E, Ponomarev V, Sandström M, Mild KH, Medvedev S (1998) Steady-state visual evoked potentials to computer monitor flicker. Int J Psychophysiol 28:285–290

Müller MM, Junghöfer M, Elbert T, Rockstroh B (1997) Visually induced gamma-band responses to coherent and incoherent motion: a replication study. Neuroreport 8:2575–2579

Ossenblok P, Spekreijse H (1991) The extrastriate generators of the EP to checkerboard onset. A source localization approach. Electroencephalogr Clin Neurophysiol 80:181–193

Pulvermüller F, Keil A, Elbert T (1999) High-frequency brain activity: perception or active memory. Trends Cog Sci 3:250–252

Rager G, Singer W (1998) The response of cat visual cortex to flicker stimuli of variable frequency. Eur J Neurol 10:1856–1877

Regan D (1989) Human brain electrophysiology: evoked potentials and evoked magnetic fields in science and medicine. Elsevier, New York
Schürmann M, Başar E (1994) Topography of alpha and theta responses upon auditory and visual stimuli in humans. Biol Cybern 72:161–174
Schürmann M, Başar-Eroglu C, Başar E (1997) A possible role of evoked alpha in primary sensory processing: common properties of cat intracranial recordings and human EEG. Int J Psychophysiol 26:149–170
Silberstein RB (1995) Steady-state visually evoked potentials, brain resonances, and cognitive processes. In: Nunez PL (ed) Neocortical dynamics and human EEG rhythms. Oxford University Press, Oxford, pp 272–303
Stam CJ, Pijn JPM, Suffczynski P, Lopes da Silva FH (1999) Dynamics of the human alpha rhythm: evidence for non-linearity? Clin Neurophysiol 110:1801–1813
Takahashi T (1993) Activation methods. In: Niedermeyer E, Lopes da Silva F (eds) Electroencephalography, basic principles, clinical applications and related fields. William & Wilkins, pp 241–262
Tallon-Baudry C, Bertrand O (1999) Oscillatory gamma activity in humans and its role in object representation. Trends Cog Sci 3:151–162
Tallon C, Bertrand O, Bouchet P, Pernier J (1995) Gamma-range activity evoked by coherent visual stimuli in humans. Eur J Neurosci 7:1285–1291
Tallon-Baudry C, Bertrand O, Peronnet F, Pernier J (1998) Induced γ-band activity during the delay of a visual short-term memory task in humans. J Neurosci 18:4244–4254
Tass P (1995) Cortical pattern formation during visual hallucinations. J Biol Phys 21:177–210
Tass P (1997) Oscillatory cortical activity during visual hallucinations. J Biol Phys 23:21–66
Tiitinen H, Sinkkonen J, Reinikainen K, Alho K, Lavikainen J, Näätänen R (1993) Selective attention enhances the auditory 40-Hz transient response in humans. Nature 364:59–60

Erklärung

Hiermit erkläre ich, daß ich die vorliegende Habilitationsschrift selbständig verfaßt habe und keine anderen, als die angegebenen Quellen und Hilfsmittel benutzt habe, sowie wörtlich oder inhaltlich übernommene Stellen als solche gekennzeichnet habe.

Dr. Christoph Herrmann

Curriculum Vitae

Persönliche Daten:

Name:	Dr. Christoph Siegfried Herrmann
Nationalität:	Deutsch
Geburt:	20. August 1966 in Celle
Wohnadresse	Wettiner Str. 16, 04105 Leipzig
Telephon:	0341 9940 250 (Büro)
	0341 9808 360 (zu Hause)
Fax:	0341 9940 204
Email:	herrmann@cns.mpg.de
Webseite:	www.csherrmann.de
Büroadresse :	Max Planck Institut für neuropsychologische Forschung, Stephanstr. 1, 04103 Leipzig

Ausbildung:

1986 - 1992:	Studium der Elektrotechnik an der Technischen Universität Darmstadt
Okt. 1992:	Diplom in Elektrotechnik
1993 - 1996:	Promotion am Fachgebiet Intellektik (FB Informatik) an der Technischen Universität Darmstadt
1996:	Dissertation *Ein hybrides KI–System zur medizinischen Befundung: am Beispiel der Elektroenzephalographie*

Berufserfahrung:

Mai 1996 - Nov. 1996:	Wissenschaftlicher Mitarbeiter an der Universitätsklinik Mainz
Dez. 1996 - Sept. 1997:	Wissenschaftlicher Mitarbeiter an der Technischen Universität Darmstadt
Seit Sept. 1997:	Wissenschaftlicher Mitarbeiter am Max-Planck-Institut für neuropsychologische Forschung

Auslandserfahrung:

1989:	Auslandssemester am The College of New Jersey, USA
1997:	3 Monate Forschungsaufenthalt an der Hokkaido University in Sapporo, Japan
2000:	3 Monate Forschungsaufenthalt an der University of California in Berkeley, USA

Drittmittelprojekte:

1998–2001:	Koordinator des Verbundprojekts *Künstlich intelligente funktionelle Gehirnanalyse* durch das Bundesministerium für Bildung und Forschung (BMBF). Weitere Projektpartner: Uniklinik Mainz, Firma Walther Graphtek
1998–2001:	Bewilligung eines Forschungprojekts zum Thema *Automatische EEG–Analyse* in obigem BMBF–Verbundprojekt
2001–2003:	Bewilligung eines Forschungprojekts zum Thema *Differenzierung des visuellen Arbeitsgedächtnisses von Merkmalsbindung und selektiver Aufmerksamkeit* durch die Deutsche Forschungsgemeinschaft (DFG) im Rahmen der Forschergruppe Arbeitsgedächtnis (Prof. Schröger, Leipzig)
2002–2004:	Vorläufige Bewilligung eines Forschungprojekts zum Thema *Merkmalsbindung und 40 Hz: Elektrophysiologische Korrelate räumlicher und zeitlicher Bindung* durch die Deutsche Forschungsgemeinschaft (DFG) im Rahmen der Forschergruppe Bindung (Prof. Lindenberger, Saarbrücken)

Mitgliedschaften in wissenschaftlichen Vereinigungen:

Seit 1995	Gesellschaft für Informatik (FG Künstliche Intelligenz)
Seit 1997	Deutscher Hochschulverband
Seit 1998	Society of Psychophysiological Research
Seit 1999	Cognitive Neuroscience Society
Seit 2000	Gesellschaft für Kognitionswissenschaften
Seit 2000	Deutsche Gesellschaft für Psychologie

Gutachter für folgende Zeitschriften:

Seit 1996	Artificial Intelligence
Seit 1998	Neuropsychobiology
Seit 1999	Proceedings of the National Academy of Sciences USA
Seit 2000	Psychophysiology
Seit 2000	Visual Cogntition
Seit 2001	Neuroscience and Biobehavioural Reviews
Seit 2001	International Journal of Psychophysiology
Seit 2001	Consciousness & Cognition
Seit 2001	Neuroscience Letters

Organisation von Kongressen:

Sept. 1996	Workshop *Wissensrepräsentation in neuronalen Netzen* auf der 20. Deutschen Jahrestagung für Künstliche Intelligenz in Dresden
März 1999	Workshop *Gamma activity in the human EEG* in Leipzig
März 2000	Symposium *Binding in space and time* in Leipzig
Sept. 2001	*5. Fachtagung der Gesellschaft für Kognitionswissenschaft* in Leipzig

MPI Series in Cognitive Neuroscience

1. Anja Hahne
   Charakteristika syntaktischer und semantischer Prozesse bei der auditiven Sprachverarbeitung: Evidenz aus ereigniskorrelierten Potentialstudien
2. Ricarda Schubotz
   Erinnern kurzer Zeitdauern: Behaviorale und neurophysiologische Korrelate einer Arbeitsgedächtnisfunktion
3. Volker Bosch
   Das Halten von Information im Arbeitsgedächtnis: Dissoziationen langsamer corticaler Potentiale
4. Jorge Jovicich
   An investigation of the use of Gradient- and Spin-Echo (GRASE) imaging for functional MRI of the human brain
5. Rosemary C. Dymond
   Spatial Specificity and Temporal Accuracy in Functional Magnetic Resonance Investigations
6. Stefan Zysset
   Eine experimentalpsychologische Studie zu Gedächtnisabrufprozessen unter Verwendung der funktionellen Magnetresonanztomographie
7. Ulrich Hartmann
   Ein mechanisches Finite-Elemente-Modell des menschlichen Kopfes
8. Bertram Opitz
   Funktionelle Neuroanatomie der Verarbeitung einfacher und komplexer akustischer Reize: Integration haemodynamischer und elektrophysiologischer Maße
9. Gisela Müller-Plath
   Formale Modellierung visueller Suchstrategien mit Anwendungen bei der Lokalisation von Hirnfunktionen und in der Diagnostik von Aufmerksamkeitsstörungen
10. Thomas Jacobsen
    Characteristics of processing morphological structural and inherent case in language comprehension
11. Stefan Kölsch
    Brain and Music: A contribution to the investigation of central auditory processing with a new electrophysiological approach
12. Stefan Frisch
    Verb-Argument-Struktur, Kasus und thematische Interpretation beim Sprachverstehen
13. Markus Ullsperger
    The role of retrieval inhibition in directed forgetting - an event-related brain potential analysis

14. Martin Koch
    Measurement of the Self-Diffusion Tensor of Water in the Human Brain

15. Axel Hutt
    Methoden zur Untersuchung der Dynamik raumzeitlicher Signale

16. Frithjof Kruggel
    Detektion und Quantifizierung von Hirnaktivität mit der funktionellen Magnetresonanztomographie

17. Anja Dove
    Lokalisierung an internen Kontrollprozessen beteiligter Hirngebiete mithilfe des Aufgabenwechselparadigmas und der ereigniskorrelierten funktionellen Magnetresonanztomographie

18. Karsten Steinhauer
    Hirnphysiologische Korrelate prosodischer Satzverarbeitung bei gesprochener und geschriebener Sprache

19. Silke Urban
    Verbinformationen im Satzverstehen

20. Katja Werheid
    Implizites Sequenzlernen bei Morbus Parkinson

21. Doreen Nessler
    Is it Memory or Illusion? Electrophysiological Characteristics of True and False Recognition

22. Christoph Herrmann
    Die Bedeutung von 40-Hz-Oszillationen für kognitive Prozesse

23. Christian Fiebach
    Working Memory and Syntax during Sentence Processing. A neurocognitive investigation with event-related brain potentials and functional magnetic resonance imaging